OCRWM	MODEL COVER SHEET	1. QA: QA Page 1 of 204

DOC.20030826.0001

2. Type of Mathematical Model

☒ Process Model ☒ Abstraction Model ☐ System Model

Describe Intended Use of Model

The purpose of this Model Report is to document the abstraction of drift seepage, conducted to provide seepage-relevant parameters and their probability distributions for use in Total System Performance Assessment for License Application (TSPA-LA).

3. Title

Abstraction of Drift Seepage

4. DI (including Rev. No. and Change No., if applicable):

MDL-NBS-HS-000019 REV00

5. Total Attachments	6. Attachment Numbers - No. of Pages in Each
5	I-2, II-2, III-6, IV-4, V-4

	Printed Name	Signature	Date
7. Originator	J.T. Birkholzer	SIGNATURE ON FILE	8/20/03
8. CSO	M. Zhu	SIGNATURE ON FILE	8/20/03
9. Checker	P. Persoff	SIGNATURE ON FILE	8/20/03
10. QER	S. Harris	SIGNATURE ON FILE	8/20/03
11. Responsible Manager/Lead	J.S.Y. Wang/S. Finsterle	SIGNATURE ON FILE	8/20/03
12. Responsible Manager	P. Dixon	SIGNATURE ON FILE	8/20/03

13. Remarks

Comments made in Section 6.5.3 (Model E.3-1) and 6.5.4 (Model E.3-2) of the report *Model Validation Status Review*, TDR-WIS-MD-000005 REV 00 (BSC 2001 [156257]), have been addressed in this Model Report.

Technical Error Report (TER) log number discussed in this Model Report

TER-02-0062

MODEL REVISION RECORD

2. Model Title:
Abstraction of Drift-Seepage

3. DI (including Rev. No. and Change No., if applicable):
MDL-NBS-HS-000019 REV00

4. Revision/Change No.	5. Description of Revision/Change
	This report is a revision of an Analysis/Model Report by the same title--Document Identifier ANL-NBS-MD-000005 (CRWMS M&O 2001 [154291]). The revision includes the following main changes: New data analyses and modeling results have become available. As a result, the abstraction model has been substantially revised. Major revisions include the incorporation of new seepage calibration data and new predictive modeling results from the SMPA, improved treatment of seepage during the period of thermally perturbed flow conditions, disposition of mechanical and chemical alterations based on process models, new probability distributions for variability and uncertainty, and a revised concept for flow focusing.
REV00	In this new model report, the entire documentation was revised. Side bars are not used because the changes were too extensive to use Step 5.9d)1) per AP-SIII.10Q Rev. 1/ICN 2.

TABLE OF CONTENTS

TABLE OF CONTENTS (Continued)

TABLE OF CONTENTS (Continued)

INTENTIONALLY LEFT BLANK

LIST OF FIGURES

LIST OF FIGURES (Continued)

LIST OF FIGURES (Continued)

INTENTIONALLY LEFT BLANK

LIST OF TABLES

INTENTIONALLY LEFT BLANK

ACRONYMS

1-D	one-dimensional
2-D	two-dimensional
3-D	three-dimensional
AC	Acceptance Criteria
AP	Administrative Procedure (DOE)
BSC	Bechtel SAIC Company, LLC
CRWMS	Civilian Radioactive Waste Management System
DFNM	discrete fracture network model
DIRS	Document Input Reference System
DOE	Department of Energy
DST	Drift Scale Test
DTN	Data Tracking Number
DRKBA	Discrete Region Key Block Analysis
ECRB	Enhanced Characterization of Repository Block
ESF	Exploratory Studies Facility
FEPs	Features, Events, and Processes
LA	License Application
LBNL	Lawrence Berkeley National Laboratory
M&O	Management and Operating Contractor
OCRWM	Office of Civilian Radioactive Waste Management
PA	Performance Assessment
Q	Qualified
QIP	Quality Implementing Procedure

ACRONYMS (Continued)

SCM	Seepage Calibration Model
SD	standard deviation
SE	standard error of mean
SMPA	Seepage Model for Performance Assessment
TDMS	Technical Data Management System
TH	thermal-hydrological
THC	thermal-hydrological-chemical
TSPA-LA	Total System Performance Assessment for License Application
TWP	Technical Work Plan
UZ	unsaturated zone
UZ Model	Unsaturated Zone Flow and Transport Model
YMP	Yucca Mountain Project
YMRP	*Yucca Mountain Review Plan, Final Report*

1. PURPOSE

The purpose of this Model Report is to document the abstraction of drift seepage, conducted to provide seepage-relevant parameters and their probability distributions for use in Total System Performance Assessment for License Application (TSPA-LA). Drift seepage refers to the flow of liquid water into waste emplacement drifts. Water that seeps into drifts may contact waste packages and potentially mobilize radionuclides, and may result in advective transport of radionuclides through breached waste packages (BSC 2002 [160780], Section 3.3.2). The unsaturated rock layers overlying and hosting the repository form a natural barrier that reduces the amount of water entering emplacement drifts by natural subsurface processes. For example, drift seepage is limited by the capillary barrier forming at the drift wall, which decreases or even eliminates water flow from the unsaturated fractured rock into the drift. During the first few hundred years after waste emplacement, when above-boiling rock temperatures will develop as a result of heat generated by the decay of the radioactive waste, vaporization of percolation water is an additional factor preventing seepage. Estimating the effectiveness of these natural barrier capabilities and predicting the amount of seepage into drifts is an important aspect of assessing the performance of the repository.

Abstraction is defined as the process of purposely simplifying a mathematical model (component, barrier, or subsystem process model) for incorporation into an overall system model of the geological repository (BSC 2002 [158794], Section 3.1.1). Thus, the purpose of this Model Report is to modify the information generated by the seepage process models into a form that can be used in the TSPA-LA. The simplifications and assumptions made in this abstraction process must be realistic and appropriate. In particular, uncertainties and spatial variabilities of the primary process models for seepage must be represented in the abstraction model and must be propagated to TSPA-LA (see Section 4.2).

A suite of primary process models provides seepage model results used as input to the abstraction performed in this report. The following three models—compatible and consistent in their conceptual treatment of flow diversion and capillary barrier behavior—provide the basis for seepage abstraction:

1. The *Seepage Calibration Model (SCM)*
   This process model provides the conceptual basis for seepage modeling and derives seepage-relevant parameters through calibration of the model against seepage-rate data from liquid-release tests (BSC 2003 [162267]).
2. The *Seepage Model for Performance Assessment (SMPA)*
   This process model predicts drift seepage rates for long-term ambient conditions at Yucca Mountain, for a wide range of seepage-relevant parameters and for potentially important perturbing effects. The latter include the effect of rock bolts on flow paths and the impact of drift shape changes caused by degradation (BSC 2003 [163226]). Drift degradation is expected as a result of thermal stresses, seismic events, and time-dependent decrease in rock strength.

3. The *Thermal-Hydrological Seepage Model (TH Seepage Model)*
   This process model predicts drift seepage during the period when water-flow processes in the drift vicinity are perturbed by heating of the rock (BSC 2003 [161530]).

Additional input from scientific analyses or from process models is required to define probability distributions that appropriately cover uncertainty and spatial variability of seepage-affecting parameters. In addition to the capillary strength in the fractures close to the drift—calibrated with the SCM—the most important parameters defining the amount of seepage are the local percolation flux and the formation's permeability close to the drifts (BSC 2003 [162267]). Information on these parameters is mainly derived from the following sources:

1. Site-scale and Intermediate-scale UZ Flow Simulations
   The *UZ Flow and Transport Model* provides three-dimensional site-scale flow fields to derive the local percolation flux (BSC 2003 [163045]). In addition, flow focusing factors account for intermediate-scale heterogeneity that is not represented in the layer-averaged *UZ Flow and Transport Model*. These are estimated from an intermediate-scale flow focusing model BSC (2001 [156609], Section 6.4.2).

2. *In situ* Testing at Yucca Mountain
   Air-injection tests performed at different scales and locations provide estimates of local fracture permeability (BSC 2001 [158463]).

Finally, results from the coupled thermal-hydrological-mechanical (THM) and thermal-hydrological-chemical (THC) models are utilized to assess whether seepage-relevant parameters may be affected by mechanical and/or chemical processes. These processes occur in response to the heat generated in the repository (BSC 2003 [162050] and BSC 2003 [162318]). The relationship and the information flow between the suite of primary process models important for seepage and the seepage abstraction are schematically illustrated in Figure 1-1. A more detailed description is given in Section 6.3.

The seepage abstraction described in this Model Report synthesizes and simplifies the relevant input from the above sources, and provides a realistic and appropriate abstraction model for TSPA-LA. The scope of this work is to (1) develop an appropriate abstraction methodology for drift seepage, considering both the nominal scenario and disruptive scenarios such as seismic and igneous events, (2) determine the uncertainty and spatial variability of seepage-relevant parameters, (3) provide look-up tables for seepage into nondegraded and collapsed drifts as a function of these parameters, (4) evaluate and discuss the impact of additional factors affecting seepage, such as THM, THC processes, rock bolts, and igneous events, (5) validate the seepage abstraction methodology, and (6) evaluate and discuss all seepage-related features, events, and processes (FEPs). The analyses documented in this report were conducted under the *Technical Work Plan (TWP) for: Performance Assessment Unsaturated Zone*, TWP-NBS-HS-000003 REV 02 (BSC 2002 [160819]). The relevant TWP sections for this work are Section 1.13.5, entitled "Update Seepage Abstraction Model," and Attachment I, entitled "Model Validation Plans," Section I-4-3. There are no deviations from the work scope described in the TWP.

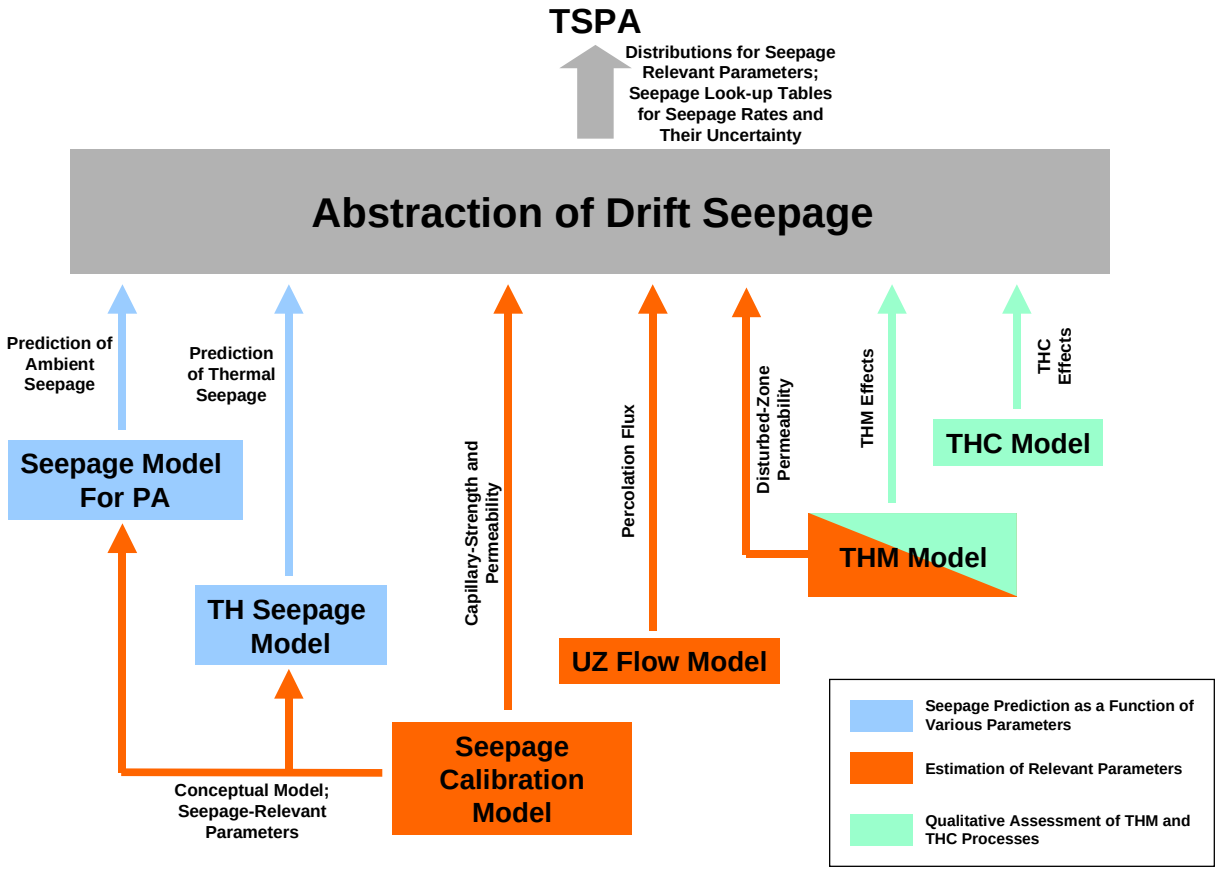

Figure 1-1. Relationship and Information Flow between Primary Process Models and Seepage Abstraction

The primary limitations in the scope of this Model Report and its results are as follows:

- The results of the seepage abstraction model are based on the available data and the available analyses/models, as listed above and in Section 4.1 and 6.4. Limitations reported in analyses or model reports that directly support this Model Report are implicit limitations of seepage abstraction. The limitations of predictive models (process models), for example, are defined by the conceptual model, as described in the pertinent sections of the respective Model Reports.

- The predictive seepage models and the seepage abstraction model are probabilistic models that provide estimates of seepage fluxes averaged over drift segments. These models are not expected to predict individual seepage events or to provide the precise spatial seepage distribution along the drifts and within the repository. This is consistent with the probabilistic seepage calculation conducted in the TSPA-LA simulation.

INTENTIONALLY LEFT BLANK

2. QUALITY ASSURANCE

Development of this Model Report on seepage abstraction and the supporting analyses/modeling activities have been determined to be subject to the Yucca Mountain Project's quality assurance (QA) program as documented in *Technical Work Plan for: Performance Assessment Unsaturated Zone*, TWP-NBS-HS-000003 REV 02 (BSC 2002 [160819], Section 8.2, Work Package AUZM09). Approved QA procedures identified in the TWP (BSC 2002 [160819], Section 4) have been used to conduct and document the activities described in this Model Report. Electronic management of information was evaluated in accordance with Administrative Procedure (AP)-SV.1Q, *Control of the Electronic Management of Information* and controlled under YMP-LBNL-QIP-SV.0, *Management of YMP-LBNL Electronic Data*, as planned in BSC (2002 [160819], Section 8.4).

This Model Report documents the abstraction of drift seepage in order to provide seepage-related parameters and their probability distributions for use in TSPA-LA. It provides insight into the performance of natural barriers that are important to the demonstration of compliance with the postclosure performance objectives prescribed in 10 CFR 63.113 [156605]. Therefore, it is classified as a "Quality Level – 1" with regard to importance to waste isolation, as defined in AP-2.22Q, *Classification Criteria and Maintenance of the Monitored Geologic Repository Q-List*. The report contributes to the analysis and modeling data used to support performance assessment; the conclusions do not directly impact engineered features important to safety, as defined in AP-2.22Q.

INTENTIONALLY LEFT BLANK

3. USE OF SOFTWARE

Only standard off-the-shelf commercially available software was used for this Model Report. These are not subject to software quality assurance requirements of AP-SI.1Q. The software used was *Microsoft Excel 97 SR-2* for calculations and graphical display, *Mathcad 11* for calculations, and Tecplot V9.0 for graphical display. All information needed to reproduce the calculations using these standard software programs, including the input, computation and output as required by AP-SIII.10Q, is included in this report, with references specified (see Attachments I through V).

INTENTIONALLY LEFT BLANK

4. INPUTS

4.1 DATA AND PARAMETERS

Table 4.1-1 summarizes the input data and parameters used in this Model Report. All input data and parameters needed for seepage abstraction are obtained from the Technical Data Management System (TDMS). These data are considered appropriate as input for the seepage abstraction model (see Section 6). The parameter values used for abstraction, as well as the spatial variability and uncertainty associated with these values, are presented and discussed in detail in Section 6.

Table 4.1-1. Input Data and Parameters Used in This Model Report

Item	Data Name	Data Source/DTN *Roadmap (if applicable)*	Parameters *Comments*
1	Ambient Seepage Prediction Results	DTN: LB0304SMDCREV2.002 [163687] *The data file from the DTN: LB0304SMDCREV2.002.zip must be unzipped. File Fig6-3toFig6-8.dat contains a seepage look-up table for non-degraded drifts. Another file Fig6-3toFig6-8.xls contains seepage results for all 20 individual realizations. This file opens in a subdirectory "Supporting data for tecplot input".*	Predicted ambient seepage rates and uncertainty for suite of simulation cases *Ambient seepage was predicted by the SMPA. Seepage results are given as a function of permeability, capillary-strength parameter, and percolation flux. Simulation cases cover parameter distributions required for TSPA. The SMPA is documented in BSC (2003 [163226]).*
2	Ambient Seepage Prediction Results for THM Effects	DTN: LB0304SMDCREV2.004 [163691] *The data file from the DTN: LB0304SMDCREV02.004.zip must be unzipped. File Fig6-22.wmf contains a figure comparing seepage results for ambient conditions versus THM altered conditions.*	Predicted seepage rates from ambient model compared to model including THM permeability changes *Seepage results were obtained using the Drift-Scale THM Model. Two cases are studied and compared. The first one calculates seepage using the initial permeability field, the second one calculates seepage using the altered permeability at 10,000 years after emplacement. The two cases are compared. The THM simulation model and results are documented in BSC (2003 [162318]).*
3	Ambient Seepage Prediction Results for Collapsed Drifts	DTN: LB0307SEEPDRCL.002 [164337] *The data file from the DTN: LB0307SEEPDRCL.002.zip must be unzipped. File ResponseSurfaceSMPACollpasedDrift.dat contains a seepage look-up table for a collapsed drift.*	Predicted seepage rates and uncertainty for suite of simulation cases for the collapsed drift scenario *Ambient seepage was predicted by the SMPA. Seepage results are given as a function of permeability, capillary-strength parameter, and percolation flux. Simulation cases cover parameter distributions required for TSPA.*

Table 4.1-1. Input Data and Parameters Used in This Model Report (Continued)

Item	Data Name	Data Source/DTN *Roadmap (if applicable)*	*Parameters* *Comments*
4	Thermal Seepage Prediction Results (TOUGH2 Simulation Files)	DTN: LB0303DSCPTHSM.001 [163688] *File Readme.doc explains the different simulation cases included in the DTN. There are five compressed data files that need to be unzipped onto a large enough disc. A directory structure with different result data files opens, as explained in the Readme document. The temporal evolution of relevant TH parameters is given in simulation files named si_heat.obs. Use the Readme document to relate simulation cases and subdirectories.*	Thermal seepage modeling results *The future drift-scale TH conditions were predicted for selected simulation cases, using the TH Seepage Model. The DTN gives the entire suite of simulation input and output files. The thermal seepage model and results are documented in BSC (2003 [161530]).*
5	Thermal Seepage Prediction Results	DTN: LB0301DSCPTHSM.002 [163689] *File Readme.doc explains the different simulation cases included in the DTN. The data file TH_Seepage_Model.data_summary.tar.gz must be unzipped. A directory structure with different result data files opens, as explained in the Readme document. The thermal seepage results are given in developed data files named seep_relrate.tec. Use the Readme document to relate simulation cases and subdirectories.*	Thermal seepage percentage *Thermal seepage was predicted for selected simulation cases, using the TH Seepage Model. Evolution of seepage with time is given for different rock properties and two geological units. The thermal seepage model and results are documented in BSC (2003 [161530]).*
6	Seepage Calibration Results	DTN: LB0302SCMREV02.002 [162273] *File LB0302SCMREV02.002.zip must be unzipped. Zip-file contains one informational README file and one word document that contains permeability data in Tables 1 and 2, and calibrated capillary-strength parameters in Table 3.*	Post-excavation air permeability statistics and calibrated capillary-strength parameters for niches and systematic testing boreholes *Calibration was conducted by the SCM. The SCM and model results are documented in BSC (2003 [162267]).*
7	Drift Design and Waste-Package Geometry	800-IED-EBS0-00201-000-00A (BSC 2003 [164069])	Drift diameter, waste-package spacing
		800-IED-WIS0-00201-000-00B (BSC 2003 [164603])	Average waste-package length
		800-IED-WIS0-00302-000-00A (BSC 2003 [164101])	Ground support
8	Repository Area	800-IED-EBS0-00401-000-00C (BSC 2003 [162289])	Repository Layout

Table 4.1-1. Input Data and Parameters Used in This Model Report (Continued)

Item	Data Name	Data Source/DTN *Roadmap (if applicable)*	*Parameters* *Comments*
9	Air Permeability Data	DTN: GS960908312232.013 [105574] *Data are in Table S01163_001.*	Air permeability data from vertical boreholes
10		DTN: LB990901233124.004 [123273] *Data are in Table S00017_002.*	Pre-excavation air permeability summary statistics from niches *Analysis is documented in BSC (2001 [158463], Table 6.1.2-3).*
11		DTN: LB0012AIRKTEST.001 [154586] *Data are in Table S01048_001.*	Pre-excavation air permeability data from Niche 1620 (also referred to as Niche 5)
12		DTN: LB980901233124.101 [136593] *Data for Niche 3107 are in Table S99469_001.* *Data for Niche 4788 are in Table S99469_002.*	Pre-excavation air permeability data from Niches 3107 (Niche 3) and 4788 (Niche 4)
13		DTN: LB0011AIRKTEST.001 [153155] *Data for Niche 3650 are in Tables S00434_006 through S00434_009, S00434_011, S00434_013, and S00434_015 (each borehole in separate table).* *Data for Niche 3566 are in Tables S00434_001, S00434_002, and S00434_005 (each borehole in separate table).*	Pre-excavation air permeability data from Niches 3650 (Niche 2) and 3566 (Niche 1)
14	Flow Field Simulations for Different Climate Scenarios	DTN: LB0302PTNTSW9I.001 [162277] *File LB0302PTNTSW9I.001.zip must be unzipped. Zip-file contains one informational README file and nine percolation flux data files, each representing one climate period and one climate scenario.*	Percolation fluxes at the PTn/TSw interface *Fluxes have been predicted by the UZ model. Results are given for three climate periods (present-day, monsoon, and glacial-transition) and three climate scenarios (mean, upper, lower). The simulation model and results are documented in BSC (2003 [163045]).*
15	Alternative Flow Field Simulations for Climate Scenarios	DTN: LB0305PTNTSW9I.001 [163690] *File LB0305PTNTSW9I.001.zip must be unzipped. Zip-file contains one informational README file and nine percolation flux data files, each representing one climate period and one climate scenario.*	Percolation fluxes at the PTn/TSw interface for alternative conceptualization of flow in the PTn *Fluxes have been predicted by the UZ model. Results are given for three climate periods (present-day, monsoon, and glacial-transition) and three climate scenarios (mean, upper, lower). The simulation model and results are documented in BSC (2003 [163045]).*

Table 4.1-1. Input Data and Parameters Used in This Model Report (Continued)

Item	Data Name	Data Source/DTN ***Roadmap (if applicable)***	***Parameters*** ***Comments***
16	UZ Model Columns Representative of Repository Area	DTN: LB03033DSSFF9I.001 [163047] *File xcheckutil.tar.gz must be unzipped. One of the extracted files is REPO_ZONE.cell. This file provides a list of repository zone elements.*	Repository Element Names *The repository element names are used to extract the fluxes over the repository area from DTN: LB0302PTNTSW9I.001 [162277]. Only the repository fluxes are needed for seepage abstraction.*
17	Flow Focusing Factor Distribution	DTN: LB0104AMRU0185.012 [163906] See figures in Sheet 1 of file CumuRE_final.xls	Flow Focusing Factor *Cumulative probability distribution of flow focusing factors is given as a regression curve, derived from a stochastic modeling analysis of a vertical cross-section of Yucca Mountain.*
18	Degraded Drift Profiles	DTN: MO0306MWDDPPDR.000 [164736] *Depending on which scenario number is considered, a file named scenarioNN.zip must be unzipped (NN is the number). A directory opens containing an eps plot file with a figure of the drift profile.*	Degraded Profiles For Several Scenarios *Drift profiles have been calculated for several scenarios, such as from thermal stresses, seismic events, and time-dependent reduction in rock strength..*

4.2 CRITERIA

Technical requirements to be satisfied by performance assessment (PA) are stated in 10 CFR 63.114 [156605] (*Requirements for Performance Assessment*). Technical requirements to be satisfied in relation to multiple barriers are given in 10 CFR 63.115 [156605] (*Requirements for Multiple Barriers*). These technical requirements are also identified in the Yucca Mountain *Project Requirements Document* (Canori and Leitner 2003 [161770]).

The acceptance criteria that will be used by the Nuclear Regulatory Commission (NRC) to determine whether the technical requirements have been met are identified in the *Yucca Mountain Review Plan, Final Report* (YMRP; NRC 2003 [163274]). Seepage abstraction is based on the current understanding of flow paths in the unsaturated zone (UZ) at Yucca Mountain to provide information about the quantity of water seeping into drifts and potentially contacting waste packages. Thus the abstraction must meet acceptance criteria in both Section 2.2.1.3.6.3, *Flow Paths in the UZ*, and Section 2.2.1.3.3.3, *Quantity and Chemistry of Water Contacting Engineered Barriers and Waste Forms*, of the YMRP (NRC 2003 [163274]). Additional acceptance criteria are identified in Section 2.2.1.1.3, System Description and Demonstration of Multiple Barriers, of the YMRP (NRC 2003 [163274]). Each of these criteria has several subcriteria, not all of which are applicable to seepage abstractions.

The pertinent requirements and acceptance criteria for this Model Report are summarized in Table 4.2-1. Differences between this list and the acceptance criteria identified in the TWP (BSC 2002 [160819], Table 3-1) are as follows: (1) YMRP section numbers are different as a result of the recent revision of the YMRP; and (2) Acceptance Criteria (AC) 1 and 2 from NRC (2003 [163274], Section 2.2.1.3.6.3), AC 1 to 5 from NRC (2003 [163274], Section 2.2.1.3.3.3), and AC 1 to 3 from NRC (2003 [163274], Section 2.2.1.1.3) are considered applicable to seepage abstraction and were thus added to the list, i.e., the list discussed in this Model Report is more comprehensive than that in the TWP (BSC 2002 [160819], Table 3-1).

Table 4.2-1. Project Requirements and YMRP Acceptance Criteria Applicable to This Model Report

Requirement Number[a]	Requirement Title[a]	10 CFR 63 Link	YMRP Acceptance Criteria
PRD-002/T-014	Performance Objectives for the Geologic Repository after Permanent Closure	10 CFR 63.113 (a) [156605]	Criteria 1 to 3 for *System Description and Demonstration of Multiple Barriers*[d].
PRD-002/T-015	Requirements for Performance Assessment	10 CFR 63.114 (a-c,e,g) [156605]	Criteria 1 to 5 for *Quantity and Chemistry of Water Contacting Engineered Barriers and Waste Forms*[b]; Criteria 1 to 5 for *Flow Paths in the Unsaturated Zone*[c].
PRD-002/T-016	Requirements for Multiple Barriers	10 CFR 63.115 (b) [156605]	Criteria 1 to 3 for *System Description and Demonstration of Multiple Barriers*[d].

NOTES: [a] from Canori and Leitner (2003 [161770])
[b] from NRC (2003 [163274], Section 2.2.1.3.3.3)
[c] from NRC (2003 [163274], Section 2.2.1.3.6.3)
[d] from NRC (2003 [163274], Section 2.2.1.1.3)

The main acceptance criteria identified in the YMRP are given below, followed by a list of the subcriteria that apply to this Model report, and a discussion on how these selected subcriteria are

being addressed in the document. This discussion is separate for the three relevant sections of the YMRP. Seepage abstraction uses input information from several sources, which provide measured data as well as model results. While the validity of these measured data and model results is briefly discussed in this abstraction report, we refer to the respective upstream reports for a more detailed description of methods, assumptions, initial and boundary conditions, data justification, model validation, alternative conceptual models, and sensitivity studies. References to upstream reports are given throughout this document.

- **Acceptance Criteria from Section 2.2.1.3.6.3, *Flow Paths in the UZ***

  Acceptance Criterion 1, *System Description and Model Integration Are Adequate*:

  - Subcriterion (1): Couplings between thermal, hydrological, mechanical, and chemical processes in the fractured rock are incorporated in the abstraction as appropriate (Sections 6.4.3, 6.4.4, 6.5.1.4, and 6.5.2).
  - Subcriterion (2): All aspects of geology, hydrology, geochemistry, and physical phenomena affecting flow paths in the UZ are adequately considered in the seepage abstraction. Conditions and assumptions are readily identified and consistent with data (Sections 6.3, 6.4, and 6.5).
  - Subcriterion (3): Seepage abstraction uses assumptions, technical bases, data, and models that are appropriate and consistent with abstractions of upstream analyses (UZ flow paths, climate, and infiltration). Seepage abstraction utilizes results from UZ flow path simulations (which are based on climate and infiltration) without any additional simplifications (Section 6.6.4) and integrates them with seepage-relevant information from drift-scale models. The descriptions and technical bases are transparent and traceable to site and design data.
  - Subcriterion (5): Sufficient data and technical bases are provided to assess the degree to which features, events, and processes have been included in this abstraction (Section 6.2).
  - Subcriteria (6) and (7): Several process-level models feed into seepage abstraction (Section 6.4). Adequate spatial variability of model parameters and boundary conditions are employed in these process-level models used to estimate flow paths in the unsaturated zone, percolation flux, and seepage flux. Average parameter estimates used in process-level models are representative of the temporal and spatial discretizations considered in the model.

  Acceptance Criterion 2, *Data Are Sufficient for Model Justification*:

  - Subcriteria (1), (2), (5), (6), and (7): These acceptance criteria mainly address the justification of upstream models that feed into the seepage abstraction. Adequate descriptions of how these upstream models meet the several subcriteria are provided in detail in the respective model reports (as referenced in Section 6.4). It is demonstrated in these reports that the input parameters used in the models are justified. Accepted and well-documented procedures have been used to construct and calibrate the numerical models. The models are technically defensible and based on data collected using acceptable techniques. Sensitivity analyses have been conducted to assess data sufficiency.

- Subcriterion (2): The main hydrological properties (air permeability and the capillary-strength parameters) used in the seepage abstraction are based on adequately designed air injection and liquid release tests. From the seepage rates measured in the liquid release tests, effective capillary-strength parameters have been calibrated with an appropriate inverse model (Section 6.4.1).
- Subcriterion (3): The percolation flux distributions used in the seepage abstraction are based on a technically defensible UZ flow model that reasonably represents the physical system and is calibrated using site-specific hydrological, geological, and geochemical data (Section 6.6.4.1). These distributions provide the appropriate spatial and temporal variability of model parameters, including climate-induced changes in infiltration. Percolation fluxes are further adjusted using flow focusing factors to account for intermediate-scale heterogeneity (Section 6.6.4.2).
- Subcriterion (4): Appropriate thermal-hydrological tests have been designed and conducted, so that critical thermal-hydrological-mechanical-chemical processes could be observed, and values for relevant model parameters estimated (see references in Sections 6.4.3 and 6.4.4).

Acceptance Criterion 3, *Data Uncertainty Is Characterized and Propagated through the Model Abstraction:*

- Subcriteria (1) and (2): Seepage abstraction uses parameter values, ranges, probability distributions, and/or bounding assumptions that are technically defensible, reasonably account for uncertainties and variabilities, and do not result in an under-representation of risk (Section 6.5). The technical bases for the parameter values used in this abstraction are provided (Section 6.6).
- Subcriterion (3): Possible statistical correlations between parameters have been evaluated in this abstraction. An adequate technical basis or bounding argument is provided for neglected correlations (Section 6.5.1.1).
- Subcriterion (5): The impact of coupled processes is adequately represented in the seepage abstraction (Sections 6.5.1.4 and 6.5.2).
- Subcriterion (6): Uncertainties in the characteristics of the natural system are explicitly considered in the seepage abstraction (see summary in Section 6.7.2, detailed discussions in Sections 6.5 and 6.6).

Acceptance Criterion 4, *Model Uncertainty Is Characterized and Propagated through the Model Abstraction*:

- Subcriterion (1): Alternative modeling approaches have been investigated in all upstream models that feed into this abstraction (Section 6.4). The results are appropriately considered in the abstraction (Section 6.5).
- Subcriterion (2): The bounds of uncertainty created by the process-level models are considered in the abstraction (Sections 6.5 and 6.6).
- Subcriterion (3): Consideration of conceptual model uncertainty is consistent with available site characterization data, laboratory experiments, field measurements, natural analog information and process-level modeling studies. The treatment of conceptual

model uncertainty does not result in an under-representation of risk (Sections 6.5 and 6.6).

Acceptance Criterion 5, *Model Abstraction Output Is Supported by Objective Comparisons:*

- Subcriteria (1), (2), and (3): The abstraction results implemented in the TSPA-LA are based on and consistent with output from detailed process-level models, as demonstrated by comparison. For example, results from the process-level model for ambient seepage are incorporated in the seepage abstraction without any simplifications. Other abstractions of process-level models conservatively bound the process-level predictions (Section 6.4 and 6.5).

- **Acceptance Criteria from Section 2.2.1.3.3.3, *Quantity and Chemistry of Water Contacting Engineered Barriers and Waste Forms***

Acceptance Criterion 1, *System Description and Model Integration Are Adequate*:

- Subcriteria (1) and (2): Physical phenomena and couplings are adequately incorporated in the seepage abstraction. The assumptions, technical bases, data, and models used in the seepage abstraction are appropriate and consistent with the abstractions for UZ flow paths and for climate and infiltration (Section 6.6.4) as well as for drift degradation (Section 6.5.1.5). The descriptions and technical bases are transparent and traceable.
- Subcriterion (4): Spatial and temporal abstractions appropriately address physical couplings from thermal, hydrological, mechanical, and chemical processes (Sections 6.5.1.4 and 6.5.2). Flow perturbations resulting from these processes, which could potentially lead to increased flux of water towards drifts, have been analyzed by appropriate testing and modeling studies (Sections 6.4.3 and 6.4.4) and have been accounted for in the abstraction (Section 6.5.1.4 and 6.5.2).
- Subcriterion (5): Sufficient technical data and justification are provided for assumptions and approximations regarding the coupled effects on seepage and flow (Sections 6.4.3 and 6.4.4). The effects of flow distribution on the amount of water contacting waste packages are consistently addressed (Sections 6.4 for small-scale variability, Section 6.6.4 for intermediate-scale variability).
- Subcriterion (8): Adequate technical bases are provided, including independent modeling, laboratory, and field data, or sensitivity studies, for inclusion of any thermal-hydrological-mechanical-chemical couplings and features, events, and processes (Sections 6.4.3 and 6.4.4).
- Subcriterion (9): Performance-affecting processes that have been observed in thermal-hydrological tests and experiments are included in the seepage abstraction. It has been demonstrated that refluxing water will not enhance seepage at Yucca Mountain (Sections 6.4.3 and 6.5.2).

Acceptance Criterion 2, *Data Are Sufficient for Model Justification*:

- Subcriteria (1) and (2): This acceptance criterion mainly addresses the justification of upstream process-level models that feed into the seepage abstraction. Adequate descriptions of how these models meet the several subcriteria are provided in detail in the

respective model reports (as referenced in Section 6.4). It is demonstrated that the geological, hydrological and geochemical values used in these upstream process-level models are adequately justified. Sufficient data were collected on the characteristics of the natural system to establish initial and boundary conditions for these models.

- Subcriterion (3): Thermal-hydrological tests have been designed and conducted with the explicit objectives of observing thermal-hydrological processes for the temperature ranges expected for the repository conditions and making measurements for process-level models (see references in Section 6.4.3). The data collected are sufficient to verify that the thermal-hydrological conceptual models capture the relevant thermal-hydrological phenomena (Section 6.4.3).

Acceptance Criterion 3, *Data Uncertainty Is Characterized and Propagated through the Model Abstraction:*

- Subcriterion (1): Seepage abstraction uses parameter values, ranges, probability distributions, and bounding assumptions that are technically defensible, reasonably account for uncertainties and variabilities, and do not result in an under-representation of risk (Sections 6.5 and 6.6).
- Subcriterion (2): The parameter values, ranges, probability distributions, and bounding assumptions used in seepage abstraction are based on data from the Yucca Mountain region, including results from heater tests and niche liquid-release tests, from field measurements, and process-modeling studies, corroborated by natural analog research (Sections 6.4, 6.5 and 6.6).
- Subcriterion (3): The input information used in the TSPA seepage calculations is derived from and consistent with measured data or parameters provided by process-level models (Section 6.4). Possible statistical correlations between input values have been evaluated in this abstraction (Section 6.5.1.1). The impact of coupled processes is adequately represented in the seepage abstraction (Sections 6.5.1.4 and 6.5.2). Reasonable or conservative ranges of parameters or functional relations are established (Section 6.6).
- Subcriterion (4): Uncertainties in the characteristics of the natural system are explicitly considered in the seepage abstraction (see summary in Section 6.7.2, detailed discussions in Sections 6.5 and 6.6).

Acceptance Criterion 4, *Model Uncertainty Is Characterized and Propagated through the Model Abstraction*:

- Subcriteria (1), (2), and (4): Alternative model approaches of features, events, and processes have been investigated in all upstream models that feed into this abstraction. The results are appropriately considered in the abstraction. The selected modeling approaches are consistent with available data and current scientific understanding. Alternative approaches not considered in the final analysis, and the limitations and uncertainties of the upstream models, are described in the respective Model Reports (Section 6.4). Adequate consideration is given to effects of thermal-hydrological-mechanical-chemical processes in the assessment of alternative conceptual models.
- Subcriterion (3): Consideration of conceptual model uncertainty is consistent with available site characterization data, laboratory experiments, field measurements, natural

analog information and process-level modeling studies. The treatment of conceptual model uncertainty does not result in an under-representation of risk (Sections 6.5 and 6.6).

- Subcriterion (5): The process-level models feeding into the seepage abstraction are based on an equivalent continuum assumption for flow and transport in the fractured network and in the matrix blocks. As discussed in Section 6.4, these models have been validated by comparison with measured data and are appropriate for their use in seepage abstraction. Alternative models, such as the discrete fracture models, are briefly discussed in Section 6.4.1.2, and references to a more in-depth discussion are given therein. It was demonstrated that seepage predictions with a continuum model were consistent with seepage predictions from a discrete model.

Acceptance Criterion 5, *Model Abstraction Output Is Supported by Objective Comparisons:*

- Subcriterion (1): The abstraction results implemented in the TSPA-LA are based on and consistent with output from detailed process-level models (Sections 6.4 and 6.5).
- Subcriterion (2): Abstracted models for thermal-hydrological-mechanical-chemical effects on seepage and flow are based on the same assumptions and approximations used for process-level models (Sections 6.4.4). Note that the ambient seepage process-level model results (estimating flow diversion of percolation flux around from drifts) are incorporated in the seepage abstraction without any simplifications (Section 6.5.1). Other abstractions of process-level models conservatively bound the process-level predictions (e.g., abstraction of thermally induced parameter changes discussed in Section 6.5.1.4).
- Subcriterion (3): Accepted and well-documented procedures have been used to construct and test the numerical models that simulate coupled effects of seepage and flow, providing the basis for this abstraction (see references in Section 6.4).

- **Acceptance Criteria from Section 2.2.1.1.3, *System Description and Demonstration of Multiple Barriers***

Acceptance Criterion 1, *Identification of Barriers Is Adequate*:

- Subcriterion (1): The unsaturated zone above the repository forms a natural barrier important to waste isolation. This Model Report addresses the amount of water seeping into drifts relative to the amount of percolation to provide a basis for evaluating the barrier capability (see probabilistic seepage evaluation in Section 6.8).

Acceptance Criterion 2, *Description of Barrier Capability to Isolate Waste Is Acceptable*:

- Subcriteria (1) and (2): The capability of the identified barriers to prevent or limit the amount of water seeping into waste emplacement drifts is adequately identified and described, including changes during the compliance period. The uncertainty associated with barrier capabilities is adequately described (see Section 6.8).

Acceptance Criterion 3, *Technical Basis for Barrier Capability Is Adequately Presented*:

- Subcriterion (1): The technical bases for this seepage abstraction are consistent with the technical basis for TSPA-LA. The technical basis for assertions of barrier capability is commensurate with the importance of the barrier's capability and the associated

uncertainties (see description of technical basis for barrier capability in Sections 6.3 and 6.4).

4.3 CODES AND STANDARDS

No specific formally established standards have been identified as applying to this modeling activity.

INTENTIONALLY LEFT BLANK

5. ASSUMPTIONS

The following assumptions pertain to this abstraction model as follows:

- *Assumption 1*

  Capillary diversion depends upon the difference in capillary strength ($1/\alpha$) between the interior of the drift and the rock surrounding the drift. For a collapsed drift filled with rubble rock material, it is assumed that the capillary strength of the rubble rock material is 100 Pa. This assumption is used in Section 6.4.2.4.2.

  Rationale
  The bulk porosity of the rubble rock material in the drift is much greater than the porosity of intact rock, because it includes large voids between chunks of fragmented rock. The chunks of fragmented rock are expected to have sizes on the order of centimeters to decimeters (BSC 2003 [162711], Section 8.1). The voids are similar in size to the chunks of rubble and have zero capillary strength. The resulting capillary strength of the rubble-filled drift is therefore much weaker than that of the intact surrounding rock. Also note that an open space is expected to form between the solid rock at the ceiling of the drift and the collapsed rubble material (because of consolidation of the rubble material). This open space would even result in a zero capillarity at the drift ceiling, maintaining the full diversion potential for percolating water. The value of 100 Pa is therefore chosen as a conservative, non-zero value to represent the effective capillary strength of the rubble-filled drift with an air gap forming at the ceiling. This assumption is considered adequate and requires no further confirmation.

- *Assumption 2*

  Seepage into open drifts depends on the fracture permeability and the effective capillary-strength parameter of the fractured rock in the drift vicinity. These properties, which are influenced by the impact of stress redistribution during drift excavation, have been measured and/or calibrated in field experiments and associated modeling work. It is assumed for seepage into collapsed drifts that the properties of the intact rock above the rubble-filled cave are similar to the properties of the excavation-disturbed zone around non-degraded drifts. This assumption is used in Sections 6.5.1.4 and 6.5.1.5.

  Rationale
  This assumption is a reasonable starting point for the analysis of seepage into rubble-filled collapsed drifts, but requires further confirmation ([164617]). Supporting analyses with the Drift-Scale THM Model are ongoing.

- *Assumption 3*

  Analysis of thermal seepage, as described in Section 6.4.3, was conducted for non-degraded drifts, and the abstraction methodology for thermal seepage in Section 6.5.2 was developed based on these non-degraded drift results. It is assumed that the abstraction methods are also valid for thermal seepage into collapsed drifts. This assumption is used in Section 6.5.2.

Rationale
This assumption is a reasonable starting point for the abstraction of thermal seepage into rubble-filled collapsed drifts, but requires further confirmation ([164618]). Supporting analyses with the TH Seepage Model are ongoing.

In addition to the above assumptions, several assumptions pertain to the upstream analyses that provided input information to the seepage abstraction. These assumptions are explained and justified in the following model reports:

- *Seepage Calibration Model and Seepage Testing Data* (BSC 2003 [162267], Section 5)
- *Seepage Model for PA Including Drift Collapse* (BSC 2003 [163226], Section 5; [163017])
- *Drift-Scale Coupled Processes (DST and TH Seepage) Models* (BSC 2003 [161530], Section 5)
- *Drift-Scale THM Model* (BSC 2003 [162318], Section 5)
- *Drift-Scale Coupled Processes (DST and THC Seepage) Models* (BSC 2003 [162050], Section 5)
- *In Situ Field Testing of Processes* (BSC 2002 [158463], Section 5)

6. MODEL DISCUSSION

6.1 OBJECTIVES AND DEFINITIONS

6.1.1 Objectives

The following sections describe the development of the abstraction model for seepage of water into waste emplacement drifts. The purpose of seepage abstraction is to synthesize and simplify the relevant input for the seepage calculations to be conducted in the TSPA-LA. This input stems from several different sources, such as drift- and site-scale simulation models, as well as from *in situ* testing conducted in the unsaturated zone (UZ) at Yucca Mountain.

Seepage is treated as a stochastic process in the TSPA-LA simulations (e.g., CRWMS M&O 2000 [148384], Section 6.3.1.2). It is recognized that the amount of seepage is sensitive to key hydrological parameters that are both spatially variable and uncertain. One of the main tasks of this seepage abstraction model is therefore to define appropriate probability distributions that represent this spatial variability and uncertainty in a cautiously realistic manner. Using these distributions in the Monte Carlo analysis, the probability of seepage will be calculated in the TSPA-LA simulations under explicit consideration of spatial variability and uncertainty.

The TSPA calculations use seepage look-up tables that provide the seepage rate (and related estimation uncertainty) as a function of key hydrological properties. These look-up tables have been developed from modeling results of the predictive Seepage Model for Performance Assessment (SMPA), as described in BSC (2003 [163226]), and from additional studies conducted for collapsed drifts (a result of thermal stress combined with joint cohesion changes or seismic events). Since this model accounts for seepage at ambient and somewhat idealized conditions, the SMPA results may need to be adjusted for the impact of additional factors. These factors include thermal perturbation in response to the heat emitted from the radioactive waste, transient changes in rock properties as a result of mechanical and chemical processes, and rock bolts providing potential pathways for seepage. Based on scientific analyses from several sources, seepage abstraction considers the relative importance of these factors and develops appropriate and realistic methods for incorporating them into the TSPA-LA simulations.

The abstraction model is an extension of the previous seepage abstraction model developed for Total System Performance Assessment for Site Recommendation (TSPA-SR) (CRWMS M&O 2001 [154291]). Since then, new data analyses and modeling results have become available. As a result, the abstraction model has been substantially revised. Major revisions include the incorporation of new seepage calibration data and new predictive modeling results from the SMPA, improved treatment of seepage during the period of thermally perturbed flow conditions, disposition of mechanical and chemical alterations based on process models, new probability distributions for variability and uncertainty, and a revised concept for flow focusing.

Sections 6.1.2 through 6.1.4 below provide definitions of seepage properties, relevant scales, and uncertainties. In Section 6.2, all seepage-related features, events, and processes (FEPs) are evaluated, and their disposition for TSPA-LA is discussed. Section 6.3 describes basic processes and factors that can be important for seepage. In Section 6.4, several drift-scale process models used in the abstraction are introduced and main results are briefly presented. The seepage

abstraction methodology, developed mainly based on these model results, is explained in detail in Section 6.5. Probability distributions covering spatial variability and uncertainty in relevant parameters for seepage are generated in Section 6.6. A summary of the proposed seepage abstraction methodology is provided in Section 6.7. Finally, using the proposed abstraction methodology and the probability distributions for seepage-relevant parameters, a stochastic Monte Carlo analysis is conducted to illustrate the probability for seepage into the waste emplacement drifts at Yucca Mountain as a function of time (Section 6.8).

The scientific notebooks listed in Table 6-1 provide details supporting the work discussed in this Model Report.

Table 6-1. Scientific Notebook

LBNL Scientific Notebook ID	M&O Scientific Notebook ID	Relevant Pages	Citation
YMP-LBNL-JTB-2	SN-LBNL-SCI-231-V1	1–146	Birkholzer 2003 [164526]
YMP-LBNL-JTB-3	SN-LBNL-SCI-231-V2	1–142	Birkholzer 2003 [164525]
YMP-LBNL-JTB-4	SN-LBNL-SCI-231-V3	1–48	Wang 2003 [163702]

6.1.2 Definition of Seepage Properties

Seepage is defined as flow of liquid water into an underground opening such as a niche or a waste emplacement drift. According to this definition, seepage does not include advective or diffusive vapor flow into the opening or condensation of water vapor on surfaces, which may lead to drop formation and drop detachment. Some of the water entering an underground opening may evaporate or flow along the wall, thus not contributing to seepage in the narrow sense defined here. Note, however, that evaporation, condensation, and film flow along the surface of the opening affect the moisture conditions in the waste emplacement drift and may thus impact repository performance.

Thermal seepage refers to the seepage of water during the time period when water flow processes in the drift vicinity are perturbed from heating of the rock.

Seepage flux is the amount of water seeping into the opening per unit of time per unit area.

Seepage rate is the amount of water seeping into the opening per unit of time. A 5.1 m long drift section (the approximate length of a waste package plus the 0.1 m spacing between waste packages (BSC 2003 [164603] and BSC 2003 [164069])) is used as the reference scale for calculating the seepage rate. Thus, the seepage rate refers to seepage per time and waste package.

Seepage percentage is defined as the ratio of seepage rate divided by percolation rate across the reference area multiplied by 100. The reference area is given by the footprint area of a 5.1 m long drift section.

Seepage threshold is defined here as the critical percolation flux below which no seepage occurs, i.e., all percolating water is diverted around the opening, evaporates, or flows along the drift surface as a thin water film.

Seepage fraction is defined as the fraction of waste packages affected by seepage. This is equivalent to the fraction of 5.1 m long drift sections that exhibit a nonzero seepage percentage.

6.1.3 Definition of Barriers

The surficial soils and topography, the rock layers overlying the repository, the host rock, and the rock layers below the repository are *natural barriers* to flow and transport (BSC 2002 [160819], Section 2.1.1). The work described in this abstraction report analyzes one of the barrier functions associated with the host rock layers, i.e., to reduce the amount of water entering emplacement drifts (seepage). These natural processes are (1) capillary forces holding water in the fractured rock around drifts, and (2) reduction of flow towards drifts as a result of vaporization. While these two processes are not barriers in the terminology of LA, they are referred to in this abstraction report as (1) *capillary barrier* and (2) *vaporization barrier*, respectively.

6.1.4 Definition of Spatial Scales

Seepage abstraction utilizes simulation results from UZ process models that represent different spatial model scales. These relevant model scales for seepage abstraction are defined as follows:

Drift-Scale Model:
Model that focuses on the processes occurring in the vicinity of waste emplacement drifts. A typical model domain includes appropriate rock portions covering a few drift diameters. The discretization in the drift vicinity is relatively fine (much smaller than the drift diameter), while the geometry of the drift is explicitly accounted for in the model discretization.

Site-Scale Model:
Model that represents the entire unsaturated zone at Yucca Mountain extending from the ground surface to the water table, including several stratigraphic units and major faults. Due to the size of the model domain, explicit consideration of individual drifts is not taken into account in site-scale models.

Abstraction needs to consider spatial variability in properties and processes that occur on different spatial scales. The relevant heterogeneity scales for seepage abstraction are defined as follows:

Small-Scale Heterogeneity:
Heterogeneity on a resolution much smaller than the typical drift-scale model domain. An example is the small-scale variability of fracture permeability (resolution of about 1 foot) considered in the seepage process models.

Intermediate-Scale Heterogeneity:
Heterogeneity on a resolution similar to the typical drift-scale model domain. An example is the spatial distribution of the calibrated capillary-strength parameter used in the drift scale seepage models throughout different sections of the repository.

Large-Scale Heterogeneity:
Heterogeneity on a resolution much larger than the typical drift-scale model domain. In seepage abstraction, large-scale variability refers to the variability between the different stratigraphic units at Yucca Mountain, which is explicitly accounted for by considering separate rock property sets for each unit. (Intermediate-scale heterogeneity, on the other hand, is heterogeneity *within* stratigraphic units, on a drift-scale model resolution.)

6.1.5 Definition of Uncertainty and Spatial Variability

Seepage is treated as a probabilistic process in this model abstraction. Probabilistic models need to account for the variability and uncertainty of parameters (BSC 2002 [158794], Section 4.1):

Variability, also referred to as aleatory uncertainty, arises due to natural randomness or heterogeneity. This first type of uncertainty cannot be reduced through further testing and data collection; it can only be better characterized. Thus, this first type of uncertainty is also referred to as irreducible uncertainty. It is typically accounted for using geostatistical approaches, e.g., using appropriate probability distribution functions.

Uncertainty, also referred to as epistemic uncertainty, arises from lack of knowledge about a parameter because the data are limited or there are alternative interpretations of the available data. This second type of uncertainty can be reduced because the state of knowledge can be improved by further testing or data collection. As a consequence, this second type of uncertainty is also referred to as reducible uncertainty.

In this Model Report, the term *variability* is used for aleatory uncertainty, and the term *uncertainty* is used for *epistemic* uncertainty.

Uncertainty may have different sources as follows, depending on the respective method of deriving the parameter in question (e.g., derived from measurements, analyses, or models):

Measurement uncertainty refers to the exactness of the actual measurement method and related data processing.

Spatial variability uncertainty refers to the uncertainty in parameters describing the spatial variability of data, typically arising from the limited number of samples.

Conceptual model uncertainty arises when the most appropriate conceptual model for a system is uncertain.

Estimation uncertainty arises if the resulting parameter is estimated from a random process (e.g., from noisy data or from a Monte Carlo analysis), giving a range of possible results.

6.2 FEATURES, EVENTS, AND PROCESSES

Results of this model abstraction provide the technical basis for treatment of features, events, and processes (FEPs) that are relevant to this Model Report as discussed in the *Total System Performance Assessment—License Application Methods and Approach* (BSC 2002 [160146], Section 3.2.2). Table 6.2-1 provides FEPs taken from the LA FEP List (DTN: MO0301SEPFEPS1.000 [161496]). The LA FEP List is a revision to the previous project FEP list (Freeze et al. 2001 [154365]) used to develop the list of included FEPs in the *Technical Work Plan for: Performance Assessment Unsaturated Zone* (BSC 2002 [160819], Table 2-6). The selected FEPs are those taken from the LA FEP List that are associated with the subject matter of this report, regardless of the anticipated status for exclusion or inclusion in TSPA-LA as represented in BSC (2002 [160819]).

The table provides the proposed FEPs disposition for TSPA-LA seepage evaluation and lists the relevant upstream reports used in the seepage abstraction process. The cross-reference for each FEP to the relevant sections of this report is also given in the table.

The results of this and other model reports are used to fully document the technical basis for the include/exclude status of these FEPs for TSPA-LA. The UZ Department's documentation for the included FEPs listed in Table 6.2-1 is compiled from this and other model reports, and can be found in the model abstraction reports as described in Sections 2.1.2 and 2.4 of the TWP (BSC 2002 [160819]) and the UZ FEP report as described in Section 1.12.10 of the TWP (BSC 2002 [160819]). Excluded FEPs are to be documented in the UZ FEP report as described in Section 1.12.10 of the TWP (BSC 2002 [160819]).

Table 6.2-1. FEPs Addressed in This Model Report

FEP No.	FEP Name	Upstream Reports Used for FEP Disposition	FEP Description (from LA FEP List) ***Summary Disposition for TSPA Seepage Evaluation***
1.1.01.01.0B	Influx through holes drilled in drift wall or crown	BSC (2003 [163226])	Holes may be drilled through the drift walls or crown for a variety of reasons including, but not limited to, rock bolt and ground support, monitoring and testing, or construction-related activities. These openings may promote flow or seepage into the drifts and onto the waste packages. *TSPA Disposition: Excluded* *Detailed simulations were made using the predictive SMPA to study the effect of rock bolts in the drift crown. From these results, the presence of rock bolts is not considered a relevant factor for seepage into drifts (Section 6.4.2.5). The impact of rock bolts is therefore neglected in the seepage abstraction (Section 6.5.1.6).*

Table 6.2-1. FEPs Addressed in This Model Report (Continued)

FEP No.	FEP Name	Upstream Reports Used for FEP Disposition	FEP Description (from LA FEP List) ***Summary Disposition for TSPA Seepage Evaluation***
1.1.02.02.0A	Pre-closure Ventilation	BSC (2003 [161530])	The duration of pre-closure ventilation acts together with waste package spacing (as per design) to control the extent of the boiling front. *TSPA Disposition: Included* *Preclosure ventilation in drifts will remove a considerable amount of the heat output from the waste canisters. The preclosure period is 50 years, during which the major fraction of the thermal load is removed from the drifts. This effect of preclosure ventilation on the thermal load provided to the rock is explicitly simulated with the TH Seepage Model that feeds into seepage abstraction, by using time-dependent boundary conditions for the thermal load (Section 6.4.3.1). These boundary conditions reflect the current emplacement design (waste package spacing, average heat output of waste canisters, etc.), as provided in design drawings 800-IED-EBS0-00201-000-00A (BSC 2003 [164069]) and 800-IED-WIS0-00201-000-00B (BSC 2003 [164603]). Thus, the TH modeling results from the TH Seepage Model (DTN: LB0301DSCPTHSM.002 [163689]) directly account for the impact of preclosure ventilation and waste package spacing on the TH conditions in the near-drift rock. As discussed in Section 6.5.2.1, the abstraction of thermal seepage utilizes these modeling results to develop an appropriate thermal seepage abstraction methodology. Note that preclosure ventilation also causes initial rock drying in the drift vicinity as a result of evaporation effects. The reduced relative humidity in the emplacement drifts leads to evaporation of water at the drift surfaces and the development of a small zone of reduced saturation in the drift vicinity. This early dryout as a result of evaporation is neglected in the TH Seepage Model, because seepage into ventilated drifts is highly unlikely (Section 6.5.2.1).*

Table 6.2-1. FEPs Addressed in This Model Report (Continued)

FEP No.	FEP Name	Upstream Reports Used for FEP Disposition	FEP Description (from LA FEP List) ***Summary Disposition for TSPA Seepage Evaluation***
1.2.02.01.0A	Fractures	BSC (2003 [162267]) BSC (2003 [163226]) BSC (2003 [161530]) BSC (2003 [162050]) BSC (2003 [162318])	Groundwater flow in the Yucca Mountain region and transport of any released radionuclides may take place along fractures. The rate of flow and the extent of transport in fractures are influenced by characteristics such as orientation, aperture, asperity, fracture length, connectivity, and the nature of any linings or infills. *TSPA Disposition: Included* *Flow processes in fractures or other channels are important for seepage abstraction because the amount of seepage is determined by the diversion capacity of the fracture flow in the drift vicinity (Section 6.3.1). These flow processes are influenced by the fracture characteristics, such as orientation, aperture, asperity, length, connectivity, and fillings. All the seepage process models that feed into seepage abstraction explicitly simulate the flow processes in fractures using appropriate continuum properties that represent these characteristics (Section 6.4). For ambient seepage, the relevant continuum properties are the continuum permeability and the effective fracture capillary-strength in the drift vicinity. For seepage abstraction, probability distributions describing spatial variability and uncertainty of these parameters have been developed in Section 6.8.1, based on air-permeability measurements and liquid release tests combined with inverse modeling (Section 6.6 and 6.4.1). Ambient seepage calculations will be conducted within the TSPA-LA by sampling from these probability distributions and interpolating seepage rates from the look-up tables given in DTNs LB0304SMDCREV2.002 [163687] and LB0307SEEPDRCL.002 [164337]. During the thermal period, the ambient seepage rates will be adjusted based on the TH modeling results from TH Seepage Model, which explicitly simulates the thermally perturbed fracture flow conditions. Results are given in DTN LB0301DSCPTHSM.002 [163689]. The abstraction methodology for thermal seepage is developed in Section 6.5.2.1.THM and THC effects on the fracture characteristics are evaluated with process models that explicitly account for fracture flow affected by THM and THC parameter alterations (Sections 6.4.4.1 and 6.4.4.2). It was demonstrated that these potential alterations can be neglected in the TSPA-LA, because the expected changes would lead to less seepage (Section 6.5.1.4).*
1.3.01.00.0A	Climate change, global	BSC (2003 [163045])	Climate change may affect the long-term performance of the repository. This includes the effects of long-term change in global climate (e.g., glacial/interglacial cycles) and shorter-term change in regional and local climate. Climate is typically characterized by temporal variations in precipitation and temperature. *TSPA Disposition: Included* *Potential effects of climate change on the amount of infiltration and percolation at Yucca Mountain are taken into account in the seepage abstraction by considering different climate stages and climate scenarios (see Section 6.6.4). Seepage is calculated in the TSPA-LA using percolation flux distributions based on results from the UZ Flow and Transport Model (Section 6.6.4.1), given in DTNs LB0302PTNTSW9I.001 [162277] and LB0305PTNTSW9I.001 [163690]. These flux distributions include different climate stages and scenarios.*

Table 6.2-1. FEPs Addressed in This Model Report (Continued)

FEP No.	FEP Name	Upstream Reports Used for FEP Disposition	FEP Description (from LA FEP List) ***Summary Disposition for TSPA Seepage Evaluation***
1.4.01.01.0A	Climate modification increases recharge	BSC (2003 [163045])	Climate modification (natural or artificial) causes an increase in re-charge in the Yucca Mountain region. Increased recharge might lead to increased flux through the repository, perched water, or water table rise. *TSPA Disposition: Included* *Potential effects of climate change on the amount of flux through the repository are taken into account in the seepage abstraction by considering different climate stages and climate scenarios (see Section 6.6.4). Seepage is calculated in the TSPA-LA using percolation flux distributions that are based on results from the UZ Flow and Transport Model (Section 6.6.4.1), given in DTNs LB0302PTNTSW9I.001 [162277] and LB0305PTNTSW9I.001 [163690]. These flux distributions include different climate stages and scenarios.*
2.1.08.01.0A	Water influx at the repository	BSC (2003 [163045])	An increase in the unsaturated water flux at the repository affects thermal, hydrological, chemical, and mechanical behavior of the system. Increases in flux could result from climate change, but the cause of the increase is not an essential part of the FEP. *TSPA Disposition: Included* *The potential increase in the magnitude of percolation flux at the repository, as a result of climate changes or flow focusing effects, is accounted for in the seepage abstraction by considering different climate stages, climate scenarios, and introducing flow focusing factors (see Section 6.6.4). Seepage is calculated in the TSPA-LA using percolation flux distributions that are based on results from the UZ Flow and Transport Model (Section 6.6.4.1), given in DTNs LB0302PTNTSW9I.001 [162277] and LB0305PTNTSW9I.001 [163690]. These flux distributions include different climate stages and scenarios. The potential focusing of flow towards individual drift sections is accounted for by a distribution of flow focusing factors, as discussed in Section 6.6.4.2. This distribution is given in DTN LB0104AMRU0185.012 [163906]. The local percolation flux distribution used for the seepage calculations in the TSPA-LA is derived by multiplying the percolation flux values from the site-scale model with the randomly sampled flow focusing factors (Section 6.8.1).*
2.1.08.02.0A	Enhanced influx at the repository	BSC (2003 [162267]) BSC (2003 [163226]) BSC (2003 [161530])	An opening in unsaturated rock alters the hydraulic potential, affecting local saturation around the opening and redirecting flow. Some of the flow is directed to the opening where it is available to seep into the opening. *TSPA Disposition: Included* *The impact of an underground opening on the unsaturated flow field (including capillary barrier effect and flow diversion around the drifts) and its relevance for seepage is explicitly captured in the seepage process models used for the seepage abstraction (see Sections 6.4.1, 6.4.2, and 6.4.3). From these model simulations, seepage predictions are available in form of look-up tables in DTNs LB0304SMDCREV2.002 [163687] and LB0307SEEPDRCL.002 [164337]. These will be used in the TSPA-LA to calculate ambient seepage, by sampling parameter cases of seepage-relevant parameters from the probability distributions that are defined in Section 6.8.1 of this Model Report. These seepage-relevant parameters are the effective capillary-strength parameter, the permeability, and the local percolation flux. The percolation flux distributions include flow focusing effects, as discussed in Section 6.6.4.2. During the thermal period, the ambient seepage rates will be adjusted based on the TH modeling results from DTN LB0301DSCPTHSM.002 [163689], using the abstraction methodology developed in Section 6.5.2.1.*

Table 6.2-1. FEPs Addressed in This Model Report (Continued)

FEP No.	FEP Name	Upstream Reports Used for FEP Disposition	FEP Description (from LA FEP List) ***Summary Disposition for TSPA Seepage Evaluation***
2.1.09.12.0A	Rind (chemically altered zone) forms in the near-field	BSC (2003 [162050])	Thermal-chemical processes involving precipitation, condensation, and re-dissolution alter the properties of the adjacent rock. These alterations may form a rind, or altered zone, in the rock, with hydrological, thermal, and mineralogical properties different from the initial conditions. *TSPA Disposition: Excluded* *The impact of THC processes such as precipitation and dissolution of minerals on fracture surfaces is explicitly simulated with a coupled THC Model (Section 6.4.4.2). The impact of these alterations on seepage may be important, because a "precipitation umbrella" is expected to evolve several meters above drifts, which could divert percolating water. However, these potentially beneficial THC effects on seepage are not accounted for in the seepage abstraction because of the considerable uncertainty related to these predictions (Section 6.5.1.4). As indicated by the THC predictions, neglecting THC parameter alteration leads to an overestimation of seepage.*
2.2.01.01.0A	Mechanical effects of excavation/ construction in the near field	BSC (2001 [158463]) BSC (2003 [162267]) BSC (2003 [162318])	Excavation will produce some disturbance of the rocks surrounding the drifts due to stress relief. Stresses associated directly with excavation (e.g., boring and blasting operations) may also cause some changes in rock properties. Properties that may be affected include rock strength, fracture spacing, block size, and hydrological properties such as permeability. *TSPA Disposition: Included* *Excavation effects are taken into account in the seepage abstraction through the use of post-excavation air-permeability data (Table 6.6-3) and the estimation of a capillary-strength parameter determined from seepage tests (Table 6.6-1). These data reflect the impact of excavation around a large opening (niche or drift). The measured post-excavation air-permeability data are supported by THM modeling results (Section 6.6.2.1). The probability distributions for permeability and capillary strength given in Section 6.8.1 are based on the values given in Tables 6.6-3 and 6.6-1, respectively, and thus account for such excavation effects. These distributions will be used in the TSPA-LA to calculate seepage from the seepage look-up tables, using the methodology defined in Section 6.8.1 of this Model Report.*
2.2.01.02.0A	Thermally-induced stress changes in the near-field	BSC (2003 [162318]) BSC (2003 [163226])	Changes in host rock properties result from thermal effects or other factors related to emplacement of the waste. Properties that may be affected include rock strength, fracture spacing and block size, and hydrologic properties such as permeability and sorption. *TSPA Disposition: Excluded* *The effect of thermal stresses on host rock properties in the drift vicinity is explicitly simulated with a coupled THM Model (Section 6.4.4.1). The impact of these stress-induced alterations on seepage is rather small, however, as described in Section 6.4.4.1. In fact, the seepage rates obtained from the SMPA model that neglects thermal expansion are slightly higher than those with a THM model (Figure 6.4-17). For reasons given in Section 6.5.1.4, effects of THM parameter changes on seepage are therefore neglected in the seepage abstraction, leading to a slight overestimation of the seepage rates.*

Table 6.2-1. FEPs Addressed in This Model Report (Continued)

FEP No.	FEP Name	Upstream Reports Used for FEP Disposition	FEP Description (from LA FEP List) ***Summary Disposition for TSPA Seepage Evaluation***
2.2.03.01.0A	Stratigraphy	BSC (2003 [161530]) BSC (2003 [162050]) BSC (2003 [162318]) BSC (2003 [163045])	Stratigraphic information is necessary information for the performance assessment. This information should include identification of the relevant rock units, soils and alluvium, and their thickness, lateral extents, and relationships to each other. Major discontinuities should be identified. *TSPA Disposition: Included* *Ambient seepage as a result of flow diversion around drifts is a local process that is simulated by drift-scale models such as the SCM and the SMPA (Sections 6.4.1.1 and 6.4.2.1). In these models, the stratigraphy below and above the repository unit can be neglected. In contrast, the UZ Flow and Transport Model (which provides the percolation flux distributions used for seepage calculations) explicitly accounts for the various geological units and major faults in the UZ. This is because the overall distribution of percolation flux at the repository horizon is influenced by stratigraphic layering and by major discontinuities. For example, the PTn- unit overlying the Topopah Spring welded tuff units can divert a fraction of percolating water to intercepting faults and fault zones, thereby changing the spatial distribution of fluxes (Section 6.4.1.1). The drift-scale process models addressing TH, THM, and THC processes (Sections 6.4.3.1, 6.4.4.1, and 6.4.4.2) also represent the stratigraphy in the UZ at Yucca Mountain in an explicit manner. This is needed because the thermal perturbation of the unsaturated rock extends far into the overlying and underlying geological units. Thus, the stratigraphy information is automatically embedded in the respective model results from the UZ Flow and Transport Model and the TH, THM, and THC drift-scale models.*
2.2.03.02.0A	Rock properties of host rock and other units	BSC (2003 [162267]) BSC (2003 [163226]) BSC (2003 [161530]) BSC (2003 [162318]) BSC (2003 [162050]) BSC (2003 [163045])	Physical properties such as porosity and permeability of the relevant rock units, soils, and alluvium are necessary for the performance assessment. Possible heterogeneities in these properties should be considered. Questions concerning events and processes that may cause these physical properties to change over time are considered in other FEPs. *TSPA Disposition: Included* *All the seepage process models that feed into seepage abstraction explicitly represent the physical properties of the unsaturated rock and their heterogeneity (Section 6.4). Small-scale heterogeneity is accounted for by a stochastic continuum representation of fracture permeability. Thus, heterogeneity on this scale is implicitly embedded in the model output from the SCM, the SMPA, and the TH Seepage Model (provided in DTNs LB0304SMDCREV2.002 [163687], LB0307SEEPDRCL.002 [164337], and LB0301DSCPTHSM.002 [163689]). The intermediate-scale spatial variability and uncertainty of seepage-relevant rock properties are accounted for by appropriate probability distributions that were developed in this abstraction (Sections 6.6.1 and 6.6.2). Potential alterations of these properties, as a result of THM or THC processes, have been assessed using drift-scale process models (Sections 6.4.4.1 and 6.4.4.2). It was demonstrated that these potential alterations can be neglected in the TSPA-LA, as the expected changes would lead to less seepage (Section 6.5.1.4). Percolation flux distributions are provided by the UZ Flow and Transport Model (Section 6.6.4.1), which accounts for rock properties and their variation on a larger scale, e.g., stemming from stratigraphy effects.*

Table 6.2-1. FEPs Addressed in This Model Report (Continued)

FEP No.	FEP Name	Upstream Reports Used for FEP Disposition	FEP Description (from LA FEP List) ***Summary Disposition for TSPA Seepage Evaluation***
2.2.07.02.0A	Unsaturated groundwater flow in the geosphere	BSC (2003 [162267]) BSC (2003 [163226]) BSC (2003 [161530]) BSC (2003 [162050]) BSC (2003 [162318]) BSC (2003 [163045])	Groundwater flow occurs in unsaturated rocks in most locations above the water table at Yucca Mountain, including at the location of the repository. See other FEPs for discussions of specific issues related to unsaturated flow. See related FEPs 2.2.07.03.0A (capillary rise), 2.2.07.04.0A (focusing of unsaturated flow), 2.2.07.05.0A (effects of episodic infiltration), 2.2.07.07.0A (perched water), 2.2.07.08.0A (fracture flow), 2.2.07.09.0A (matrix imbibition), 2.2.07.10.0A (condensation zone forms), 2.2.07.11.0A (resaturation of dryout zone), and 2.2.10.10.0A (two-phase flow/heat pipes). *TSPA Disposition: Included* *Unsaturated flow processes are accounted for in the seepage abstraction by using results from process models that explicitly account for various relevant aspects of unsaturated groundwater flow. All the seepage process models that feed into seepage abstraction simulate groundwater flow processes in unsaturated rock (Section 6.4). For ambient seepage, the fracture flow processes in the drift vicinity and the resulting seepage rates are predicted by model simulations from the SMPA (Section 6.4.2). Results are available as look-up tables in DTNs LB0304SMDCREV2.002 [163687] and LB0307SEEPDRCL.002 [164337]. These will be used in the TSPA-LA to calculate ambient seepage, by sampling parameter cases of seepage-relevant parameters from the probability distributions that are defined in Section 6.8.1 of this Model Report. During the thermal period, the ambient seepage rates will be adjusted based on the TH modeling results from TH Seepage Model, which explicitly simulates the thermally-perturbed groundwater flow processes. Results are given in DTN LB0301DSCPTHSM.002 [163689]. The abstraction methodology for thermal seepage is developed in Section 6.5.2.1.THM and THC effects on fracture flow processes are evaluated with process models that explicitly account for groundwater flow processes affected by THM and THC parameter alterations (Sections 6.4.4.1 and 6.4.4.2). It was demonstrated that these potential alterations can be neglected in the TSPA-LA, as the expected changes would lead to less seepage (Section 6.5.1.4). Percolation flux distributions are provided by the UZ Flow and Transport Model (Section 6.6.4.1), which accounts for groundwater flow on a larger scale, influenced by climate changes, infiltration variability and stratigraphy effects. All related FEPs listed above that are important for seepage are included in this FEP table.*

Table 6.2-1. FEPs Addressed in This Model Report (Continued)

FEP No.	FEP Name	Upstream Reports Used for FEP Disposition	FEP Description (from LA FEP List) ***Summary Disposition for TSPA Seepage Evaluation***
2.2.07.04.0A	Focusing of unsaturated flow (fingers, weeps)	BSC (2003 [162267]) BSC (2003 [163226]) BSC (2003 [161530])	Unsaturated flow can differentiate into zones of greater and lower saturation (fingers) that may persist as preferential flow paths. Heterogeneities in rock properties, including fractures and faults, may contribute to focusing. Focused flow may become locally saturated. *TSPA Disposition: Included* *Intermediate-scale focusing of flow from the site scale to the drift scale is accounted for in the seepage abstraction by using appropriate flow focusing factors (Section 6.6.4.2). Small-scale preferential flow is explicitly simulated in the seepage process models that feed into the abstraction, by use of heterogeneous fracture permeability fields (Sections 6.4.1.1, 6.4.2.1, and 6.4.3.1). Thus, preferential flow is automatically embedded in the seepage look-up tables for ambient seepage given in DTNs LB0304SMDCREV2.002 [163687] and LB0307SEEPDRCL.002 [164337], and in the thermal seepage results provided in DTN LB0301DSCPTHSM.002 [163689]. The abstraction methodology for both ambient and thermal seepage is described in Section 6.8.1 of this Model Report. The possibility of episodic finger flow is accounted for with an alternative conceptual model analyzed in the thermal seepage model report. Results from this alternative conceptual model are consistent with results from the TH Seepage Model used for this abstraction (see Section 6.4.3.2).*
2.2.07.05.0A	Flow in the UZ from episodic infiltration	BSC (2003 [163045])	Episodic flow occurs in the UZ as a result of episodic infiltration. See also FEP 2.2.07.02.0A (unsaturated groundwater flow), 2.3.11.03.0A (infiltration), 2.2.07.04.0A (focusing of UZ flow), and 1.3.01.00.0A (climate change). Episodic flow may affect transport; for example, colloidal transport may be enhanced by episodic flow (FEP 2.2.08.10.0A). *TSPA Disposition: Excluded* *The process that drives infiltration in the unsaturated zone is precipitation, which is episodic in nature. Studies of episodic infiltration and percolation have found, however, that matrix-dominated flow in the PTn dampens out the transient nature of the percolation such that unsaturated zone flow below the PTn is essentially steady (CRWMS M&O 1998 [100356], Section 2.4.2.8). Furthermore, the PTn is found over the entire repository block (in Underground Layout Configuration BSC 2003 [164325]). This damping of transient flow is due to capillary forces and high matrix permeability in the PTn that lead to matrix imbibition of water from fractures. Therefore, this FEP is excluded, because the unsaturated zone flow is steady at the repository and along radionuclide transport pathways (BSC 2003 [163045], Section 6.2.6). Very small amounts of fracture flow do appear to penetrate as transients through fault zones between the ground surface and the repository elevation, as evidenced by high ^{36}Cl concentrations in samples taken from the ESF (Fabryka-Martin et al. 1997 [100145]). Higher concentrations of this isotope found in the ESF can only be explained through surface deposition of ^{36}Cl from nuclear weapons testing and subsequent aqueous transport to certain ESF sampling locations over a period of approximately 50 years. However, the flow and transport models indicate that the quantity of water and dissolved constituents that do penetrate the PTn as flow transients is negligible with respect to repository performance (CRWMS M&O 1998 [100356], Section 2.4.2.8), generally less than 1% of the total infiltration (CRWMS M&O 1997 [124052], Section 6.12.4).*

Table 6.2-1. FEPs Addressed in This Model Report (Continued)

FEP No.	FEP Name	Upstream Reports Used for FEP Disposition	FEP Description (from LA FEP List) ***Summary Disposition for TSPA Seepage Evaluation***
2.2.07.08.0A	Fracture flow in the UZ	BSC (2003 [162267]) BSC (2003 [163226]) BSC (2003 [161530]) BSC (2003 [162050]) BSC (2003 [162318]) BSC (2003 [163045])	Fractures or other analogous channels act as conduits for fluids to move into the subsurface to interact with the repository and as conduits for fluids to leave the vicinity of the repository and be conducted to the SZ. Water may flow through only a portion of the fracture network, including flow through a restricted portion of a given fracture plane. *TSPA Disposition: Included* *Flow processes in fractures or other channels are important for seepage abstraction because the amount of seepage is determined by the diversion capacity of the fracture flow in the drift vicinity (Section 6.3.1). All the seepage process models that feed into seepage abstraction simulate flow processes in fractured rock (Section 6.4). Spatial variability in the fracture flow, potentially leading to water flow through only a portion of the fracture network, is accounted for by using a stochastic continuum representation. For ambient seepage, the fracture flow processes in the drift vicinity and the resulting seepage rates are predicted by model simulations from the SMPA (Section 6.4.2). Results are available as look-up tables in DTNs LB0304SMDCREV2.002 [163687] and LB0307SEEPDRCL.002 [164337]. These will be used in the TSPA-LA to calculate ambient seepage, by sampling parameter cases of seepage-relevant parameters from the probability distributions that are defined in Section 6.8.1 of this Model Report. During the thermal period, the ambient seepage rates will be adjusted based on the TH modeling results from the TH Seepage Model, which explicitly simulates thermally perturbed fracture flow conditions. Results are given in DTN LB0301DSCPTHSM.002 [163689]. The abstraction methodology for thermal seepage is developed in Section 6.5.2.1.THM and THC effects on fracture flow processes are evaluated with process models that explicitly account for fracture flow affected by THM and THC parameter alterations (Sections 6.4.4.1 and 6.4.4.2). It was demonstrated that these potential alterations can be neglected in the TSPA-LA, because the expected changes would lead to less seepage (Section 6.5.1.4). Percolation flux distributions are provided by the UZ Flow and Transport Model (Section 6.6.4.1), which accounts for fracture flow on a larger scale (influenced by climate changes), infiltration variability, and stratigraphy effects. Flow focusing effects are included as discussed in Section 6.6.4.2.*
2.2.07.09.0A	Matrix Imbibition in the UZ	BSC (2003 [161530]) BSC (2003 [162050]) BSC (2003 [162318]) BSC (2003 [163045])	Water flowing in fractures or other channels in the UZ is imbibed into the surrounding rock matrix. This may occur during steady flow, episodic flow, or into matrix pores that have been dried out during the thermal period. *TSPA Disposition: Included* *Ambient seepage is mainly governed by flow in the fractures, as discussed in Sections 6.4.1.1 and 6.4.2.1. Thus, in the predictive model for ambient seepage, i.e., the SCM and the SMPA, matrix imbibition is neglected. In contrast, the drift-scale process models addressing TH, THM, and THC processes (Sections 6.4.3.1, 6.4.4.1, and 6.4.4.2) explicitly account for matrix imbibition using appropriate dual-permeability modeling concepts. This is needed because the thermal perturbation of the unsaturated rock results in significant transfer of liquid and gas from the matrix into the fractures and vice versa. The UZ Flow and Transport Model (which provides the percolation flux distributions used for seepage calculations) also accounts for the impact of matrix imbibition in an explicit manner (Section 6.6.4.1). Thus, matrix imbibition effects are automatically embedded in the respective model results used for this abstraction.*

Table 6.2-1. FEPs Addressed in This Model Report (Continued)

FEP No.	FEP Name	Upstream Reports Used for FEP Disposition	FEP Description (from LA FEP List) ***Summary Disposition for TSPA Seepage Evaluation***
2.2.07.10.0A	Condensation zone forms around drifts	BSC (2003 [161530])	Condensation of the two-phase flow generated by repository heat forms in the rock where the temperature drops below the local vaporization temperature. Waste package emplacement geometry and thermal loading will affect the scale at which condensation caps form (over waste packages, over panels, or over the entire repository), and to the extent to which "shedding" will occur as water flows from the region above one drift to the region above another drift or into the rock between drifts. *TSPA Disposition: Included* *The coupled processes of vapor condensation forming a condensation cap above the drifts and occurrence of "shedding" between drifts (Section 6.3.2) are explicitly simulated with the TH Seepage Model that feeds into the seepage abstraction. Using this model, the impact of condensation and shedding on seepage is assessed for various simulation cases (Section 6.4.3.3). Thus the TH modeling results from DTN LB0301DSCPTHSM.002 [163689] automatically include these effects. As discussed in Section 6.5.2.1, the abstraction of thermal seepage utilizes these modeling results to develop an appropriate thermal-seepage abstraction methodology.*
2.2.07.11.0A	Resaturation of geosphere dryout zone	BSC (2003 [161530])	Following the peak thermal period, water in the condensation cap (see FEP 2.2.07.10.0A) may flow downward into the drifts. Influx of cooler water from above, such as might occur from episodic flow, may accelerate return flow from the condensation cap by lowering temperatures below the condensation point. Percolating groundwater will also contribute to resaturation of the dryout zone. Vapor flow, as distinct from liquid flow by capillary processes, may also contribute. *TSPA Disposition: Included* *Resaturation of the dryout zone around drifts, and the potential of return flow from the condensation zone back to the drifts, are explicitly simulated with the TH Seepage Model that feeds into seepage abstraction. Using this model, the impact of resaturation and reflux (on) seepage is assessed for various simulation cases (Section 6.4.3.3). Thus, the TH modeling results from DTN LB0301DSCPTHSM.002 [163689] automatically include these effects. As discussed in Section 6.5.2.1, the abstraction of thermal seepage utilizes these modeling results to develop an appropriate thermal seepage abstraction methodology. The impact of potential episodic flow was addressed with an alternative conceptual model for thermal seepage, as discussed in Section 6.4.3.2. It was shown that results from this alternative conceptual model are consistent with the process model results from the TH Seepage Model used for this abstraction.*

Table 6.2-1. FEPs Addressed in This Model Report (Continued)

FEP No.	FEP Name	Upstream Reports Used for FEP Disposition	FEP Description (from LA FEP List) ***Summary Disposition for TSPA Seepage Evaluation***
2.2.07.18.0A	Film flow into the repository	BSC (2003 [162267])	Water entering waste emplacement drifts may occur by a film-flow process. This differs from the traditional view of flow in a capillary network where the wetting phase exclusively occupies capillaries with apertures smaller than some level defined by the capillary pressure. As a result, a film-flow process could allow water to enter a waste emplacement drift at non-zero capillary pressure. Dripping into the drifts could also occur through collection of the film flow on the local minima of surface roughness features along the crown of the drift. *TSPA Disposition: Included* *The potential impact of film flow is represented in the SCM results that are used for the seepage abstraction; i.e., in the calibrated values of the capillary-strength parameter given in Table 6.6-1 (DTN LB0302SCMREV02.002 [162273]). If water originating from film flow seeps into the opening during a liquid-release test, it is reflected in the corresponding seepage data point used for model calibration, i.e., film flow is automatically accounted for in the estimated seepage-related capillary-strength parameter from the SCM, and thus in the prediction of seepage into waste emplacement drifts (Section 6.4.1.1). Note that in theory, film flow behavior may be influenced by the elevated temperatures in the drift vicinity during the first several thousand years after emplacement. This effect is not included in the ambient liquid-release tests. However, the potential changes in film flow as a result of temperature increase are not expected to be significant for drift seepage.*
2.2.07.20.0A	Flow diversion around repository drifts	BSC (2003 [162267]) BSC (2003 [163226]) BSC (2003 [161530])	Flow in unsaturated rock tends to be diverted by openings such as waste emplacement drifts due to the effects of capillary forces. The resulting diversion of flow could have an effect on seepage into the repository. Flow diversion around the drift openings could also lead to the development of a zone of lower flow rates and low saturation beneath the drift, known as the drift shadow (see FEP 2.2.07.21.0A). *TSPA Disposition: Included* *The impact of flow diversion around the drifts and its relevance for seepage is explicitly captured in the seepage process models used for the seepage abstraction (see Sections 6.4.1, 6.4.2, and 6.4.3). From these model simulations, seepage predictions are available in form of look-up tables in DTNs LB0304SMDCREV2.002 [163687] and LB0307SEEPDRCL.002 [164337]. These will be used in the TSPA-LA to calculate ambient seepage, by sampling parameter cases of seepage-relevant parameters from the probability distributions that are defined in Section 6.8.1 of this Model Report. These seepage-relevant parameters are the effective capillary-strength parameter permeability, and local percolation flux. During the thermal period, the ambient rates will be adjusted based on the TH modeling results from DTN LB0301DSCPTHSM.002 [163689], using the abstraction methodology developed in Section 6.5.2.1. Note that FEP 2.2.07.21.0A, regarding the drift shadow zone, is not discussed in this report.*

Table 6.2-1. FEPs Addressed in This Model Report (Continued)

FEP No.	FEP Name	Upstream Reports Used for FEP Disposition	FEP Description (from LA FEP List) ***Summary Disposition for TSPA Seepage Evaluation***
2.2.10.04.0A	Thermo-mechanical stresses alter characteristics of fractures near repository	BSC (2003 [162318]) BSC (2003 [163226])	Heat from the waste causes thermal expansion of the surrounding rock, generating changes in the stress field that may change the fracture properties (both hydrologic and mechanical) of fractures in the rock. Cooling following the peak thermal period will also change the stress field, further affecting fracture properties near the repository. *TSPA Disposition: Excluded* *The effect of thermal stresses on fracture properties in the drift vicinity is explicitly simulated with a coupled THM Model (Section 6.4.4.1). The impact of these stress-induced alterations on seepage is rather small, however, as described in Section 6.4.4.1. In fact, the seepage rates obtained from the SMPA model that neglects thermal expansion are slightly higher than those with a THM model (Figure 6.4-17). For reasons given in Section 6.5.1.4, effects of THM parameter changes on seepage are therefore neglected in the seepage abstraction, leading to a slight overestimation of the seepage rates.*
2.2.10.10.0A	Two-phase buoyant flow / heat pipes	BSC (2003 [161530])	Heat from waste generates two-phase buoyant flow. The vapor phase (water vapor) escapes from the mountain. A heat pipe consists of a system for transferring energy between a hot and a cold region (source and sink respectively), using the heat of vaporization and movement of the vapor as the transfer mechanism. Two-phase circulation continues until the heat source is too weak to provide the thermal gradients required to drive it. Alteration of the rock adjacent to the drift may include dissolution, which maintains the permeability necessary to support the circulation (as inferred for some geothermal systems). *TSPA Disposition: Included* *The coupled processes causing heat-pipe behavior (Section 6.3.2) are explicitly simulated with the TH Seepage Model that feeds into the seepage abstraction. Using this model, the impact of heat-pipe behavior on seepage is assessed for various simulation cases (Section 6.4.3.3). Thus, the TH modeling results from DTN LB0301DSCPTHSM.002 [163689] automatically include the effect of heat pipes. As discussed in Section 6.5.2.1, the abstraction of thermal-seepage utilizes these modeling results to develop an appropriate thermal seepage abstraction methodology.*
2.2.10.12.0A	Geosphere dry-out due to waste heat	BSC (2003 [161530])	Repository heat evaporates water from the UZ rocks near the drifts as the temperature exceeds the vaporization temperature. This zone of reduced water content (reduced saturation) migrates outward during the heating phase (about the first 1,000 years) and then migrates back to the containers as heat diffuses throughout the mountain and the radioactive sources decay. *TSPA Disposition: Included* *The coupled processes of vaporization, dryout, and resaturation are explicitly simulated with the TH Seepage Model that feeds into the seepage abstraction. Using this model, the impact of such coupled processes on seepage is assessed for various simulation cases (Section 6.4.3.3). Thus, the TH modeling results from DTN LB0301DSCPTHSM.002 [163689] automatically include these effects. As discussed in Section 6.5.2.1, the abstraction of thermal seepage utilizes these modeling results to develop an appropriate thermal-seepage abstraction methodology.*

6.3 SEEPAGE PHENOMENA AND IMPORTANT FACTORS FOR SEEPAGE

To help explain seepage phenomena in unsaturated fractured tuff and to identify the factors affecting seepage, this Model Report describes the basic processes involved. This description is based on and consistent with the related discussion found in the scientific literature (see, for example, Philip et al. (1989 [105743]); Finsterle (2000 [151875]) and references therein for the capillary barrier effect; Pruess et al. (1990 [100819]) and Birkholzer and Tsang (2000 [154608]) for TH processes). The sections below distinguish between seepage at ambient conditions (Section 6.3.1) and seepage at thermal conditions (Section 6.3.2). In the framework of seepage modeling, "ambient" conditions refer to the time period where the flow and seepage processes in the drift vicinity are *not* significantly influenced by thermal effects; i.e., the period that rock temperature is above boiling has ended and the local flow and saturation perturbations have mostly equilibrated. "Thermal" conditions, on the other hand, are defined as conditions where the flow and seepage processes are strongly perturbed in the drift vicinity, because boiling of water either occurs or has just recently occurred (BSC 2003 [161530], Section 6.1). "Thermal" seepage refers to seepage during the time period that thermal conditions prevail. Typically, the time period with "thermal conditions" may cover the first 1,000 to 2,000 years after waste emplacement. Afterwards, rock temperatures are still higher than ambient as a result of the slow heat transfer processes and the slow decay of the radioactive waste, but the local flow conditions are essentially back to ambient; i.e., the fractures and the rock matrix at the drift wall have saturation levels similar to the ambient state. These conditions can be treated as "ambient" in the seepage evaluation (see Section 6.5). Additional factors for seepage (e.g., stemming from drift degradation and ground support), are briefly discussed in Section 6.3.3.

6.3.1 Seepage Under Ambient Conditions

Underground openings in unsaturated rock have a tendency to divert water around them because of the capillary barrier effect at the interface between the rock and the opening, which retains the wetting fluid in the pore space. As a result, a significant fraction of the water that percolates down the Yucca Mountain UZ can be prevented from seeping into the emplacement drifts. The barrier effect leads to a local saturation build-up and the development of a boundary layer in the formation immediately adjacent to the drift. If capillarity and tangential permeability of the fracture network within this boundary layer are sufficiently high, all or a portion of the water is diverted around the drift under partially saturated conditions. Locally, however, the water potential in the formation may be higher than that in the drift, and then water exits the formation and enters the drift. At the drift surface, the water either evaporates, or follows the inclined, rough wall in a thin film, or forms a drop that grows and eventually detaches (Or and Ghezzehei 2000 [144773]). Only this last mechanism is considered drift seepage according to the definition in Section 6.1.2.

For an emplacement drift of given shape, the seepage threshold—and the amount of seepage once this threshold is exceeded—depend on the local flow conditions in the drift vicinity (Figure 6.3-1). These are mainly influenced by the local percolation flux reaching the drift and by the rock properties in the immediate vicinity of the opening. This is because the capillary barrier effect occurs in a relatively small region around the opening, with the thickness of this layer approximately given by the height to which the water rises on account of capillarity. (This height can be estimated by dividing the capillary-strength parameter $1/\alpha$ by water density and

gravitational acceleration.) The key rock properties for seepage are (1) the capillary strength and (2) the tangential conductivity in the boundary layer near the drift wall. Geological formations with strong capillarity and high tangential conductivity exhibit a high seepage threshold (i.e., low seepage), whereas a weak capillary barrier effect (i.e., high seepage) is expected if water retention is small or if the tangential permeability is insufficient to promote flow diversion. Thus, evaluation and description of these local rock properties is essential for seepage calculations. Because the matrix permeability is small, the tangential conductivity is governed by the properties of the fracture network. For flow diversion to occur, the fracture system must have sufficient connectivity and permeability to provide the necessary effective conductivity in the tangential direction around the drift. Small-scale heterogeneity increases the probability of locally breaching the capillary barrier, because it promotes the existence of flow channeling and local ponding (Birkholzer et al. 1999 [105170]).

In addition to the considerable heterogeneity of seepage-relevant properties that needs to be described in appropriate spatial detail, alterations of these properties may occur with time. Initially, the undisturbed rock properties around the openings are likely to be altered as a result of stress redistribution during drift excavation, which typically leads to local opening of fractures and potentially the creation of new microfractures in the drift vicinity (BSC 2001 [158463], Section 6.1.2.2; Wang and Elsworth 1999 [104366], pp. 752–756). These changes affect porosity, permeability, and capillarity of the fracture system in the vicinity of emplacement drifts. Later, the heat emanating from the radioactive material will induce thermal-hydrological-mechanical (THM) and thermal-hydrological-chemical (THC) changes (see Section 6.3.2 below). For example, thermal expansion of the rock matrix induces changes in fracture apertures. Also, thermal effects lead to dissolution and precipitation of minerals, again affecting the porosity, permeability, and capillarity of the fracture system as well as fracture-matrix interaction. The impact of these alterations needs to be assessed in seepage abstraction.

Another key factor for seepage is the percolation flux arriving at the drifts. Seepage is initiated if the local percolation fluxes in individual flow channels and their accumulation near the drift ceiling exceed the diversion capacity of the capillary barrier. The fate of water percolating through the Yucca Mountain UZ and eventually encountering the immediate vicinity of a waste emplacement drift is influenced by various factors. The ultimate source of percolation flux at Yucca Mountain is net infiltration at the ground surface, stemming from precipitation events. Net infiltration is the fraction of precipitation that moves through the ground surface to a depth where the liquid water can no longer be removed by evaporation or transpiration. Net infiltration varies in space (as a result of several factors such as vegetation, morphology, and soil and bedrock conditions) and in time. Time variations are short-term as a result of daily or seasonal fluctuations and long-term as a result of climate changes. As infiltrating water percolates through the UZ, driven by gravity and capillary forces, the initial infiltration and flow patterns will change depending on the hydrogeologic properties in the UZ and their related heterogeneities. On a large scale, several stratigraphic units of volcanic rock can be distinguished at Yucca Mountain, with significant differences in fracture frequency, matrix porosity, and lithophysal characteristics. Variations between units reflect the type of volcanic eruption, the rate of cooling, and the intensity of postdepositional processes. Tilted contacts between hydrogeologic units (especially between welded and nonwelded tuffs) can divert flow laterally. Welded units typically have lower matrix porosities and high fracture densities, whereas the nonwelded and bedded tuffs have relatively high matrix porosities and lower fracture densities (Bodvarsson et al.

1999 [120055], Section 2). These nonwelded units can dampen short-term infiltration patterns, homogenizing the unsaturated flow below them.

The repository would be located about 300 m below the surface in the Topopah Spring welded unit (TSw). Unsaturated flow in the TSw is primarily in the fractures, because the small matrix permeability in many of the TSw subunits can support flows of only a few millimeters per year. Several subunits are defined in the TSw based on the different degrees of lithophysal content. According to BSC (2003 [163938], Attachment VIII), where the current repository design was analyzed, the Topopah Spring Tuff lower lithophysal unit (Tptpll) is by far the most important unit with respect to the part of the repository located in geological units (about 81%), followed by the Topopah Spring middle nonlithophysal unit (Tptpmn) (about 12%). Less important are two additional geological units, the Topopah Spring Tuff upper lithophysal unit (Tptpul) and Topopah Spring Tuff lower nonlithophysal unit (Tptpln).

On an intermediate scale, there is also considerable heterogeneity *within* stratigraphic units. This kind of heterogeneity can focus water towards one drift location while diverting it away from another. Flow focusing and diversion of flow paths also happens *within* a rough-walled fracture, where asperity contacts and locally larger fracture openings lead to small-scale redistribution of water within the fracture. In addition, asperity-induced flow instabilities may cause small-scale episodic flow within fractures, leading to high-frequency fluctuations. All the above factors determining the spatial and temporal variation of local percolation flux need to be considered in seepage calculations.

The overall drift size and geometry may also impact the seepage threshold and the seepage amount in the unsaturated fractured rock. As demonstrated by Philip et al. (1989 [105743]) for homogeneous media, a large drift exhibits a significantly lower seepage threshold because more water accumulates in the boundary layer as it migrates over a longer diversion distance around the wide opening. Also shown was that the effectiveness of a capillary barrier is highest if the shape of the cavity follows an equipotential surface. Parabolic cavities are more efficient in preventing seepage than circular or flat-roofed openings. Small-scale surface roughness on the drift wall tends to increase seepage because it may encourage drop detachment.

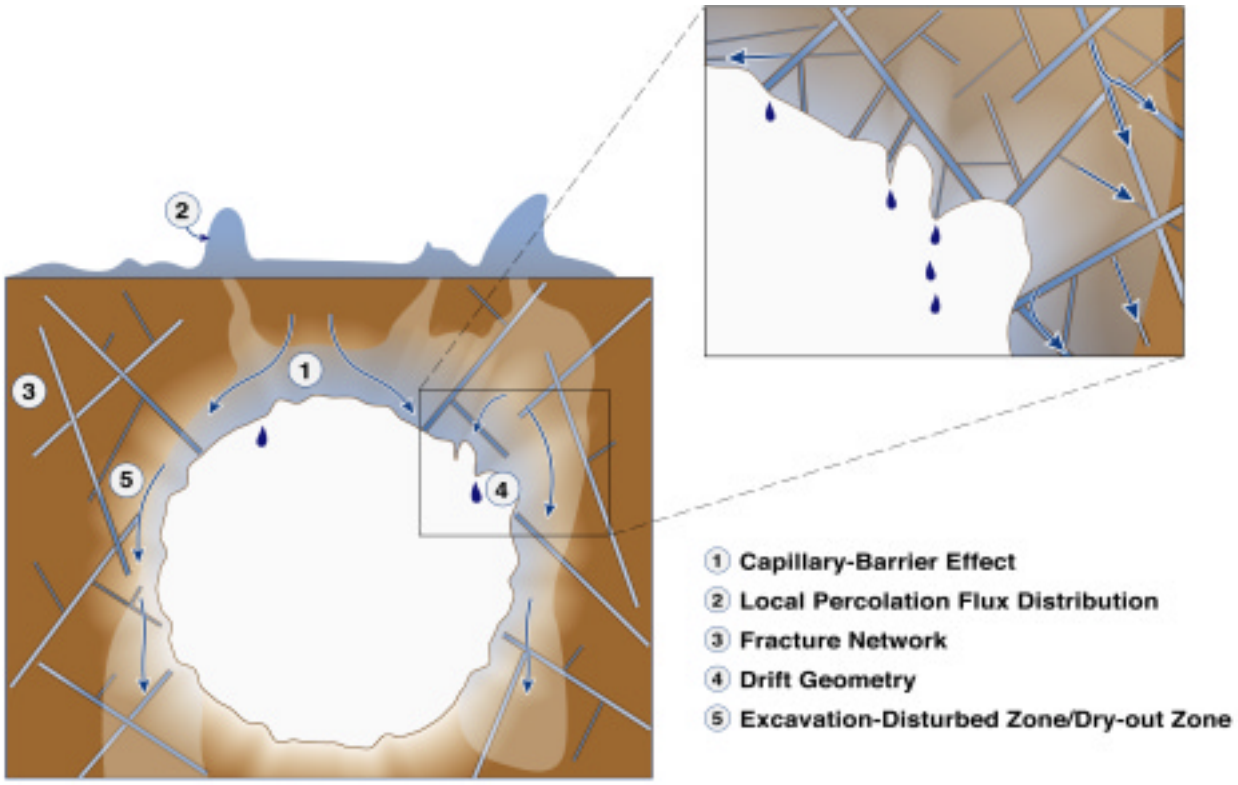

Source: Revised from CRWMS M&O (2000 [151940], Figure 3.9-1)

Figure 6.3-1. Schematic of Phenomena and Processes Affecting Drift Seepage

It is possible that the initially circular-shaped open emplacement drifts degrade with time as a result of thermal stress, seismic ground motion, and time-dependent degradation of rock strength. Thermal stresses are caused by the heat generated from the decaying nuclear waste. Significant stresses can also be caused by seismically related ground motion. Time-dependent degradation of rock strength (joint mechanical properties) may be a result of over-stressing from thermal heating and of static fatigue of the rock resulting from stress corrosion mechanisms. All these effects may lead to rock mass damage and rock fall in emplacement drifts, changing the drift shape and size. Depending on the type of rock, the stress conditions, and the time-dependent rock mechanical properties, damage to the drifts may be rather small, with local rock fall at the ceiling of otherwise intact drift openings, or, in extreme cases, may result in partial or complete drift collapse, with rubble rock material filling the enlarged drifts. These changes affect the potential for drift seepage. Local breakouts in the drift ceiling may lead to geometry changes (e.g., topographic lows) which can reduce or prevent flow diversion around the opening. The larger size and potentially different shape of collapsed drifts can also reduce the potential for flow diversion; furthermore, the larger footprint of the collapsed drift leads to an increase in the total amount of percolation flux arriving at the drifts, which in turn can affect the total amount of seepage. In addition, the capillary-barrier behavior at the drift wall may be affected by the rubble rock particles filling the opening, as the capillary strength inside the opening will be different from the zero capillarity condition in the initially open drift. Finally, drift degradation may lead to fracture dilation or the generation of new fractures in the vicinity of emplacement drifts. Fracture dilation would increase the permeability, thereby promoting flow diversion around the

drift, but at the same time decrease the fracture capillary strength, which could lead to less flow diversion around the drift. The generation of new fractures in the drift vicinity—with apertures comparable to the existing fractures—would promote flow diversion around the drift opening because of the related increase in fracture permeability, but would not affect the fracture capillary strength.

Another factor potentially affecting seepage is the ground support in the emplacement drifts. In previous repository designs, the main method of ground support for emplacement drifts at Yucca Mountain was grouted rock bolts (BSC 2001 [155187]). Rock bolts are steel rods emplaced into a borehole normal to the drift wall (BSC 2001 [155187], Section 6.5.1.2.2). While the new LA design is not finalized, it is expected that the updated drift ground support system will use about 3 m long rock bolts without grout (BSC 2003 [164101]). Both main repository units, the Tptpll and Tptpmn, will need ground support. There may be up to 10 such bolts in a drift cross section, at a spacing of about 1 m along the drifts. Rock bolts pose a concern with respect to seepage because they may provide a direct flow conduit to the drift wall and may increase the likelihood of seepage into drifts.

6.3.2 Thermal Seepage

The heat generated by the decay of the radioactive waste results in rock temperatures elevated from ambient for thousands of years after emplacement. For the current repository design, these temperatures will be high enough to cause boiling conditions in the drift vicinity, giving rise to local water redistribution and altered flow paths. Key TH processes occurring around a drift are shown schematically in Figure 6.3-2, for an idealized circular-shaped drift. The figure indicates that heating of the rock causes pore water in the rock matrix to boil and vaporize. The vapor moves away from the drift through the permeable fracture network, driven primarily by a pressure increase caused by boiling. In cooler regions away from the drift, the vapor condenses in the fractures, where it can drain either toward the heat source from above or shed around the drift into the zone below the heat source. Condensed water can also imbibe from fractures into the matrix, leading to increased liquid saturation in the rock matrix. With continuous heating, a superheated dryout zone may develop closest to the heat source, separated from the condensation zone by a nearly isothermal zone maintained at about the boiling temperature. This nearly isothermal zone is characterized by a continuous process of boiling, vapor transport, condensation, and migration of water back towards the heat source (either by capillary forces or gravity drainage), and is often referred to as a heat pipe (Pruess et al. 1990 [100819]).

For the current repository design at Yucca Mountain, the dryout zone around drifts will extend to a maximum distance of approximately 5 to 10 meters from the drift wall (BSC 2003 [161530], Section 6.2). Boiling conditions in the rock are expected to exist for about 1,000 years after emplacement. While these values reflect average conditions, there may be significant heterogeneity of the TH conditions within the repository. One factor causing heterogeneity is the spatial and temporal variability of the thermal load in different drift sections, stemming from heat output variation between individual waste packages and emplacement-time differences. Another factor is the variability of the formation properties and the local percolation fluxes. Thermal rock properties such as thermal conductivity directly affect the conductive transport of heat. Hydrological properties and local percolation fluxes, on the other hand, affect the significance of TH coupling as they determine the effectiveness of convective heat transport.

While heat conduction is the major component of energy transport in Yucca Mountain tuff, the impact of TH coupling can be quite large. For example, a large percolation flux above a drift segment, combined with relatively high permeability, may cause strong heat-pipe effects that give rise to rock temperatures much lower and boiling periods much shorter than at average conditions (BSC 2003 [161530], Section 6.2.1.4).

Heating of the rock in the drift vicinity can affect seepage in two different ways:

(1) Boiling of rock water will directly affect the seepage-relevant flow processes close to the drift wall. For above-boiling conditions, vaporization of percolating water in the fractured rock overlying the repository provides an additional barrier to seepage. Percolating water is expected to boil off in the superheated rock zone before reaching the drift crown. Therefore, thermal seepage is unlikely as long as boiling conditions exist. On the other hand, condensed water forms a zone of elevated water saturation above the rock dryout zone. Water from this zone may be mobilized to flow rapidly down towards the drift, in particular during later heating stages when the effect of vaporization has already diminished. This flow mobilization may promote seepage.

(2) Rock properties relevant for seepage may be affected by reversible and irreversible THM and THC effects. Stress-induced THM changes tend to close existing fractures, leading to a general decrease in fracture permeability and porosity, combined with an increase in fracture capillary strength. Aperture changes that occur during the thermal period could be fully reversible, meaning that these properties would recover to pre-emplacement conditions after the temperature has declined to ambient. Thermal stresses could also induce permeability enhancement through fracture shear slip with accompanying shear dilation opening. Such permeability changes would be irreversible and remain after the temperature has declined to ambient. THC processes such as mineral precipitation and dissolution in fractures and matrix also have the potential for modifying permeability, porosity, and capillary strength of the system. Because the molar volumes of minerals created by hydrolysis reactions (i.e., anhydrous phases, such as feldspars, reacting with aqueous fluids to form hydrous minerals, such as zeolites or clays) are commonly larger than the molar volumes of the primary reactant minerals, dissolution-precipitation reactions commonly lead to porosity (and permeability) reductions. The extent of mineral-water reaction is controlled by the surface areas of the mineral phases in contact with the aqueous fluid, as well as heterogeneity in the initial distribution of minerals in the fractures. Therefore, changes in porosity and permeability caused by these processes may also be heterogeneously distributed. Typically, THC effects on hydrological properties are irreversible.

Note that during the first 50 years after emplacement, the repository drifts will be ventilated to allow access. Ventilation in the drifts will cause initial rock drying in the drift vicinity and will also remove a significant amount of heat during this preclosure period.

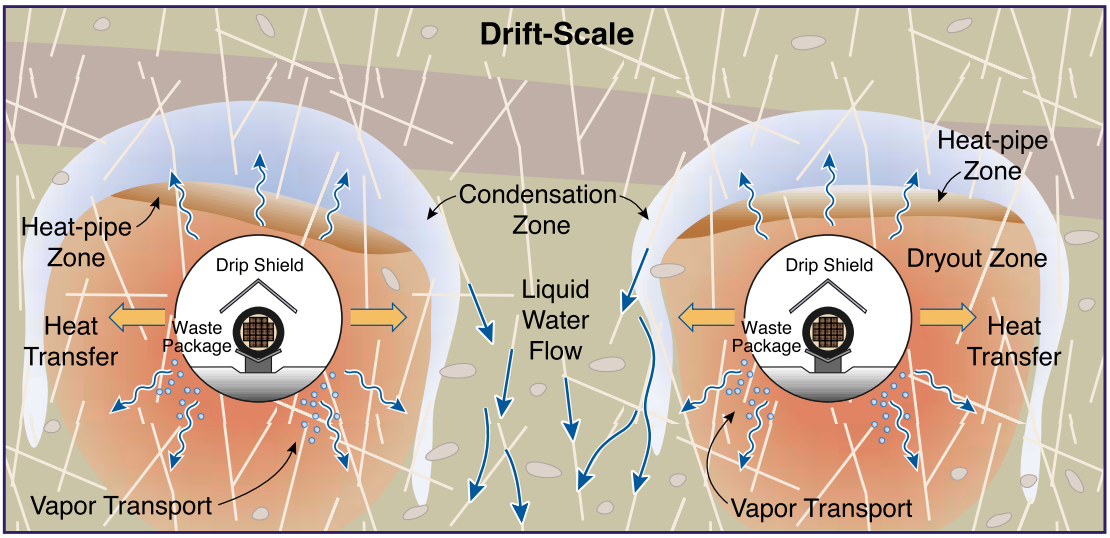

Source: Revised from BSC (2003 [161530], Figure 6.1-1)

Figure 6.3-2. Schematic of TH Processes Occurring in the Drift Vicinity as a Result of Repository Heating

As mentioned in Section 6.3.1, emplacement drifts may collapse in extreme cases as a result of thermal and seismic stresses and degradation of joint mechanical properties. The thermal conditions in a collapsed drift will be different from those in an open drift, mainly because the thermal-hydrological processes in a drift filled with rubbly rock fragments are different from those in an open, gas-filled drift. The extent to which these differences can be important for thermal seepage is governed by the time at which the drift collapse occurs. Significant differences should only be expected when drift collapse occurs during the time period of strongly elevated temperatures.

6.4 PROCESS MODELS PROVIDING INPUT TO SEEPAGE ABSTRACTION

Seepage abstraction uses modeling results from several upstream drift-scale process models. These process models can be categorized into (1) models that directly calculate seepage rates for a given set of seepage-relevant properties and boundary conditions, and (2) supporting models that provide information about the potential alteration of relevant properties as a result of THM and THC processes. These upstream models are introduced in the following Sections 6.4.1 through 6.4.3 (seepage process models) and 6.4.4 (supporting models), and relevant model results are provided. Note that, if not otherwise mentioned, the modeling studies below have been conducted assuming open drifts that have not been affected by drift degradation or collapse (non-degraded drifts).

6.4.1 Seepage Calibration Model

The Seepage Calibration Model (SCM) provides the conceptual basis for modeling of ambient seepage processes (BSC 2003 [162267], Section 6.3). It also provides estimates of the seepage-relevant capillary-strength parameter through calibration of the model against seepage data obtained from *in situ* liquid-release tests.

6.4.1.1 Model Description

The key element of the approach chosen to simulate seepage and determine seepage-relevant parameters is to treat seepage as a stochastic process while relying on inverse modeling for the estimation of relevant parameters. Given the complexity of the seepage process in a fractured porous medium, it was recognized that (1) a detailed deterministic simulation of individual seeps is not necessary to estimate average seepage rates into waste emplacement drifts, (2) the impact of certain second-order factors affecting seepage can be lumped into an effective parameter, making explicit consideration of such factors in the model unnecessary, and (3) calibrating and validating the model against data from seepage experiments ensures that the model captures the relevant processes for ambient seepage (BSC 2003 [162267], Section 6.3.4). Based on these considerations, the SCM was developed as a three-dimensional (3-D) drift-scale calibration model that describes the small-scale heterogeneity of the fractured rock using a stochastic continuum representation.

As explained in BSC (2003 [162267], Section 6), the SCM model domain includes appropriate rock portions above and sideways of niches in the Exploratory Studies Facility (ESF) and the ECRB (a few meters of rock from the niche walls) where liquid-release tests have been conducted (see Figure 6.4-1). Different meshes have been generated representing the different niches and their respective shapes and test geometries in the Tptpmn and the Tptpll. The small-scale fracture permeability variation in each test location was described using spatially correlated stochastic fields based on analysis of air-permeability data measured at that location. These measurements were taken in close proximity to the drifts *after* drift excavation; thus the generated stochastic fields represent the impact of stress redistribution on permeability. The resolution of the stochastic fields is 0.1 m uniform in each direction, slightly smaller than the measurement resolution of the air-injection tests (1-foot intervals). Multiple realizations of the permeability fields were generated and used for the modeling analysis.

No attempt was made in the SCM to describe the excavation-induced alterations of rock properties in spatial detail. In general, the impact of excavation is largest immediately at the opening, and decreases with increasing distance into the rock. However, the extent of the zone affected by alterations (e.g., approximately one drift diameter) is larger than the rock portion affected by the liquid release above the niches, which approximately corresponds to the extent of the model domain. This zone is also much larger than the rather small boundary layer at the drift wall that is important for seepage-related flow processes. It is therefore appropriate for seepage models to represent the impact of excavation within the model domain with averaged excavation-disturbed properties. Thus, the stochastic permeability fields used in the SCM have a uniform mean permeability, independent of the distance to the opening; similarly, the calibrated capillary-strength parameter is uniform in the model domain.

Applying the imposed liquid-release rates of each test, inverse modeling runs were conducted with the SCM to calibrate the effective capillary-strength parameter of the fractured rock in the niche vicinity. Seepage data from multiple test events in one borehole, using different liquid-release rates, were calibrated simultaneously in the inverse modeling approach. Only long-term seepage experiments were considered, where near-steady seepage rates are no longer affected by storage effects. Therefore, because seepage processes are mainly determined by the properties of the fracture system, the SCM is a single continuum model that does not explicitly account for imbibition and flow in the rock matrix. Note that evaporation effects, stemming from forced ventilation in the Enhanced Characterization of Repository Block (ECRB) cross drift, were explicitly accounted for in the model (BSC 2003 [162267], Section 6.6.1.3).

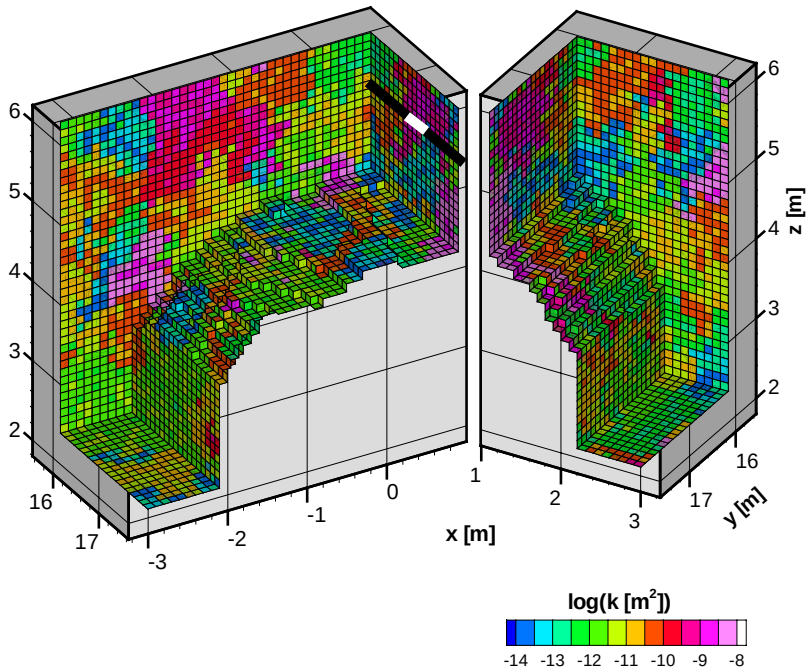

Source: BSC (2003 [162267], Figure 15a)

NOTE: In this visualization, the mesh is split into two parts to expose the boreholes (indicated by thick black lines) and the injection interval (thick white line).

Figure 6.4-1. Example of Numerical Grid and Permeability Distribution used for the SCM Simulation of Liquid-Release Tests Conducted in Niche 1620, Showing Injection into Borehole #4

The calibrated capillary-strength parameter $1/\alpha$ provided by the SCM is an effective process parameter for seepage that is specifically determined for its intended use in drift seepage models. This effective parameter not only represents the average capillary characteristics of the fracture network, but also accounts for seepage factors that are not explicitly implemented in the conceptual model (BSC 2003 [162267], Section 6.3.3). Such processes include effects from (1) small-scale roughness within individual fractures, potentially leading to preferential flow and/or high-episodicity flow, (2) individual fractures cutting into the opening, (3) small-scale surface roughness at the drift ceiling, (4) film flow within fractures and along the drift surface, (5) drop formation and detachment, and (6) fracture-aperture changes as a result of excavation effects. For the Tptpll unit, the effect of lithophysal cavities is also captured in the effective capillary-strength parameter, making the explicit representation of lithophysal cavities into the process model unnecessary. While modeling these factors is theoretically possible, the necessary characterization data needed to warrant such a detailed simulation are not available. As discussed in BSC (2003 [162267], Section 6.3.2), the calibrated capillary-strength parameter is not correlated to the local permeability.

6.4.1.2 Model Validation

The SCM model was validated in comparison with measured data from liquid release tests (BSC 2003 [162267], Section 7). Observed and predicted seepage data were compared for various tests that had not been used for the calibration of the model. It was demonstrated that the calibrated model was capable of reproducing the measured seepage data. As summarized in BSC (2003 [162267], Section 7.4), the seepage observations (1) fell within the range of pre-test predictions of seepage rates in all test cases for the lower lithophysal zone, and in almost all test cases for the middle nonlithophysal zone, or (2) were lower than the predicted seepage rates in a few cases, i.e., the model prediction was conservative. In addition, alternative conceptual models for seepage prediction at Yucca Mountain were qualitatively evaluated. The most important alternative conceptual model is a model that simulates flow through discrete fractures rather than through a stochastic continuum. This alternative, referred to as the discrete fracture network model (DFNM), is discussed in great detail in Finsterle (2000 [151875]), and in lesser detail in BSC (2003 [162267], Section 6.4) and BSC (2003 [161530], Section 6.3.5). It has been concluded that the full development of a DFNM as a potential alternative to the stochastic continuum model is not feasible and not necessary, for the following reasons:

(1) A continuum representation of unsaturated fracture flow is appropriate when the fracture density is high and a well-connected fracture network forms at the scale of interest. As evidenced in fracture mapping data from the ESF and the ECRB, the repository units at Yucca Mountain have a high fracture density, and these fractures form a well-connected 3-D system at the relevant scale (BSC 2003 [163226], Section 6.3).

(2) The development of a defensible DFNM requires collecting a very large amount of geometric and hydrological data. The databases required to develop a defensible DFNM are currently not available and are generally difficult or even impossible to obtain for site-specific simulations. As a result, the cumulative effect of all the input uncertainties is likely to outweigh the apparent advantage of a detailed representation of

the fracture network. To reduce prediction uncertainties, the DFNM must be calibrated against hydrogeologic data—an approach very similar to that used in the SCM.

(3) Seepage calculations with a calibrated DFNM are likely to corroborate the results of a calibrated stochastic continuum model. For example, Finsterle (2000 [151875]) used synthetically generated data from a model that exhibits discrete flow and seepage behavior to calibrate a simplified fracture continuum model. The calibrated continuum model was used to predict seepage rates. The extrapolated seepage predictions performed with the continuum model were consistent with the synthetically generated data from the discrete-feature model.

Three other possible alternative approaches for seepage estimation are discussed in BSC (2003 [162267], Section 6.4): estimating seepage from the local ponding probability (Birkholzer et al. 1999 [105170]), estimating seepage from deposition rates of calcite and opal in lithophysal cavities, and estimating the seepage threshold directly from the liquid-release tests. These approaches are not carried further for the reasons presented in BSC (2003 [162267], Section 6.4). Nevertheless, they corroborate the general concept and the findings of the SCM.

Natural analogues as those reported in TDR-NBS-GS-000027 REV 00 ICN 02, *Natural Analogue Synthesis Report* (BSC 2002 [160405], Section 8) provide additional evidence that the concept of seepage exclusion describes a process that actually occurs in caves, lava tubes, rock shelters, and buildings. Quantitative seepage measurements from limestone caves in a fractured karst terrain have demonstrated that seepage is considerably smaller than the pertinent percolation flux, corroborating the seepage testing and modeling results at Yucca Mountain (BSC 2003 [162267], Section 7.2.1). Precipitation at these cave locations exceeds current rates at Yucca Mountain and those predicted for future climates as well. In addition, various other natural analogue sites provide qualitative evidence that most of the infiltrating water is diverted around underground openings and does not become seepage.

It was concluded that the SCM provides a solid conceptual basis and sufficient characterization data for predicting seepage into waste emplacement drifts in the repository host rock (BSC 2003 [162267], Section 8). Specific recommendations were provided concerning the use of the conceptual model in predictive seepage models such as the SMPA and the TH Seepage Model. These recommendations are as follows (BSC 2003 [162267], Section 8.4):

(1) Seepage predictions should be conducted with a process model similar to the SCM, capable of simulating unsaturated flow under viscous, capillary pressure, and gravitational forces.

(2) A stochastic continuum model should be employed that captures the small-scale heterogeneity of permeability on a spatial resolution similar to the SCM.

(3) The permeability values should capture the impact of excavation effects in the vicinity of the emplacement drifts.

(4) The calibrated capillary-strength parameters derived from the SCM should be used for the fractured tuff in the vicinity of emplacement drifts.

(5) Several second-order factors are lumped into the effective capillary-strength parameter. These factors should not be explicitly considered in the model. (For example, small-scale roughness of the drift wall or lithophysal cavities should not be explicitly discretized.)

(6) A specific boundary condition should be employed at the rock-drift interface, similar to the one chosen in the SCM.

(7) Multiple prediction runs with different realizations of the underlying heterogeneous permeability field should be performed.

6.4.1.3 Model Results

The calibrated values of the effective capillary-strength parameter provided by the SCM are directly used in seepage abstraction. A total of 22 liquid release tests conducted in ten test intervals at different locations along the ESF and the ECRB were used in the SCM model calibration (13 tests conducted in the Tptpll and 9 in the Tptpmn). The resulting capillary-strength parameter values and their associated estimation uncertainty, provided in DTN: LB0302SCMREV02.002 [162273], are presented and discussed in Section 6.6.4 of BSC (2003 [162267]). Parameter values range roughly between 400 and 800 Pa.

Appropriate probability distributions developed in Section 6.6 of this Model Report cover the potential spatial variability and uncertainty of the capillary-strength parameter. A detailed discussion of the calibrated parameter values and the derived parameter distributions is presented in Section 6.6.1.

6.4.2 Seepage Model for Performance Assessment

The Seepage Model for Performance Assessment (SMPA) adopts the conceptual framework from the SCM to conduct systematic predictions of ambient seepage fluxes into waste emplacement drifts (BSC 2003 [163226]). Isothermal flow simulations are performed for selected key parameters that vary over wide ranges. Results are provided in the form of a look-up table (DTN: LB0304SMDCREV2.002 [163687]), giving seepage rates and related seepage estimation uncertainty as a function of these key parameters. Note that appropriate distributions describing the spatial variability and uncertainty of these key parameters are developed in Section 6.6 of this model report. The simulation cases studied with the SMPA sufficiently cover the parameter range defined by these distributions.

6.4.2.1 Model Description

Consistent with the SCM, the predictive SMPA is a 3-D drift-scale model applying a stochastic continuum representation of the small-scale heterogeneity of fractured rock in the drift vicinity. The modeling framework and the processes studied are identical to the SCM; the recommendations for predictive seepage modeling as listed in Section 6.4.1.2 are strictly followed in the SMPA. The major difference between the two models is their scope. The SCM is applied to simulate field test data for calibration and validation purposes, while the SMPA is employed to conduct predictive simulations.

The 3-D model domain of the SMPA is shown in Figure 6.4-2, representing the fractured rock adjacent to the upper left half of a circular-shaped, 8 ft long drift segment with diameter 5.5 m (BSC 2003 [164069]). (Potential changes in the drift shape as a result of drift degradation are considered with adjusted SMPA grids, as discussed in Section 6.4.2.4.) Based on symmetry considerations, the numerical mesh was reduced to a half-drift model, increasing the computational efficiency of the simulation. (More than 50,000 simulation runs had to be conducted to fully cover the required parameter space for TSPA.) The size of the model domain and the discretization were selected according to the following criteria: (1) the model domain above the drift should be large enough to allow for flow channeling independent of boundary effects, (2) the lateral boundary should cover the region where lateral flow diversion is important, (3) the mesh resolution should be similar to the SCM, and (4) the simulation runs must be computationally efficient. Satisfying these criteria, the upper boundary of the model domain was chosen to be at 10 m above the drift axis. The lateral boundary is at 4 m from the drift axis. Grid resolution is identical to the SCM in the plane normal to the drift axis, where flow diversion is most important (i.e., 0.1 m). Along the drift axis, grid cells are slightly larger at 1-foot length (consistent with the SCM grid design of the ECRB). While the side boundaries have no-flow conditions assigned to them, a constant flux boundary is imposed at the top of the domain. This flux boundary represents the local percolation flux arriving at the considered drift segment.

The key parameters affecting ambient seepage are the effective capillary-strength parameter $1/\alpha$, the statistical parameters defining the small-scale stochastic permeability field, and the local percolation flux $q_{perc,ff}$ imposed at the upper model boundary. Only these relevant parameters are varied in the predictive SMPA simulation runs, while other model parameters are kept constant, with their values similar to the parameter choices made in the SCM (BSC 2003 [163226], Section 6.3). Note that the SCM modeling framework calls for the use of an effective capillary-strength parameter not correlated to the local permeability. Thus, this parameter is taken to be uniform within the model domain.

Similar to the SCM, no attempt was made in the SMPA to describe the excavation-induced alterations of rock properties in spatial detail, despite the fact that the extent of the zone affected by alterations (e.g., approximately one drift diameter) is smaller than the vertical extent of the model area above the drift. Thus, in theory, hydrogeological parameters representing the excavation-disturbed zone should be used within the first diameter from the drift, while undisturbed rock properties should be applied outside of this region. For simplification, however, the SMPA assumes a uniform mean permeability in the entire model domain, representative of the excavation-disturbed zone, and also applies a uniform capillary-strength parameter as calibrated from the SCM. This is because it is most important for seepage simulations to appropriately represent the conditions in the close vicinity of the drifts. Changes in the hydrogeological properties further away from the drifts do not significantly affect the seepage results. In fact, the seepage rates would most likely be reduced if the undisturbed rock properties were explicitly accounted for outside of the 1-diameter region around drifts. For example, the capillary-strength parameters representative of the undisturbed fractured continuum in the Tptpmn and the Tptpll, determined in BSC (2003 [160240], Table 11), are much larger than the effective capillary-strength parameters calibrated with the SCM (by a factor of 10 or more). (Note that tsw34 in BSC (2003 [160240], Table 11) corresponds to the Tptpmn unit when using the nomenclature of the Geological Framework Model (BSC 2002 [159124]). Similarly, the

tsw35 corresponds to the Tptpll unit.) Thus, as a result of capillarity effects in the transition zone between undisturbed rock and the excavation-disturbed zone, the percolation flux would partially be diverted before reaching the vicinity of the drifts (BSC 2003 [161530], Section 6.2.2.1.4).

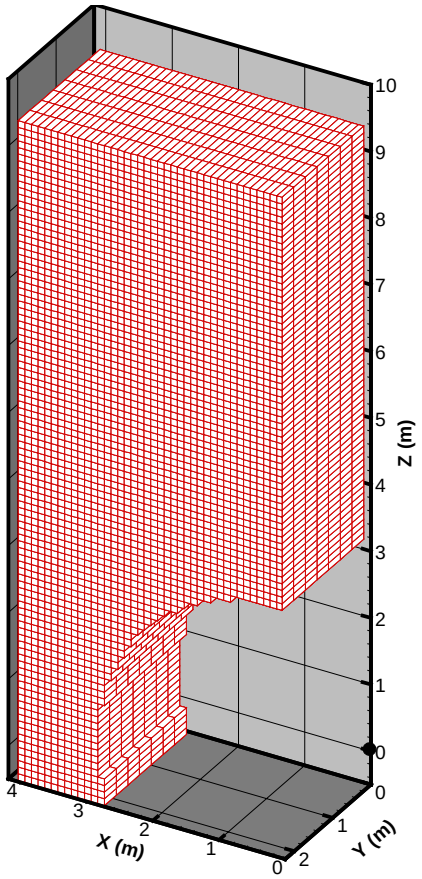

Source: BSC (2003 [163226], Figure 6-1)

NOTE: The plot shows the center nodes of grid blocks and the grid block connections. The point shown at (z = 0 and x = 0) indicates the drift axis.

Figure 6.4-2. Model Domain and Mesh Design of the SMPA

The parameters defining the stochastic permeability fields are the mean permeability μ_S, for simplification hereafter referred to as k (in log10), the standard deviation σ_S (in log10) and the correlation length λ_S. While the mean permeability varies over a wide range in the SMPA simulation runs, corresponding to the significant variability of this parameter over the repository area, the standard deviation and the correlation length of the small-scale permeability fields are kept at constant values of σ_S = 1.0 and λ_S = 1 foot, respectively. These parameter choices are based on post-excavation air-permeability data measured using 1-foot-injection intervals that are appropriate to derive small-scale variability. Standard deviations derived from these data range from 0.72 to 1.31, while the correlation structure is described as essentially random (BSC 2003 [162267], Table 10 and Section 6.6.2.1). Sensitivity analyses were conducted to estimate the impact of varying the standard deviation and correlation length of the random fields (BSC 2003 [163226], Section 6.6.2, Figures 6-12 and 6-13). It was demonstrated that even significant parameter variation produced seepage rates comparable to the base case (i.e., for a standard

deviation of 2.0 in log10) or smaller than the base case (i.e., correlation length of 1.0 and 2.0 m). This indicates that the selected constant values of standard deviation and correlation length are appropriate, and that seepage can be treated as a function of three rather than five key parameters. Note that the SCM modeling framework requires the permeability distribution to be representative of the excavation-disturbed zone in the drift vicinity.

The range of percolation flux $q_{perc,ff}$ imposed at the top boundary needs to cover the potential flux variability at Yucca Mountain for present and future climate scenarios. Since small-scale flow channeling is explicitly modeled within the SMPA, only the spatial variability on a resolution equal to or larger than the model domain needs to be considered. As explained in Section 6.6.4, appropriate spatial distributions of percolation fluxes as input to the SMPA can be developed using results of the UZ Flow and Transport Model (BSC 2003 [163045]) under additional consideration of flow focusing effects. These percolation fluxes are considered constant during three distinct long-term climate periods, based mainly on daily or seasonal fluctuations in net infiltration being effectively dampened in the overlying PTn nonwelded tuff unit (see Section 6.2, FEP 2.2.07.05.0A, and Section 6.6.4). Therefore, the SMPA model runs are conducted for steady-state flow conditions, applying a constant flux condition at the top boundary.

As was already mentioned in Section 6.3, the local flow conditions will be strongly altered by thermal effects during the first 1,000 to 2,000 years after waste emplacement. In a strict interpretation, the derived seepage results from the isothermal SMPA should only be applied for late time periods when both the rock temperatures and saturations have returned to "ambient" state. However, results from the TH Seepage Model presented in Section 6.4.3 demonstrate that ambient seepage rates from the SMPA are reasonably accurate (slightly conservative), provided that the rock temperatures have decreased below boiling and that the fractured rock close to the drift wall has resaturated. This means that the SMPA results can be used to abstract seepage during most of the 10,000-year compliance period. The potential impact of THM and THC effects on the applicability of the SMPA is discussed in Section 6.4.4.

6.4.2.2 Model Validation

Since the SMPA and the SCM are similar models that differ only in their scope, validation of the SMPA has been mainly achieved by comparison with results from the SCM. In other words, confidence in the model results was gained by comparison with another model that is validated against field data and other observations (BSC 2003 [163226], Section 7.1). The discussion and conclusions regarding alternative conceptual approaches in Section 6.4.1.2 apply similarly to the SCM and the SMPA.

6.4.2.3 Model Results: Systematic Study of Ambient Seepage

The systematic simulations performed by the SMPA cover a wide range of capillary-strength values $1/\alpha$ (100 Pa to 1,000 Pa in steps of 100 Pa), mean permeability values k (–14 to –10 in steps of 0.25, given in log10), and percolation flux values $q_{perc,ff}$ (1, 5, 10, 20, 50, 100 through 1,000 mm/yr in steps of 100 mm/yr). For each combination of the above values, a total of 20 realizations of the heterogeneous permeability fields were simulated. It was demonstrated that the number of 20 realizations was sufficient to ensure sufficiently stable estimates of the simulation outputs (BSC 2003 [163226], Section 7.1). Comparison of selected simulation cases

conducted with 10 vs. 20 realizations indicated differences of 2% or less in the mean seepage rates (BSC 2003 [163226], Table 7-1).

The resulting seepage values, provided in DTN: LB0304SMDCREV2.002 [163687] in the form of a look-up table, are presented and discussed in detail in BSC (2003 [163226], Section 6.6.1). Seepage rates and seepage percentages are given for a reference drift section of 5.1 m length, corresponding to the length of a waste canister plus the 0.1 m spacing between canisters (see definitions of seepage rate and percentage in Section 6.1.2). The SMPA results used in abstraction are the seepage mean and the standard deviation calculated over the 20 realizations, but values from individual realizations are provided as well. To derive a seepage rate for a particular set of key parameters $1/\alpha$, k_s, and $q_{perc,ff}$ analyzed in TSPA, the corresponding seepage results need to be interpolated from the seepage values given in the look-up table (DTN: LB0304SMDCREV2.002 [163687]).

Example results from the SMPA are illustrated in Figures 6.4-3 through 6.4-6. The figures give contours of the simulated seepage percentage as a function of the capillary-strength parameter and the mean fracture permeability (in log10 space), for selected percolation fluxes of 5, 50, 200, and 500 mm/yr. Presenting results in the form of seepage percentages (absolute seepage into a drift section relative to the amount of percolation over this drift section) is useful because the effectiveness of flow diversion is immediately evident. As expected, the seepage percentage is large for small capillary strength, small permeability, and large percolation flux. In these cases, seepage may be as high as 100%; i.e., there is no flow diversion at the drift wall, and the entire fraction of the percolation flux seeps into the drift. In contrast, the seepage percentage is small for all cases with strong capillarity, large permeability, and small percolation flux. In many of these cases, there is no seepage at all; i.e., the entire percolation flux is diverted around the drift by capillary forces, because the percolation flux is below the seepage threshold for the parameters given.

Note that the resulting seepage percentages in the look-up table are identical for simulation cases that have the same ratio of percolation flux $q_{perc,ff}$ over permeability given in m^2 (e.g., the seepage percentages for cases a permeability of 10^{-13} m^2 and $q_{perc,ff}$ = 5 mm/yr are identical to cases with a permeability of 10^{-12} m^2 and $q_{perc,ff}$ = 50 mm/yr and cases with a permeability of 10^{-11} m^2 and $q_{perc,ff}$ = 500 mm/yr; see Figures 6.4-3 through 6.4-5). This is because the steady-state capillary pressure and saturation conditions are determined by the ratio of percolation flux over permeability. As a result, it would be possible to reduce the number of key parameters for ambient seepage, and thus the size of the look-up table. However, to be consistent with previous abstractions, the look-up table is not changed for the TSPA-LA.

It should be recognized that identical seepage percentages for different percolation flux scenarios may correspond to vastly different seepage rates. For example, a seepage percentage of 50% at 1 mm/yr percolation relates to a seepage rate of approximately 14 kg/yr per waste package. At 500 mm/yr, the same percentage relates to a seepage rate of 7,013 kg/yr per waste package.

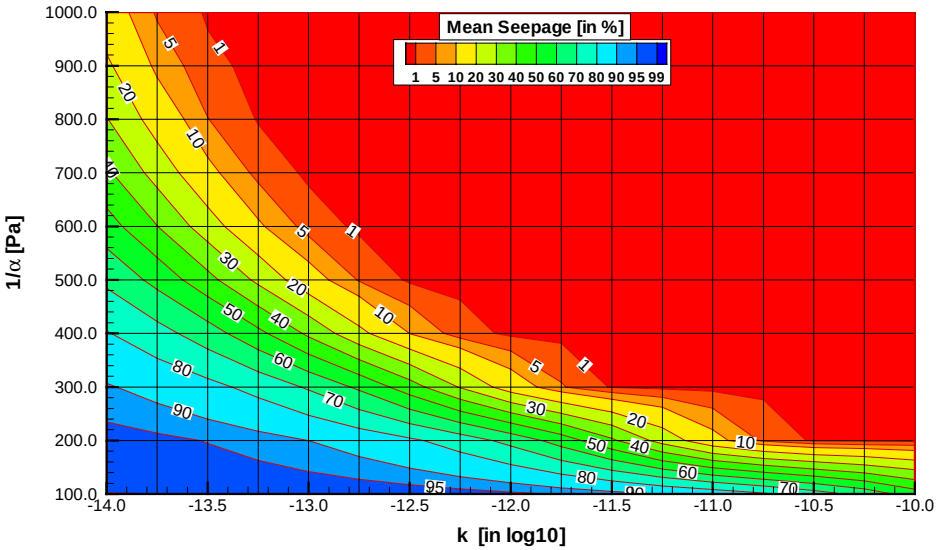

Source: LB0304SMDCREV2.002 [163687] (using file Fig6-3toFig6-8.dat)

NOTE: Horizontal and vertical lines indicate simulated parameter cases.

Figure 6.4-3. Mean Seepage Percentage as a Function of Capillary-Strength Parameter and Mean Permeability for a Percolation Flux of 5 mm/yr

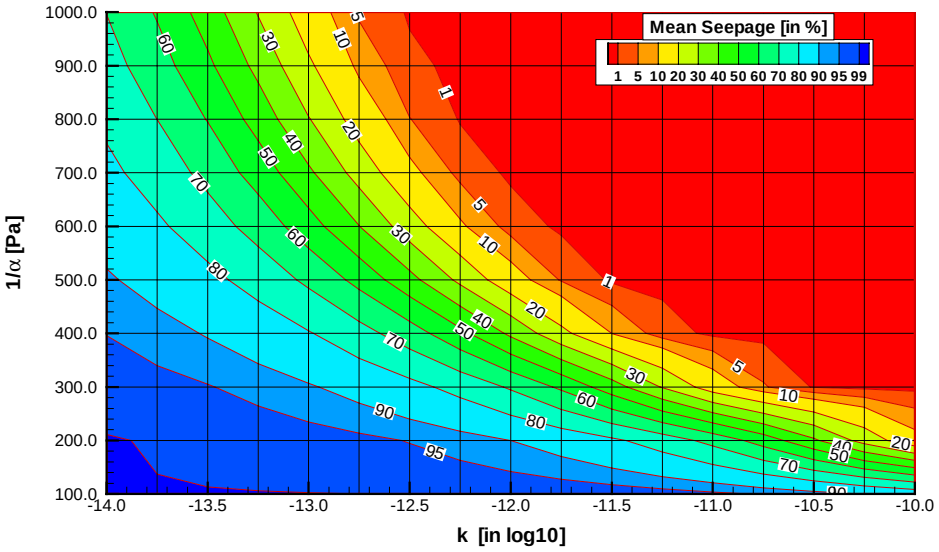

Source: LB0304SMDCREV2.002 [163687] (using file Fig6-3toFig6-8.dat)

NOTE: Horizontal and vertical lines indicate simulated parameter cases.

Figure 6.4-4. Mean Seepage Percentage as a Function of Capillary-Strength Parameter and Mean Permeability for a Percolation Flux of 50 mm/yr

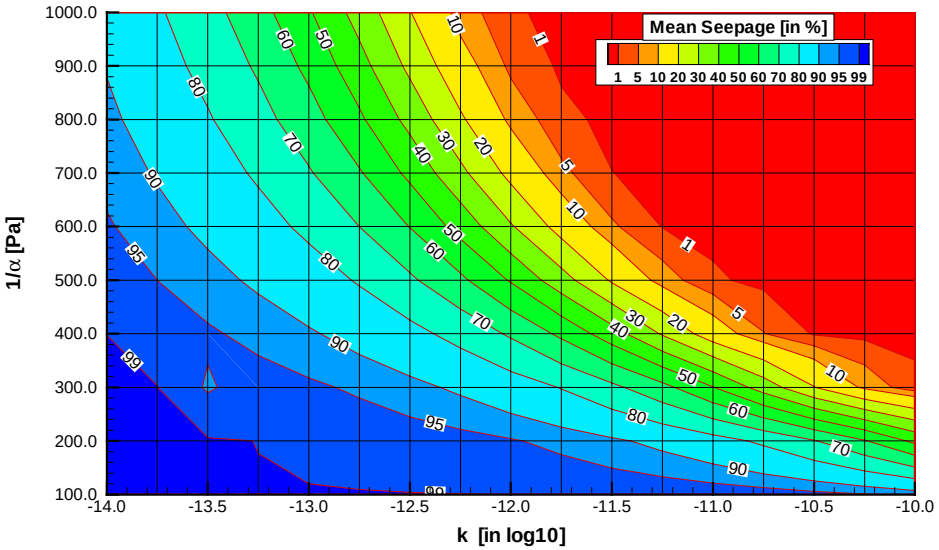

Source: LB0304SMDCREV2.002 [163687] (using file Fig6-3toFig6-8.dat)

NOTE: Horizontal and vertical lines indicate simulated parameter cases.

Figure 6.4-5. Mean Seepage Percentage as a Function of Capillary-Strength Parameter and Mean Permeability for a Percolation Flux of 200 mm/yr

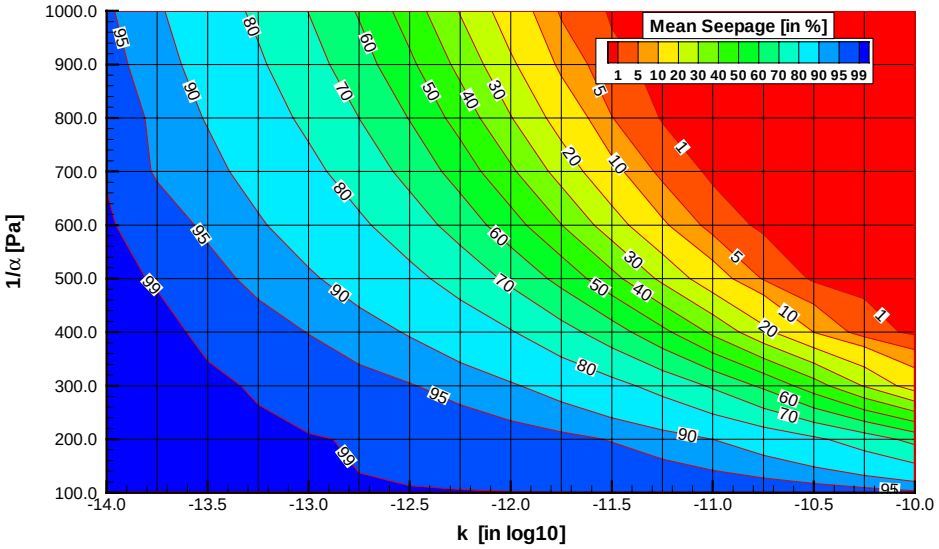

Source: LB0304SMDCREV2.002 [163687] (using file Fig6-3toFig6-8.dat)

NOTE: Horizontal and vertical lines indicate simulated parameter cases.

Figure 6.4-6. Mean Seepage Percentage as a Function of Capillary-Strength Parameter and Mean Permeability for a Percolation Flux of 500 mm/yr

The range of results observed from the 20 realizations provides information about the estimation uncertainty in the predicted seepage rates, on account of uncertainty in the stochastic small-scale heterogeneity. As shown in Figures 6-9, 6-10, and 6-11 of BSC (2003 [163226]), the differences obtained between realizations of the random permeability field can be quite large. Thus, this estimation uncertainty should be included in and propagated through seepage abstraction. This can be done using appropriate uncertainty distributions defined on the basis of the standard deviations provided in DTN: LB0304SMDCREV2.002 [163687]. Note that these standard deviations can be different for each simulated parameter combination; typically, the larger the derived seepage rate, the larger the associated standard deviation of the seepage rate. It is not evident from the discussion in BSC (2003 [163226], Section 6.6.1) which type of uncertainty distribution is best suited to represent the observed statistical spread. Therefore, histograms of the distribution of seepage percentage over the 20 realizations have been calculated for selected parameter cases, chosen to represent cases with small, average, and large seepage (see Attachment I). However, evaluation of these histograms did not reveal a consistent trend (see examples of histograms in Figure 6.4-7). It is therefore recommended for TSPA to use a simple uniform probability distribution to account for the estimation uncertainty of the SMPA results.

6.4.2.4 Model Results: Impact of Drift Degradation

Whereas the systematic study of the previous section assumed a circular drift design, additional simulation cases were conducted to analyze the potential impact of changes in the drift shape on seepage. Such shape changes, a possible result of thermal stress and joint cohesion degradation as well as seismic motion, have been evaluated in different revisions of the Model Report *Drift Degradation Analysis* (Revision 01 in BSC (2001 [156304]), Revision 02 in BSC 2003 [162711]). Revision 01 of the Model Report *Drift Degradation Analysis* (BSC (2001 [156304]) was based on a Discrete Region Key Block Analysis (DRKBA) to determine the potential rock fall at the repository horizon. Key blocks are critical rock blocks in the surrounding rock mass of an excavation which are removable and oriented in an unsafe manner so that they are likely to fall into the opening unless ground support is provided. It was later recognized, however, that the DRKBA analysis presented in BSC (2001 [156304]) needed improvement in several areas. For example, the DKRBA could not be used to explicitly apply dynamic loads (due to seismic ground motion) or thermal stresses. The DRKBA analysis, which determines structurally controlled key-block failure, was also not applicable to lithophysal units, where failure is essentially stress controlled (BSC 2003 [162711], Section 1.1). Therefore, an improved degradation analysis was presented in Revision 02 of the Model Report *Drift Degradation Analysis* (BSC 2003 [162711]), using additional approaches such as two-dimensional and three-dimensional discontinuum analysis with explicit representation of seismic and thermal loads. Results from this revised analysis indicate more drastic drift shape changes in the lithophysal rocks compared to the earlier revision, including cases with partial or complete collapse of drifts.

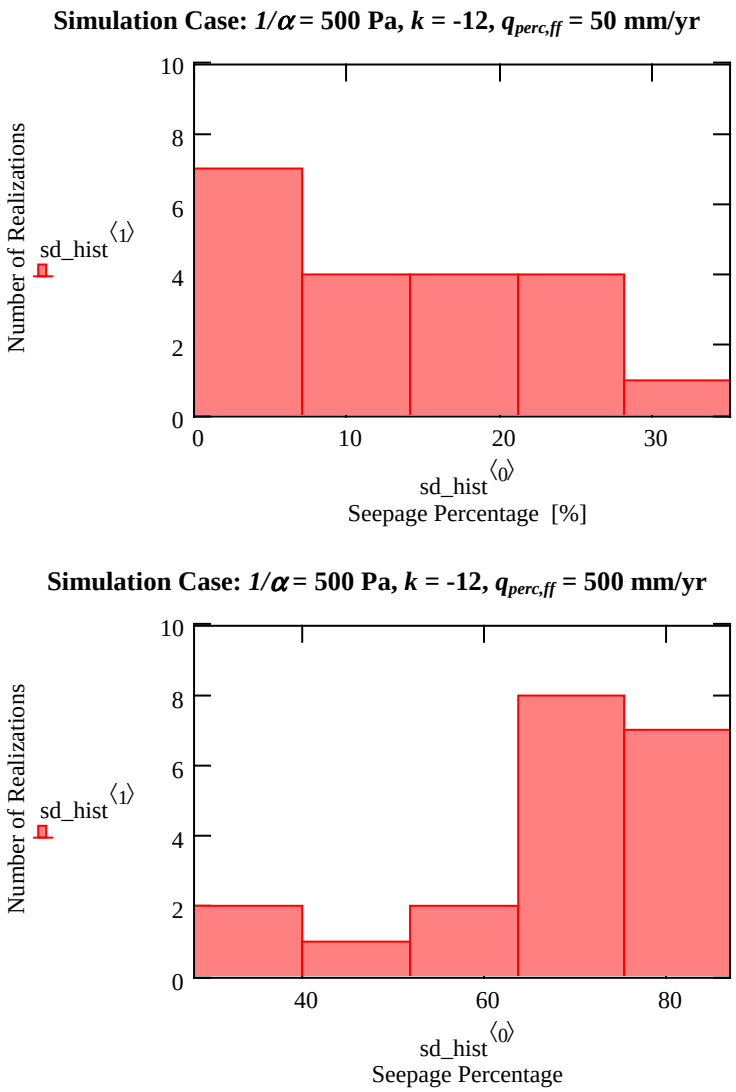

Source: LB0304SMDCREV2.002 [163687] (using file Fig6-3toFig6-8.xls, see Attachment I)
NOTE: The symbols in the histograms (i.e., sd_hist$^{<0>}$ and sd_hist$^{<1>}$) denote the variable names given in the *Mathcad 11* spreadsheet used for the calculation. The histogram ranges are derived using the largest and the smallest seepage percentage of the 20 realizations of each simulation case, and dividing the difference by the bin number of 5. For $q_{perc,ff}$ = 50 mm/yr, the largest value is 34.8%, the smallest value is 0.4. For $q_{perc,ff}$ = 500 mm/yr, the largest value is 86.9%, the smallest value is 28.3%.

Figure 6.4-7. Example Histograms of Seepage Percentage from 20 Realizations for Two Selected Parameter Cases

Note that the SMPA simulation cases for drift degradation effects reported in BSC (2003 [163226], Sections 6.4 and 6.6.3) were based on the previous DRKBA results, as the latest Revision 02 of the Model Report *Drift Degradation Analysis* was not yet available (BSC 2003 [163226], Section 5; [163017]). Since the studied degradation cases are still useful for understanding seepage in moderately degraded drifts, the simulated cases are presented and discussed in Section 6.4.2.4.1 below. In response to the new drift degradation results obtained in Revision 02 of the Model Report *Drift Degradation Analysis* (BSC 2003 [162711]), additional seepage analyses have been conducted. These analyses are documented in Section 6.4.2.4.2.

6.4.2.4.1 Seepage Analysis for Revision 01 Drift Degradation Results

The drift degradation analysis reported in Revision 01 of the Model Report *Drift Degradation Analysis* (BSC 2001 [156304]) considered three different levels of seismic events in conjunction with thermal effects and a moderate time-dependent decrease in rock strength. The seismic events were defined as follows: Level 1, corresponding to a 1,000-year event with a peak ground acceleration of 0.14 g, Level 2, corresponding to a 5,000-year event with a peak ground acceleration of 0.30 g, and Level 3, corresponding to a 10,000-year event with a peak ground acceleration of 0.43 g (BSC 2001 [156304], Section 4.1, Table 4). None of these levels leads to significant drift degradation. Typically, the degraded drift profiles showed indication of local rock fall of key blocks at the ceiling of the drift, while the drifts remained essentially intact and the horizontal extent was not affected. In general, these results were similar for the Tptpmn and the Tptpll.

Selected drift profile predictions from the drift degradation analyses were adopted for the seepage analysis conducted with the SMPA (BSC 2003 [163226], Sections 6.4 and 6.6.3). The selected profiles were the 75 percentile profile and the worst-case profile of the seismic Level 3 case for both geological units, as presented in BSC (2001 [156304], Figures 39 and 40, Table 43). The 75 percentile profile for a particular unit and seismic event indicates that 75% of the drift length within that unit will have less (or no) drift profile deterioration. The worst-case profile represents the most severely degraded profile of the probabilistic analysis. The SMPA seepage simulations used the selected drift profiles and the fall-off rock volumes to construct 3-D numerical grids that explicitly represent the predicted changes in drift shape (BSC 2003 [163226], Section 6.4). On these discretized drift profiles, seepage was calculated with 10 realizations of the heterogeneous permeability field. Calculations were carried out for both the Tptpmn and the Tptpll units. Seepage simulations were conducted for selected parameter cases, using a capillary strength of 600 Pa and a percolation flux of 200 mm/yr. The mean permeability value used was -11.86 in the Tptpmn unit and -10.84 in the Tptpll unit (in log10). No-degradation results with the same parameter values were also calculated for comparison, to study the impact of drift degradation on seepage.

The simulation results obtained from the SMPA analysis indicate that the effects of drift shape changes are limited for all Revision 01 degradation cases. It was demonstrated that, for both considered drift profiles and both geological units, the average seepage rates as well as the average seepage threshold calculated over the 10 realizations were almost identical to the no-degradation cases (BSC 2003 [163226], Section 6.6.3). This result indicates that the impact of geometry changes at the drift ceiling as a result of local breakout of key blocks can be neglected, as long as the drifts stay essentially intact and the horizontal extent remains mostly unchanged. Thus the seepage look-up table derived for the initially circular drift design should be applicable

for such moderately degraded drifts. However, note that the statistical spread among the 10 realizations was considerably stronger than in the no-degradation case.

6.4.2.4.2 Seepage Analysis for Revision 02 Drift Degradation Results

The improved drift degradation analysis, as reported in Revision 02 of the Model Report *Drift Degradation Analysis* (BSC 2003 [162711]), also considers different levels of seismic events, thermal stresses, and time-dependent reduction in rock strength. The seismic events were defined by their probabilistic seismic hazard level, giving the annual probability that certain levels of ground motion would be exceeded. The three annual hazard levels considered are a 5×10^{-4} annual probability of exceedance, a 1×10^{-6} annual probability of exceedance, and a 1×10^{-7} annual probability of exceedance (BSC 2003 [162711], Table 9). These levels correspond to a 2,000-year event with a peak ground acceleration between 0.16 and 0.19g, to a 1,000,000-year event with a peak ground acceleration between 6.86 and 10.46g, and to a 10,000,000-year event with a peak ground acceleration between 13.15 and 16.28g, respectively. The latter two seismic levels are significantly larger than the ones analyzed in Revision 01 of the drift degradation analysis (see Section 6.4.2.4.1). In fact, as pointed out in Section 8.2 of BSC (2003 [162711]), some of the ground motions used are larger than the largest ground motions observed and may not be realistic. Therefore, the drift degradation predictions for the 1×10^{-6} and the 1×10^{-7} hazard levels can be considered worst-case scenarios.

The impact of rock strength reduction was analyzed by selected cases using different levels of joint-cohesion reduction and tensile-strength reduction. Because no information on the most probable values of strength reduction was available, the analysis covered the entire range of possible joint cohesion loss, with the two extreme scenarios being the 0% reduction case (i.e., present-day rock strength) and the 100% reduction case (complete loss of cohesion strength). The other cases assume 20, 40, 60, and 80% reduction in joint cohesion. Since information on the cohesion reduction as a function of time was not available either, the cohesion parameters were stepwise adjusted and the model was run to an equilibrium state, without considering the time scale for cohesion reduction. Therefore, the temporal evolution is not known; only the ultimate extent of drift degradation for the different reduction levels is provided by this analysis.

Results from the drift degradation analysis demonstrate fundamental differences between the nonlithophysal and the lithophysal rocks. Drift degradation in the hard, strong, jointed rock of the nonlithophysal units is limited to local gravitational drop of rock blocks at the drift ceiling, even for the extreme seismic cases and complete loss of joint cohesion (BSC 2003 [162711], Figures 101 through 105). The drifts remain intact openings with the horizontal extent essentially unchanged, similar to the results obtained in the earlier Revision 01 of the Model Report *Drift Degradation Analysis* (BSC 2001 [156304], compare with profiles in Figures 39 and 40). Thus the seepage prediction studies discussed in the previous section are still applicable to the nonlithophysal rocks. Thus, in the Tptpmn and the Tptpln, the impact of drift degradation on the predicted mean seepage is almost negligible.

In contrast, significant drift degradation is predicted for the relatively deformable lithophysal rock (BSC 2003 [162711], Section 6.4). In this geologic unit, most of the extreme simulation cases, among them the 1×10^{-6} and the 1×10^{-7} seismic hazard levels and the 80% through 100% strength reduction cases, result in complete drift collapse, as discussed in BSC (2003 [162711], Sections 6.4.1.1 and 6.4.2.4). How this may affect seepage is discussed in the paragraphs below.

No significant rock fall is predicted for the thermal stress case, the 5×10^{-4} seismic hazard case, and most of the 0% through 60% strength reduction cases (BSC 2003 [162711], Sections 6.4.1.2, 6.4.1.1, and 6.4.2.4). In these cases, the impact of drift degradation on seepage is expected to be small, similar to the nonlithophysal unit.

During collapse, either sudden or gradual, the rock mass above an underground opening disintegrates into a number of fragments that fall down and begin to fill the open space. Because there are large voids between the rock fragments, the bulk porosity of the fragmented rubble is much larger than the intact rock. As a result, the open space of the original excavation plus the collapsed portion of rock above completely fill with rubble at a certain stage. When this occurs, the broken rock provides backpressure, which prevents further collapse of the rock mass (BSC 2003 [162711], Section 6.4.2.1). Therefore, the final situation after drift collapse can be categorized as follows: The original opening has increased in size, but is filled with fragmented rubble and large voids. The solid wall rock surrounding the rubble-filled opening is intact, but may have increased permeability because of the dynamic motion and the stress redistribution (see Section 6.4.4.1). For convenience, we refer to the rubble-filled opening as a "collapsed drift", although technically there is no drift after collapse. The size and the shape of a collapsed drift mainly depend on the porosity of the rubble material and on the type of caving mechanism as collapse occurs. This explains why the collapsed drift profiles provided in DTN: MO0306MWDDPPDR.000 [164736] are all similar, independent of the event leading to collapse (i.e., seismic stress or rock fatigue). (Note that these profiles are also depicted in Attachment XVIII of BSC (2003 [162711]).) Collapsed drifts are shown for Scenarios 2 through 5, 11, 12, 17, 18, 23, 24, 28, 29, and 30. All drifts remain approximately circular after collapse. However, the diameter of collapsed drifts approximately doubles to about 11 m.

It was already discussed in Section 6.3.1 that complete drift collapse may lead to significantly different seepage behavior. However, even though the collapsed drifts are filled with rubble material, capillary barrier effects still give rise to considerable flow diversion at the interface between the solid rock and the rubble-filled drift opening. This is because of the large scattered voids between the fragmented rock particles (particle sizes on the order of centimeters and decimeters (BSC 2003 [162711], Section 8.1)), suggesting that the capillary strength parameter in the rubble filled drift is very small, most likely close to the zero capillarity of an air-filled opening. Also, an open space can be expected between the solid rock at the ceiling and the collapsed rubble material. Therefore, capillary-driven flow diversion remains an important mechanism reducing seepage in collapsed drifts, which should be included in the seepage abstraction. Additional simulation cases were conducted with the SMPA to study seepage into collapsed drifts. A worst-case drift profile was selected representative of the drift collapse scenarios depicted in MO0306MWDDPPDR.000 [164736] (see also Attachment XVIII of BSC (2003 [162711])). The chosen profile has a circular shape with a diameter of 11 m. A capillary strength parameter of 100 Pa was used for the fragmented rock material within the collapsed drift (see Section 5). This value is considered a conservative choice for seepage calculations, because the capillarity of the rubble material is most likely smaller. Otherwise, the conceptual model of the seepage simulations remains identical to the SMPA analysis for non-degraded drifts (see Section 6.4.2.1).

Systematic seepage simulations for the collapsed drift case were conducted for the full set of parameter combinations, with capillary strength values ranging from 100 Pa to 1,000 Pa, mean permeability values ranging from –14 to –10 (in log10), and percolation flux values ranging from 1 mm/yr to 1,000 mm/yr. (These are the same parameter cases as simulated for the non-degraded drift in Section 6.4.2.3). The resulting seepage values are provided in a seepage look-up table for the collapsed drift scenario (DTN: LB0307SEEPDRCL.002 [164337]). The format of this look-up table is identical to the non-degraded drift case in Section 6.4.2.3. Thus, to account for collapsed drifts, seepage abstraction would simply sample from this second look-up table, without changing the basic abstraction methodology (see Section 6.5.1.5). The collapsed drift look-up table in DTN: LB0307SEEPDRCL.002 [164337] is based on results from 10 realizations.

Example results for the collapsed drift scenario are illustrated in Figures 6.4-8 through 6.4-11, showing contours of simulated seepage percentage. Comparison with results from the non-degraded drift scenario (Figures 6.4-3 through 6.4-6) indicates a moderate increase in seepage percentage, caused by the larger size of the collapsed drift (reducing the effectiveness of flow diversion around the drift) and by the non-zero capillary strength in the drift (reducing the effectiveness of the capillary barrier). The simulation results demonstrate that most of the percolation flux is still diverted around the collapsed drift for most of the considered parameter range. Note, however, that the related seepage rates for the collapsed drift scenario are much larger than for nondegraded drifts. This is because the footprint of the drifts has doubled in size, thereby doubling the amount of percolation flux arriving at the collapsed drift. (As defined in Section 6.1.2, seepage denotes the flow of liquid water into a drift. Whether the seeping water can actually contact waste packages is not considered in this definition. Obviously, the larger the horizontal extent of a drift, the higher the possibility that seeped water does not hit a waste package.)

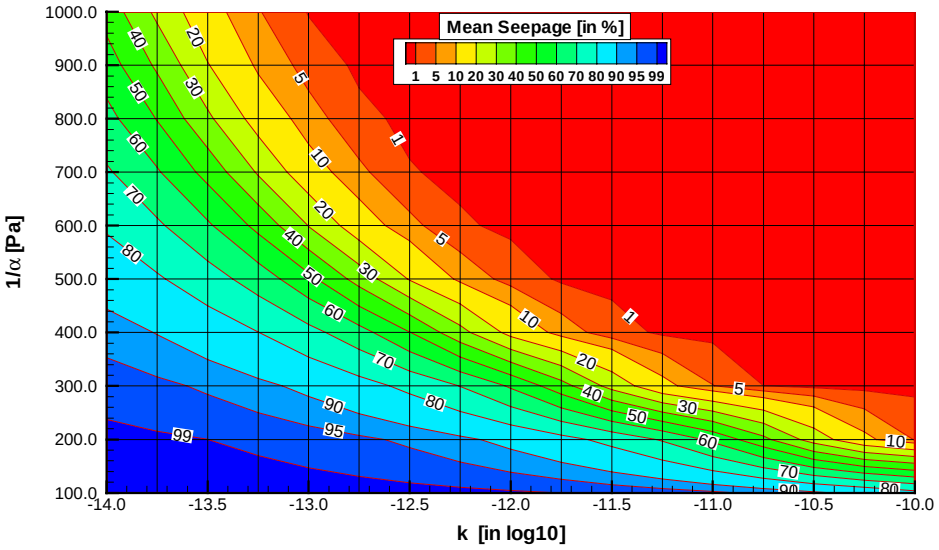

Source: LB0307SEEPDRCL.002 [164337]

NOTE: Horizontal and vertical lines indicate simulated parameter cases.

Figure 6.4-8. Mean Seepage Percentage for the Collapsed Drift Scenario as a Function of Capillary-Strength Parameter and Mean Permeability for a Percolation Flux of 5 mm/yr

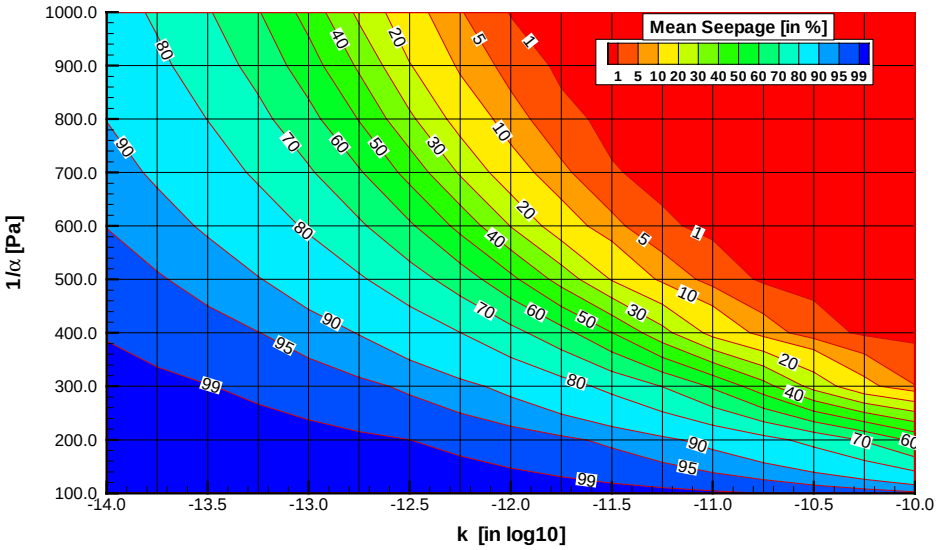

Source: LB0307SEEPDRCL.002 [164337]

NOTE: Horizontal and vertical lines indicate simulated parameter cases.

Figure 6.4-9. Mean Seepage Percentage for the Collapsed Drift Scenario as a Function of Capillary-Strength Parameter and Mean Permeability for a Percolation Flux of 50 mm/yr

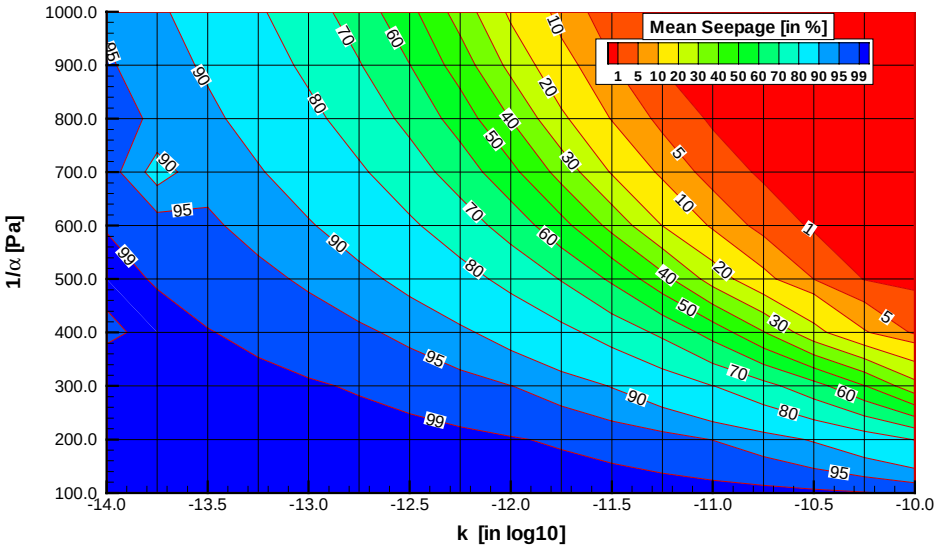

Source: LB0307SEEPDRCL.002 [164337]

NOTE: Horizontal and vertical lines indicate simulated parameter cases.

Figure 6.4-10. Mean Seepage Percentage for the Collapsed Drift Scenario as a Function of Capillary-Strength Parameter and Mean Permeability for a Percolation Flux of 200 mm/yr

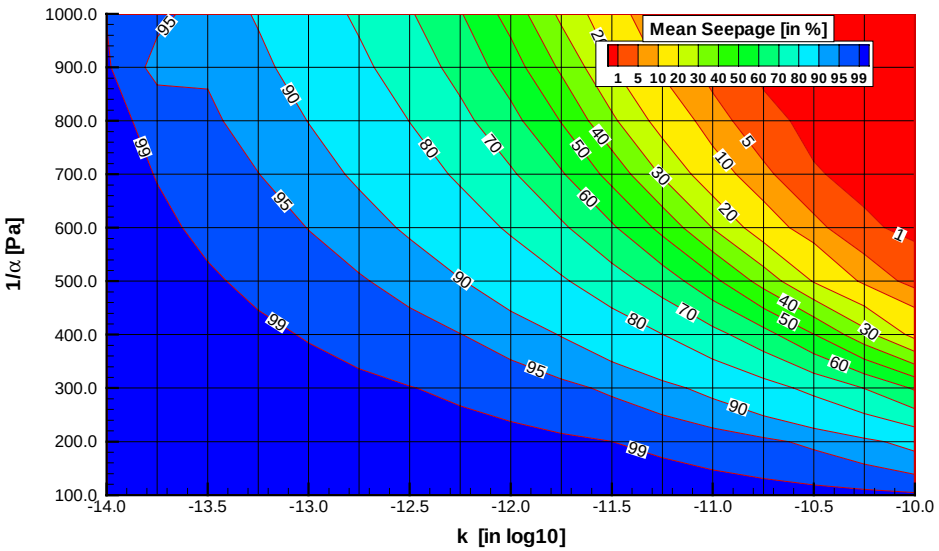

Source: LB0307SEEPDRCL.002 [164337]

Figure 6.4-11. Mean Seepage Percentage as a Function of Capillary-Strength Parameter and Mean Permeability for a Percolation Flux of 500 mm/yr

6.4.2.5 Model Results: Impact of Rock Bolts

To evaluate the potential impact of rock-bolt ground support on seepage, a refined seepage model including rock bolts was developed (BSC 2003 [163226], Section 6.5). The model features a 3 m long rock-bolt borehole extending vertically upward from the crown of a drift. A fine discretization was chosen at the interface between the rock and the borehole, using grid elements as small as 0.1 mm. The simulated radius of the borehole was 1 inch. This is comparable to the probable rock bolt design, which is given in BSC (2003 [164101]). The small differences are not relevant for the model results. The model was applied to several selected simulation cases, using a representative range of formation properties and percolation fluxes.

As pointed out in Section 6.3.1, the current repository design uses rock bolts without grout. In contrast, the base-case simulation model considered grouted boreholes, which is consistent with previous repository designs. A wide range of grout properties was simulated to account for the fact that the grout would most likely not retain its designed hydraulic properties over many thousands of years. In particular, one sensitivity case, designated to represent completely disintegrated grout in the borehole, used a large grout permeability of 10^{-10} m^2 and a small capillary strength of 10 Pa, which corresponds essentially to an open rock-bolt borehole (BSC 2003 [163226], Figure 6-3, Case G2). This is the simulation case relevant for seepage abstraction.

Results of the SMPA simulations with explicit consideration of rock bolts are described in BSC (2003 [163226], Section 6.6.4). Essentially, no seepage enhancement was found for the simulation case representing an open rock-bolt borehole without grout (BSC 2003 [163226], Table 6-4, Case G2). This result is understandable, considering that the open borehole acts as a capillary barrier to flow in the fractured rock, similar to the barrier that exists at the rock-drift interface. Also, the cross-sectional area between the borehole and the rock is rather small. Thus the presence of open rock-bolt boreholes is not considered a major factor for seepage into drifts.

6.4.3 TH Seepage Model

The TH Seepage Model is employed to evaluate the coupled TH processes—and their impact on seepage processes—in the vicinity of waste emplacement drifts during the heating phase of the repository (BSC 2003 [161530]). This drift-scale process model is designed to analyze the combined effect of the two barriers that may prevent seepage into drifts at elevated temperatures: (1) the capillary barrier, which is independent of the thermal conditions, and (2) the vaporization barrier, which is in effect only if boiling temperatures prevail. While incorporating the conceptual framework for ambient seepage from the SCM, the TH Seepage Model accounts for all important flow and energy transport processes in response to the heat emplacement. Transient simulations were performed to explicitly calculate fluid flow down to the drift during the heating phase of the repository, and to directly calculate transient seepage rates into the drift. Results of this model are used in the seepage abstraction to develop an appropriate methodology of adjusting the SMPA results to account for thermally perturbed conditions. The thermal analyses with the TH Seepage Model is conducted for nondegraded drifts. Modeling analyses on the impact of drift collapse on the TH behavior is ongoing (Assumption 3 in Section 5 [164618]).

6.4.3.1 Model Description

Simulation of the coupled TH processes in fractured rock requires a modeling framework of considerable complexity. The processes described by the TH Seepage Model include the movement of both gaseous and liquid phases, transport of latent and sensible heat, phase transition between liquid and vapor, and vapor pressure lowering (BSC 2003 [161530], Section 6.2.1.1). While fluid flow is described with a multiphase extension of Darcy's law, heat flow occurs by conduction (with heat conductivity a function of saturation) and convection. The thermodynamic conditions are based on a local equilibrium model of the three phases (liquid, gas, and solid rock). In contrast to the SCM and the SMPA, where only the fracture continuum is represented, the contribution of the rock matrix cannot be neglected in TH simulations. The fractured rock is therefore treated as a dual-permeability domain, accounting for the fractures and the rock matrix as two separate, overlapping continua (Doughty 1999 [135997]). The active fracture model (AFM) is employed to account for the fact that unsaturated flow may be restricted to a limited number of (active) fractures and that flow within a fracture is likely to be channelized (Liu et al. 1998 [105729], p. 2636). Both effects may effectively reduce fracture-matrix interaction, and thus have to be considered in TH simulations where strong transfer of vapor and condensate is expected between the fractures and the matrix. For further details on the conceptual framework of the TH Seepage Model, see BSC (2003 [161530], Section 6.2.1). Note that this conceptual framework is consistent with other models for unsaturated flow and transport at Yucca Mountain (CRWMS M&O 2000 [141187], Section 6.4.5). Rock-property changes as a result of THM and THC effects are not considered in the TH Seepage Model. These are evaluated with separate models as discussed in Section 6.4.4.

Based on the recommendations listed in Section 6.4.1.2 of this report, the conceptual framework for seepage in the TH Seepage Model is similar to the SCM and SMPA conceptualization. A stochastic continuum model is implemented for fractures near the drift, that considers the small-scale variability of permeability to account for flow channeling, and the capillary-strength parameter close to the drift wall is derived from the properties provided by the SCM calibration (BSC 2003 [161530], Section 6.2.1.1.2). Also, the specific seepage boundary condition used in the SCM is implemented for all fracture continuum gridblocks immediately at the rock-drift interface. Seepage from the rock matrix into the drift is unlikely because of the strong capillarity and low permeability of the matrix; thus, seepage from the matrix into the drift is neglected in the TH Seepage Model. Note that predictions of thermal seepage have been previously conducted with the Multiscale Thermohydrologic Model, as presented in BSC (2001 [158204], Section 6.14). However, in this model, the conceptual framework for the capillary barrier at the drift wall was not based on the recent experimental and modeling analyses of seepage into niches, as described in BSC (2003 [162267]).

In contrast to ambient seepage, the thermal seepage behavior of the fractured rock is simulated with a 2-D model, in a vertical model domain perpendicular to the drift axis. Considering that several simulation cases must be studied to account for the variability in rock properties and boundary conditions important for thermal seepage, a full 3-D simulation of the coupled processes is not feasible because of computational limitations. Similar to the SCM and the SMPA, the TH Seepage Model needs to focus on near-drift conditions, using a refined discretization in the drift vicinity. However, at the same time, the TH simulation requires a large vertical model domain because the thermally disturbed zone extends far into the overlying and

underlying geological units. The main deviations between a 3-D and a 2-D model occur at the end of each emplacement drift and at the edges of the repository. Such effects are accounted for in BSC (2003 [161530], Sections 6.2.2.1.3 and 6.2.4.2) by considering several sensitivity cases for the thermal load. Also note that, with respect to the effectiveness of the capillary barrier for seepage into drifts, a 2-D representation gives a conservative prediction of seepage for most cases of heterogeneous fracture permeability fields because the potential diversion of flow in the third dimension is neglected.

To account for the two main host-rock units of the repository, two submodels with slightly different numerical gridding and different stratigraphy were studied with the TH Seepage Model. The first one, the Tptpmn Submodel, considers a drift located in the Topopah Spring tuff middle nonlithophysal unit (Tptpmn unit). The second one is the Tptpll Submodel, considers a drift located in the Topopah Spring tuff lower lithophysal unit (Tptpll unit). In both submodels, the discretization in close vicinity to the drift is identical; the differences occur only at some distance from the drifts where geological contacts to other rock units are encountered. As an example, Figure 6.4-12 shows the discretization chosen for the Tptpmn Submodel, illustrating the entire vertical mesh and a close-up view of the drift vicinity. The model extends from the ground surface at the top—with an open atmosphere boundary condition—to the water table at the bottom—represented as a flat, stable surface. Symmetry considerations were applied to reduce the model domain in the lateral direction, perpendicular to the drift axis, to increase the computational efficiency of the simulation runs. The current repository design of parallel drifts spaced at 81 m can be represented as a series of symmetrical, identical half-drift models with vertical no-flow boundaries between them. Accordingly, the numerical mesh was reduced to a half-drift model with a width of 40.5 m, extending from the drift center to the midpoint between drifts.

Note that the grid design of the TH Seepage Model is different from the ambient seepage studies, in that it uses radial symmetry and small gridblocks in the drift vicinity with gradual conversion into larger cartesian gridblocks at increasing distance from the drift. This is important for TH models because sufficient resolution is provided at key locations where steep gradients of TH properties occur, while maintaining computational efficiency. At the drift wall, gridblocks are about 20 cm in the radial direction, which is twice the size of the uniform gridblocks used in ambient seepage models. To account for spatial variability in the drift vicinity, stochastic permeability values with random correlation structure and a standard deviation of to $\sigma_s = 0.84$ (in log10 space) are mapped to the gridblocks. This standard deviation is slightly smaller than the value used in the current revisions of SMPA modeling analysis (BSC 2003 [163226], Section 6.3.3). It was taken from BSC (2003 [162267], Table 10), representing the maximum standard deviation from small-scale air permeability tests conducted in Tptpmn niches. The differences in the grid design and the stochastic parameter representation will bring out differences in the model results between the ambient and thermal seepage models, which are analyzed in Section 6.2.2.2.2 of BSC (2003 [161530]). The relevance of these differences for seepage abstraction is discussed in Section 6.5.2 of this Model Report.

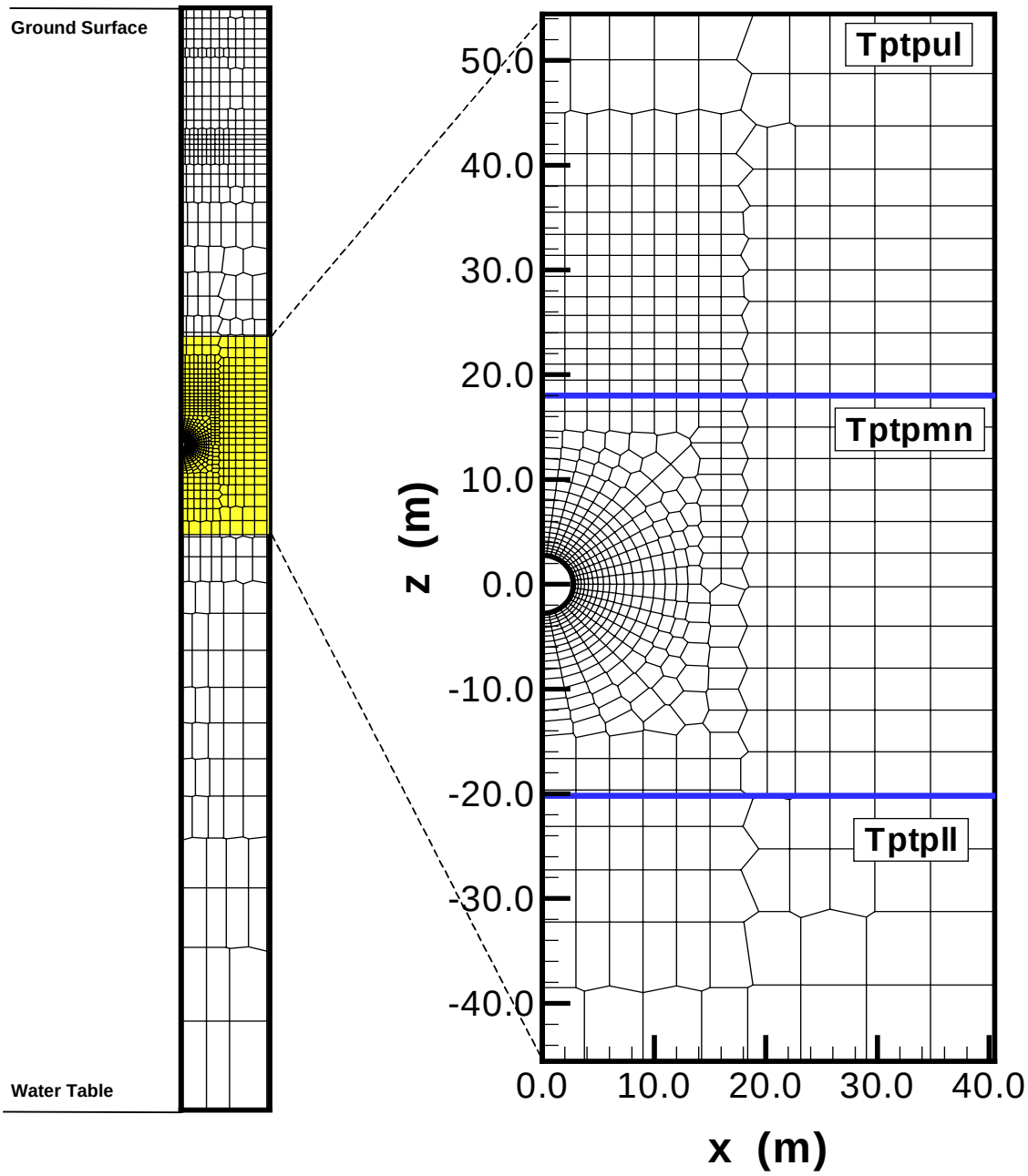

Source: BSC (2003 [161530], Figure 6.2.1.2-1)

NOTE: In this example, the emplacement drift is located in the Tptpmn unit (Tptpmn Submodel).

Figure 6.4-12. Example of Numerical Grid for the TH Seepage Model

Predictive simulations with the TH Seepage Model were performed for two main suites of simulation cases. The first suite of cases addresses the relevant TH conditions in the drift vicinity, mainly for informative purposes. The second suite of cases focuses specifically on the potential of thermal seepage for further use in seepage abstraction and TSPA, applying the specific modeling framework for seepage that was outlined in Section 6.4.1. Because modeling of coupled processes is so computationally intensive, it was not feasible to conduct a systematic study with thousands of parameter combinations as done with the SMPA. Thus it was not possible to arrive at similar look-up tables that would provide the rate of thermal seepage as a function of various parameters. Instead, sensitivity analyses were performed with selected simulation cases, varying a small number of parameters that are important for thermal seepage. The scope of this study was to demonstrate that thermal seepage can be described by a simple abstraction method that uses the ambient seepage rates as a base estimate. Thus, modeling results from the TH Seepage Model are not expected to provide the exact quantitative amount of seepage for all possible parameter combinations. Rather, the model is expected to *qualitatively* describe the evolution of seepage in comparison to the ambient seepage rates. Enough sensitivity cases must be considered to demonstrate that the proposed simple abstraction method for thermal seepage holds for the relevant ranges of parameters (see Section 6.4.3.3).

The relevant parameters varied in the evaluation of thermal seepage are the thermal operating mode, the local percolation flux, and selected rock properties. The parameter ranges studied were chosen to cover the expected variability and uncertainty in these relevant factors. The temperature conditions, for example, will vary considerably in the repository, arising from heat-output variation among individual waste packages, emplacement-time differences among repository sections, and three-dimensional (3-D) edge effects (e.g., BSC 2001 [158204], Sections 6.12 and 6.14). Therefore, four different thermal operating modes were analyzed with the TH Seepage Model (BSC 2003 [161530], Table 6.2.1.3-1). The “reference mode” denotes a thermal load representative of the average thermal conditions for the current repository design, resulting in maximum rock temperatures above the boiling point of water for several hundred years close to the emplacement drifts. The other thermal-operating modes are studied as sensitivity cases, resulting in rock temperature conditions that can be as high as 143°C (“high-temp” mode), that will barely exceed boiling temperature (“additional heat mode”), and that will never even reach boiling conditions (“low-temp mode”). In each case, the thermal load is reduced by a large percentage during the preclosure period—as the forced ventilation effectively removes heat from the emplacement drifts—and decreases with time as a result of the radioactive decay (BSC 2003 [161530], Section 6.2.1.3.3).

As explained in Section 6.6.4.1, the local percolation fluxes arriving at emplacement drifts can vary considerably in space, and will be affected by future climate changes. The TH Seepage Model accounts for this spatial and temporal variation by using appropriate flux boundary conditions at the top of the model domain. Consistent with the future climate analyses for the Yucca Mountain (USGS 2001 [158378]; USGS 2001 [160355]), the model considers three long-term climate periods with constant net infiltration: the present-day climate (up to 600 years from now), the monsoon climate (600–2,000 years from now), and the glacial transition climate (more than 2,000 years from now). The base-case simulation has assigned percolation fluxes of 6, 16, and 25 mm/yr, respectively, for these three periods (BSC 2003 [161530], Table 6.2.1.4-1), slightly larger than the average fluxes over the repository area for the mean climate scenario (see Table 6.6-11). These average fluxes may vary because of spatial variability in surface

infiltration, heterogeneity in rock properties, flow diversion at stratigraphic contacts, and flow focusing, giving maximum fluxes much larger than the average values (see Section 6.6.4). Additional flux scenarios have been studied with the TH Seepage Model to cover the expected range of percolation fluxes within the repository units. These scenarios are defined by multiplying the boundary fluxes of the base case using factors of 5, 10, and 20. For the three climate periods, the resulting fluxes are: (1) 30, 80, and 125 mm/yr for a multiplication factor of 5; (2) 60, 160, 250 mm/yr for a multiplication factor of 10; and (3) 120, 320, and 500 mm/yr for a multiplication factor of 20. Together, these cases cover the major fraction of the parameter distributions for percolation flux developed in Section 6.6.4. As discussed in Section 6.6.4.3, the probability of local percolation fluxes larger than the range defined by these cases is very small.

As mentioned above, the percolation flux boundary condition is applied at the top of the model domain, which represents the ground surface. The ground surface was selected as the top boundary because appropriate boundary conditions for temperature, pressure, and saturation can be easily defined. It is important to note, however, that the definition of boundary fluxes at this location faces a conceptual difficulty for a drift-scale model such as the TH Seepage Model. This is because the percolation flux distribution below the Paintbrush nonwelded hydrogeological unit (PTn), which defines the TH conditions in the repository units, is considerably different from the distribution of net infiltration at the ground surface, mainly a result of lateral diversion in the PTn. Since the TH Seepage Model is essentially a vertical column model, it cannot account for lateral flow diversion in the PTn. Therefore, instead of using the net infiltration rates at the top boundary, the TH Seepage Model needs to use boundary fluxes representative of the fluxes within the repository units. Thus, the flux boundary conditions at the top of the model domain are designated to represent the range of percolation fluxes below the PTn rather than the range of net infiltration at the ground surface. (Note that this approach is appropriate because the PTn fluxes are hardly affected by TH processes.) As discussed in Section 6.6.4.1, the distribution of percolation fluxes below the PTn is provided by simulation results from the three-dimensional UZ Flow and Transport Model (BSC 2003 [163045]).

The rock properties assigned to the various stratigraphic units in the TH Seepage Model have been mainly derived from site-scale calibration runs (most hydrological properties) and supplemental data analyses (thermal properties). Since these properties are different for the Tptpmn and the Tptpll host-rock units, some effect of parameter variation is already accounted for by analyzing the Tptpmn and the Tptpll submodels. The rock properties that have the strongest impact on the TH conditions in the fractured tuff are the thermal properties, most importantly the bulk thermal conductivity (important for conductive heat transport) and the fracture permeability (important for moisture redistribution). In the TH Seepage Model, the bulk thermal conductivity varies by about 10% between the Tptpmn and the Tptpll, while fracture permeability varies by about one-half order of magnitude (BSC 2003 [161530], Table 4.1-2). These parameter ranges are smaller than the estimated variability of these properties over the repository area. For comparison, the standard deviation describing the variability of bulk thermal conductivity was reported on the order of 0.25 W/m/K in the Tptpmn and the Tptpll units (Table 7-10 of BSC (2002 [160319]), while the standard deviation of mean permeability is 0.34 and 0.47 (in log10) for the two units, respectively (see Section 6.7.1.1). Effects of variation of these parameters beyond the range explicitly accounted for by the thermal seepage simulation were qualitatively discussed in Section 6.2.4.3 of BSC (2003 [161530]), based on sensitivity analyses reported in BSC (2001 [155950], Sections 5.3.1.4.7 and 5.3.1.4.8). These analyses demonstrate

that the potential variability in thermal conductivity and fracture permeability is expected to result in considerable variability in the TH conditions. However, it was concluded that the validity of the simple abstraction method for thermal seepage should not be affected. This assessment was based on the fact that the range of TH conditions expected from the variability of these properties is smaller than the range of TH conditions explicitly addressed in the modeling analysis by varying the thermal load and using vastly different percolation rates.

For consistency with the ambient seepage models, the capillary-strength parameters close to the drift wall must be based on the effective properties provided by the SCM calibration. In the TH Seepage Model, these calibrated parameters were applied to the entire unit hosting the emplacement drifts, for reasons explained in BSC (2003 [161530], Section 6.2.2.1.4). A base-case value of $1/\alpha = 589$ Pa was assigned to both the Tptpmn and the Tptpll unit, similar to the mean value of the respective probability distribution developed in Section 6.4.1 of this report (591 Pa). As a sensitivity case, the capillary-strength parameter was set to a smaller value of 400 Pa (i.e., a parameter choice promoting seepage), similar to the lower bound of the respective probability distribution that describes the spatial variability of this parameter (402 Pa). Additional sensitivity analyses were conducted to evaluate the impact of different conceptual models for fracture-matrix interaction. The AFM, used for the base-case simulations, was compared to a standard dual-permeability method in which all fractures are considered "actively" flowing. It was demonstrated that the seepage rates calculated with the AFM are slightly higher than the DKM results. Note that the AFM is not needed for the drift-scale seepage models considering ambient conditions, such as the SCM and the SMPA. This is because (1) fracture-matrix interaction is not relevant for the steady-state simulations employed in these ambient seepage predictions, and (2) the effect of flow channeling on ambient seepage is already accounted for through explicit modeling of small-scale heterogeneity in the SCM and the SMPA. Also, the potential impact of all AFM effects on ambient seepage are automatically reflected in the observed seepage-rate data from liquid release tests and thus represented in the effective capillary-strength parameters calibrated by the SCM (BSC 2003 [162267], Section 6.3.2).

6.4.3.2 Model Validation

The TH Seepage Model was validated in comparison with three *in situ* heater tests conducted at Yucca Mountain (BSC 2003 [161530], Section 7). Particular focus was on the Drift Scale Test (DST), which is best suited for validation of the local TH processes because of its geometric setup. The model validation included quantitative evaluation of continuously measured temperature data—with a detailed analysis of subtle temperature signals indicative of TH coupling—as well as qualitative evaluation of periodic measurements that monitored moisture redistribution processes, using geophysical methods, air-injection data, and withdrawal of liquid water in packed-off boreholes. It was concluded from the good overall agreement between model and data that the uncertainty of predicted temperature, saturation, and water flux data was within acceptable ranges, implying that the model is essentially validated.

As pointed out in BSC (2003 [161530], Section 8.2), there are limitations related to the validation of the TH Seepage Model. While the DST results—as well as results from the other *in situ* tests—allow for a unique model validation with respect to the strongly perturbed near-field TH conditions in the rock mass, they offer no seepage data (observed seepage rates) that could be used directly for thermal seepage validation purposes. Direct validation of thermal seepage

would require a heater test operated at artificially enhanced percolation fluxes, to observe the seepage potential for extreme percolation conditions. Also, there was concern that the setup of the DST was allowing vapor to escape from the heated drift through the bulkhead (BSC 2003 [161530], Section 7.3.4). The issue of heat and mass losses through the bulkhead was discussed and evaluated in several thermal workshops. It was concluded that the objectives of the DST—acquiring a more in-depth understanding of the coupled TH processes and validating the conceptual models in comparison with data—were being met despite these heat and mass losses. However, it was also understood that the measurements in the DST should not be directly used to evaluate the potential of seepage into drifts during the thermal period, because the potential of seepage in the DST might be reduced as a result of the vapor losses. As a result of these limitations, validation of the seepage part of the TH Seepage Model is an indirect one, based on a separate assessment of the two relevant barriers. Validation of the coupled TH processes (using the DST data and data from other *in situ* tests) provides confidence regarding the predicted effectiveness of the vaporization barrier, while validation of the ambient-seepage conceptual model (using liquid-release data) provides confidence regarding the predicted effectiveness of the capillary barrier. (The conceptual framework for the capillary barrier treatment in the TH Seepage Model can already be considered validated, because the conceptual model is identical to the one validated and successfully applied in the SCM [see Section 6.4.1.1].) However, some uncertainty remains, since no direct test data on thermal seepage at extreme flux conditions are available. Another limitation stems from the fact that all three thermal tests have been conducted in the Tptpmn unit at Yucca Mountain; so far, there has been no testing in the lower lithophysal unit. Thus, validation of the TH Seepage Model does not include direct comparison with measured data from the Tptpll. While application of the validated model to the Tptpll unit is appropriate since similar TH processes need to be described, some uncertainty remains about the rock properties in this unit and the influence of lithophysal cavities.

The TH Seepage Model predictions regarding the effectiveness of the vaporization barrier were also tested in comparison with an alternative conceptual model of water flow in the superheated rock environment (BSC 2003 [161530], Section 6.3). In this model, the thermally perturbed downward flux from the condensation zone towards the superheated rock zone is conceptualized to form in episodic preferential-flow patterns. The effectiveness of the vaporization barrier was then tested for these extreme conditions where downward flux is fast and large in magnitude compared to average flow. A semi-analytical solution (Birkholzer 2003 [163686]) was employed to simulate the complex flow processes of episodic finger flow in a superheated fracture. With this solution, the maximum penetration distance into the superheated rock was determined for specific episodic flow events and thermal conditions, and the amount of water arriving at the drift crown was calculated.

It was demonstrated in BSC (2003 [161530], Section 6.3) that results of the alternative conceptual model are fairly consistent with the process-model results obtained with the TH Seepage Model. Most importantly, it was shown that finger flow is not likely to penetrate through the superheated rock during the first several hundred years of heating, when rock temperature is high and boiling conditions exist in a sufficiently large region above the drifts. These are the conditions when the largest thermal perturbation occurs, or, in other words, when the potential for episodic finger flow is highest. Only later, when the boiling zone is small and the impact of vaporization is limited, can finger flow arrive at the drift crown. The fact that water can reach the drift during the period of above-boiling temperatures makes the alternative

conceptual model distinct from the TH Seepage Model. However, the strong thermal perturbation observed at early heating stages has already diminished during this time period, and the net result of water arrival at the drift—considering the combined impact of water buildup in the condensation zone and vaporization in the superheated zone—is similar to ambient percolation. It was pointed out (BSC 2003 [161530], Section 6.3) that seepage of water into the drift is not expected from this limited water arrival, because the flow should be effectively diverted around the drift by the capillary barrier capability of the cavity. Note that these findings were consistent over a wide range of finger flow characteristics studied in a sensitivity analysis, covering the potential uncertainty in finger flow patterns. Thus the alternative conceptual model results clearly supports the main findings of the TH Seepage Model, adding confidence into the model and reducing the conceptual model uncertainty.

6.4.3.3 Model Results

The TH Seepage Model was applied to simulate the TH coupled processes for a period of 4,000 years after waste emplacement. This is the period when the main flow perturbations are expected to occur as a result of heating. A series of selected simulation cases was conducted for both the Tptpmn and Tptpll Submodels, comprising different thermal loads, various percolation flux scenarios, different capillary-strength parameters, and different conceptual models for fracture-matrix interaction (see overview of simulation cases in BSC 2003 [161530], Section 6.2.1.6). The resulting simulation data sets are provided in DTN: LB0303DSCPTHSM.001 [163688]. Transient seepage rates that were developed from these simulation data sets are given in DTN: LB0301DSCPTHSM.002 [163689]. The simulation results relevant for seepage abstraction are briefly discussed below.

For a given rock-property set, the predicted TH conditions are strongly driven by the thermal load placed into the drifts and by the local percolation flux. Example results are provided in Figure 6.4-13 in the form of rock temperature evolution along the perimeter of the drift. For the reference thermal mode, the heat generated from the waste canisters results in maximum rock temperatures at the drift wall between 120°C and 130°C, depending on the amount of percolation considered (see Figure 6.4-13a). The period of above-boiling rock temperature is about 1,000 years for the base-case flux scenario (i.e., 6, 16, and 25 mm/yr for the three climate states), and rock temperature at the end of the simulation period is still as high as 65°C. Increasing the percolation flux has considerable impact on the temperature evolution. Elevated percolation leads to cooler temperatures and a shorter boiling period. Strong heat-pipe signals become particularly evident for the simulation case with a flux multiplication factor of 20, where the percolation fluxes imposed at the top model boundary are 120, 320, and 500 mm/yr. Note that the intensity of heat pipes varies locally as a result of heterogeneity, giving rise to considerable differences along the drift wall in the duration of the boiling period. Three of the four thermal modes depicted in Figure 6.4-13b result in boiling conditions in the drift vicinity, with the maximum temperature and the duration of the boiling period depending on the respective heat load. Only one thermal mode, the low-temp mode, results in rock temperatures that never reach boiling conditions. Thermal effects on flow and seepage are negligible in this case, so that the potential for thermal seepage can be estimated from ambient seepage results.

As a first assessment of the potential for thermal seepage, the moisture redistribution processes in response to boiling of rock water have been analyzed in BSC (2003 [161530], Section 6.2) for

all simulation cases. In general, thermal seepage is possible only when (a) water arrives at the drift wall, depending on the vaporization impact, and (b) the saturation at the drift wall exceeds a given threshold value, defined by the capillary barrier effect at the rock-drift interface. The modeling results consistently demonstrate that the thermal perturbation of the flow field—causing increased downward flux from the condensation zone towards the drifts—is strongest during the first few hundred years after closure, corresponding to the time period when rock temperature is highest and the vaporization barrier is most effective. Even for high percolation fluxes into the model domain, and strong flow channeling as a result of fracture heterogeneity, water cannot penetrate far into the superheated rock during the time that rock temperature is above boiling. Thus, the potential for seepage is small. The majority of the vaporized (and subsequently condensed) matrix water is diverted around the dryout zone and drains away from the drift. At the time when temperature has returned to below-boiling conditions, fractures start rewetting at the drift wall. However, while the vaporization barrier has become ineffective, the capillary barrier at the drift wall may continue to reduce (or prevent) water seepage into the drift, as long as the seepage threshold saturation at the drift wall has not been exceeded. These transient processes are illustrated in Figure 6.4-14, giving the evolution of fracture saturation at all gridblocks adjacent to the drift wall. A representative simulation case has been selected with large percolation flux so that seepage is eventually observed (BSC 2003 [161530], Simulation Case MN-HET-03). The saturation curves show that no water arrives at the drift during the boiling period of approximately 500 years duration. As rock temperature decreases to and below the boiling point, and the first stepwise change in the percolation boundary condition occurs at 600 years, the saturation values build up strongly, while significant variability in saturation becomes evident. Water starts seeping into the drift at about 1,400 years after emplacement when the seepage threshold saturation is exceeded.

In a second step, transient seepage rates were explicitly calculated by the TH Seepage Model to directly quantify the potential for seepage during the thermally perturbed time period. These transient seepage rates were compared with results from ambient (steady-state) simulations that were conducted to provide reference values for evaluating the vaporization barrier. This allows for comparison of seepage results considering the combined effectiveness of the vaporization and the capillary barrier with seepage results considering only the capillary barrier contribution. Ambient seepage rates were derived by running the thermal seepage model without thermal load until a steady state was achieved (BSC 2003 [161530], Sections 6.2.2.2.2 and 6.2.3.2.2). This is done separately for each climate period using the respective percolation-flux boundary condition.

Example results illustrating the evolution of thermal seepage are given in Figure 6.4-15, for the same simulation case as selected in Figure 6.4-14. The magnitude of seepage is provided in percent, relative to the total liquid flux percolating with constant boundary flux through an area corresponding to the footprint of the drift. There is no seepage until about 1,400 years after waste emplacement. Seepage starts to occur several hundred years after the rock temperatures have dropped below boiling conditions, the delay caused by the retarded saturation buildup in the fractures. Initially, thermal seepage is considerably smaller than the respective ambient seepage value. With the stepwise increase of percolation flux at 2,000 years, the thermal seepage percentage increases considerably, but still remains smaller than ambient seepage. There is no enhanced seepage as a result of reflux of water (because most of the condensate has long before drained down away from the drift). At the end of the simulation period, the thermal seepage percentage is at 17%, slightly less than the ambient value of 20%.

Note that the ambient seepage percentage for the present-day infiltration rate with multiplication factor 10—i.e., 60 mm/yr—is zero in this case. In other words, even without heating of the repository, the capillary barrier at the drift wall is predicted to be fully effective during the first 600 years after waste emplacement. This provides additional confidence, as two barriers prevent seepage simultaneously and independently. It also suggests that incorporating the effect of vaporization into seepage abstraction may be less important than expected. This is because the period when vaporization processes are most effective always coincides with the period of present-day climate, where percolation flux is comparably small and ambient seepage is much less likely than during the monsoon and the glacial transition climate.

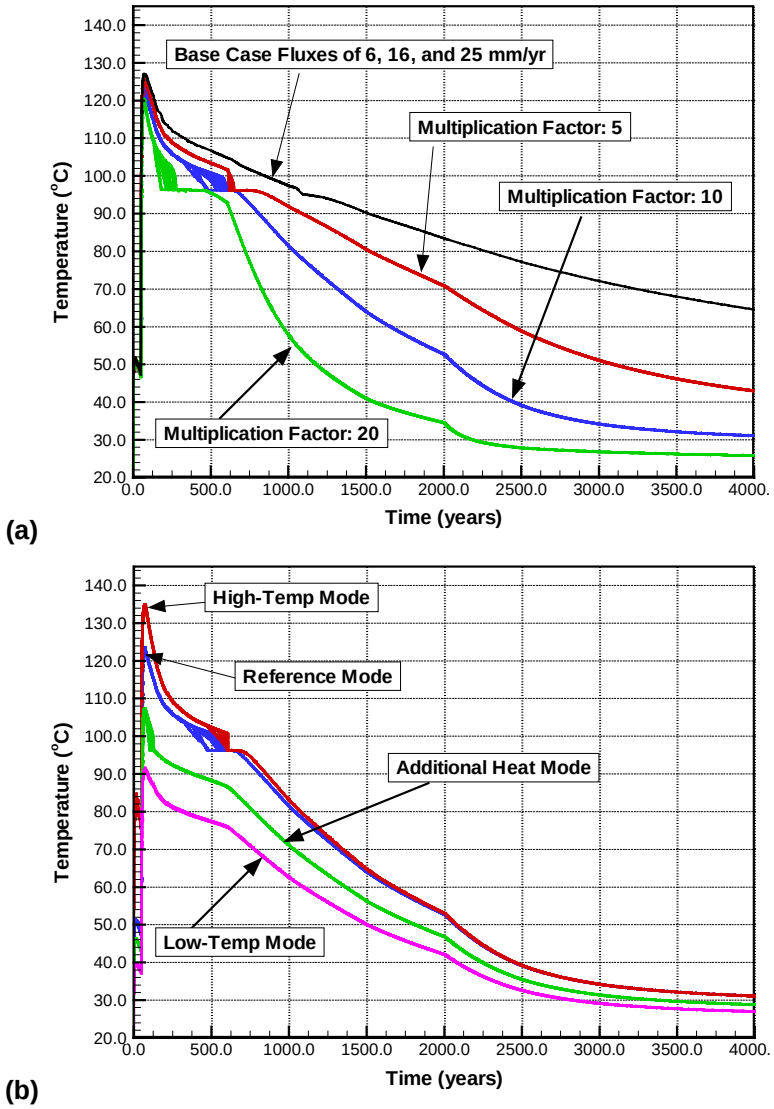

Source: DTN LB0303DSCPTHSM.001 [163688][1]

Figure 6.4-13. Rock Temperature Evolution at the Drift Wall for Tptpmn Submodel Showing (a) Different Percolation Flux Scenarios for Reference Thermal Mode, and (b) Different Thermal Modes for Percolation Flux Scenario with a Multiplication Factor of 10. For each scenario, the temperature histories in all gridblocks along the drift perimeter are depicted in the same color.

[1] The Readme document in DTN LB0303DSCPTHSM.001 [163688] explains where the various simulation cases can be found in the DTN data set. Figure 6.4-13a uses results from simulation cases MN-HET-01, MN-HET-02, MN-HET-03, and MN-HET-04. Figure 6.4-13b uses results from simulation cases MN-HET-03, MN-HET-05, and MN-HET-06. The simulation case for the Low-Temp Mode in Figure 6.4-13b is not named in the Readme document. Here, the results are in subdirectory /tptpmn_hetero_focus10_real1.dir/heat_lowtemp.dir. All results are for Realization 1 of the random permeability field.

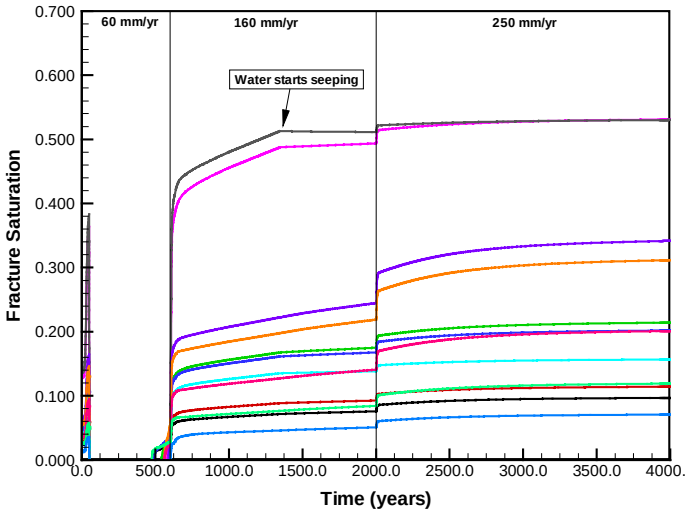

Source: BSC (2003 [161530], Figure 6.2.2.2-7a), underlying simulation results available in DTN LB0303DSCPTHSM.001 [163688], Simulation Case MN-HET-03, Realization 1

Figure 6.4-14. Fracture Saturation in Different Grid blocks along Drift Perimeter for Tptpmn Submodel and Reference Thermal Mode Using Percolation Flux Scenario with Multiplication Factor 10

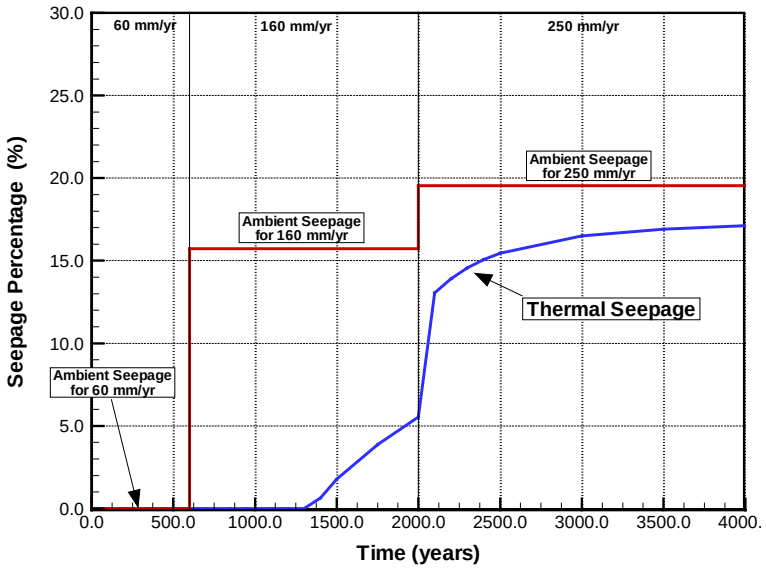

Source: BSC (2003 [161530], Figure 6.2.2.2-7b), underlying simulation results available in DTN LB0301DSCPTHSM.002 [163689], Simulation Case MN-HET-03, Realization 1

Figure 6.4-15. Seepage Percentage for Tptpmn Submodel and Reference Thermal Mode Using Percolation Flux Scenario with Multiplication Factor 10

As mentioned above, the different simulation cases studied with the TH Seepage Model show considerable variability with respect to the TH conditions in the rock. Despite this variability, there were several important observations with respect to thermal seepage that are common to all cases (BSC 2003 [161530], Sections 6.2.4 and 8.1):

(1) Thermal seepage was never observed in simulation runs where the respective ambient seepage was zero.

(2) Thermal seepage never occurred during the period of above-boiling temperatures in the rock close to the emplacement drifts.

(3) In simulation cases where ambient seepage was obtained, thermal seepage was initiated at several hundred to a few thousand years after rock temperature has returned below boiling.

(4) Thermal-seepage rates were always smaller than the respective ambient reference values. The ambient seepage values provide an asymptotic upper limit for thermal seepage.

While these main conclusions hold for all simulation cases, considerable variability exists among simulation runs with respect to the thermal-seepage initiation time, the evolution of seepage with time, and the long-term rate of thermal seepage. From the quantitative and qualitative results presented in BSC (2003 [161530], Sections 6.2.2.2.4, 6.2.3.2.3, 6.2.4.2, 6.2.4.3), the key parameters affecting thermal seepage can be categorized as follows: (1) parameters mainly affecting the TH conditions, (2) parameters mainly affecting the capillary barrier behavior, and (3) parameters with impact on both the TH conditions and the capillary barrier behavior.

The thermal load and thermal conductivity, for example, belong to the first category. Varying these parameters results in considerable differences in the duration of the boiling period and the predicted maximum temperature in the rock. These conditions are important for the initiation time and the evolution of thermal seepage, but do not change the ambient seepage rate (which defines the asymptotic upper limit for thermal seepage at later stages). Results showing the sensitivity of thermal seepage to the thermal load are given in Figures 6.2.4.2-3 and 6.2.4.2-4 of BSC (2003 [161530]). Fracture capillary strength belongs to the second category. This parameter has minor impact on the TH behavior in the fractured rock, as shown in Section 6.2.2.1.4 of BSC (2003 [161530]), but significantly affects the asymptotic upper limit for thermal seepage at later stages. As a result of the different seepage threshold saturation, the initiation time and evolution of thermal seepage can also be affected. Results for a small capillary-strength parameter of $1/\alpha$ = 400 Pa are presented in BSC (2003 [161530], Figure 6.2.4.2-5), to be compared with the respective simulation case using $1/\alpha$ = 589 Pa (BSC 2003 [161530], Figure 6.2.2.2-7b, which is also Figure 6.4.11 in the present report).

The third category comprises parameters that are important for ambient seepage and also affect the intensity of TH coupling. Large percolation fluxes, for example, are typically related to large ambient seepage rates (see Section 6.4.1.2). At the same time, increased percolation flux gives rise to a reduction of temperature and a shorter duration of the boiling period. Thus, for large percolation fluxes, thermal seepage may start earlier *and* approach larger asymptotic values at later stages of heating. Example results illustrating the impact of percolation flux changes are given in Figures 6.2.4.2-3 and 6.2.4.2-4 of BSC (2003 [161530]).

Changes in fracture permeability can also affect both the vaporization and the capillary barrier, but are expected to have counteracting effects on these barriers. Large permeabilities are generally beneficial for the performance of the capillary barrier, because they allow for more flow diversion around the drifts. The vaporization barrier, on the other hand, may be less effective because large permeabilities may cause strong heat-pipe processes that would result in

considerably lower rock temperatures. This discussion indicates that the relationship between the relevant parameters and the seepage results can become very complicated when coupled TH processes are considered.

6.4.4 Supporting THM and THC Models

This section briefly describes the conceptual framework and modeling results from the coupled THM and THC simulation models. The information provided by these models is utilized in the seepage abstraction to assess the magnitude and impact of mechanical and chemical parameter alterations of relevant rock properties during the heating phase of the repository. Note that these models do not directly calculate seepage rates. Having coupled THM or THC models directly provide seepage rates is desirable, but not feasible because of the computational burden involved in such simulations—in particular because seepage calculations have to be available for a large number of parameter sets to cover spatial variability and uncertainty of relevant properties.

6.4.4.1 Drift-Scale THM Model

The Drift-Scale THM Model is applied to assess the magnitude and distribution of stress-induced changes in hydrological properties and to analyze the impact of such changes on the percolation flux in the rock mass around a repository drift (BSC 2003 [162318]). Heating of the rock will cause thermal expansion of the rock, which in turn will change the stress field around emplacement drifts. Thermally induced changes in the stress field will act upon pre-existing fractures, with the result of changing the hydrological properties of the rock mass. Note that the model analysis focuses on these thermal expansion effects; the impact of drift collapse on the hydrological properties of the remaining rock above the rubble-filled cave—a potential result of joint cohesion loss or seismic events—has not been considered in this THM analysis.

The Drift-Scale THM Model uses the simulation tool TOUGH2-FLAC for the thermal-hydrological-mechanical processes, based on joining together the multiphase flow and transport simulator TOUGH2 V1.6 (LBNL 2003 [161491]) with the rock and soil mechanics industry-standard FLAC3D V2.0 code (LBNL 2001 [154783]; BSC 2003 [162318], Section 6.2). The modeling framework for the TH processes—boundary conditions and rock properties—is similar to the TH Seepage Model as described in Section 6.4.3. However, while the TH Seepage Model focuses on the TH conditions to evaluate seepage rates for various seepage-relevant parameter cases, the THM simulations concentrate on the heat-induced stress changes and resulting impact on the flow field. Predictive simulations were conducted with the Drift-Scale THM Model for 10,000 years after waste emplacement. Careful model validation was performed in comparison with rock-mass displacement data (for TM processes) and air-permeability data (for HM processes) measured during the heating phase of the DST (BSC 2003 [162318], Section 7). Generally, the model captured the THM behavior in the heated DST rock mass reasonably well. In particular, the THM Model was capable of representing the transient changes in air-permeability data, stemming from two simultaneous processes: fracture aperture changes in response to stress changes and relative permeability changes in response to water saturation changes (BSC 2003 [162318], Section 7.4.3). Note that the air-injection results from the DST were also used to calibrate the stress-permeability relationship that is needed for coupled THM simulations. For the predictive model runs, a conservative estimate of this relationship was adopted. This relationship is conservative in the sense that it is calibrated to capture the strongest

observed changes in air permeability in the DST (BSC 2003 [162318], Section 7.4.3). The predictive model results are thus likely to overestimate the impact of stress on the flow processes compared to a more moderate relationship.

Results from the THM predictive simulations are given in Sections 6.5 (for a drift located in the Tptpmn unit) and 6.6 (for a drift located in the Tptpll unit) of BSC (2003 [162318]). Both simulation cases assume average thermal loads and percolation boundary conditions. At the drift ceiling (i.e., the region important for seepage), the calculations show generally a decrease in vertical permeability as a result of temperature-induced stresses, while the horizontal permeabilities remain essentially unchanged from the initial post-excavation values (BSC 2003 [162318], Figures 6.5.4-3, 6.5.4-4, 6.6.1-4 and 6.6.1-5). The vertical permeability changes are much more pronounced in the Tptpmn unit compared to the Tptpll. In both units, the transient permeability changes are strongest at around 100 to 500 years after emplacement. At later stages, the declining temperatures allow the stresses and the vertical permeability values to recover somewhat, but not to their initial values because the rock temperatures are still higher than ambient. For example, in the Tptpmn, the vertical permeability immediately above the drift crown at 10,000 years after emplacement still remains one order of magnitude below its initial value.

The impact of these permeability changes on the flow field was investigated in BSC (2003 [162318], Sections 6.5.5 and 6.6.2) by comparison of the fully coupled THM simulations with TH simulations where the stress-induced property changes were neglected. This analysis indicated that the flow field differences are small to moderate, but that the reduction in vertical permeability combined with the basically unchanged horizontal permeability appeared to give rise to less water reaching the drift crown (Figure 6.4-16). It was suggested in BSC (2003 [163226], Section 6.7) that these anisotropic THM property changes would increase the likelihood of flow being diverted around the drift and thus decrease the potential for seepage.

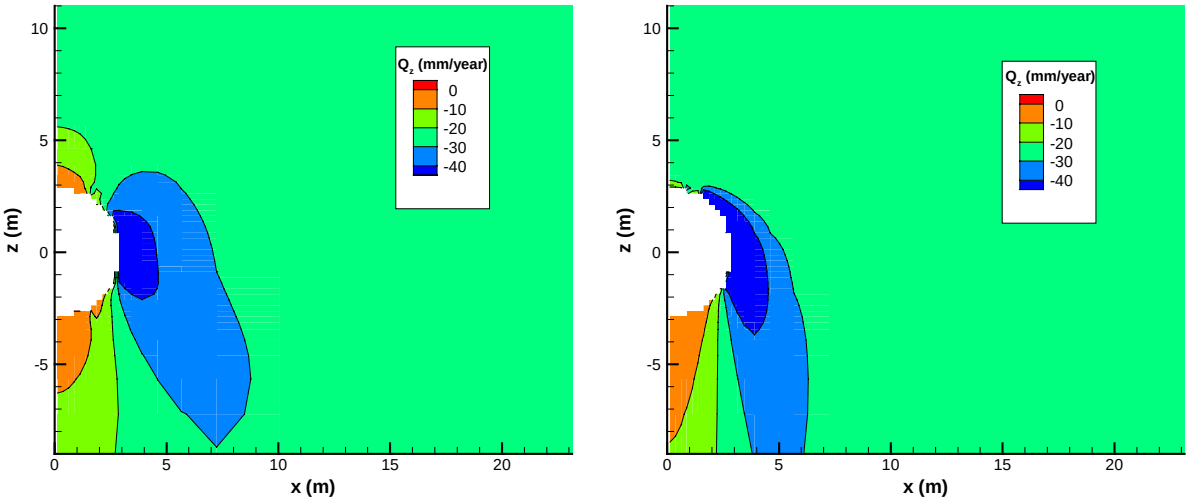

Source: BSC (2003 [162318], Figure 6.5.5-5)

Figure 6.4-16. Example Result Illustrating the Difference in Vertical Percolation Flux in the Fractures at 10,000 Years for a (a) Fully Coupled THM Simulation and (b) TH Simulation (Tptpmn Model Domain)

To confirm this point, ambient seepage calculations were conducted with the THM model using the initial post-excavation permeability field without THM changes (BSC 2003 [162318], Figure 6.5.1-1) and the permeability field at 10,000 years after emplacement including THM changes (BSC 2003 [162318], Figures 6.5.4-3(d) and 6.5.4-4 (d)). The conceptual framework applied for these seepage calculations was similar to that of the SMPA, except that the small-scale heterogeneity in the permeability field was neglected. Results from these simulations are shown in Figure 6.4-17. The calculated seepage rates for the THM permeability field are reduced by about 10% from the values calculated for the initial permeability field, over the entire range of percolation fluxes analyzed (0 mm/yr to 3,000 mm/yr). It was concluded in BSC (2003 [163226], Section 6.7), that an ambient seepage model without consideration of anisotropic THM property changes is capable of predicting seepage rates with sufficient accuracy. Thus, the SMPA results are representative over most of the 10,000-year compliance period, with the possible exception of the first 1,000 to 2,000 years where the TH processes are strongly perturbed from boiling.

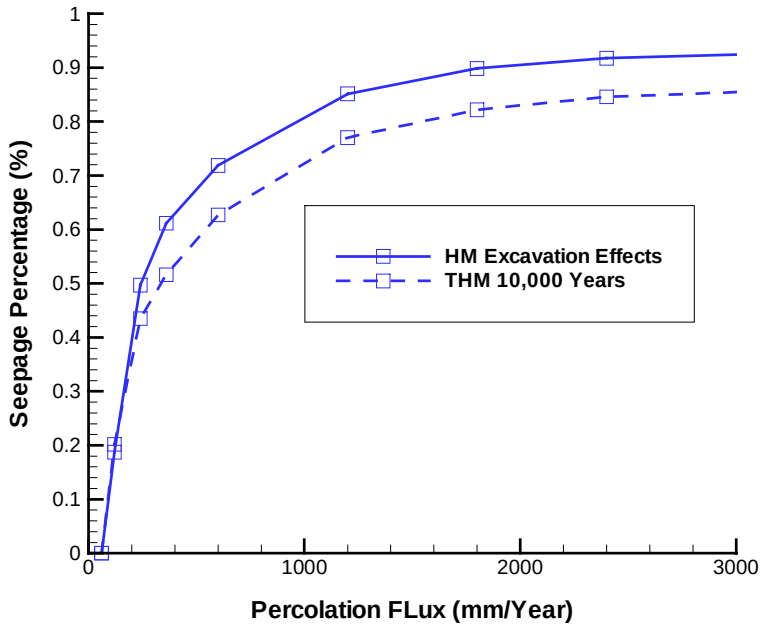

Source: DTN: LB0304SMDCREV2.004 [163691] (File Fig6-22.wmf)

Figure 6.4-17. Seepage Percentage as a Function of Percolation Flux Simulated Using the Initial Post-Excavation Permeability Field without THM Changes (HM Excavation Effects) and the Permeability Field at 10,000 years after Emplacement Including THM Changes (THM 10,000 Years)

6.4.4.2 THC Seepage Model

The THC Seepage Model is a drift-scale process model for predicting (1) the composition (not the rate) of gas and water that could enter waste emplacement drifts and (2) the effects of mineral alteration on flow in rocks surrounding drifts (BSC 2003 [162050]). The latter effect can be important for seepage abstraction: Mineral precipitation is predicted to form “precipitation” caps of calcite, silica, and other minerals above emplacement drifts, leading to changes in fracture porosity, permeability, and local percolation.

The THC Seepage Model is based on the thermal-hydrological model introduced in Section 6.4.3. As a result, the modeling framework for the thermal-hydrological simulations—including grid design, boundary conditions, and rock properties—is similar in these models. However, whereas the TH Seepage Model focuses on the TH conditions to evaluate seepage rates for various seepage-relevant parameter cases, the THC simulations concentrate on the chemical processes and their related sensitivities. Predictive simulations are conducted with the THC Seepage Model for a time period of 100,000 years after waste emplacement. The model includes a wide range of major and minor aqueous species and minerals. Sensitivity studies were performed to evaluate the impact of, for example, alternative geochemical systems, initial water compositions, and reaction rates. Careful model validation was conducted in comparison with measured gas compositions, water chemistry, and analyses of mineral composition in the DST (BSC 2003 [162050], Section 7). Model results were also compared with measured water compositions from a laboratory plug-flow dissolution experiment. In addition, a fracture-sealing laboratory experiment was simulated to compare precipitation data. In general, the model captured the trends in gas composition, water chemistry, and mineral precipitation reasonably well.

The effects of mineral precipitation and dissolution of flow processes in the drift vicinity are discussed in Section 6.8.5.4 of BSC (2003 [162050]). The simulation results suggest that a thin region of significantly decreased fracture permeability will form several meters above the drift crown, created by mineral deposition at the boiling front (mainly silica, to a lesser extent calcite). Mineral precipitation is particularly strong in this region because the boiling front remains at this location for several hundred years. Note that there is no indication that significant precipitation may occur immediately at the drift wall. This means that the local permeability and porosity in the boundary layer above the drift wall, important for the capillary barrier behavior, are not affected by THC alterations. Figure 6.4-18 illustrates the spatial distributions of permeability changes and demonstrates its impact on the flow conditions at 2,400 years after emplacement. While the permeability values directly at the drift wall remain unchanged, there is a permeability decrease by a factor of 10 in an area 7-8 m above the drift. As a result, percolating water is partially deflected sideways at this low-permeability zone, so that less water arrives at the drift crown (BSC 2003 [162050], Figure 6.8-42). Since the amount of seepage is correlated to the local percolation flux, this kind of “umbrella effect” would give rise to less seepage compared to a simulation without permeability changes. Note that the permeabilities shown at 2,400 years remain essentially unchanged for the rest of the simulation period of 100,000 years, because the silica solubility decreases with declining temperature.

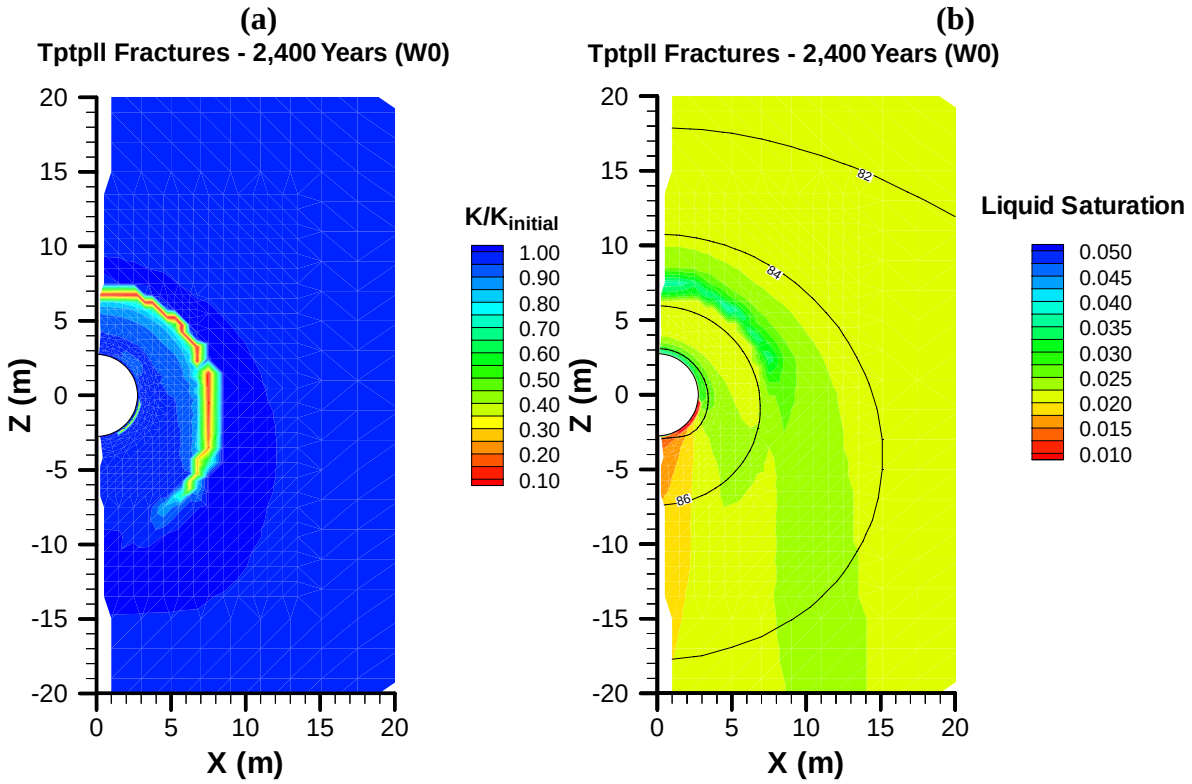

Source: BSC (2003 [162050], Figure 6.8-40)

Figure 6.4-18. Example of Effects of Mineral Alteration as Predicted by the THC Seepage Model: Contour Plot of Modeled (a) Permeability Change and (b) Liquid Saturation and Temperature Contours (^{o}C) at 2,400 Years

BSC (2003 [162050], Section 6.8.5.4) presents several sensitivity cases for mineral alteration results using different initial water compositions (Water W0 through W5), showing significantly different permeability changes using these waters. Fracture porosity changes also depend strongly on the initial porosity estimate for the fracture continuum, which is hard to quantify (BSC 2003 [162050], Section 8.2). It is also expected that variability in the TH conditions (e.g., stemming from thermal-load differences, percolation-flux variability) will bring out strong differences in the precipitation patterns. This variability was not addressed in the THC simulation runs.

6.5 SEEPAGE ABSTRACTION METHODOLOGY

The purpose of the seepage component in TSPA-LA is to calculate the seepage rate (amount of seepage per time) and the seepage fraction (the fraction of waste packages affected by seepage) as a function of time and location in the repository (CRWMS M&O 2000 [148384], Section 6.3.1.2). The calculation is performed using a probabilistic approach that accounts for the spatial and temporal variability and inherent uncertainty of seepage-relevant properties and processes. The resulting information takes the form of probability distributions for seepage events. These distributions are used for subsequent TSPA calculations that may handle, for example, waste form degradation or radionuclide transport. Depending on the downstream modules, the resulting distributions may be directly used or propagated in simplified form (histograms, sorting in bins).

The purpose of this seepage abstraction is to provide the necessary methodology, tools, parameter distributions, look-up tables, and simplifications to the TSPA-LA, so that the seepage calculations can be performed by the respective TSPA module. The abstraction does *not* provide TSPA-LA with the resulting distributions of seepage rate and seepage fraction over the repository area. However, Section 6.8 of this Model Report does include a stochastic evaluation of seepage, where the probabilistic seepage calculation of the TSPA module is adopted in a simplified manner. The purpose of this stochastic evaluation is (1) to demonstrate the barrier capability of the UZ above the repository, and (2) to derive the sensitivity of seepage results to various parameters. The latter helps to justify some of the choices made in the abstraction process (e.g., the choice of particular shapes of probability distribution functions). While the results of Section 6.8 are not directly utilized in the TSPA-LA, they may be useful as corroborative information for comparison with results from the TSPA seepage module.

Seepage is variable in space because of variability in percolation flux and heterogeneity in key hydrological properties. In addition, seepage may be affected by heat output from the decaying radioactive waste, from changes in hydrological properties as a result of mechanical and chemical effects, from changes in the drift shape due to drift degradation, and from the presence of rock bolts used for ground support. Several of these factors are also time-dependent, such as percolation flux and thermal effects. The methodology of incorporating each of these factors in seepage abstraction is directly based on the process-model results as described in Section 6.4. The general procedure has two main steps, as follows:

(1) The ambient seepage results derived from the SMPA provide the basis for the quantitative evaluation of seepage as a function of key hydrological properties. The key hydrological parameters defining ambient seepage—capillary-strength $1/\alpha$, permeability k, and local percolation flux $q_{perc,ff}$—are described by appropriate probability distributions, as defined in Section 6.6. For a particular set of these key parameters, sampled from the respective distributions, the ambient seepage rate and its inherent estimation uncertainty are interpolated from the seepage look-up tables provided by the SMPA. The sampling and interpolation procedure is further explained in Section 6.5.1. Depending on the considered TSPA event, the sampling will be either conducted from the look-up table for non-degraded drifts (presented in Section 6.4.2.3) or from the look-up table for collapsed drifts (presented in Section 6.4.2.4.2). Specifics to the abstraction of drift degradation effects are provided in Section 6.5.1.5.

(2) The ambient seepage rates are then adjusted to account for potentially important factors such as thermal effects on seepage, drift degradation, and rock bolts, if necessary. Thermal effects on seepage include potential changes in key properties (Section 6.5.1.4) as well as changes in the resulting seepage rates (Section 6.5.2). These adjustments involve simplifications of complex model results. The simplification approaches and their scientific bases are explained in detail in the subsections below.

The TSPA procedure of calculating seepage is schematically illustrated in Figure 6.5-1. The TSPA calculations run over several time steps to account for the temporal variability of relevant processes (e.g., CRWMS M&O 2000 [148384], Section 6.3.1.2). Within each time step, random sampling of uncertainty distributions is conducted for a sufficiently large number of realizations R. Within each realization R, the seepage rate is evaluated at a sufficiently larger number of spatial locations r in the repository area. Over all locations, the resulting number of locations with seepage, relative to the total number of locations, defines the seepage fraction f_{seep} for the realization and the time considered. Details are provided in the following subsections.

Note that abstraction as outlined above attempts to extract the salient features of the expected seepage behavior by compiling and reviewing field data and by simplifying the results previously obtained with complex process models (such as the SMPA and Thermal Seepage Model). No new mathematical model was developed for seepage abstraction, and consequently there are no related equations, algorithms, numerical methods, or other software/computational methods that need to be discussed in this Model Report. Statistical concepts and methods are used to develop parameter distributions; the related computations are fully documented in this Model Report, specifically in Attachments I through V.

6.5.1 Abstraction of Ambient Seepage

The seepage component in TSPA directly uses the seepage look-up tables provided by the SMPA model results to calculate ambient seepage rates. There is no simplification or other processing of these results involved that would need to be developed within the abstraction process. Thus, the relevant small-scale processes simulated with the ambient-seepage process models are inherently included in TSPA without loss of information. One important role of seepage abstraction is to derive the appropriate probability distributions for seepage-relevant parameters that feed into the look-up tables for seepage. The probability distributions developed within the abstraction need to account for the spatial variability and the uncertainty of these seepage-relevant parameters. The impact of additional factors, such as THC and THM parameter changes, drift degradation, and rock bolts, needs to be assessed and appropriately accounted for.

6.5.1.1 Random Sampling Methodology

The key hydrological parameters for ambient seepage are the capillary strength $1/\alpha$, local permeability k and percolation flux $q_{perc,ff}$. According to the conceptual model of the seepage process models (SCM and SMPA, see sections 6.4.1 and 6.4.2), the following guidelines apply for defining the respective parameter distributions:

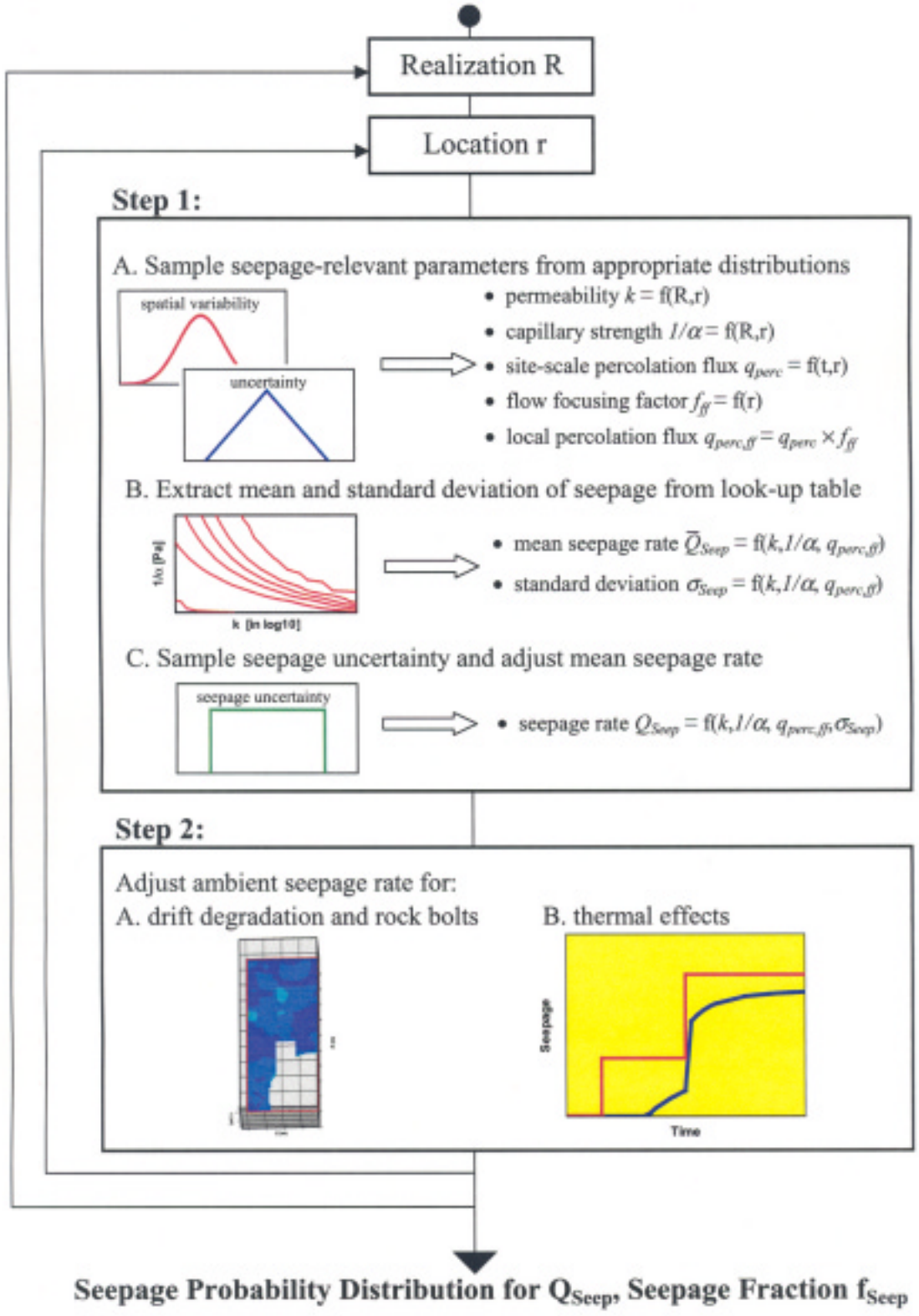

Figure 6.5-1. Probabilistic TSPA Procedure for Calculating Seepage at Selected Time Steps

Since small-scale heterogeneity (on the order of 1 foot or less) is explicitly accounted for in the SMPA, the spatial variability to be described by probability distributions is the variability over the repository area that occurs on the spatial resolution of a few drift diameters or more (intermediate-scale heterogeneity).

(1) The capillary-strength parameter distribution must be representative of the effective parameter values calibrated from the SCM.

(2) The permeability parameter distribution provided to the TSPA must represent the mean values of the small-scale permeability fields used in the SMPA. The standard deviation and the correlation structure of these small-scale fields are not varied in the TSPA because the "best" parameter estimates produced seepage rates that were either comparable to or larger than seepage rates calculated from selected sensitivity cases (Section 6.4.2).

(3) The permeability distribution must be representative of the excavation–disturbed zone in the vicinity of the drifts.

Following this guidance and based on evaluation of available measurements and model data, appropriate probability distributions are developed in Section 6.6 of this report. For permeability and capillary strength, the resulting distributions are representative of the ambient conditions in the drift vicinity prior to heating of the rock. The abstraction methodology for incorporating time-dependent changes in these properties, e.g., stemming from THM or THC effects, will be discussed in Section 6.5.1.4. It will be demonstrated that these changes can be neglected in seepage abstraction, so that the derived parameter distributions are valid for the entire 20,000-year TSPA period. The percolation flux, on the other hand, is time-dependent, as a result of future climate changes. Three different spatial distributions representative of three future climate stages are used to account for the temporal evolution of percolation flux (Section 6.6.4).

The probabilities assigned to the relevant parameters distinguish explicitly between spatial variability and uncertainty, using separate distributions. Distinguishing between aleatory and epistemic uncertainty is not important for estimates of mean risk, but helps us to better understand the respective contributions of variability and uncertainty (BSC 2002 [158794], Section 4.1.2). As explained in Section 6.6, spatial variability of permeability is described by a log-normal probability distribution, whereas spatial variability of the capillary-strength parameter is expressed by a uniform distribution. The uncertainty of both parameters is represented by triangular distributions, with a mean of zero and a range value defining the uncertainty of the parameter (Mishra 2002 [163603], Section 2.3). Potential sources of uncertainty included in this triangular distribution are (1) measurement uncertainty, (2) spatial variability uncertainty, (3) conceptual model uncertainty, and (4) estimation uncertainty (Section 6.6). A schematic illustration of the random sampling procedure is given in Figure 6.5-2. In the outer calculation loop over realizations R, the spatial variability distributions for permeability and capillary strength are adjusted to account for uncertainty, using random samples of the triangular uncertainty distribution. The inner calculation loop of the TSPA seepage component conducts random sampling of the adjusted spatial variability distributions at each of the several thousand locations r in the repository area, to derive values of permeability and capillary strength. Separate distributions of r are used for each realization R, accounting for the uncertainty in the generated random fields. Note that the two main host-rock units, the Tptpll and

the Tptpmn, may have separate distributions to account for differences in the hydrological properties.

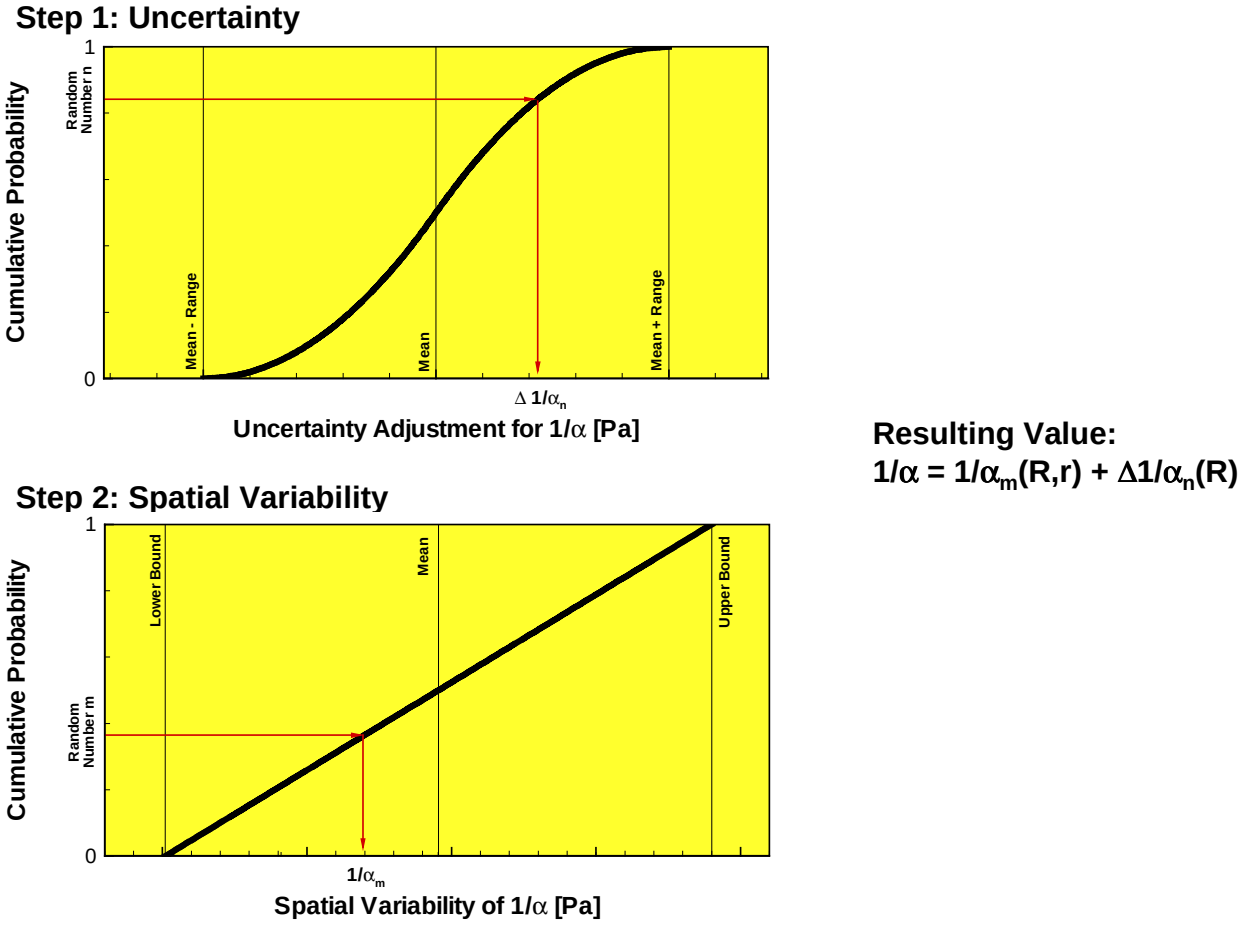

Figure 6.5-2. Schematic Illustration of Random Sampling Procedure for Capillary-Strength Parameter 1/α, Using Cumulative Probability Distributions for Spatial Variability (Uniform) and Uncertainty (Triangular)

The procedure for sampling of local percolation fluxes $q_{perc,ff}$ is slightly different from sampling of the other parameters. As explained in Section 6.6.4, the flux variability is provided by model results from the UZ Flow and Transport Model (BSC 2003 [163045], Section 6.6). These fluxes are provided for three different climate stages (present-day climate, monsoon climate, and glacial transition climate), during which the UZ model flow fields are considered steady state. Which one of these flow fields is to be used for sampling depends on the time step considered in the TSPA calculation. For each time step, the local fluxes at the several thousand locations r in the repository area are interpolated from the simulated flux distributions. Uncertainty inherent in these flux distributions is expressed by using several alternative scenarios of spatial flux distributions, each of them associated with a certain occurrence probability. These scenarios are the mean, the upper-bound and the lower-bound scenario, available for two different conceptualizations of flow in the PTn unit. Because each scenario covers three climate periods, there are 18 different flux distributions altogether. (However, only nine of them are relevant for

TSPA, as shown in Sections 6.6.4.1 and 6.8.2.) For reasons discussed in Section 6.6.4, the local flux values need to be multiplied with flow focusing factors f_{ff} that lead to increased fluxes in some areas, while reducing them in others. These factors, also spatially variable and thus randomly sampled in r, account for intermediate-scale heterogeneity not represented in the above mentioned flux distributions. Multiplication of the local fluxes q_{perc} from the site-scale model with the flow focusing factors f_{ff} gives the local percolation flux $q_{perc,ff}$ to be used in the TSPA calculation.

Note that the respective probability distributions for capillary strength, permeability, and percolation flux are not correlated. This means that the random variables used to sample from the respective distributions should be generated independently in the TSPA. There are theoretical reasons to expect that the permeability and the capillary strength in a single fracture should be negatively correlated, since both are related to the fracture aperture. Overall, such negative correlation would give rise to smaller seepage estimates compared to a no-correlation assumption. This is because, for each sampled parameter set, a parameter value promoting seepage (e.g., large capillary strength $1/\alpha$) would coincide with a parameter value reducing seepage (e.g., small permeability k), and vice versa. These opposite effects would partially cancel out so that there would be fewer "extreme" seepage cases, leading to an overall reduction in seepage. However, the calibrated capillary-strength parameter derived from the SCM is not just related to fracture aperture; it is an effective continuum process parameter that implicitly accounts for many additional factors affecting seepage (see Section 6.4.1.1). Thus, no predictable correlation exists between permeability and the effective capillary-strength parameter, and the no-correlation model should be used in TSPA (Section 6.6.1.1). One might also expect that local permeability and flux were positively correlated (which is the case in saturated flow). Though this would again give rise to less seepage, TSPA should not assume such a correlation. The flow patterns in the heterogeneous, unsaturated rock at Yucca Mountain are determined by various factors (e.g., boundary conditions, geological structure) in addition to local properties.

6.5.1.2 Seepage Interpolation

Seepage rates are calculated for each set of seepage-relevant parameters derived in the random sampling procedure over R realizations and r locations, using the seepage look-up tables provided by the SMPA. The sampling and interpolation procedure is identical for the two look-up tables provided for non-degraded and collapsed drifts. Seepage results should be derived from a linear interpolation between the seepage values in the SMPA look-up table. The tabulated value resolution provided by the systematic SMPA simulation runs is fine enough to justify linear interpolation, even though the functional relation between seepage results and input parameters may be nonlinear overall. The look-up tables (DTN: LB0304SMDCREV02.002 [163687]) generated by the SMPA contain the mean seepage value $\overline{Q}_{seep}$ and the standard deviation σ_{seep} over 20 realizations, given either as seepage rate per waste package or as seepage percentage.

The finite probability distributions chosen for the capillary-strength parameter are sufficiently bracketed by the parameter range covered in the SMPA results (i.e., 100 Pa to 1,000 Pa, see Section 6.4.2.3). In contrast, the unbounded distribution for permeability can possibly exceed the range simulated with the SMPA (i.e., –14 to –10 in log10, see section 6.4.2.3). However, the

probability that sampled permeability values fall outside of the SMPA range is very small, as demonstrated in Section 6.8.2. (For comparison, the 99% confidence interval for the spatial variability distributions developed in Section 6.6.2 ranges approximately from –13.2 to –11.2 for the Tptpmn and from –12.9 to –10.1 for the Tptpll). In the unlikely case that a sampled log-permeability value is smaller than –14, it should be set to –14. Similarly, log-permeability values exceeding the upper bound of –10 should be set to –10. The impact of this truncation on seepage results is insignificant.

A similar methodology is recommended for truncating the local percolation-flux distributions $q_{perc,ff}$. Flux values smaller than 1 mm/yr should be set to 1 mm/yr, the smallest percolation flux simulated with the SMPA. At such small fluxes, seepage is only expected for extreme parameter combinations, so that this flux adjustment has almost no effect on the seepage results. Percolation fluxes larger than 1,000 mm/yr should be set to 1,000 mm/yr. As pointed out in Section 6.6.4.3, local percolation fluxes larger than 1,000 mm/yr are theoretically possible (as a result of climate changes, spatial variability, and flow focusing), but extremely unlikely. Therefore the impact on the seepage results is negligible.

6.5.1.3 Ambient Seepage Uncertainty

The uncertainty inherent in the ambient seepage results is a result of uncertainty in the key input parameters to the model, as well as uncertainty that arises from the modeling methodology independent of the model input. As mentioned above, uncertainty in the input parameters is accounted for in the TSPA by feeding appropriate probability distributions into the seepage look-up tables derived from the SMPA. These distributions are developed in Section 6.6. Uncertainty inherent in the modeling methodology can stem from uncertainty in the conceptual model used for the seepage simulations (conceptual model uncertainty) and from uncertainty about the local heterogeneity considered in the SMPA (estimation uncertainty). These are accounted for in the abstraction as follows:

(1) The conceptual model used in the SMPA is adopted from the conceptual framework of the seepage calibration analyses, conducted with the SCM. As pointed out in Section 6.4.1, the SMPA and the SCM are in fact similar models that are used for different purposes. Both are sophisticated seepage-process models considering the scale and the conditions of interest. The modeling framework is consistent with the conceptual and numerical models used for calculating flow and transport in the UZ at Yucca Mountain. The calibrated SCM with the appropriate effective parameters is capable of reproducing and predicting observed seepage data from liquid-release tests conducted above and below the seepage threshold. The SMPA predictions are thus likely to yield reasonable estimates of seepage into waste emplacement drifts. Alternative conceptual models that corroborate the findings of the SCM have been qualitatively discussed in BSC (2003 [162267], Section 6.4). Altogether, the conceptual model uncertainty should be small compared to other sources of uncertainty that are explicitly accounted for using cautiously realistic uncertainty estimates. Therefore, the contribution of conceptual model uncertainty is neglected in the abstraction of ambient seepage.

(2) Because the exact structure of local heterogeneity in the drift vicinity is unknown, multiple realizations of stochastic permeability fields were studied with the SMPA. The

spread of results stemming from these realizations defines the estimation uncertainty of seepage. This uncertainty contribution, as described by the standard deviation values given above, must be accounted for in the TSPA calculations. As recommended in Section 6.4.2, a uniform probability distribution should be used to describe the estimation uncertainty. This uniform distribution, which is different for each parameter set, has a mean of zero and a range defined by the interpolated value of the seepage standard deviation. It can be easily shown that the upper bound of a uniform distribution with mean zero and standard deviation σ_{seep} is given as $+1.732\ \sigma_{seep}$, the lower bound is $-1.732\ \sigma_{seep}$ (derived from Mishra 2002 [163603], Section 2.3; see Scientific Notebook Birkholzer 2003 [164526], p. 123). Seepage uncertainty values are randomly sampled from the uniform uncertainty distribution and then used to adjust the mean seepage values. After adjusting the seepage rates, the results must be checked for consistency. Seepage rates smaller than zero are set to zero. Seepage rates that correspond to a seepage percentage of more than 100% (i.e., the resulting seepage is larger than the percolation flux over the drift segment) are set to a seepage rate corresponding to a seepage percentage of 100%.

6.5.1.4 Abstraction of THM and THC Parameter Alterations

The section below explains why the expected time-dependent alterations of seepage-relevant properties, stemming from THM and THC effects in response to the elevated temperatures in the repository, can be (or should be) neglected in the seepage simulations conducted in the TSPA. In other words, the ambient SMPA results can be directly applied for most of the 20,000-year TSPA period (except for the time period of strongly perturbed thermal conditions). Also, the parameter distributions for capillary strength and permeability can be considered constant in the seepage abstraction.

THM Parameter Alterations

The THM simulations discussed in Section 6.4.4.1 suggest that temperature-induced stress changes give rise to changes in the vertical fracture permeability in the vicinity of waste emplacement drifts, in particular in the Tptpmn unit. It was demonstrated, however, that these permeability changes do not result in significant changes in the flow fields. In particular, the seepage rates calculated for a permeability field including THM permeability changes were similar to, but slightly smaller than those calculated for a permeability field representative of the initial post-excavation conditions. The SMPA simulation results provide reasonably accurate (slightly conservative) estimates of the expected seepage rates at long-term conditions with coupled THM property changes. Therefore, the impact of THM property changes is neglected in the seepage abstraction. The seepage abstraction model uses the ambient seepage rates without accounting for the transient THM changes in seepage-relevant properties. The rationale for neglecting THM effects is listed below:

(1) Including the impact of THM property changes would result in slightly smaller seepage rates in the TSPA analyses. However, the limited benefit of including THM effects does not justify the complexity of implementing these processes in the TSPA analyses.

(2) The THM simulation results were conducted for average TH conditions using best THM property estimates. Because of computational limitations, the potential variability in these conditions and properties could not be fully addressed in the THM simulation.

(3) The stress-permeability relationship used in the predictive THM simulations is relatively conservative; i.e., the permeability changes predicted by the model are likely to be overestimated.

(4) While the DST displacement results indicate predominantly elastic reversible mechanical behavior during the heating phase of the test, cooling-phase data had not been available at the time of conducting the THM analysis to support this assessment. Also, some uncertainty remains regarding the predicted THM behavior on the Tptpll, because of the lack of *in situ* heater tests in this unit (BSC 2003 [162318], Section 8.2). These uncertainties are not relevant for the suggested simple THM abstraction model, but would need to be considered for a less conservative abstraction using a time-dependent representation of the THM property changes.

Note that the THM model analysis is restricted to thermal expansion effects on seepage-relevant properties. Analysis of the impact of drift collapse on the hydrological properties of the remaining rock above the rubble-filled cave—a potential result of joint cohesion loss or seismic events—is ongoing. It is assumed that these properties are similar to the properties of the initial excavation-disturbed zone around nondegraded drifts (Assumption 2 in Section 5 [164617]).

THC Parameter Alterations

The THC simulations discussed in Section 6.4.4.2 suggest formation of a precipitation cap about 7–8 m above the drift crown. The zone of decreased fracture permeability acts as an "umbrella" that partially deflects percolating water sideways, limits the amount of flux at the drift crown, and reduces seepage. Seepage abstraction does not incorporate this effect, considering the considerable uncertainty and potential variability in these simulated results. As pointed out in BSC (2003 [162050], Section 8.1), both natural variability and process uncertainties exist in modeling the coupled THC processes because of the large amount of input data needed and the complexity of the natural system. Studies conducted with different initial water compositions have demonstrated significant sensitivity of the predicted permeability changes. Other relevant sources of uncertainty are the initial fracture porosity and the relation between porosity and permeability changes. In addition, the THC simulations were conducted using average thermal-hydrological conditions. The location and magnitude of the precipitation "umbrella" can change considerably if the boiling front or the duration of boiling is different from these average conditions. A final note on the DST measurements used for the model validation: While the predicted locations and relative abundances of secondary minerals were consistent with *in situ* sidewall core samples retrieved from zones that had undergone boiling in the DST, the total amount of mineral precipitation was small and did not create measurable permeability changes. This is because the DST heating phase of 4 years was too short to allow for mineral alteration strong enough to affect permeability.

Because of these uncertainties inherent in the THC results, the seepage abstraction model uses the ambient seepage rates from the SMPA without accounting for the "umbrella" effect. It should be recognized, however, that the simulated trend of a precipitation cap forming at some distance above the drift crown appears to be reliable in a qualitative sense. This adds confidence in the

seepage abstraction results, in that the amount of seepage is likely to be smaller than the abstracted seepage because of THC effects. Note that the general conceptual model for seepage simulations of the SMPA is still valid independent of THC alterations, as pointed out in BSC (2003 [163226], Section 6.7). This is because the seepage-relevant flow diversion occurs in a boundary layer of less than 1 m from the drift wall; they are not affected by these THC porosity and permeability changes.

6.5.1.5 Abstraction of Drift Degradation

As pointed out in Section 6.4.2.4, drift degradation can occur as a result of thermal stresses, seismic ground motion, and rock strength decrease. The degree to which drift degradation occurs is fundamentally different between drifts located in nonlithophysal and lithophysal rocks. Moderate drift degradation, limited to local rock fall at the drift ceiling, is predicted for nonlithophysal rocks, regardless of the considered event leading to degradation. The SMPA seepage simulations discussed in Section 6.4.2.4.1 suggest that local breakout at the drift ceiling is not likely to increase seepage, as long as the drifts stay essentially intact and the horizontal extent remains mostly unchanged. In lithophysal units, the degree of drift degradation depends on the considered stress scenario. Moderate drift degradation similar to the nonlithophysal results is predicted for the thermal stress cases, the 5×10^{-4} seismic hazard case, and most of the 0% through 60% strength reduction cases. Other events, among them the 1×10^{-6} and the 1×10^{-7} seismic hazard levels and the 80% through 100% strength reduction cases, result in complete drift collapse, leading to enlarged openings filled with fragmented rock material. Systematic seepage simulations have been conducted for a selected (worst-case) drift collapse scenario, modeling seepage into a rubble-filled drift of 11 m diameter. Results from these simulations are available in a seepage look-up table similar in structure to the one developed for non-degraded drifts (DTN: LB0307SEEPDRCL.002 [164337]).

For seepage abstraction, the different degrees of drift degradation simulated in BSC (2003 [162711]) are categorized as follows: The first category comprises degraded drifts that may show local rock breakout but stay essentially intact. In this category, seepage is interpolated from the look-up table for nondegraded drifts in DTN: LB0304SMDCREV2.002 [163687]. All drifts located in nonlithophysal rock are automatically included in Category 1. For drifts located in lithophysal rock, the thermal stress case, the 5×10^{-4} seismic hazard case and the 0% through 40% strength reduction cases are included in Category 1. The second category comprises the cases with complete drift collapse. These are the 1×10^{-6} and the 1×10^{-7} seismic hazard levels and the 80% through 100% strength reduction cases for lithophysal rock units. Note that this assessment is based on a visual analysis of the drift profiles given in MO0306MWDDPPDR.000 [164736] (see also Figures XVIII-1 through XVIII-30 in Attachment XVIII of BSC (2003 [162711])). While most scenarios in these figures can be clearly identified as belonging to Category 1 or 2, the 60% strength reduction case has ambiguous results, depending on which random generation seed is used in the degradation analysis. To be conservative, the 60% strength reduction case should be included in Category 2, representing collapsed drifts. Based on this categorization, the TSPA seepage simulation will sample seepage rates and percentages from either the non-degraded drift or the collapsed drift look-up tables, depending on the considered geologic unit, the selected nominal or disruptive scenarios, and the assumed rock strength reduction case. Note that information on the time-dependence of rock fatigue is not available at this time. Therefore, the collapsed drift look-up table should be used for the entire postclosure

period when one of the strength-induced collapsed drift scenarios is considered in TSPA. On the other hand, given that the time of a seismic event leading to drift collapse is considered in TSPA, the collapsed drift scenario should be used starting with the assumed time of the seismic event.

Quantitative assessment of uncertainties involved in the assessment of seepage for degraded drifts is not easy. There may be uncertainty in the drift degradation analysis (degradation profiles) as well as uncertainty in the seepage simulation results for these scenarios. However, it should be recognized that most cases leading to complete drift collapse are based on very conservative assumptions and represent worst-case scenarios. The ground motions associated with the 10^{-6} and the 10^{-7} seismic hazard scenarios, for example, or the cohesion losses of 80% or 100% may not be realistic and may overestimate the importance of time-dependent rock strength degradation in the lithophysal rocks. Therefore, the following procedure is suggested for covering uncertainty in the seepage predictions for degraded drifts. For all cases in Category 2, (uses the seepage look-up table for collapsed drifts), uncertainty is fully accounted for by the conservatism involved in the worst-case analysis. For all cases in Category 1 (uses the seepage look-up table for nondegraded drifts), the interpolated seepage rates are increased by 20%, to account for uncertainty associated with the seepage evaluation for these cases. This uncertainty stems in part from the limited number of simulation cases studied for moderately degraded drifts, but is mainly related to the large estimation differences between the stochastic realizations conducted for these cases (see Section 6.4.2.4.1). The maximum standard deviation of seepage percentage for degraded drifts was found to be above 30%, compared to about 16% for non-degraded cases. The proposed increase of seepage by 20% accounts for the impact of large estimation differences between realizations.

It was already pointed out in Section 6.3.1 that drift collapse may have an impact on the hydrological properties of the remaining rock above the rubble-filled cave. It is assumed that these properties—local fracture permeability and capillary strength—are similar to the properties of the initial excavation-disturbed zone around nondegraded drifts (Assumption 2 in Section 5 [164617]). This means that the respective parameter distributions for these properties, developed in Section 6.6.1 and 6.6.2, are applicable to both the nondegraded and the collapsed drift cases.

6.5.1.6 Abstraction of Rock-Bolt Effects

The simulated rock-bolt cases in Section 6.4.2.5 indicated that there is essentially no seepage enhancement for nongrouted boreholes housing rock bolts. The impact of rock bolts is therefore neglected in the seepage abstraction.

6.5.1.7 Abstraction for Igneous Events

Igneous intrusions (BSC 2003 [161839]) are likely to introduce large thermal, mechanical, and chemical perturbations both within the intersected emplacement drifts and in the surrounding rock. These perturbations may greatly affect the integrity of the natural and engineered barriers in the vicinity of and within the waste emplacement drifts.

Several different configurations are possible after an igneous intrusion event, when magma has filled intersected emplacement drifts and eventually cooled off. One possible scenario is that thermal contraction gives rise to numerous fractures or joints in the cooling magma, such that the

drift would be filled with fractured magma of relatively high permeability and small capillarity. In case this capillarity is much smaller than the capillarity of the surrounding rock (or if a small gap opens at the magma-rock interface as a result of cooling), the capillary barrier and flow diversion potential at the interface between the magma and the rock would be maintained. The magma may also drain out of the drift interior, leaving an air space that would also maintain the capillary barrier capability. Such processes are evident, for example, in the formation of lava tubes present in basaltic lavas (Williams and McBirney 1979 [164334], pp. 106–108). To determine the water inflow into magma-filled drifts with the capillary barrier potential still in place, the use of the seepage table for a nondegraded drift would provide a reasonable seepage estimate for the abstraction (DTN: LB0304SMDCREV2.002 [163687]). However, in view of the considerable uncertainty about the in-drift conditions after an igneous event, it may be reasonable to use a second abstraction method providing more conservative seepage estimates. This abstraction method would use the look-up table for collapsed rubble-filled drifts (DTN: LB0307SEEPDRCL.002 [164337]). Both look-up tables account for the effects of site-scale flow focusing and small-scale flow channeling, as caused by drift-scale heterogeneity. This abstraction recommendation should be an acceptable simplification for implementation of these low-probability and localized disruptive events into TSPA.

Another possible in-drift configuration after an igneous event is that the waste may be encapsulated by solidified magma with few cooling joints. In this case, there will be no capillary barrier at the interface between the magma and the fractured tuff. However, water contact with the waste would be limited by the small permeability of the solidified magma. A conservative abstraction method for such cases is to set the seepage percentage in intersected drifts to 100%; i.e., the seepage flux potentially contacting the waste is equal to the local percolation flux arriving at the drifts. This is equivalent to assuming that the cooled magma and the surrounding tuff have the same hydrological properties, leading to an undistorted flow field in the vicinity and through the drifts. This third method is easily implemented into TSPA by setting seepage flux equal to percolation flux.

Information on which one of the different in-drift conditions after an igneous event is to be expected at Yucca Mountain is not available. It is therefore recommended that TSPA conduct sensitivity analyses with the three abstraction methods described above. The more conservative seepage estimates should be chosen and propagated to the downstream TSPA modules. If the time of an igneous intrusion event is considered in TSPA, the selected abstraction method for igneous intrusion should be used, starting with the assumed time of the event.

6.5.2 Abstraction of Thermal Seepage

Thermal seepage is accounted for in TSPA using results from the TH Seepage Model as introduced in Section 6.4.3. This seepage process model simulates the coupled TH processes occurring as a result of the heat generated by the radioactive waste and explicitly calculates seepage rates during the time period of significant flux perturbation. Having a sophisticated thermal-seepage-process model available for seepage abstraction is a significant improvement to previous TSPA approaches for seepage, such as the *Total System Performance Assessment (TSPA) for the Site Recommendation* (CRWMS M&O 2000 [153246], Section 3.3.3.2.3) and the Fiscal Year *(FY)01 Supplemental Science and Performance Analyses, Volume 2: Performance Analyses* (BSC 2001 [154659], Section 3.2.2.6).

As pointed out in Section 6.4.3.1, the TH Seepage Model was applied to selected simulation cases by varying parameters that are important for thermal seepage (e.g., thermal-operating mode, local percolation flux, and seepage-relevant rock properties). Because of computational limitations, the number of thermal-seepage-simulation cases was much smaller than in the systematic SMPA analysis of ambient seepage. It was not practical to derive thermal seepage look-up tables that would allow direct interpolation of thermal seepage for any given combination of key properties. Therefore, the seepage abstraction approach developed in this Model Report uses the thermal seepage results to *qualitatively* describe the evolution of seepage in comparison to the ambient seepage rates. The first step of this approach is to interpolate the ambient seepage rates for the respective parameter case, as described in Section 6.5.1. Depending on the time step considered in the TSPA calculation, the ambient rate is then adjusted to account for the transient impact of thermal seepage, based on the qualitative results of the TH Seepage Model. For time steps that fall into the period of above-boiling rock temperatures, the ambient seepage rates may be set to zero as seepage is effectively suppressed. For late periods, on the other hand, there is no need to distinguish between thermal and ambient seepage, because the thermal perturbation has become insignificant. The abstraction approach for thermal seepage implicitly defines (and justifies) the time period when seepage can be treated with ambient seepage estimates.

Another advantage of this approach is that results from the TH Seepage Model are not required to provide the exact quantitative amount of seepage. It was already pointed out in Section 6.4.3.1 that the TH Seepage Model and the SMPA are not expected to arrive at identical simulation results of ambient seepage because of unavoidable differences in the model setups. From the two models, the SMPA results are considered quantitatively more reliable than the results from the TH Seepage Model. This is because (1) the SMPA is a 3-D model similar to the SCM, (2) the grid orientation and resolution of the SMPA, as well as the stochastic parameter representation, are identical to the SCM, and (3) the SMPA considers a much larger number of stochastic realizations. The TH Seepage Model, on the other hand, has a radially oriented 2-D and slightly different grid resolution in the drift vicinity. Also, the standard deviation of the stochastic permeability field is slightly smaller than the one used in the SMPA. Because the scope of the thermal seepage abstraction is to derive qualitative seepage rates, these model-setup differences between the SMPA and the TH Seepage Model are not relevant for the abstraction results. Using the SMPA results as the quantitative basis for ambient *and* thermal seepage ensures consistency in the time-dependent seepage rate.

The abstraction methodology for thermal seepage, relative to the ambient seepage results, is based on the consistent trends that were observed in the thermal seepage results (see Section 6.4.3.3). Despite different thermal loads, percolation conditions, rock properties, and host rock units studied in various simulation cases, the modeling results from the TH Seepage Model demonstrated that thermal seepage did not occur at above-boiling temperatures and that the ambient seepage values provide an asymptotic upper limit for thermal seepage. It was concluded in BSC (2003 [161530], Sections 6.2.4 and 8.1) that these qualitative trends hold for all relevant TSPA parameter cases. This assessment was based on the wide range of simulation cases explicitly addressed with the TH Seepage Model, corroborated by additional analysis of sensitivity studies conducted in BSC (2001 [155950], Section 5.3.1.4.8).

While these consistent trends are helpful in developing a simplified abstraction methodology using ambient seepage rates as base estimates, the complex transient nature of the TH coupled processes makes a detailed time-dependent seepage abstraction very tedious. The modeling results presented in BSC (2003 [161530], Section 6.2) demonstrate considerable variability among simulation runs with respect to the duration of the boiling period, the transient rewetting processes, the initiation time of thermal seepage, and the evolution of thermal seepage in comparison with the ambient seepage rates. As pointed out in Section 6.4.3.3, the key parameters affecting these processes are not only those important for ambient seepage—percolation flux, capillary strength, and permeability—but also the thermal load generated by the waste and the thermal conductivity of the rock. In addition, the TH coupling occurring in the superheated rock results in highly nonlinear relationships between these key parameters and the observed TH conditions in the rock. For example, a large percolation flux may not only promote ambient seepage, but also suppress the temperature build-up in the rock, giving rise to a less extended boiling period and faster rewetting at the drift wall. Thus, implementation of a detailed time-dependent seepage abstraction in TSPA involve prediction of the transient local TH conditions throughout the repository, dependent on a number of spatially varying key parameters.

6.5.2.1 Alternative Thermal-Seepage-Abstraction Approaches

The benefit of a detailed time-dependent abstraction of thermal seepage may not merit the difficulty of implementing it into the TSPA. Therefore, two alternative abstraction approaches are proposed for the seepage calculation component in TSPA, based on the recommendations made in Section 6.2.4.1 of BSC (2003 [161530]). Both approaches define thermal seepage relative to the ambient seepage rates for the respective climate stages—one using a very simple model, one with considerably more complexity. They are defined as follows:

Abstraction Model 1:

This simplified abstraction model sets thermal seepage equal to the respective ambient seepage throughout the entire TSPA period of 20,000 years. The abstraction is based on the model finding that ambient seepage provides an asymptotic upper limit for thermal seepage (i.e., there is no enhanced seepage as a result of thermal perturbation). The approach does not incorporate the vaporization barrier that prevents seepage during the period of above-boiling temperatures. Implementation in TSPA is straightforward, since the time-dependent evolution of thermal seepage is not accounted for in this abstraction model.

Abstraction Model 2:

This abstraction model sets thermal seepage to zero for the period of above-boiling temperatures in the drift vicinity. For the remaining time period, thermal seepage is set equal to the respective ambient seepage. The abstraction is based on model findings that thermal seepage never occurs at above-boiling temperatures and that the ambient seepage values provide an asymptotic upper limit for thermal seepage. The transient seepage result obtained from this abstraction model is more realistic, since the model does not incorporate the vaporization barrier limiting water flux towards the drifts. For implementation of this model, detailed information is required about the duration of the boiling period for a large number of parameter cases. These cases need to cover the

spatial variability and uncertainty in the above-mentioned relevant parameters for thermal seepage.

Figures 6.5-3 and 6.5-4 give examples of the proposed abstraction models for two simulation cases where seepage occurs. The first figure shows the simulation case that was already presented in Section 6.4.3.3 of this Model Report (see Figures 6.4-9, 6.4-10 and 6.4-11). The second figure gives the same simulation case, except that a smaller capillary-strength parameter was used. The assumed percolation fluxes are relatively large compared to the average flux conditions expected for present-day and future climate stages, totaling 60 mm/yr during the present-day climate, 160 mm/yr during the monsoon climate, and 250 mm/yr during the glacial transition climate. In both cases, the period of above-boiling rock temperature covers only the first 500 years after emplacement. This means that the boiling period is shorter than the present-day climate period (up to 600 years from emplacement), where percolation fluxes (and seepage rates) are typically smaller than at later times. In Figure 6.5-3, for example, ambient seepage does not occur during the present-day climate, because the capillary barrier is fully effective at a percolation flux of 60 mm/yr. This explains why both abstraction models arrive at the same abstraction result in this simulation case.

On the other hand, in Figure 6.5-4, the capillary-strength parameter is small enough to allow for ambient seepage even during the present-day climate period. In this case, there are distinct differences between the two approaches. While Abstraction Model 1 results in seepage at all times, Abstraction Model 2 does not allow seepage during the above-boiling period. Note that the 100^{o}C-isotherm of the fracture continuum is used as the threshold temperature to define the duration of the boiling period for abstraction (to be measured at the drift wall). This temperature is a few degrees centigrade higher than the nominal boiling point of water at prevailing pressures. This guarantees that no heat pipe conditions occur in the fractures close to the drift (because temperature would be at boiling) and also accounts for some uncertainty in the modeling results (see Section 6.5.2.2). Furthermore, because of potential variability in the TH conditions, the boiling period should be evaluated locally for all the grid elements along the drift wall, and the shortest period should be used for abstraction. In the selected simulation case, the resulting time period associated with fracture temperature above 100^{o}C is about 420 years.

Note that the simulated thermal seepage rates in Figure 6.5-4 are equal to the ambient ones at the onset of the simulation runs. However, they drop to zero shortly after the 50-year ventilation period, as soon as the rock temperatures approach boiling conditions. This early seepage is merely an artifact of the TH Seepage Model that neglects the impact of reduced relative humidity as a result of forced ventilation with dry air during the 50-year preclosure period (BSC 2003 [161530], Section 6.2.1.3.3). The reduced relative humidity in the emplacement drifts leads to evaporation of water at the drift surfaces and the development of a dryout zone in the drift vicinity. For the range of present-day percolation fluxes expected at Yucca Mountain, seepage in ventilated drifts is highly unlikely. As stated in Wang et al. (1996 [101309], Section 5), forced ventilation in drifts is expected to evaporate the equivalent of 100 mm/yr to more than 200 mm/yr percolation flux from the rock surfaces of the drifts. Since the predicted percolation fluxes during this time period are much smaller (see Section 6.6.4.1), seepage during the preclosure period can be neglected in both abstraction models.

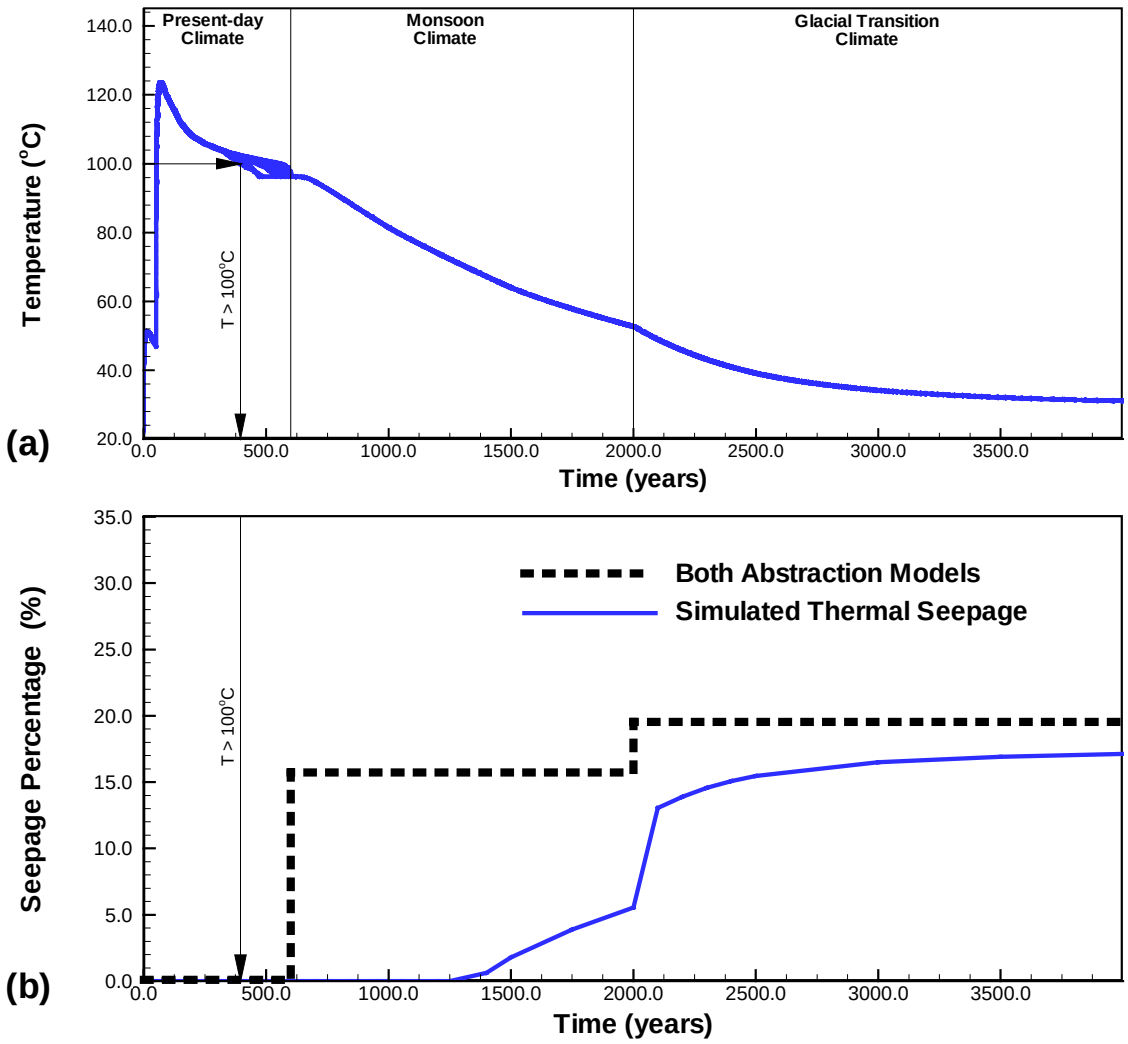

Source: Temperature Evolution from DTN: LB0303DSCPTHSM.001 [163688], Simulation Case MN-HET-03, Realization 1. Seepage Percentage from DTN: LB0301DSCPTHSM.002 [163689], Simulation Case MN-HET-03, Realization 1.

Figure 6.5-3. Illustration of Recommended Seepage Abstraction Models 1 and 2 for Simulation Case with Tptpmn Submodel, Reference Thermal Mode, Percolation Flux Multiplication Factor 10, and Capillary-Strength Parameter $1/\alpha$ = 589 Pa: (a) Temperature Evolution of Fracture Continuum at the Drift Wall; (b) Abstracted Seepage Percentage as a Function of Time.

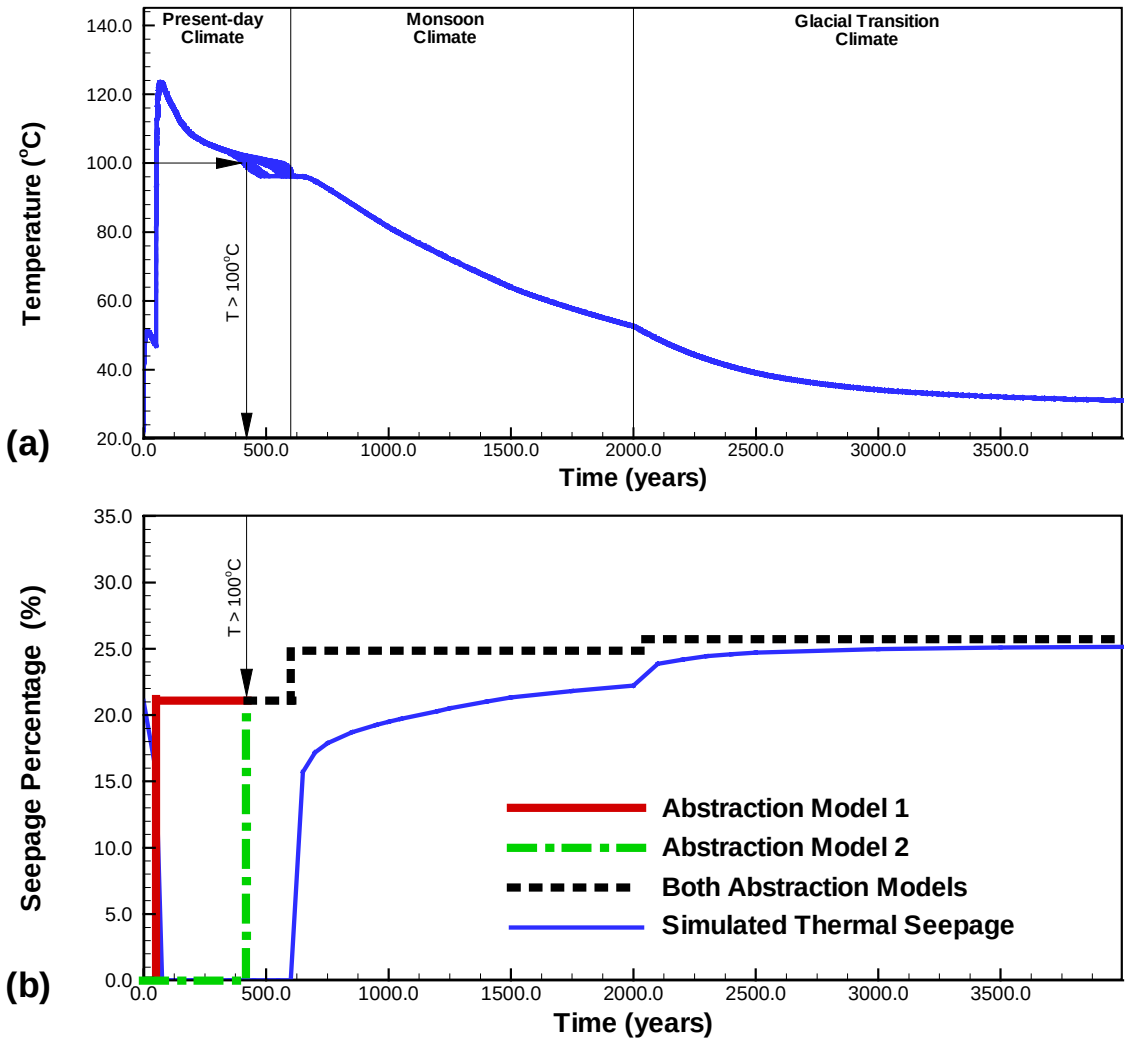

Source: Temperature Evolution from DTN: LB0303DSCPTHSM.001 [163688], Simulation Case MN-HET-09, Realization 1. Seepage Percentage from DTN: LB0301DSCPTHSM.002 [163689], Simulation Case MN-HET-09, Realization 1.

Figure 6.5-4. Illustration of Recommended Seepage Abstraction Models 1 and 2 for Simulation Case with Tptpmn Submodel, Reference Thermal Mode, Percolation Flux Multiplication Factor 10, and Capillary-Strength Parameter $1/\alpha$ = 400 Pa: (a) Temperature Evolution of Fracture Continuum at the Drift Wall; (b) Abstracted Seepage Percentage as a Function of Time

Neither of the proposed abstraction models for thermal seepage incorporates the time-dependent saturation buildup at the drift wall after boiling conditions have ended. As demonstrated in Figures 6.5-3 and 6.5-4 (and in additional simulation cases presented in BSC (2003 [161530], Section 6.2), thermal seepage is usually initiated at a few hundred to a few thousand years into the post-boiling period, the delay caused by the retarded rewetting of the dryout zone. These rewetting processes and their temporal evolution depend on many of the key properties for thermal seepage that were mentioned in the previous section—as well as on matrix capillarity, permeability, and fracture-matrix interface area. With so many key properties involved, prediction of the time-dependent buildup of saturation is a formidable task, and the related variabilities and uncertainties are hard to quantify. Seepage abstraction therefore assumes immediate increase in saturation to the respective ambient value at the end of the boiling period.

The decision regarding which one of the two abstraction models should be used will be made during the TSPA process, weighing the benefit of less seepage in Abstraction Model 2 against the complexity of implementing it into the TSPA. Note that in many parameter cases, the two abstraction models are identical. These are the parameter cases giving no seepage at any time, as well as most of the cases where seepage is possible during future climate periods with higher net infiltration, but does not occur at the present-day climate stage with comparably small net infiltration. This is because vaporization processes are most intense during the first several hundred years after emplacement, falling into the time period where the capillary barrier is fully effective in many parameter cases. An estimate of the potential merit of Abstraction Model 2 is provided in Section 6.8.1 of this Model Report.

Both abstraction models are implicitly valid for repository drifts where the local rock temperatures never reach boiling (e.g., as a result of 3-D edge effects or heat-load variability among waste packages). As pointed out in Section 6.4.3.3, thermal effects on flow and seepage are negligible in such cases, so that the potential for thermal seepage is similar to ambient seepage results. For nonboiling temperatures, both abstraction models per definition use the ambient seepage rates at all times.

Note that the thermal simulation analyses with the TH Seepage Model were conducted only for nondegraded drifts. As pointed out in Section 6.3.1, the thermal behavior in the fractured rock around collapsed drifts can be different from the conditions in the vicinity of an open drift. Modeling analyses for the impact of drift collapse on TH behavior is ongoing. Until supporting results become available, it is assumed that the two abstraction methods for thermal seepage are also applicable to the conditions in collapsed drifts (Assumption 3 in Section 5 [164618]).

6.5.2.2 Thermal Seepage Uncertainty

Uncertainty in the abstracted thermal seepage results is a result of (1) uncertainty in the ambient seepage estimates used as the quantitative basis of the abstraction, and (2) uncertainty in the evolution of thermal seepage compared to the ambient seepage estimates. The first contribution to thermal seepage uncertainty is automatically included in the thermal abstraction, because the abstracted ambient seepage rates explicitly account for the conceptual model uncertainty and the uncertainty in seepage-relevant parameters (see Section 6.5.1.3). The second contribution to thermal seepage uncertainty needs further discussion.

As pointed out in Section 6.4.3.2, conceptual model uncertainty related to the TH Seepage Model has been addressed in BSC (2003 [161530], Sections 7 and 8.2) by careful validation of the coupled TH processes in comparison with *in situ* heater tests. This validation provides confidence regarding the thermally induced flux processes and the predicted effectiveness of the vaporization barrier. In addition, validation of the ambient seepage conceptual model (in comparison with liquid-release tests) provides confidence in the predicted effectiveness of the capillary barrier. Results of an alternative conceptual model, considering the potential penetration of episodic preferential flow into the superheated zone above emplacement drifts, corroborate the main findings of the thermal-seepage process model. Based on this discussion, the conceptual model uncertainty of the TH Seepage Model is expected to be small. It is recognized, however, that some conceptual model uncertainty remains because the *in situ* heater tests used for model validation were operated at natural percolation, which is comparably small, and heater tests were conducted only in the Tptpmn unit. Thus, they do not provide seepage data for extreme percolation conditions and cannot account for the potential effect of lithophysal cavities on the TH conditions (Section 6.4.3.2). The two abstraction models account for conceptual model uncertainty as follows:

Abstraction Model 1:

This conservative abstraction model does not incorporate the vaporization barrier formed as a result of heating. The abstraction merely requires that no enhanced seepage occurs during the thermal period compared to ambient seepage estimates. Enhanced seepage could only occur when strong reflux of condensate coincides with late heating periods when vaporization is not effective. However, model results clearly demonstrate that this potential can be neglected in the abstraction, since the thermal perturbation is strongest early in the heating period when vaporization is most intense (see Section 6.4.3.3). The model validation, corroborated by the alternative conceptual model, provides sufficient confidence to support this conservative abstraction model without explicit consideration of conceptual model uncertainty.

Abstraction Model 2:

This abstraction model assumes that no thermal seepage occurs during the period of above-boiling temperatures in the drift vicinity. Here, the remaining uncertainty related to the predictive effectiveness of the vaporization barrier needs to be accounted for in the abstraction. This is done by using a threshold temperature higher than the nominal boiling temperature to define the duration of the boiling period for abstraction. As explained above, it is recommended to use the 100^{o}C isotherm of the fracture continuum as the threshold temperature. This ensures that the boiling isotherm is at some distance from the drift (and there is a small dryout zone around the wall) when the zero seepage is switched back to ambient seepage in the abstraction. Additional confidence is provided because the abstraction model does not incorporate the delayed seepage initiation caused by the time-dependent saturation buildup at the drift. Thus, Abstraction Model 2, despite assuming no seepage for rock temperature above 100^{o}C, still gives conservative seepage estimates compared to the predicted thermal seepage results.

Another source of uncertainty in the thermal-seepage modeling results is uncertainty in the relevant input parameters to the model. The selected sensitivity cases analyzed in BSC (2003 [161530], Section 6.2) provide enough confidence that the recommended abstraction procedures are valid over the required range of conditions and values used in TSPA. In other words, it can be stated that the general conclusions about the qualitative magnitude and evolution of thermal seepage—i.e., no seepage during boiling and thermal seepage bounded by ambient seepage estimates—remain consistent for all parameter combinations of capillary strength, permeability, percolation flux, thermal load, and/or thermal conductivity studied in the TSPA calculations. They also remain consistent for the three different realizations analyzed in BSC (2003 [161530], Section 6.2); consequently, there is no estimation uncertainty regarding these conclusions.

Based on this assessment, Abstraction Model 1 can be immediately implemented into TSPA, because the abstraction is independent of the thermal processes. Abstraction Model 2, on the other hand, requires detailed knowledge about the duration of the boiling period in the vicinity of emplacement drifts. In this case, the spatial variability and uncertainty of additional parameters relevant for the thermal conditions in the repository must be described (e.g., thermal load, thermal conductivity), and more thermal simulation cases have to be analyzed for various combinations and stochastic realizations of these additional parameters. The latter tasks are not included in this Model Report.

6.6 PARAMETER DISTRIBUTIONS FOR SEEPAGE-RELEVANT PROPERTIES

This section explains the background, methodology, and results of a data analysis intended to derive probability distribution functions for the seepage-relevant properties varied within the TSPA calculations. Separate probability distributions are developed for spatial variability and for uncertainty of these properties. As explained in Section 6.5, the seepage component in TSPA-LA will sample from these distributions at spatial locations r and uncertainty realizations R.

The relevant parameters to be described are the capillary-strength parameter $1/\alpha$, the permeability k, and the percolation flux $q_{perc,ff}$. These parameters are defined according to the conceptual framework of the ambient-seepage process models; thus, the parameter distributions developed must correspond to the designated use of these parameters within the SMPA simulation model (see Section 6.4.2). This means that (1) the capillary strength is the calibrated effective parameter as estimated from the SCM, (2) the permeability represents the mean value of the small-scale stochastic permeability fields in the SMPA domain, and (3) the percolation flux is the local flux arriving at the upper boundary of the SMPA model (Section 6.5.1.1). It also means that these parameters are representative of properties or processes derived for a typical drift-scale model domain. The spatial variability distributions need to cover the intermediate-scale distribution of these drift-scale parameters within the repository units. According to the definition given in Section 6.1.3, intermediate-scale heterogeneity defines heterogeneity on a resolution similar to the typical drift-scale model domain.

The following Sections 6.6.1 and 6.6.2 explain the development of the parameter distributions for the capillary-strength parameter and the permeability, respectively. The discussion focuses on the two main repository units, the Tptpll and the Tptpmn. Both these units have been extensively characterized by underground testing in the Exploratory Studies Facility (ESF) and the Enhanced Characterization of Repository Block (ECRB), to provide sufficient basis for predictive modeling and seepage abstraction. How the less important Tptpul and Tptpln units are treated in the seepage abstraction is briefly explained in Section 6.6.3. Finally, the magnitude and distribution of percolation fluxes is provided in Section 6.6.4.

Only the key properties for *ambient* seepage are included in the following sections. Whether additional probability distributions need to be developed for parameters affecting the local TH conditions depends on the method of choice for the abstraction of *thermal* seepage (Section 6.5.2).

Note that, in addition to active testing of seepage-relevant properties (liquid-release tests, air injection tests), the fracture inventory of the repository units has been extensively characterized from geological mapping and scanline surveys along the ESF and the ECRB Cross Drift as well as from borehole cores and video logs. In general, the distribution of fractures in the units exposed is similar in the Cross Drift and the ESF in terms of frequency, character, and orientation (Mongano et al. 1999 [149850], p. 44). The information gathered in the scanline surveys includes location, orientation, trace length, width, and roughness. The average fracture frequencies calculated from these data indicate a high degree of fracturing in both the Tptpll (tsw35) and the Tptpmn (tsw34), with about three fractures per meter in the Tptpll versus four fractures per meter in the Tptpmn (BSC 2003 [161773], Table 7). The calculated fracture porosities, reported in the same table in BSC (2003 [161773]) are 9.6×10^{-3} in the Tptpll vs. 8.5

$\times 10^{-3}$ in the Tptpmn. Small fractures with a trace length of less than one meter are not included in this analysis, because the scanline surveys were mostly conducted using a 1 m cutoff threshold (CRWMS M&O 2000 [152286], Section 6.2.2). These small fractures, however, may be important for seepage, which is governed by small-scale flow processes in the drift vicinity. Other fracture characteristics differ between the geological units. As reported in CRWMS M&O (2000 [151945], Section 4.6.6.2.3), fractures in the Tptpmn tend to be planar or arcuate, with low surface roughness, while fractures within the Tptpll are mainly subplanar and have rougher surfaces. CRWMS M&O (2000 [151945], Section 4.6.6.2.3) states that the average fracture length in the Tptpmn is larger than in the Tptpll. This, however, is not supported by the quantitative data given in Table 13 of CRWMS M&O (2000 [152286]), where the trace lengths in the Tptpll are slightly larger than in the Tptpmn.

6.6.1 Capillary-Strength Parameter

The local capillary-strength parameter $1/\alpha$ of the fractured rock is one of the key parameters affecting the capillary barrier behavior at the drift crown. The larger this parameter, the stronger the capillary force, which holds water in the fractures and prevents it from seeping into the drift. A value of zero is the lower limit for the capillary-strength parameter, corresponding to a fractured rock with zero capillary forces.

6.6.1.1 Supporting Information

As explained in Section 6.4.1, appropriate estimates of the fracture capillary-strength parameter are obtained by inverse modeling; this is the main purpose of the SCM (BSC 2003 [162267]). This process model was calibrated and validated against seepage-rate data from multiple liquid-release tests conducted in three niches along the ESF (Niches 3107, 3650, and 4788), one niche in the ECRB (Niche 1620), and in three systematic-testing boreholes (SYBT-ECRB-LA#1–3) drilled into the ceiling of the ECRB. The tests were performed by sealing a short section of a borehole above the opening using an inflatable packer system, releasing water at a specified rate into the isolated test interval, and recording the amount of water dripping into the opening. For each interval tested, optimal values of a seepage-relevant capillary-strength parameter were calibrated. Seepage-rate data from multiple test events, using different liquid-release rates, were calibrated simultaneously in the inverse modeling approach. Inversions for the lower lithophysal zone were repeated for multiple realizations of the underlying stochastic permeability field to capture their influence on the calibrated results. Inversions for the middle nonlithophysal zone were conducted for only one realization of the underlying permeability field, which was justified by the smaller importance of this geologic unit for TSPA (12% of the repository is in the Tptpmn, compared to 81% in the Tptpll). The resulting capillary strength values for the Tptpmn may thus be affected by the specifics of the single realization of the permeability field, making them less robust compared to the Tptpll results. This contribution to uncertainty is accounted for in Section 6.6.1.3.

A summary of all calibrated capillary-strength values is provided in Table 6.6-1 (DTN: LB0302SCMREV02.002 [162273], also given in BSC 2003 [162267], Table 14). Data from six test intervals are available in the lower lithophysal zone: four intervals in boreholes located above the ECRB Cross Drift, and two intervals in boreholes above Niche 1620. Four intervals in the middle nonlithophysal zone have been analyzed, one interval in a borehole above Niche 3107

and three intervals in boreholes above Niche 4788. Since multiple inversions with different realizations of the underlying heterogeneous permeability field were performed for test locations in the lower lithophysal zone, the capillary-strength parameter $1/\alpha$ is calculated as the average of all inverse modeling results at that location. A standard deviation (SD) representing the related uncertainty of each inversion is computed. The standard error (SE) of the mean is calculated as SE = SD/($i^{1/2}$), where i is the number of inversions performed (between 17 and 30 inversions). The estimates for the middle nonlithophysal zone are based on a single inversion, i.e., no estimation uncertainty as a result of uncertainty in small-scale heterogeneity can be given. Note that the values provided in Table 6.6-1 reflect characterization of $1/\alpha$ that does not include the potential effects of mechanical and chemical rock alteration in response to heating the drifts. Effects of excavation, however, are implicitly accounted for in the calibrated values (Section 6.4.1).

Table 6.6-1. Summary Statistics of Estimated Capillary-Strength Parameter for Lower Lithophysal Zone and Middle Nonlithophysal Zone

Lower Lithophysal Zone (Tptpll)							
Location	**Interval**	**Number of Inversions[1]**	**Estimate $1/\alpha$ [Pa]**				
			Mean	**Std. Dev.[2]**	**Std. Error[3]**	**Min.**	**Max.**
SYBT-ECRB-LA#1	zone 2	17	534.3	56.8	13.8	447.7	674.1
SYBT-ECRB-LA#2	zone 2	21	557.1	56.4	12.3	457.1	676.1
SYBT-ECRB-LA#2	zone 3	19	534.8	57.8	13.3	443.1	645.7
SYBT-ECRB-LA#3	zone 1	23	452.0	54.7	11.4	382.8	616.6
Niche 1620	BH #4	30	671.2	223.2	40.8	356.0	1197.0
Niche 1620	BH #5	24	740.5	339.0	69.2	231.1	1840.8
Middle Nonlithophysal Zone (Tptpmn)							
Niche 3107	UM	1	741	—	—	—	—
Niche 4788	UL	1	646	—	—	—	—
Niche 4788	UM	1	603	—	—	—	—
Niche 4788	UR	1	427	—	—	—	—

[1] Each inversion is based on a different realization of the heterogeneous permeability field.

[2] Represents estimation uncertainty on account of small-scale heterogeneity (not available for estimates for the middle nonlithophysal zone).

[3] Standard error of mean.

Source: DTN: LB0302SCMREV02.002 [162273], also given in BSC (2003 [162267], Table 14)

The values given in Table 6.6-1 provide the basis for developing appropriate probability distributions that cover spatial variability and uncertainty of seepage-relevant fracture capillarity for use in TSPA-LA. For that matter, it is important to understand the nature of the calibrated parameter $1/\alpha$. From capillary theory, the capillary-strength parameter in a single fracture is governed by the aperture distribution. Aperture and capillary strength in a single fracture are

negatively correlated; i.e., large apertures are typically associated with a smaller capillary-strength parameter. Since permeability in a single fracture increases with aperture (positive correlation), the fracture permeability and capillary-strength parameter are also negatively correlated. In a fracture continuum, with $1/\alpha$ being a representative continuum parameter (as in the seepage process models), a change in continuum permeability can be related to (1) a change in fracture aperture or (2) a change in the fracture density (Birkholzer et al. 1999 [105170], Section 2). In the first case, $1/\alpha$ is approximately negatively correlated to the square root of fracture continuum permeability; in the second case, there is no change in $1/\alpha$.

Most process models for unsaturated flow at Yucca Mountain use values for $1/\alpha$ that represent the physically based capillary-strength parameter of the fracture ensemble in the rock, as discussed above (CRWMS M&O 2000 [141187], Section 6.1). Seepage process models like the SCM, however, consider $1/\alpha$ as an effective process parameter for drift seepage that implicitly accounts for a number of additional factors affecting seepage, as listed in Section 6.4.1.1. Estimating $1/\alpha$ as an effective process parameter in the inversion makes the explicit inclusion of these factors into the seepage calibration model unnecessary (BSC 2003 [162267], Section 6.3.2.2). The calibrated $1/\alpha$ value therefore represents a process-related parameter for estimating seepage with a specific conceptual model on a given spatial scale. Since some of the above-listed additional factors are not affected by intermediate-scale to large-scale rock type changes, the effective capillarity may exhibit less significant variation between and within different geological units compared to other fracture properties such as, for example, the fracture permeability. For similar reasons, the calibrated capillary-strength parameter is not expected to be correlated to the mean fracture permeability used in the seepage process models (compare with Table 6.6-3).

Note that this specific seepage-related definition of $1/\alpha$ requires that downstream models using this parameter for seepage prediction must be fully compatible with the SCM. The process models used for predicting seepage during ambient and thermally perturbed conditions (the SMPA and the TH Seepage Model, respectively) are compatible in this sense (see Section 6.4).

6.6.1.2 Spatial Variability

The intermediate-scale variability of $1/\alpha$ refers to the variation of this effective process parameter, provided on the spatial resolution similar to the SCM and SMPA model domain, within the repository rock units. Figure 6.6-1 shows a schematic illustration of the location of niches and drift sections where seepage tests have been conducted. The first three niche sites are located along the west side of the ESF in the Tptpmn and were selected for seepage testing based on their different fracture densities (BSC 2003 [162267], Section 6.5.1). Niche 3107, at construction station (CS) 31+07 in the ESF, consists of a 6.3 m long drift located in an area of relatively low fracture density. Niche 3650, at CS 36+50, consists of a 9 m long drift located in a competent rock mass exhibiting relatively moderate fracture density. Niche 4788, at CS 47+88, consists of an 8.2 m long drift located in an area exhibiting relatively high fracture density. Niche 4788 is located in a 950 m long exposure of an intensely fractured zone. Fractures in this zone are not uniformly spaced, but instead occur in clusters of closely spaced fractures. The 15.0 m long Niche 1620 is located on the south side of the ECRB Cross Drift in the Tptpll. This unit comprises many small fractures (less than 1 m long) interspersed with many lithophysal cavities,

ranging in size from 15 cm to 100 cm (BSC 2001 [158463], Section 6.11). Additional tests in the Tptpll were conducted in three systematic testing boreholes drilled into the ceiling of the ECRB Cross Drift. Note that no calibrated capillary-strength values are available for Niche 3650. Though 27 liquid-release tests have been conducted (13 of which resulted in seepage), the testing methodology was considered less reliable because of the short test duration, making the test results very sensitive to storage effects (BSC 2003 [162267], Section 7.3). All boreholes shown in Figure 6.6-1 are approximately parallel to the niche (drift) axis. Test intervals in the niches are approximately 1 ft long (0.3 m); test intervals in the systematic testing boreholes are approximately 1.8 m long.

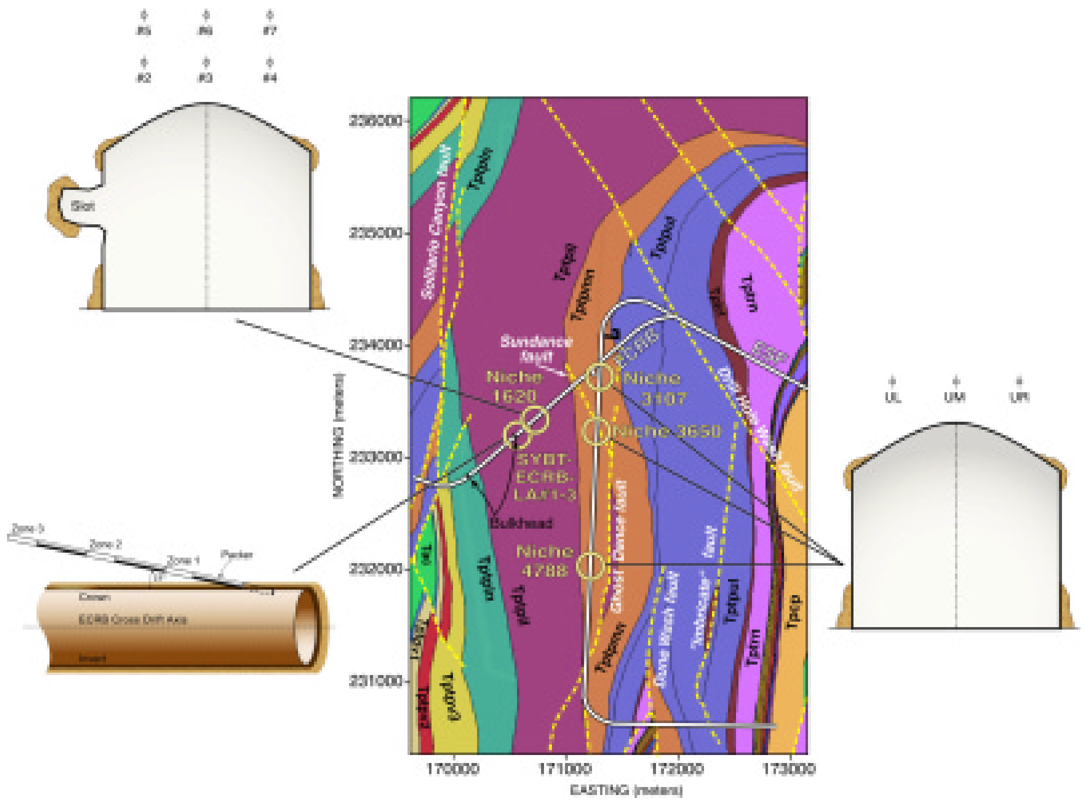

Source: BSC (2003 [162267], Figures 4 and 5)

Figure 6.6-1. Schematic Geological Map Showing Approximate Location and Schematic Setup of Niches and Systematic Testing Boreholes SYBT-ECRB-LA#1–3 (formations are depicted at the elevation of the ESF)

From Table 6.6-1 and Figure 6.6-1, calibrated 1/α values are available from ten test intervals in four different niche or drift locations. The four locations provide broad spatial coverage of the primary repository units, with a north-south distance of about 1,700 m between Niches 3107 and 4788, and an east-west distance of about 800 m between the ESF niches and the location of the systematic testing boreholes. Considering the geological units separately, the Tptpmn test locations (Niche 3107 and 4788) are separated by a distance of about 1,700 m, covering areas in the middle nonlithophysal zone with distinct fracture characteristics, while the Tptpll test locations (Niche 1620 and systematic testing boreholes) are in relatively close proximity within a 150 m long section of the ECRB Cross Drift. Where several boreholes were tested in one niche, the typical distance between test intervals was on the order of a few meters (boreholes are

typically a few meters apart). A similar distance is measured between the two tested intervals in systematic testing borehole SYBT-ECRB-LA#2 (BSC 2003 [162267], Section 6.5.1). Thus, the ten available $1/\alpha$ values are not randomly placed over the entire repository area; instead, sample points are clustered at four carefully selected test locations within two different rock types.

To develop appropriate probability distributions from these data, it is important to recall the nature of the parameter in question. If $1/\alpha$ solely represented capillary behavior of the fractured rock, one would expect this parameter to vary considerably between the two geological units, a result of potential differences in fracture aperture and fracture wall roughness. Thus, the analysis would need to be conducted separately for the two geological units. Another consequence of $1/\alpha$ solely representing capillary behavior would be that the $1/\alpha$ values available in one niche location (or drift section) could not be used to constrain the intermediate-scale variation because of the close test proximity. Therefore, these values would need to be treated as statistically dependent; one would have to use the average of the available samples at each distinct niche location (or drift section) for further statistical analysis of intermediate-scale variability. This would leave a very small sample size at two distinct locations (Niches 3107 and 4788 in the Tptpmn; Niche 1620 and systematic testing boreholes in the Tptpll) as the basis for estimating intermediate-scale variability within the repository units, making the calculated statistical measures more uncertain.

On the other hand, as pointed out earlier, seepage models derive and apply $1/\alpha$ as an effective process parameter that accounts for a number of additional factors affecting seepage. Some of these factors—drift-wall roughness, drop formation and detachment, artifacts of finite discretization—are largely independent of intermediate- and large-scale rock type variation. Other factors depend on fracture characteristics that are not significantly different for the two units. For example, the possible existence of individual fractures cutting into the opening is mainly governed by the fracture frequency. It is therefore possible that the $1/\alpha$-variability is not significantly dependent on the geological unit. In this case, analysis of statistical measures could be conducted without distinguishing between geological units. It is also possible that the variation of effective fracture capillarity is not closely tied to the location (or drift section). In this case, all ten samples could be considered as independent.

Table 6.6-2 provides statistical parameters defining spatial variability distributions—mean μ and standard deviation σ—calculated from the ten test samples provided in Table 6.6-1. (The mean of $1/\alpha$ over multiple inversions is used for the Tptpll unit.) Also given is the standard error of the mean (SE), an estimate for the uncertainty in the mean value caused by a limited number of measurements. In light of the above discussion on the possible statistical independence of the ten test intervals, these statistical parameters have been derived using four different methods. These methods are as follows:

A. Derive mean and standard deviation from all ten samples in both units.

B. Calculate average values from multiple tests in one location, then derive mean and standard deviation from the resulting four samples in both units.

C. Derive mean and standard deviation separately for geological units, from six samples in the Tptpll and four samples in the Tptpmn.

D. Calculate average values from multiple tests in one location, then derive mean and standard deviation separately for each geological unit.

Except for the standard error, the statistical values provided in Table 6.6-2 are consistent among the four calculation methods. The maximum differences in the mean (about 60 Pa) and the standard deviation (about 20 Pa) between methods A through D are significantly smaller than the variability in the calibrated 1/α-values (or the range of results from multiple inversions, see Table 6.6-1). The two geological units do not show a significant difference in the effective capillary-strength parameter. In fact, the difference of 1/α-values within a geological unit is on the same order as the difference of 1/α between geological units. However, the standard error of the mean varies between the different methods as a result of the varying sample size. The more statistically independent samples available, the more reliable the estimate of the mean.

Table 6.6-2. Intermediate-Scale Variability Statistics of Estimated Capillary-Strength Parameter over Repository Rock Block, Using Different Calculation Methods

Method	Number of Samples	Mean μ (Pa)	Std. Dev. σ (Pa)	Std. Error of Mean SE (Pa)
A ***All Samples, Both Units***	***10***	***591***	***109***[1]	***35***
B				
All Locations, Both Units	4	631	109	54
C				
All Samples in Tptpmn	4	604	131	66
All Samples in Tptpll	6	582	105	43
D				
All Locations in Tptpmn	2	650	129	91
All Locations in Tptpll	2	613	132	93

Output-DTN: LB0308AMRU0120.001

NOTE: [1] Due to rounding, the standard deviation of Method A was set to 109 Pa in this analysis instead of 110 Pa, as suggested by the Excel spreadsheet results referred to in Attachment II. This difference of less than 1% in the second moment is not relevant for the resulting parameter distributions.

Note that statistical tests are available to rigorously analyze the statistical independence of samples. However, because of the rather small sample size, such statistical tests have not provided clear indication about which one of the four methods is most appropriate for defining the spatial variability of the *1/α*-parameter. On the other hand, the sensitivity analysis conducted in Section 6.8 indicates that the overall seepage results are not significantly affected by the statistical evaluation method. It is therefore recommended that all four methods be included in TSPA as alternative representations of spatial variability and uncertainty in the *1/α*-parameter. The four methods should be uniformly sampled (i.e., equally weighted) in TSPA, incorporating the global epistemic uncertainty about these different statistical evaluation methods. The significance of this uncertainty in the seepage model can be evaluated as part of the TSPA linear regression analyses of individual dose. For further discussion of spatial variability and uncertainty treatment of *1/α* in the remainder of this document, we use the resulting mean and standard deviation of Method A as an example.

The question of which parametric probability distribution should be best suited to represent the spatial variability of the ten samples deserves further attention. Since capillary strength in a single fracture is correlated to the aperture distribution, which is approximately lognormal in most fractured rocks, one would expect $1/\alpha$ to be lognormally distributed as well. However, the histogram of the sample values in Figure 6.6-2 gives no clear indication of the parametric model, arguably because the calibrated capillary-strength parameter includes many additional factors affecting seepage. In light of this uncertainty about the relative likelihood of the data, the distribution of choice for the capillary-strength parameter is a simple uniform distribution, where all possible values between the specified minimum and maximum values are equally probable. The minimum and maximum values of this distribution can be easily calculated from the given mean and the standard deviation of the sample (Mishra 2002 [163603], Section 3.2). The minimum value is defined as $\mu - 1.732\ \sigma$, giving 402 PA using the respective values from Method A. The maximum value is defined as $\mu + 1.732\ \sigma$, which is 780 Pa. The resulting probability distribution for spatial variability of $1/\alpha$ is also depicted in Figure 6.6-2. (Note that the impact of choosing another parametric distribution, such as a normal distribution, is rather small, as shown in Section 6.8.2.) The uncertainty associated with capillary-strength parameter will be discussed in the next subsection.

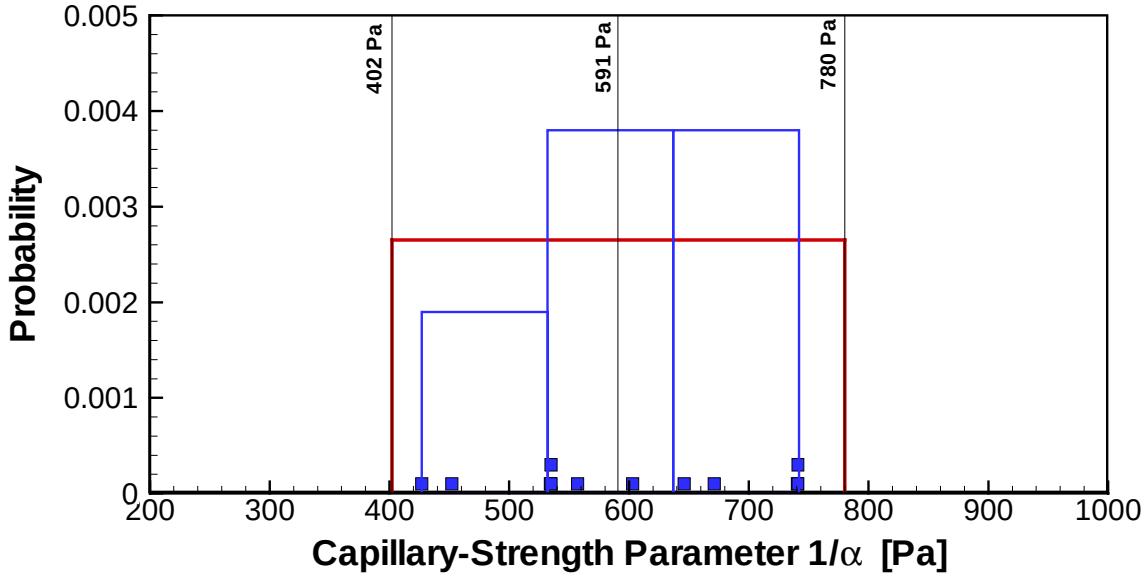

Source DTN: LB0302SCMREV02.002 [162273]

NOTE: Vertical lines indicate mean and range of distribution. Blue symbols indicate calibrated sample values.

Figure 6.6-2. Histogram and Related Probability Distribution for Spatial Variability of Capillary-Strength Parameter 1/α, Using Statistical Parameters Based on Method A.

6.6.1.3 Uncertainty

The different sources of uncertainty related to the capillary-strength parameter are as follows:

Measurement Uncertainty:

The capillary-strength parameter is determined by calibrating the SCM against seepage-rate data from liquid-release tests (Section 6.4.1). As described in BSC (2001 [158463], Sections 6.2, 6.11, 7.2.3), these tests have been carefully designed, and potential problems observed in early tests (i.e., memory effect, short test duration, ventilation) were fixed in subsequent testing phases, with tests conducted over longer periods, at various release rates, and under better control of ventilation regime and relative humidity conditions. Only these later tests were selected for calibration of the SCM, and evaporation effects were incorporated into the model (BSC 2003 [162267], Section 6.5.3). The remaining uncertainty in the measured seepage rates is mainly caused by the possibility of unaccounted water losses, e.g., from evaporation in the seepage capture system or from unaccounted storage capacity in the rock. In an attempt to obtain a complete water balance from the experimental data (including seepage, storage, evaporation, and flow diversion) a horizontal slot was designed near the spring line of Niche 1620 (see Figure 6.6-1). However, excavation and instrumentation of the slot proved difficult, and capturing of diverted water was only partially successful. While the flow diversion capability has been demonstrated, a complete water balance has not been achieved (BSC 2003 [162267], Section 6.8). Thus, uncertainty related to the measured seepage rates and potential water losses should be included in and propagated through the abstraction, using appropriate probability distribution functions.

Conceptual Model Uncertainty:

As explained in Section 6.4.1, the SCM is a sophisticated seepage process model for calibration of capillary-strength parameters on the scale and for the conditions of interest. The calibrated model with the appropriate effective parameters is capable of reproducing and predicting observed seepage data from liquid-release tests conducted above and below the seepage threshold; they are thus likely to yield reasonable seepage predictions into waste emplacement drifts. Alternative conceptual models corroborate the findings of the SCM. Altogether, the conceptual model uncertainty should be small compared to other sources of uncertainty inherent in the $1/\alpha$-values. Therefore, conceptual model uncertainty is ignored in abstraction.

Estimation Uncertainty:

The estimation uncertainty of $1/\alpha$ in the Tptpll is mainly a result of uncertainty in the small-scale fracture permeability distribution used in the inversion model. Multiple realizations were performed with different realizations of conditioned random permeability fields. It was demonstrated in BSC (2003 [162267], Section 6.6.4) that the estimation uncertainty on account of small-scale heterogeneity differences is on the order of 50 to about 300 Pa. However, it is also pointed out in BSC (2003 [162267], Section 8.2) that this source of estimation uncertainty should not be incorporated in the parameter distribution used for sampling in TSPA-LA. This is because the impact of undetermined details pertaining to small-scale heterogeneity is directly evaluated in the predictive

seepage models, i.e., the SMPA and the TH Seepage Model. Using the range of results from these models in the TSPA calculations assures that the estimation uncertainty is intrinsically included in and propagated through the abstraction (see Section 6.5.1.3). In the Tptpmn, only one realization of permeability fields was analyzed, which makes the calibration results less robust than those for the Tptpll. This contribution to uncertainty should thus be accounted for in the abstraction. Another uncertainty factor may stem from the misfit between the results and the data; i.e., from the goodness of fit between calibration model and measurement. It is stated in BSC (2003 [162267], Section 6.6.4) that uncertainty related to the misfit between the model and the data was significantly smaller than the uncertainty from small-scale heterogeneity. This contribution to the estimation uncertainty can be ignored in abstraction.

Spatial Variability Uncertainty:

Spatial variability uncertainty needs to account for uncertainty in the probability distribution chosen to represent spatial variability. This requirement stems from the fact that only a limited number of data points are available to derive the distribution parameters. The related uncertainty can be uncertainty both in the mean and in the standard deviation of $1/\alpha$, defining the potential range of the data. In measurement theory, the standard error of the mean is often used to describe the potential error in the estimated mean resulting from a limited sample size. For the analysis based on all ten $1/\alpha$ values (Method A), this error is comparably small at 35 Pa. Method D, on the other hand, arrives at much higher standard errors of 91 and 93 Pa for the Tptmn and the Tptpll units. Thus, spatial variability uncertainty needs to be included in and propagated through the abstraction, using appropriate probability distribution functions.

With most of the above discussion being a qualitative assessment of uncertainty, the assignment of quantitative measures for uncertainty—i.e., the definition of appropriate probability distributions describing uncertainty—is necessarily subjective and somewhat arbitrary, and must be based on scientific judgment. The method chosen here is to account for uncertainty by varying the mean of the chosen probability distribution for spatial variability within appropriate ranges; i.e., by shifting the uniform distribution for spatial variability to smaller or larger $1/\alpha$-values. The uncertainty distribution designated to provide this random adjustment of the mean is a symmetric triangular distribution, with a mean of zero, a maximum of three standard errors, and a minimum of minus three standard errors. For Method A, this would give a range of ±105 Pa. For Method D, as an example, this range is much higher at ±273 Pa for the Tptpmn and ±279 Pa for the Tptpll. A range of approximately plus/minus two standard errors defines the 95%-confidence interval for the estimated mean value of the sample; i.e., this uncertainty range accounts for the fact that the estimated mean value of the limited sample may be different from the mean value of the entire population. As a consequence, the chosen uncertainty distribution covers sufficient uncertainty in the estimated mean values, while leaving room for additional uncertainty sources (e.g., measurement uncertainty, estimation uncertainty for the Tptpll stemming from a limited number of realizations). The parameter range is believed to cautiously but realistically represent the potential total uncertainty in $1/\alpha$, comprising the respective contribution of measurement errors and spatial variability errors.

The triangular distribution is an appropriate model for uncertain quantities where a most likely value is known in addition to an estimated range of parameters. The triangular distribution represents the key features desired, which are that a probability distribution with a mean value of 591 Pa, a lower bound of 402 Pa, and an upper bound of 780 Pa is the most likely case; while distributions with higher or lower mean are possible, but less likely. No uncertainty distribution is assigned to the specified minimum and maximum values of the distribution. Uncertainty about these values is believed to be small in light of the above discussion about the nature of this parameter; it should be fully accounted for in the triangular probability distribution for uncertainty of the mean.

A schematic of the spatial variability and uncertainty model is given in Figure 6.6-3, using the values derived from Method A as an example. The heavy blue line shows the triangular-shaped uncertainty distribution, assigning a probability to the mean of the uniform-shaped spatial variability distribution. The most likely spatial variability distribution is the one defined in Section 6.6.1.2, with a probability of 0.0095 per Pa^{-1} corresponding to the peak value of the triangular distribution. This spatial variability distribution has a mean of 591 Pa, a minimum value of 402 Pa, and a maximum value of 780 Pa. Least likely are the two bounding cases, where the triangular distribution indicates a zero probability. The lower bounding case has a uniform spatial variability distribution with a mean of 486 Pa, a minimum value of 297 Pa, and a maximum value of 675 Pa. The upper bounding case has a uniform spatial variability distribution with a mean of 696 Pa, a minimum value of 507 Pa, and a maximum value of 885 Pa. Together, considering the combined effect of spatial variability and uncertainty, the range of 1/α-values to be used in TSPA-LA is quite large, extending from 297 Pa to 885 Pa.

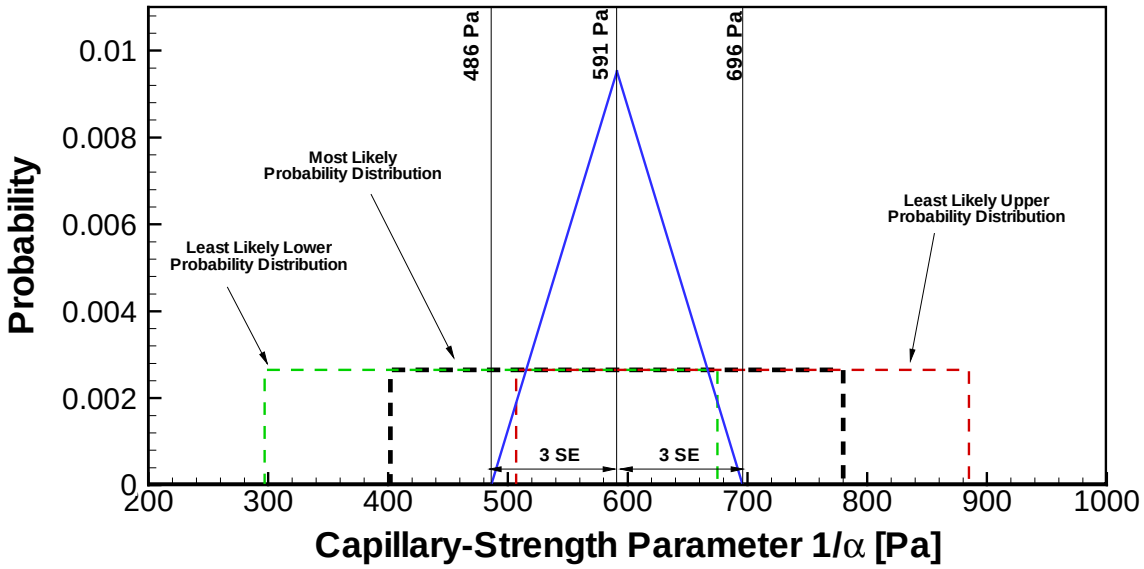

NOTE: The black dashed line shows the most likely spatial probability distribution (at the peak of the triangular distribution). The green and the red dashed lines show the least likely spatial probability distributions (at the minimum and the maximum of the triangular distribution); based on statistical parameters summarized in Table 6.6-2.

Figure 6.6-3. Triangular Probability Distribution (Heavy Blue Line) for Covering Uncertainty of the Capillary-Strength Parameter by Varying the Mean of the Spatial Probability Distribution, Using Statistical Parameters Based on Method A.

6.6.2 Fracture Permeability

The second key parameter affecting the diversion of water around drifts is the tangential fracture permeability in the boundary layer near the drift wall. The larger this parameter, the more likely is water-flow around the drift and the less likely is seepage (Birkholzer et al. 1999 [105170], Sections 3 and 5). Similar to the SCM, the predictive models for seepage—the SMPA and the TH Seepage Model—apply a stochastic continuum conceptualization for fracture permeability in the drift vicinity. The small-scale variability of the continuum permeability (resolution of about 1 foot) is implicitly accounted for in these models, using lognormal probability distributions based on air-injection measurements that were performed on the same scale. While the standard deviation of these small-scale permeability distributions, σ_S, can be treated as a constant for abstraction (see discussion in Section 6.4.2), their mean values, μ_S, may vary significantly over the repository rock units. (For simplification, these mean values of small-scale permeability were simply referred to as k in the previous sections.) For TSPA, distributions covering the intermediate-scale variability and the uncertainty of these mean values of small-scale permeability need to be developed (see Figure 6.6-4). The statistical parameters describing the distribution of intermediate-scale variability are the mean permeability μ and the standard deviation σ.

As discussed in Sections 6.4.1 and 6.4.2, the permeability values provided to the SMPA need to account for the effect of excavation. Typically, the excavation-disturbed permeabilities in the vicinity of an underground opening are larger than the permeabilities measured in undisturbed rock. It is therefore important to use permeability data for the seepage abstraction that reflect the impact of excavation (see Section 6.6.2.1 below). Additional effects potentially changing fracture permeability, stemming from THM or THC rock alteration during or after the heating phase of the repository, do not need to be included in the permeability distributions for TSPA, for the reasons presented in Section 6.5.1.4.

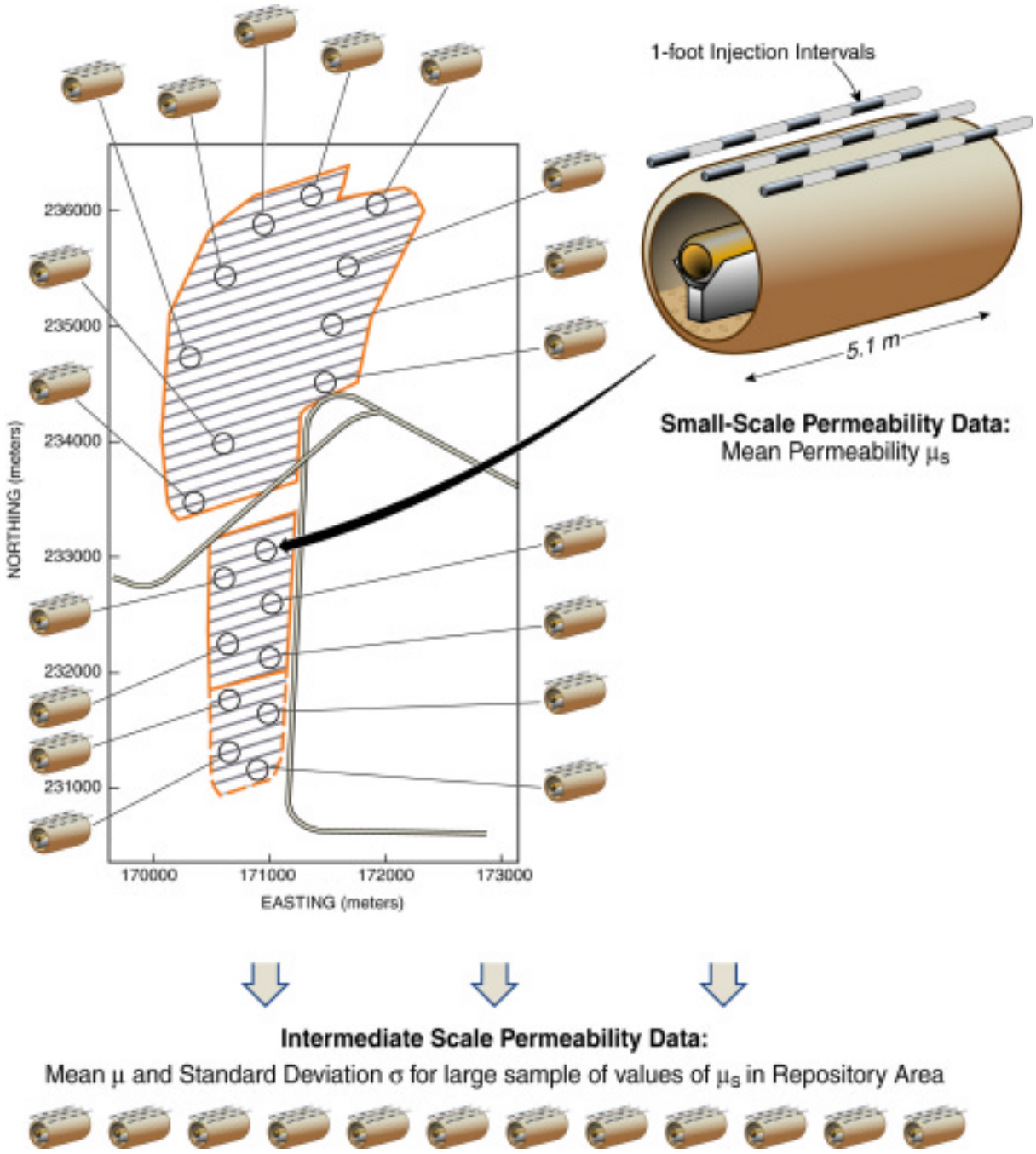

Figure 6.6-4. Schematic Showing the Relation between Statistics of Small-Scale Measurements (Mean Permeability μ_S) and the Intermediate-Scale Variability Distribution of the Repository Units (Mean μ and standard deviation σ)

6.6.2.1 Supporting Information

The most appropriate information on fracture permeability—measured on the scale of interest—stems from the air-injection testing conducted in the boreholes and niches displayed in Figure 6.6-1. The tests were performed by isolating a short section of the boreholes (1 foot [0.3 m] in niches, 6 ft [1.8 m] in systematic testing borehole SYBT-ECRB-LA#2), using an inflatable packer system, and then injecting compressed air at a constant rate into the isolated injection interval. The pressure buildup in the injection interval and in nearby observation intervals was monitored with time until steady-state conditions were reached, which typically occurred within a few minutes. Air injection was terminated after reaching steady-state pressures, and the decline in air pressure was then monitored as it recovered to its initial pre-test condition. Using the pressure response as input, the air-permeability value of the tested interval is calculated based on a commonly used analytical solution (BSC 2001 [158463], Section 6.1.2.1; LeCain 1995 [101700], p. 10, Eq. (15)). With the exception of the systematic testing boreholes, which were constructed after excavation of the drift, air-permeability values are available both before and after excavation. This is because the boreholes above Niches 3107, 3566, 3650, 4788, and 1620 had been drilled and tested prior to niche construction. Except for Niche 3566, testing was repeated using the same testing methodology and identical packer setup after excavation.

Analysis of pre-excavation measurements at Niches 3107, 3566, 3650, and 4788 is provided in BSC (2001 [158463], Table 6.1.2-3), giving the mean and standard deviation of the small-scale permeabilities (DTN: LB990901233124.004 [123273]). Statistical parameters for pre-excavation air-permeability data from Niche 1620 were calculated in this Model Report from DTN: LB0012AIRKTEST.001 [154586]; details are provided in Attachment III. Post-excavation data for Niches 3107, 3650, 4788, and 1620, as well as for systematic testing borehole SYBT-ECRB-LA#2, were analyzed in BSC (2003 [162267], Section 6.5.2 and Table 10). The resulting statistics are provided in DTN: LB0302SCMREV02.002 [162273]. Note that Niche 3566, located at CS 35+66, offers pre-excavation air-permeability data, but was not tested after excavation, as the niche was sealed with a bulkhead to conduct long-term monitoring of *in situ* conditions. No air-permeability data are available from boreholes SYBT-ECRB-LA#1 and SYBT-ECRB-LA#3 because of equipment problems during air-injection testing.

The mean values μ_S and the standard deviations σ_S of all appropriate small-scale permeability data conducted at each of the test locations are summarized in Table 6.6-3, for both undisturbed and disturbed conditions, if available. Here, standard deviations reflect spatial variability within the test bed, on a 1-foot test interval scale. Statistical analyses are conducted with log-transformed values, as the niche permeabilities are approximately log-normally distributed (BSC 2003 [162267], Section 6.6.2.1; note that log denotes base-10 logarithm in this report).

Table 6.6-3. Summary Statistics of Air Permeabilities Derived from Small-Scale Air-Injection Tests for Undisturbed and Excavation-Disturbed Conditions in the Middle Nonlithophysal Zone and the Lower Lithophysal Zone

Middle Nonlithophysal Zone (Tptpmn)						
Location	**Mean μ_S *(in log k)***			**Standard Deviation σ_S *(in log k)***		
	Undisturbed	Disturbed	Factor Dist./Undist.[3]	Undisturbed	Disturbed	Factor Dist./Undist.
Niche 3107	-13.4[1]	-12.14[2]	18.2	0.70[1]	0.80[2]	1.14
Niche 3566	-13.0[1]	—	—	0.92[1]	—	—
Niche 3650	-13.4[1]	-11.66[2]	55.0	0.81[1]	0.72[2]	0.89
Niche 4788	-13.0[1]	-11.79[2]	16.2	0.85[1]	0.84[2]	0.99
Lower Lithophysal Zone (Tptpll)						
Location	**Mean μ_S *(in log k)***			**Standard Deviation σ_S *(in log k)***		
	Undisturbed	Disturbed	Factor Dist./Undist.	Undisturbed	Disturbed	Factor Dist./Undist.
Niche 1620	-11.5[4]	-10.95[2]	3.5	1.12[4]	1.31[2]	1.17
SYBT-ECRB-LA#2	—	-10.73[2]	—	—	0.21[2]	—

Output-DTN: LB0308AMRU0120.001

NOTE: Computations documented in Attachment III

[1] Source: DTN: LB990901233124.004 [123273], also given in BSC (2001 [158463], Table 6.1.2-3)

[2] Source: DTN: LB0302SCMREV02.002 [162273], also given in BSC (2003 [162267], Table 10)

[3] Ratio of disturbed and undisturbed permeability values, not in log space.

[4] Source: Statistics were calculated from individual measurements given in DTN: LB0012AIRKTEST.001 [154586]

The small-scale mean permeabilities and their spatial variability as calculated for the four (three) niches located in the Tptpmn zone are consistent with one another, for both undisturbed and disturbed conditions. The Tptpll permeabilities show distinct differences to the Tptpmn values. Undisturbed permeability measured at one location in the lower lithophysal zone is approximately 1½ orders of magnitude larger than the respective Tptpmn value; disturbed zone permeabilities differ by approximately one order of magnitude. While the post-excavation permeabilities in the Tptpmn are between 16 and 55 times larger than the pre-excavation values, the Tptpll permeability at Niche 1620 differs by a factor of only 3.5. Possibly, these differences are related to the initially higher permeability in the Tptpll (before excavation), in case this higher permeability is a result of initially larger fracture apertures. The effect of excavation-related fracture dilation should be relatively small if the undisturbed fracture apertures are already large (Wang and Elsworth 1999 [104366]).

Note that the standard deviations in all niches are similar for the undisturbed and the disturbed conditions. Changing the mechanical stress field does not give rise to substantial changes in the small-scale variability. For the lower lithophysal unit, the variability as measured in Niche 1620 is significantly larger than that obtained in borehole SYBT-ECRB-LA#2. This is mainly a result of the injection intervals of borehole SYBT-ECRB-LA#2 being six times longer than those in Niche 1620.

As mentioned earlier, the small-scale variability of permeability σ_S is explicitly accounted for in the predictive seepage models. Most of the SMPA simulations were conducted using a base case standard deviation of 1.0 (see Section 6.4.2.1). It was demonstrated that a considerable increase in standard deviation (σ_S = 2.0) produced seepage rates that were only slightly larger than in the base case (BSC 2003 [163226], Section 6.6.2). Therefore, variation of σ_S can be neglected for seepage abstraction. On the other hand, the mean permeability μ_S and its potential intermediate-scale variation within the repository units is very important for seepage and needs to be provided to the TSPA. In the discussion below, these mean values of small-scale permeability will be simply referred to as permeability, to avoid confusion with the statistical parameters (mean μ and standard deviation σ) developed for the intermediate-scale variation of this rock property.

Supporting information on the impact of excavation on permeability distributions in the drift vicinity is available from rock-mechanical model simulations. Preliminary analyses of excavation-related permeability changes were performed (BSC 2001 [155950], Section 4.3.7.4), using a fully coupled thermal-hydrological-mechanical continuum model (TOUGH2-FLAC), which was calibrated to available niche and drift air-permeability data conducted at ambient conditions. These initial studies are complemented by more recent modeling analyses presented in BSC (2003 [162318]). In theory, the excavation-related permeability increase at the crown of a circular-shaped drift should be slightly smaller than in niches where the ceiling has a flatter, approximately elliptic shape. Thus, the disturbed-zone permeabilities for niches may need adjustments to represent permeabilities of the excavation-disturbed zone around circular-shaped emplacement drifts. Modeling results also suggest anisotropic behavior; the horizontal permeability increase at the crown can be significant while the vertical increase at the crown is almost negligible. Considering a circular drift in the Tptpmn, the permeability at the drift crown is predicted to increase by a factor of up to 19 in the tangential and by a factor of 1.5 in the radial direction (BSC 2003 [162318], Section 6.5.1, Figure 6.5.1-1). The permeability increase in the Tptpll is smaller, with a factor of up to 8 tangentially and about 1.3 radially (BSC 2003 [162318], Section 6.6.1, Figure 6.6.1-1). These values compare reasonably well with the measured changes at the crown of the niches, where the permeability increase is between 16 and 55 in the middle nonlithophysal unit (with a geometric mean of 25 over the three niches) and 3.5 in the lower lithophysal unit.

It was pointed out earlier in this Model Report that the diversion of water around drifts mainly depends on the tangential fracture permeability in the boundary layer near the drift wall. Thus, the increased tangential permeability component at the drift crown needs to be accounted for in seepage models. However, the process models developed for drift seepage predictions, like the SMPA and the TH Seepage Model, do not consider anisotropy in permeability. Therefore, the increased tangential permeability component is used in these models as an isotropic value. That the radial permeability component in the excavation-disturbed zone is overestimated as a result of such simplification makes the predicted seepage values conservative. As explained in BSC (2003 [163226], Section 6.3.2), a higher tangential permeability in conjunction with a smaller vertical permeability will facilitate the flow of water laterally around the drift and hence reduce seepage probability. Note that the tangential permeability, as predicted by the TOUGH2-FLAC model, not only increases at the crown of the drift, but also at the springline (BSC 2003 [162318], Sections 6.5.4 and 6.6.1).

Since measured and predicted permeability differences between undisturbed and disturbed conditions show reasonable agreement, there are two possible methods of defining the parameter distributions of the disturbed-zone permeability for TSPA-LA: (1) directly use the measured post-excavation air-permeability data, or (2) use pre-excavation data and adjust them according to the predicted permeability changes. In this Model Report, the more conservative of these methods is used in order to account for uncertainties in both the measured and the simulated results. For the Tptpmn, where the measured permeability change is larger than the predicted, the THM model results are applied. Based on BSC (2003 [163226], Section 6.3.2), a factor of 10 is chosen as a representative average for the tangential permeability changes in the seepage-relevant boundary layer along the crown, which is smaller than the maximum predicted increase of 19 directly at the drift crown. (As explained earlier, the impact of excavation alterations decreases with distance from the drift wall.) For the Tptpll, where the measured change is smaller than the predicted, the measured factor of 3.5 is chosen as appropriate.

6.6.2.2 Spatial Variability

The intermediate-scale variability of permeability refers to the variation of this parameter—provided as the mean μ_S of small-scale permeability measurements—within the repository rock units. From Table 6.6-3, the two main host rock units have significantly different permeability ranges, as measured in Niches 3107, 3650, and 4788 for the Tptpmn, and in Niche 1620 and borehole SYBT-ECRB-LA#2 for the Tptpll. Thus, analyses of intermediate-scale variability need to be conducted separately for the two units, which makes the sample size for developing appropriate probability distributions rather small. For the Tptpmn, pre-excavation permeability values are available at four niche locations, covering a stretch of about 1,700 m length along the ESF (see Figure 6.6-1). Post-excavation data are available at three niches. Less information is available in the lower lithophysal unit. Pre-excavation data are available at one test location only (Niche 1620); post-excavation measurements are available at two locations that are relatively close (Niche 1620 and borehole SYBT-ECRB-LA#2). Since this sample size is not sufficient to derive defensible probability distributions, information from other sources is needed to better constrain the parameter distributions. The following paragraphs describe the treatment of spatial variability separately for the Tptpmn and the Tptpll.

6.6.2.2.1 Middle Nonlithophysal Unit

Table 6.6-4 summarizes the intermediate-scale statistical parameters (mean μ and standard deviation σ) calculated from the four niches located in the Tptpmn (see Table 6.6-3). Though covering a large distance along the ESF, and despite the fact that the niche locations have been carefully selected to represent rock zones with different fracture intensity (Section 6.6.1.2), the variability σ of mean permeability observed among the four (three[1]) test locations is very small. This is consistent for both undisturbed- and disturbed-zone data, with standard deviations of 0.23 and 0.25 (in log10), respectively. Because standard deviation is small, the standard error of the mean is also small, although the number of samples is limited. This would lead to relatively narrow probability distributions for spatial variability and uncertainty.

[1] Numbers in parenthesis indicate excavation-disturbed measurement locations.

The question arises whether these statistical values accurately represent the permeability distribution over the entire host rock unit. Additional air-permeability data need to be evaluated to confirm or, if needed, to adjust the parameter distributions given in Table 6.6-3. Measurements of air permeability in the Tptpmn have been conducted in four vertical surface-based boreholes (NRG-7a, NRG-6, SD-12, and UZ#16) and in numerous boreholes drilled into the SHT and DST rock block (Alcove 5). Note that the full name of borehole UZ#16 is "UE-25 UZ#16". Out of convenience, the short name UZ#16 is used throughout this Model Report.

The locations of these air permeability measurements are illustrated in Figure 6.6-5. Boreholes NRG-6 and UZ#16 are located some distance from the ESF; thus, they cover rock areas that have not been represented by niche measurements. The packer lengths in the vertical boreholes were fairly consistent between 3.5 m and 4.6 m (more than one order of magnitude larger than in the niches), while the packer length in the heater test areas varied widely from approximately 2 to 11 m for the SHT, and 3 to 39 m in the DST.

Table 6.6-4. Intermediate-Scale Variability Statistics (Mean μ and Standard Deviation σ) of Permeability over Repository Rock Block, for Pre- and Post-Excavation Data in the Tptpmn

Parameter	Number of Samples	Mean μ (in log k)	Std. Dev. σ	Std. Error of Mean SE
Pre-excavation Permeability (undisturbed)	4	-13.2	0.23	0.12
Post-excavation Permeability (disturbed)	3	-11.9	0.25	0.14

Output-DTN: LB0308AMRU0120.001
NOTE: Computations documented in Attachment III

Figure 6.6-6 compares the mean values (in log space) of data from the pre-excavation niche measurements (from Table 6.6-1), the surface-based boreholes, and the SHT/DST area, separately for each location (BSC 2003 [161773], Section 6.1.1.1). The ranges of data, calculated as mean plus/minus one standard deviation, overlap, but generally the means of the small-scale niche data are lower than the other values. This is expected because the mean effective permeability increases as the scale of measurements increases (Neuman 1994 [105731]). (Also, the observed range of data is larger for the niche measurements. This again is expected from scaling effects, because a larger measurement scale tends to neglect the impact of small-scale variability.) Thus direct comparison of the mean permeability data observed at the niches with data from surface-based boreholes (or from the heater test block) is not appropriate; statistical analyses have to be conducted over locations with similar measurement scale. However, it can be beneficial to apply adequate scaling laws to adjust the mean permeability values obtained with different interval lengths. Also, the variability of mean permeability between surface boreholes should be similar to the variability of mean permeability between the niche locations.

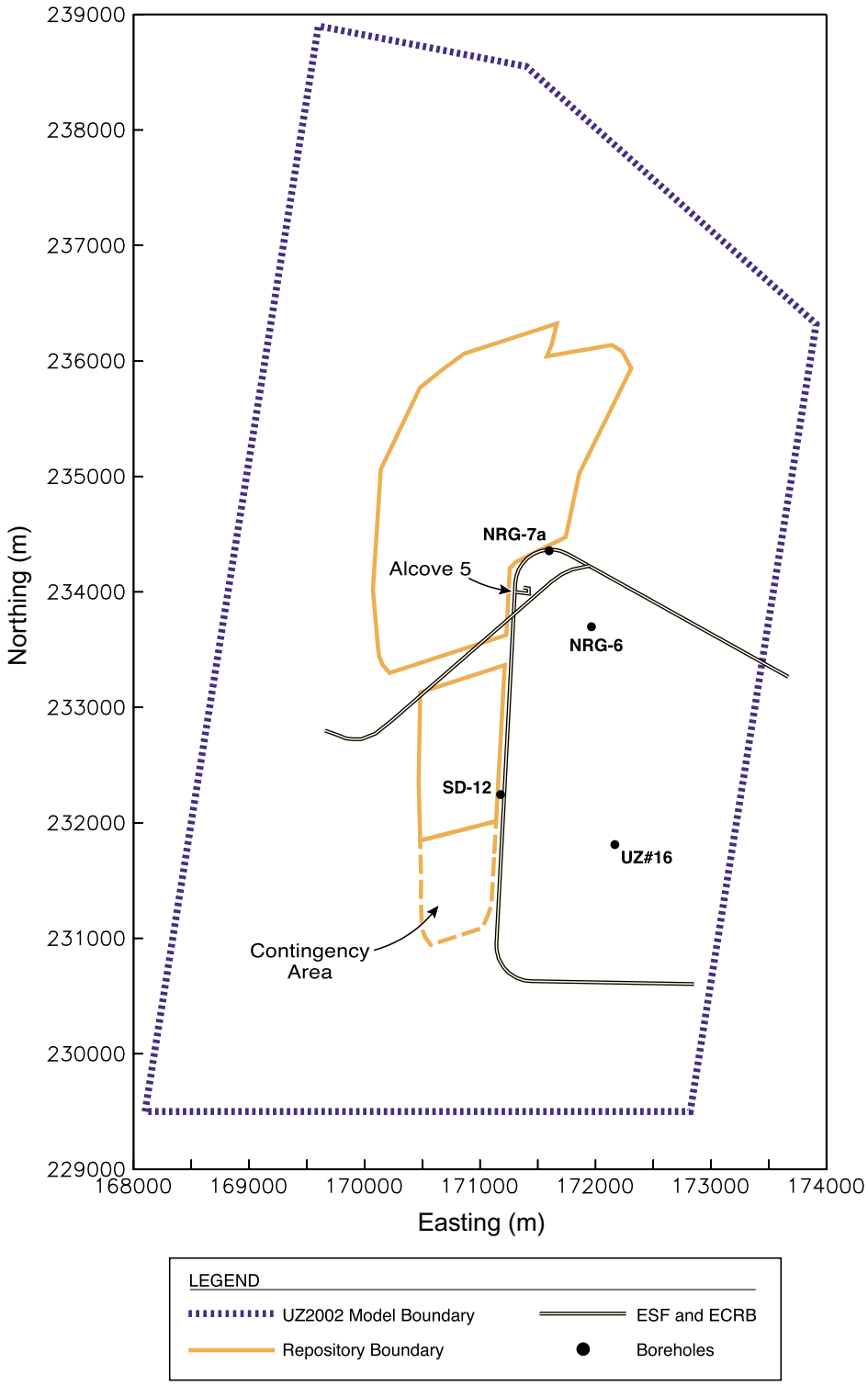

Source: Revised from BSC (2003 [160109], Figure 1b) using 800-IED-WIS0-00101-000-00A (BSC 2003 [162289])

NOTE: The boundary of the current repository design is also given.

Figure 6.6-5. Map Showing Approximate Location of Surface-Based Boreholes NRG-7a, NRG-6, SD-12, and UZ#16 and SHT/DST Heater Test Area (Alcove 5)

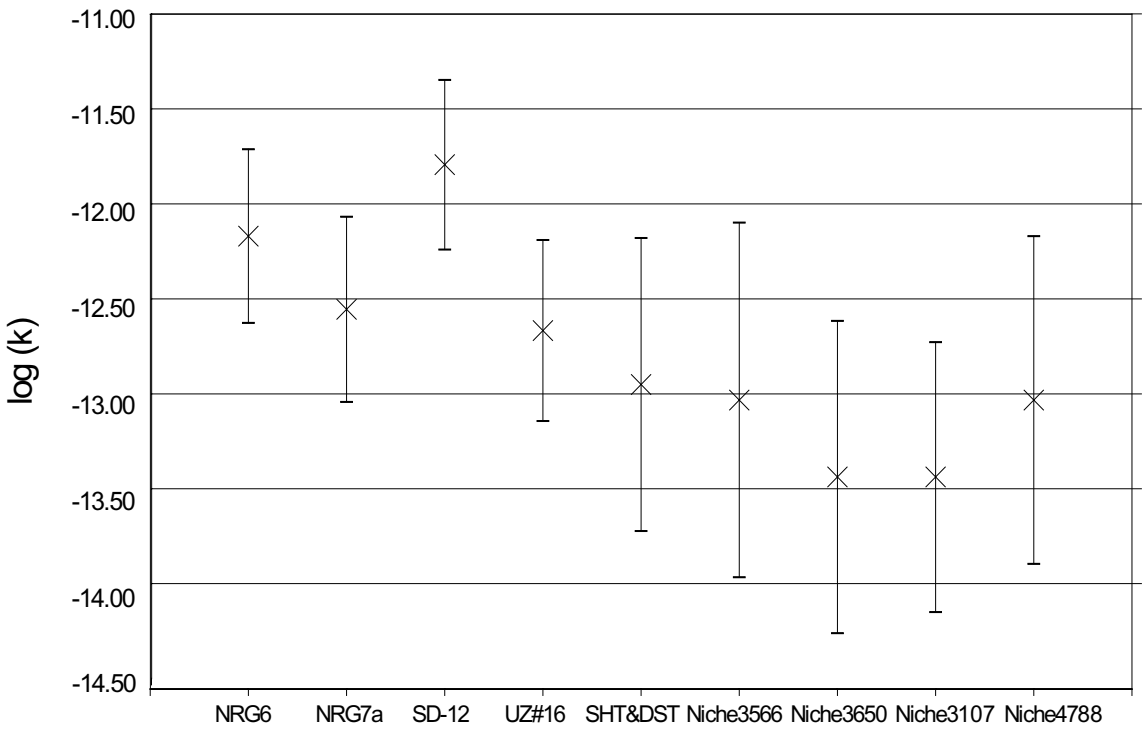

Source: BSC (2003 [161773], Figure 2)

NOTE: X are the geometric means. Bars indicate mean plus/minus one standard deviation.

Figure 6.6-6. Mean Fracture Permeabilities for Different Locations in the Tptpmn Unit

A more detailed analysis of intermediate-scale variation of permeability among the four vertical boreholes is presented in Table 6.6-5. Between 7 and 19 vertical intervals have been tested in the Tptpmn in each of these boreholes. The resulting air-permeability data for each test interval are provided in DTN: GS960908312232.013 [105574]. From these data, the mean permeability μ_{sur} was calculated for each location. In a second step, the statistics of the variation of this parameter over the repository unit were derived. Data from the SHT/DST heater test block have not been considered in this analysis, mainly because of the large, inconsistent measurement scale. Also, some of the tested boreholes are in close proximity to the alcoves or drifts, and thus they may not represent undisturbed rock. As shown in Table 6.6-5, the average of the mean log-permeability values at the four vertical boreholes is –12.2, which is one order of magnitude higher than the intermediate-scale mean μ estimated from the niche data. The standard deviation is 0.34, about 50% larger than from the undisturbed niche data. It appears that the variability inferred from the niche experiments is on the low side when compared with additional information from vertical boreholes. To define a cautiously realistic variability for TSPA-LA, the larger σ of 0.34 should be used. It will be discussed below whether the one-order-of-magnitude difference in the mean values can be fully explained by scale effects. (Note that there are minor differences in the mean permeabilities of boreholes NRG7a and UZ#16 between Figure 6.6-6 and Table 6.6-5. These differences stem from a slightly different averaging procedure. For the analysis in Table 6.6-6, air-injection intervals that intersect two geological units have been assigned to both units.)

Table 6.6-5. Mean Permeabilities of Undisturbed Rock from Tptpmn Unit Measured in Surface-Based Boreholes and Intermediate-Scale Variability Statistics over the Repository Rock Block

Location	Number of Intervals	Mean μ_{sur} *(in log k)*	Interval Length (m)	
NRG-6	7	-12.2	4.3[1]	
NRG-7a	8	-12.5	3.5	
SD-12	7	-11.8	4.6	
UZ#16	19	-12.5	4	
Statistics over All Four Locations	**Number of Locations**	**Mean μ (in log k)**	**Std. Dev. σ**	**Std. Error of Mean SE**
Tptpmn	4	-12.2	0.34	0.17

Output-DTN: LB0308AMRU0120.001

NOTE: Computations documented in Attachment III

[1] One interval length is 11.3 m in NRG-6. All others are 4.3 m.

While many theoretical upscaling approaches are available in the literature, an upscaling method for highly heterogeneous porous media is described by the following expression (Paleologos et al. 1996 [105736], p. 1336, Eq. (26)):

$$k_{eff} = k_S \exp[\sigma_S (\ln k_S)^2 (1/2 - D)] \quad \text{(Eq. 1)}$$

where k_{eff} is the effective permeability at a larger scale L (about 3.5 to 4.6 meter scale), k_S is the geometric mean of the small-scale permeability (about 1-foot scale), $\sigma_S(ln\ k_S)$ is the standard deviation of the natural log-transformed small-scale permeability, and D is a function of the spatial dimensions and the correlation scale. The exponential expression in Equation (1) is always larger than or equal to 1, indicating that the upscaled effective permeability is always larger than or equal to the small-scale geometric mean. Using an approximate value of 1 m for the correlation scale λ of permeability in the niches, estimated from BSC (2003 [162267], Table 13), and with L in the range between 3.5 and 4.6 m, the domain integral D can be evaluated from Figure 2 in Paleologos et al. (1996 [105736]) as approximately 0.3. (Note: $2\rho = 2L/\lambda$ as defined in Paleogolos et al. (1996 [105736], p. 1335) becomes 7 for L = 3.5 and λ = 1). In this case, Equation (1) becomes

$$\log(k_{eff}) = \log(k_S) + 0.46\sigma_S^2 \quad \text{(Eq. 2)}$$

where σ_S is the standard deviation of the log-transformed small-scale permeability, as given in Table 6.6-3. Note that the logarithm of the geometric mean of a sample is equal to the arithmetic mean of the log-transformed data. This relationship can be used to derive the expected value of log-transformed permeability measurements on a larger scale, μ_{eff}, from the expected value of the small-scale measurements, μ_S, given in Table 6.6-3. The resulting equation is given as:

$$\mu_{eff} = \mu_S + 0.46\sigma_S^2 \quad \text{(Eq. 3)}$$

If the differences between the niche measurements and the data from surface-based boreholes are merely a result of scale effects, these values for μ_{eff} should be consistent with the permeability values μ_{sur} from the surface-based boreholes.

Another approach for upscaling is to directly use the 1-foot permeability measurements of the niches. Estimates of effective permeabilities on a larger scale can be derived by calculating the arithmetic mean of these 1-foot values (not log-transformed) over appropriately long sections of the boreholes. It is presumed in this approach that the 1-foot data represent the exact spatial variability along the borehole, and that this exact variability is being measured using packed-off intervals of a larger interval length. It can be shown that the measured permeability over this larger interval would be the arithmetic mean of the 1-foot values within the interval. Since the arithmetic mean of heterogeneous data gives more weight to large values, the resulting effective permeability is higher than the geometric mean of the 1-foot data. The proposed upscaling approach was conducted for the four niches 3107, 3566, 3650, and 4788, using the permeability data given in the following DTNs: LB980901233124.101 [136593] and LB0011AIRKTEST.001 [153155]. A 3.6-m interval length was chosen, comprising twelve 1-foot intervals. The available sample of undisturbed small-scale permeability at each niche location was divided into groups of twelve subsequent 1-foot measurements; i.e., one group represents the length covered by a 3.6 m measurement interval. The arithmetic mean of permeability was calculated for each group. Then the means were log-transformed, and the mean of all groups belonging to one niche location was derived. The final result is the mean effective permeability μ_{eff} measured at a 3.6 m interval length, which can be compared with the mean of the small-scale measurements.

Table 6.6-6 summarizes results for both upscaling methods outlined above, giving the predicted increase of permeability as a result of scale effects, and listing the adjusted upscaled permeability values for measurements conducted on a 3.6 m scale. While both methods are consistent in their trends, there are differences in magnitude. The average permeability increase as predicted by Equation (2) is 0.3 (in log10), while the average increase estimated from the arithmetic mean data analysis is 0.6 (in log10). Much of this larger increase, however, is provided by data from Niche 3566, where the fewest small-scale measurements are available. If data from Niche 3566 were disregarded, the respective average increases would be approximately 0.3 and 0.4 for the two approaches (in log10).

Table 6.6-6. Upscaling Factors for Air Permeabilities in the Tptpmn Derived Using Two Different Upscaling Approaches

	Small-Scale Measurements		Upscaling Factor and Adjusted Mean μ_{eff}			
Location	Mean μ_S (in log k)	Std. Dev. σ_S	Using Eq. (3) (in log k)		Using Data Analysis (in log k)	
Niche 3107	-13.4[1]	0.70[1]	0.2	-13.2	0.4	-13.0
Niche 3566	-13.0[1]	0.92[1]	0.4	-12.6	1.0	-12.0
Niche 3650	-13.4[1]	0.81[1]	0.3	-13.1	0.4	-13.0
Niche 4788	-13.0[1]	0.85[1]	0.3	-12.7	0.5	-12.5
Mean All Niches	-13.2[2]	—	0.3	-12.9	0.6	-12.6

Output-DTN: LB0308AMRU0120.001

NOTE: Computations documented in Attachment III

[1] Data from Table 6.6-3 (undisturbed)

[2] Data from Table 6.6-4 (undisturbed)

The estimated scaling factors are significantly smaller than the one-order-of-magnitude difference between the mean permeability of the four niches (-13.2) and the mean permeability from the four surface-based boreholes (-12.2). Or, in other words, the effective permeability values μ_{eff} derived from upscaling the small-scale measurements are much smaller than the permeability values measured in surface-based boreholes. Thus, even though scale effects are considered to make both measurement scales comparable, the remaining difference is still half an order of magnitude. This may suggest that the four niche locations have relatively low permeability, compared to the average permeability the Tptpmn unit, and that the scale-corrected data from surface-based boreholes could be used to adjust the mean of the niches to higher values for TSPA-LA, which would generally reduce seepage. On the other hand, one should keep in mind in this abstraction process that the four niche measurements represent the more reliable data source for the purpose of seepage modeling: they represent the scale of interest. The surface-based data, on the other hand, should be handled with care because of uncertainties related to the upscaling analysis. Therefore, seepage abstraction does not incorporate this possible adjustment of the niche permeabilities to larger values. The additional information available from the surface-based boreholes is used as corroborative evidence demonstrating that the niche data provide conservative parameter estimates for mean permeability in the Tptpmn.

Based on the discussion above, the parameter distributions for permeability variation within the middle nonlithophysal unit in TSPA-LA are defined as follows: The intermediate-scale mean log-permeability of the undisturbed measurements is –13.2, derived from the mean over four niche locations (Table 6.6-4). Cautiously realistic, the intermediate-scale variability is described by a standard deviation of 0.34, derived from the four surface-based borehole locations (Table 6.6-5). This standard deviation is larger than the one calculated from the niches. The permeability increase as a result of excavation is conservatively accounted for by increasing the mean permeability by one order of magnitude. This is consistent with modeling predictions, but smaller than the measured effect of excavation. The final probability distribution is given by a mean of μ = –12.2 and a standard deviation of σ= 0.34 (log-normal distribution); the 95%-confidence interval of this distribution ranges approximately from –12.9 to –11.5. Uncertainty related to this distribution is discussed in Section 6.6.2.3.

6.6.2.2.2 Lower Lithophysal Unit

Table 6.6-7 summarizes statistical parameters for intermediate-scale variability within the Tptpll, based on the small-scale measurements conducted in Niche 1620 and borehole SYBT-ECRB-LA#2 (see Table 6.6-3). It is recognized that the supporting sample size is very small: There is only one location where pre-excavation data have been measured (Niche 1620). Two locations are available for post-excavation data (Niche 1620 and borehole SYBT-ECRB-LA#2, see Table 6.6-3), though the relatively close proximity limits the value of these data. Hence, the small standard deviation of 0.16 measured for the disturbed-zone permeabilities, relating to a small 95% confidence interval that covers about half an order of magnitude, is arguably not representative for the variability of Tptpll permeability values over the repository block. Additional air-permeability data are therefore evaluated.

Table 6.6-7. Intermediate-Scale Variability Statistics (Mean μ and Standard Deviation σ) of Permeability over the Repository Rock Block, for Pre- and Post-Excavation Data in the Tptpll

Parameter	Number of Samples	Mean μ (in log k)	Std. Dev. σ	Std. Error of Mean SE
Pre-excavation Permeability (undisturbed)	1	-11.5	—	—
Post-excavation Permeability (disturbed)	2	-10.8	0.16	0.11

Output-DTN: LB0308AMRU0120.001

NOTE: Computations documented in Attachment III

Surface-based boreholes NRG-7a and UZ#16 offer undisturbed air-permeability values for the Tptpll measured over interval lengths of 3.5 and 4 m, respectively (see Figure 6.6-5 for the location of these boreholes). The measured data are given in DTN: GS960908312232.013 [105574]. No Tptpll measurements are available at boreholes NRG-6 and SD-12, but the hydrogeologically comparable upper lithophysal unit (Tptpul) has been tested at four locations, i.e., at NRG-7a, NRG-6, SD-12, and UZ#16. Table 6.6-8 below provides the calculated mean permeability μ_{sur} at each of these borehole locations in the Tptpll and the Tptpul, and gives summary statistics of the variation of this parameter within the repository.

Both units have consistent permeability values; the values at available locations are identical (NRG-7a) or differ by only 0.1 in log space (UZ#16). Over all locations, the intermediate-scale mean μ is –12.1 in the Tptpll versus –11.8 in the Tptpul. Standard deviations are 0.58 versus 0.47, respectively. The Tptpul values are considered the more reliable estimates for the lithophysal units (because the statistical analysis is based on a sample size of four) and shall be used below. Data analysis suggests that the differences in the intermediate-scale means and standard deviations can mainly be attributed to the one permeability value of –12.5 at NRG-7a, which is significantly smaller than those at all other measurement locations.

Comparison between the summary statistics over the surface-based boreholes, given in Table 6.6-8, and the Niche 1620/borehole SYBT-ECRB-LA#2 data, given in Table 6.6-7, indicates

significant differences. It appears that the standard deviation estimated from the small-scale measurements (σ = 0.16) is not representative of the intermediate-scale spatial variability within the Tptpll. Therefore, the larger value of 0.47 derived from surface-based boreholes (while using the Tptpul value as explained above) is recommended for use in the TSPA-LA.

Table 6.6-8. Mean Permeabilities of Undisturbed Rock from Tptpll and Tptpul Units Measured in Vertical Boreholes and Intermediate-Scale Variability Statistics over Repository Rock Block

	Lower Lithophysal Unit (Tptpll)			Upper Lithophysal Unit (Tptpul)		
Location	**Number of Intervals**	**Mean μ_{sur} (in log k)**	**Interval Length (m)**	**Number of Intervals**	**Mean μ_{sur} (in log k)**	**Interval Length (m)**
NRG-6	—	—	—	5	-11.7	4.3[1]
NRG-7a	16	-12.5	3.5	10	-12.5	3.5
SD-12	—	—	—	6	-11.4	4.6
UZ#16	18	-11.7	4	5	-11.8	4
Statistics over all Locations	**Number of Locations**	**Mean μ (in log k)**	**Std. Dev. σ**	**Std. Error of Mean SE**		
Tptpll	2	-12.1	0.58	0.41		
Tptpul	4	-11.8	0.47	0.23		

Output-DTN: LB0308AMRU0120.001

NOTE: Computations documented in Attachment III

[1] Two interval lengths are 11.3 m in NRG-6. All others are 4.3 m.

As for the mean permeability, scaling effects need to be accounted for to make the different estimates from surface-based boreholes and from small-scale niche experiments comparable. Using the same two upscaling approaches as for the middle nonlithophysal unit, the upscaling factors for Niche 1620 are 0.6 from Equation (2) and 0.7 from the arithmetic-mean data analysis (Table 6.6-9). One can use these upscaling factors to adjust the mean permeability from the surface-based borehole data, making them representative of 1-foot-interval measurements. With an upscaling factor of 0.7 from the arithmetic data analysis and using the more reliable Tptpul permeability value of μ_{sur} = –11.8 (Table 6.6-8), the resulting scale-adjusted mean permeability for the surface-based borehole data is –12.5. This permeability value is one order of magnitude smaller than the mean pre-excavation permeability of μ = –11.5 from the small-scale niche measurements (Table 6.6-7). Quite possibly, Niche 1620 is located in a fairly permeable section of the lower lithophysal unit and may not be representative for all other areas in the repository. For the purpose of seepage abstraction, the permeability value measured in Niche 1620 should be adjusted to smaller values to account for the possible existence of less permeable regions in the repository. It is therefore proposed to use adjusted permeability distributions for the Tptpll with a decreased mean permeability of –12.0, which is derived from simply averaging the respective values from the niche analysis (-11.5) and the scale-adjusted surface-based data (-12.5). This shift in the parameter distribution is conservative, because smaller permeabilities generally lead to more seepage. One should keep in mind in this abstraction process that the measurements in Niche 1620 represent the more reliable data source for the purpose of seepage modeling: they represent the scale of interest. The surface-based data, on the other hand, should be handled with

care because of uncertainties related to the upscaling analysis. In light of this discussion, a permeability decrease by half an order of magnitude is a cautious, yet realistic parameter choice for the Tptpll unit.

Based on the above discussion, the parameter distributions for permeability variation within the lower lithophysal unit in TSPA-LA are defined as follows: The intermediate-scale mean log-permeability of the undisturbed measurements is –12.0, derived from the averaging the scale-adjusted mean of surface-based boreholes with the mean permeability from the niche measurements. Cautiously realistic, the intermediate-scale variability can be described by a standard deviation of 0.47, derived from the four surface-based borehole locations. This standard deviation is significantly larger than the one calculated from the niche/systematic testing data. The permeability increase as a result of excavation is conservatively accounted for by adjusting the mean permeability by a factor of 3.5 (Table 6.6-3). This is consistent with the measured effect of excavation, but less than predicted from the THM modeling studies (see Section 6.6.2.1). The final probability distribution for the Tptpll is given by a mean of μ = –11.5 and a standard deviation of σ = 0.47 (log-normal distribution); the 95% confidence interval of this distribution ranges approximately from –12.4 to –10.6. Compared to the middle nonlithophysal unit, the resulting distribution of disturbed-zone permeability in the Tptpll has a larger mean and a larger standard deviation. Uncertainty related to this distribution is discussed in Section 6.6.2.3.

Table 6.6-9. Upscaling Factors for Air-Permeability Measurements in the Tptpll Derived Using Two Different Upscaling Approaches

	Small-Scale Measurements		Upscaling Factor and Adjusted Mean μ_{eff}			
Location	Mean μ_{sf} (in log k)	Std. Dev. σ_S	Using Eq. (2) (in log k)		Using Data Analysis (in log k)	
Niche 1620	-11.5[1]	1.12[1]	0.6	-10.9	0.7	-10.8

Output-DTN: LB0308AMRU0120.001

NOTE: Computations documented in Attachment III

[1] Data from Table 6.6-3

6.6.2.3 Uncertainty

The different sources of uncertainty related to the intermediate-scale, disturbed-zone fracture permeability distribution are as follows:

Measurement Uncertainty:

Air-injection testing is the main method of estimating fracture permeability in the Yucca Mountain UZ. The measurement methodology for the niche test data—isolating borehole sections using an inflatable packer system, injecting compressed air, and monitoring the pressure response—is described in detail in Attachment I of BSC (2001 [158463]). The flow rate of air is controlled by four different sizes of mass flow controllers from 1 to 500 standard liters per minute, ensuring that the anticipated flow rates can be prescribed with sufficient accuracy (BSC 2001 [158463], Attachment I). Instrumentation error of the pressure sensors is about 0.3 kilopascals and thus negligible (BSC 2001 [158463], Attachment I). Short circuiting of gas flow between adjacent boreholes (or borehole

intervals), a potential error source of measurements conducted in the SHT (BSC 2002 [160771], Section 6.2.2.4.2) is of no concern in the niche tests because all boreholes in one niche location are packed-off with multiple packer strings at one time. Therefore, no measurement uncertainty is included in and propagated through seepage abstraction.

Conceptual Model Uncertainty:

The measured pressure response from the injection tests is converted into air-permeability values using the modified Hvorslev's formula (LeCain 1995 [101700], p. 10, Eq. (15)), derived for a steady-state ellipsoidal flow field around a finite line source. For post-excavation tests, where the niche opening acts as a constant pressure boundary, a cylindrical solution is adopted with an ambient constant pressure boundary at the external radius (BSC 2001 [158463], Section 6.1.2.1). While the formulas used are based on a simplified geometric configuration, the derived permeability values are expected to adequately represent the fracture continuum permeability of the medium. Also, due to the consistency of the conceptual models for seepage calibration (SCM) and seepage prediction (SMPA and TH Seepage Model), a possible bias in estimated air permeabilities would be removed from the predictive results because the calibrated capillary-strength parameter implicitly accounts for the impact of this bias. A final contribution to conceptual model uncertainty of fracture permeability may stem from the THM results used to constrain the choice of post-excavation parameters. However, the model results are compared (validated) with pre- and post-excavation measurements in the niches that give direct evidence of excavation effects. For abstraction, the more conservative of the resulting disturbed-zone permeability values is used to acknowledge the remaining uncertainty.

Estimation Uncertainty:

There is no estimation uncertainty for permeability because the proposed parameter distributions covering intermediate-scale permeability differences, described by a log-normal distribution with mean μ and standard deviation σ, are directly based on the permeability data from air-injection testing. Estimation uncertainty would only arise if the parameter of interest was estimated from a random process (e.g., from a Monte-Carlo analysis). Note that the impact of random variations of small-scale heterogeneity is directly evaluated in the seepage models by using several realizations of random fields.

Spatial Variability Uncertainty:

The main uncertainty source for permeability is related to the spatial variability assumed for this parameter, stemming from the limited number of data points available to derive the distribution parameters. Four (three[1]) niche locations are available in Tptpmn unit, compared to only one (two[1]) locations in the Tptpll. Therefore, additional information was used to better define appropriate probability distributions. For this purpose, data from surface-based boreholes were analyzed, adjusted to account for scale effects stemming from the longer measurement interval, and then compared to the niche data. In case of the Tptpll unit, where the surface-based data indicated that the niche measurements might represent a rather permeable section, the mean permeability was adjusted to smaller

[1] Numbers in parenthesis indicate excavation-disturbed measurement locations.

values (which gives rise to more seepage). For standard deviation σ, the larger value was chosen, to make sure that the potential variability of permeability is adequately covered. While the use of additional permeability data and the choice of conservative parameters have provided confidence in the developed parameter distributions, the spatial variability uncertainty is still considered significant because of the limited number of data points. This uncertainty is included in and propagated through the abstraction, using appropriate probability distribution functions.

Similar to Section 6.6.1, uncertainty in the parameter of interest is quantitatively accounted for by varying the mean of the chosen probability distribution for spatial variability within appropriate ranges; i.e., by shifting the log-normal distribution for spatial variability to smaller or larger permeability values. Definition of these "appropriate ranges" is necessarily subjective, since it is based on scientific judgment. As pointed out above, the main contribution to uncertainty stems from the limited sample size constraining the spatial variability distribution. The method of choice in this abstraction is to apply a triangular uncertainty distribution with upper/lower bounds defined by plus or minus four standard errors. This adds a significant amount of additional parameter variability, believed to cover the uncertainty of the permeability estimates. As pointed out before, the standard error describes the potential uncertainty in the estimated mean of a sample of given size. A range of plus or minus two standard errors covers roughly the 95% confidence interval for the estimated mean. Thus, the defined range of the triangular distribution comprises sufficient uncertainty on account of the mean permeability and includes another two SE covering other sources of uncertainty. In light of the supporting information used to corroborate niche data, and considering the conservative choices made in defining the spatial variability distributions, this uncertainty range can be considered cautious, yet realistic. Note the difference between the uncertainty range chosen for permeability (4 SE) and the uncertainty range chosen for the capillary-strength parameter in Section 6.6.1.3 (3 SE). The difference accounts for our assessment that the spatial variability distributions for permeability are more uncertain than the ones for the capillary-strength, because of (a) the smaller sample size for permeability values, and (b) the fact that $1/\alpha$ is an effective calibrated parameter that may be less dependent on rock type variability.

A schematic of the spatial variability and uncertainty model for permeability in the middle nonlithophysal unit is given in Figure 6.6-7. The heavy blue line shows the triangular-shaped uncertainty distribution, assigning a probability to the mean of the normal-shaped spatial variability distribution. The most likely spatial variability distribution is the one defined in Section 6.6.2.2, with a probability of 1.47 corresponding to the peak value of the triangular distribution. This spatial variability distribution has a mean of –12.2 in log space. The triangular distribution for shifting this mean has a range of about ±0.68 (using the standard error of 0.17 as given in Table 6.6-5). Thus, least likely are the two bounding cases with a mean of –12.9 (minimum) and –11.5 (maximum), respectively, where the triangular distribution indicates a zero probability. Together, in consideration of spatial variability and uncertainty, the range of Tptpmn permeabilities to be used in TSPA-LA is quite large; using the approximate 95% confidence intervals of the minimum and the maximum spatial variability distribution as an estimate, this range extends from –13.6 to –10.8 (almost three orders of magnitude, from about 4.0×10^{-13} m^2 to about 1.6×10^{-11} m^2).

The respective probability distributions for the lower lithophysal unit are illustrated in Figure 6.6-8. As a result of the larger standard deviation, both the spatial variability distribution and the uncertainty distribution are wider compared to the Tptpmn. The triangular distribution of uncertainty covers a range of about ±0.92 (using the standard error of 0.23 as given in Table 6.6-8). This shifts the mean of the spatial variability distribution (most likely value at –11.5 in log space) to bounding values of –12.4 (minimum) and –10.6 (maximum). The approximate 95% confidence interval of all possible spatial variability distributions ranges from –13.3 to –9.7 (almost four orders of magnitude; from about 5.0×10^{-14} m^2 to about 2.0×10^{-10} m^2).

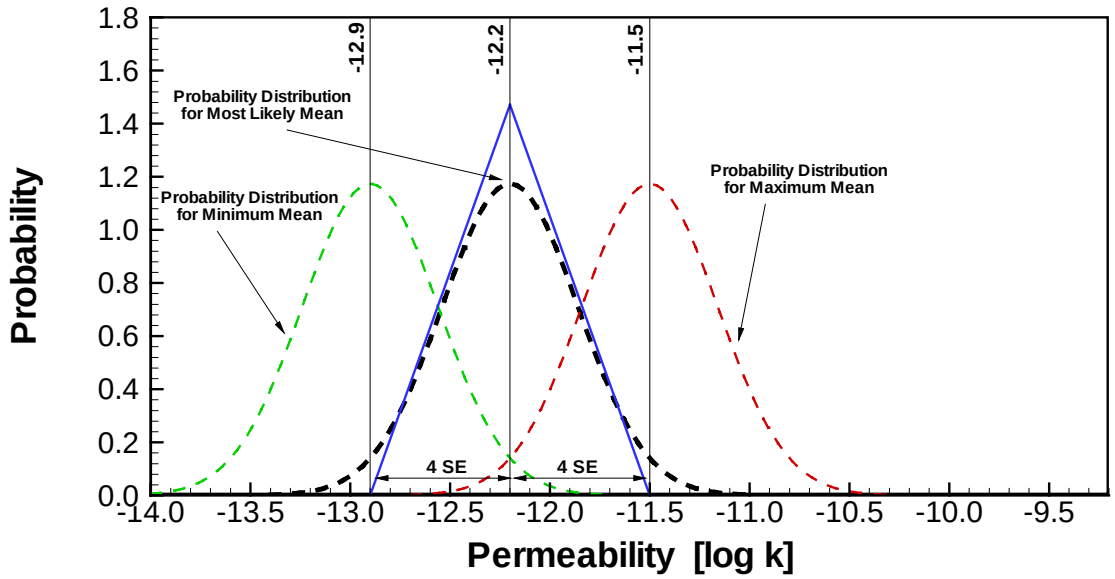

NOTE: The black dashed line shows the most likely spatial probability distribution (at the peak of the triangular distribution). The green and the red dashed lines show the least likely spatial probability distributions (at the minimum and the maximum of the triangular distribution). Based on Tables 6.6-3, 6.6-4, 6.6-5 and 6.6-6 as well as discussion in Sections 6.6.2.2 and 6.6.2.3.

Figure 6.6-7. Triangular Probability Distribution (Heavy Blue Line) for Covering Uncertainty of Permeability in the Tptpmn by Varying the Mean of the Spatial Probability Distribution

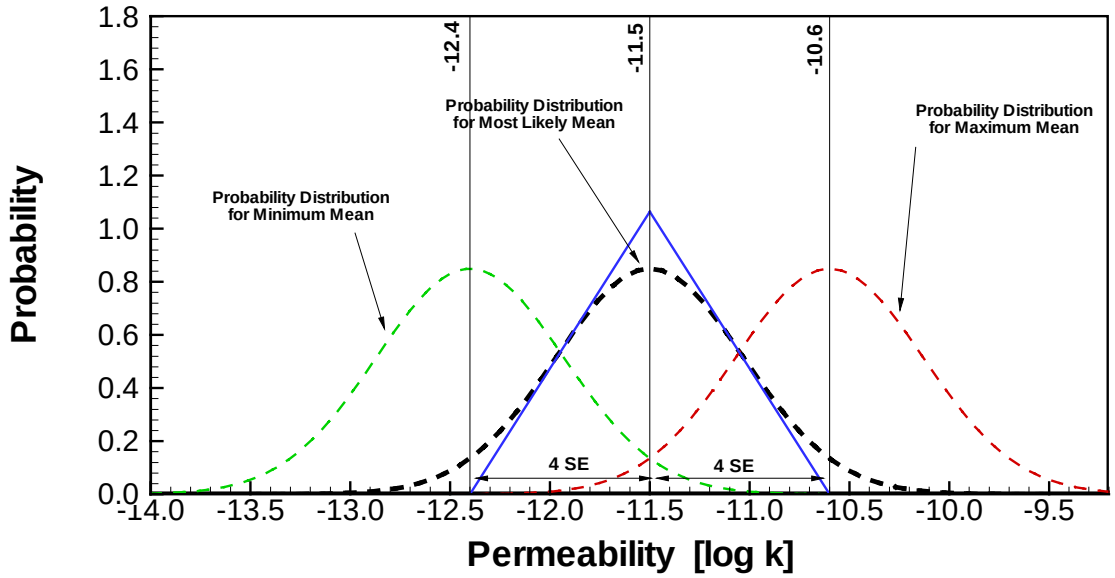

NOTE: The black dashed line shows the most likely spatial probability distribution (at the peak of the triangular distribution). The green and the red dashed lines show the least likely spatial probability distributions (at the minimum and the maximum of the triangular distribution). Based on Tables 6.6-3, 6.6-7, 6.6-8, and 6.6-9 as well as discussion in Sections 6.6.2.2 and 6.6.2.3.

Figure 6.6-8. Triangular Probability Distribution (Heavy Blue Line) for Covering Uncertainty of Permeability in the Tptpll by Varying the Mean of the Spatial Probability Distribution

6.6.3 Capillary Strength and Permeability Distributions for the Tptpul and Tptpln Units

According to the current repository design, a small fraction of the emplacement drifts will be located in the Tptpul and the Tptpln units at Yucca Mountain. Thus, additional distributions are needed that cover the spatial variability and uncertainty of the seepage-relevant parameters (capillary strength and permeability) in these units. Due to their limited importance for TSPA, results from seepage experiments and small-scale air-injection tests are not available for these units. It should be noted, however, that the Tptpul and the Tptpln are lithologically similar to the main repository units Tptpll and Tptpmn; all are welded units with moderate to intense fracturing. From such considerations, the two nonlithophysal units, the Tptpmn and the Tptpln, should have similar hydrogeological characteristics. For example, the fracture frequency in the Tptpln is four fractures per meter (BSC 2003 [161773], Table 6), which is similar to the Tptpmn. The same is expected for the units with lithophysal cavities embedded in the rock, the Tptpll and the Tptpul. However, fracturing in the Tptpul appears to be less intense than in the Tptpll. The fracture frequency in the Tptpul is about one fracture per meter compared to about three fractures per meter in the Tptpll (BSC 2003 [161773], Table 6). Note that these average fracture frequencies do not include fractures with trace lengths smaller than 1 m.

From the above discussion, the parameter distribution for the Tptpmn unit is expected to provide a reasonable estimate for the distributions of capillary-strength parameters in the Tptpln. Differences in the fracture characteristics between the Tptpll and the Tptpul may result in differences in the effective capillary strength in these units. However, as was pointed out in Section 6.6.1.2, the calibrated capillary-strength values are effective parameters that may not be strongly affected by the rock type. It may be concluded from the same logic that the distribution derived for the Tptpll should be reasonably representative of seepage behavior in the Tptpul. Therefore, and in view of the limited importance of these additional units, the capillary-strength distributions in the Tptpul and the Tptpln are based on the respective Tptpll and Tptpmn results discussed in Section 6.6.1.

While there are no small-scale permeability data in the Tptpul or the Tptpln, information on the permeability in these units can be derived from air injection tests conducted in surface-based boreholes. As pointed out in Section 6.6.2.1, permeability values from surface-based boreholes cannot be directly used for seepage evaluation purposes because (a) the measurement scale is different from the required 1-foot scale and (b) the measurements are conducted in undisturbed fractured rock. However, they are useful in comparison with available surface-based measurements conducted in the main repository units, in order to assess similarities between the respective lithophysal and nonlithophysal units. Such comparison was already conducted for the Tptpul and the Tptpll, demonstrating that both units have consistent permeability values (Table 6.6-8). Based on this assessment, the Tptpul data were utilized in Section 6.6.2.2 to support the development of permeability distributions for the Tptpll. Consequently, these permeability distributions for the Tptpll also represent the Tptpul unit.

Permeability data for the Tptpln unit are available at surface-based boreholes SD-12 and UZ#16 (DTN: GS960908312232.013 [105574]). Table 6.6-10 below provides the mean permeability of the several test intervals at each of these locations, and also gives summary statistics of the variation of this parameter. The mean permeability value over both locations is –11.9 (in log10); the standard deviation is 0.04. These values need to be compared with those given for the

Tptpmn unit (Table 6.6-5). The mean permeability of the Tptpln is slightly larger than the one measured for the Tptpmn, the spatial variability as indicated by the standard deviation is much smaller. These results would indicate that less seepage should be expected in the Tptpln unit, because both a larger mean and a smaller standard deviation would tend to reduce the overall seepage (see Section 6.8.2). However, the sample size of two surface-based boreholes is rather small, and the derived statistics may not be fully representative of the entire unit. Therefore, for seepage abstraction, the Tptpln unit has been assigned the same spatial variability and uncertainty distributions as the Tptpmn, which is a conservative parameter choice with respect to seepage.

Table 6.6-10. Mean Permeabilities of Undisturbed Rock from Tptpln Unit Measured in Surface-Based Boreholes and Intermediate-Scale Variability Statistics over the Repository Rock Block

Location	Number of Intervals	Mean μ_{sur} *(in log k)*	Interval Length (m)	
SD-12	6	-11.9	4.6	
UZ#16	14	-11.9	4	
Statistics over all two Locations	**Number of Locations**	**Mean μ (in log k)**	**Std. Dev. σ**	**Std. Error of Mean SE**
Tptpln	2	-11.9	0.04	0.03

Output-DTN: LB0308AMRU0120.001

NOTE: Computations documented in Attachment III

Thus, in summary, the parameter distributions developed for the Tptpll unit are suitable for the Tptpul unit. Similarly, the parameter distributions for the Tptpmn can be used for the Tptpln. This simplified treatment is considered cautiously realistic. Additional testing planned to be conducted in the Tptpul and the Tptpln would provide a better data basis, but is not considered necessary due to the limited importance of these units.

6.6.4 Percolation Flux and Flow Focusing

The magnitude and spatial distribution of local percolation fluxes at the repository horizon are other key parameters affecting seepage into drifts. The larger these parameters, the higher the potential for seepage to occur and the larger the amount of water that can seep into drifts. In the ambient seepage abstraction, the spatial and temporal distribution of percolation fluxes in the UZ is provided by the site-scale UZ Flow and Transport Model (BSC 2003 [163045]). This model derives relevant information on the overall flow and transport fields at the Yucca Mountain, accounting for climate changes and related uncertainties, variability in net infiltration, and the effects of different stratigraphic units and faults. However, because of the large model area, the spatial resolution of the model is much larger than the extent of drift-scale seepage models, and layer-averaged properties are used within stratigraphic units. Thus, intermediate-scale heterogeneity is not represented in the UZ Flow and Transport Model. This heterogeneity may lead to focusing of flow on a scale smaller than the resolution of the site-scale model; i.e., it may increase the site-scale fluxes in some areas, while reducing them in other areas. The additional variability and uncertainty of percolation flux stemming from this effect is accounted for in the

seepage abstraction by appropriate flow focusing factors, to be multiplied with the percolation flux distribution from the site-scale model (see Section 6.6.4.2). The resulting flux distribution is expected to represent the local percolation flux distribution needed as input to the predictive drift-scale seepage models (e.g., the SMPA or the TH Seepage Model).

6.6.4.1 Percolation Flux from the Site-Scale Model

For ambient flow conditions, the 3-D spatial flux distributions in the UZ are provided by the site-scale UZ Flow and Transport Model, as documented in BSC (2003 [163045]). The site-scale model incorporates the entire Yucca Mountain UZ; it accounts for the main stratigraphic units using layer-averaged rock properties and represents the major faults. Relevant rock properties of each hydrogeologic unit (for fractures, matrix, and fault zones) have been calibrated against saturation data, water-potential data, pneumatic-pressure data, perched-water data, temperature data, and geochemical data (BSC 2003 [160240], Section 6.2 and BSC 2003 [163045], Sections 6.2 through 6.5). The calibrated model is validated by comparison of model results with additional data that have not been used for calibration, as discussed in BSC (2003 [163045], Section 7). Model validation includes comparison with saturation, water-potential, pneumatic-pressure, perched-water, temperature, and geochemical data (carbon-14, chloride, and strontium in the pore water, calcite mineral abundance) as well as results from Alcove 8/Niche 3 seepage tests. Model predictions are conducted for three different climate conditions that are expected to occur during the 20,000-year time period considered in TSPA (USGS 2001 [158378]). The first climate stage is a continuation of the current modern-day climate conditions from present day to 600 years into the future (present-day climate). The second climate stage begins at 600 years from present day and is characterized as a monsoon climate with wetter summers than the modern climate. The third climate stage begins at approximately 2,000 years from present day and is characterized as a glacial transition climate with (on average) higher infiltration. The glacial transition climate is predicted to last the remainder of the 20,000 years.

Uncertainty in climate predictions is accounted for by defining three alternative climate scenarios referred to as the mean, the upper-bound and the lower-bound scenarios (USGS 2001 [158378]). Note that the occurrence probability of each climate scenario is provided in the Analysis Report *Analysis of Infiltration Uncertainty* (BSC 2003 [163740]). This can be used in TSPA to assign the appropriate weight to the considered site-scale flow field. The mean climate scenario is the scenario that gives the best fit between the UZ model results and the available data (BSC 2003 [163045], Sections 6.3 through 6.5). Based on the precipitation rates and temperature predicted for the future climates, distributions of net infiltration have been simulated as documented in *Simulation of Net Infiltration for Modern and Potential Future Climates* (USGS 2001 [160355]). Relatively high net infiltration rates occur generally in the northern portion of the site at high elevations and along the ridge where fractured bedrock is exposed.

The infiltration distributions, available for the three climate stages and the associated lower-bound, mean, and upper-bound scenarios, are used as direct inputs at the upper boundary of the site-scale UZ Flow and Transport Model (BSC 2003 [163045], Section 6.1.3). Steady-state simulation runs are conducted with this model for each climate stage and climate scenario, resulting in a total of nine 3-D flow fields that give the spatial distribution of percolation flux (BSC 2003 [163045], Section 6.1.4). TSPA uses the steady-state flow fields as being representative over the entire time period of the respective climate stage. Therefore, stepwise

changes in percolation flux occur at 600 years (transition from present-day to monsoon climate) and at 2,000 years (transition from monsoon to glacial transition climate). Consequently, the ambient seepage rates—calculated as a function of percolation flux—also have a stepwise change at 600 years and at 2,000 years, corresponding to climate changes. The times required for the flow conditions in the UZ to adjust to the stepwise changes in net infiltration are short compared to the duration of the different climatic stages. Therefore the steady-state conditions are representative over most of the TSPA time period, except for short durations following the stepwise changes at 600 and 2,000 years when the flow field equilibrates. Since the climate changes both lead to an increase in average percolation, the steady-state representation leads to an overestimation of seepage rates during these equilibration periods.

In general, percolation flux through the Tiva Canyon welded tuff unit, the first fractured bedrock unit below alluvial deposits, is governed by the imposed distribution of net infiltration. Flow in this unit occurs mostly in the fractures before entering the underlying Paintbrush nonwelded hydrogeological unit (PTn). With its characteristics of high matrix porosity and low fracture frequency, and the existence of tilted layers of nonwelded vitric and bedded tuff, the PTn can divert a fraction of the percolating water to intercepting faults and fault zones (CRWMS M&O 2000 [141187], Section 6.1.2; Wu et al. 2002 [161058]; BSC 2003 [163045], Section 6.2.2). Also, the PTn unit dampens and homogenizes downward-moving transient pulses from surface infiltration events. Therefore, the percolation distribution below the PTn unit is considerably different from the distribution of net infiltration, both spatially and temporally. Note that this difference is substantiated by geochemical data obtained at Yucca Mountain, as discussed in BSC (2003 [163045], Section 6.5). The geological unit below the PTn is the Topopah Spring welded tuff (TSw), a thick, densely fractured unit that hosts the repository. Results from the UZ Flow and Transport Model indicate that the flux in the TSw is mainly vertical without significant lateral diversion; as a result, the flux distribution at the PTn/TSw-interface should be similar to the flux distribution at the repository horizon.

Seepage abstraction uses the percolation flux distributions across the PTn/TSw-boundary to provide input to the seepage look-up table. These fluxes incorporate the important effects of flow dampening and lateral flow diversion in the PTn, and they are fairly representative of the fluxes at the repository horizon. The rationale for using the PTn/TSw fluxes, instead of using the flux distribution directly at the repository horizon, is mainly based on consistency considerations. The effect of flow focusing is estimated with a submodel that has the bottom of the PTn as its upper-boundary (see discussion in the following Section 6.6.4.2). Also the Multiscale Thermohydrologic Model, used for the simulation of in-drift TH conditions for feed into TSPA, has its upper boundary condition at the bottom of the PTn (to be presented in the upcoming revision to the Model Report, *Multiscale Thermohydrologic Model* (BSC 2001 [158204], which will have Document Identifier ANL-EBS-MD-000049 REV 01).

The spatial percolation flux distributions across the PTn/TSw interface are given in DTN: LB0302PTNTSW9I.001 [162277], for all three climate stages and scenarios. Flux values have been extracted from the 3-D model results for each vertical column of the model grid. Contours of these distributions are presented in Figure 6.6-9, using the glacial transition period of the mean climate scenario as an example. Note that the model domain is intersected by several major fault zones. The percolation fluxes in these fault zones are typically much larger than fluxes in

nonfault zones. In fact, the extreme values of percolation occur in these zones. Relatively high fluxes are also found in the north of the model domain and at the mountain ridge.

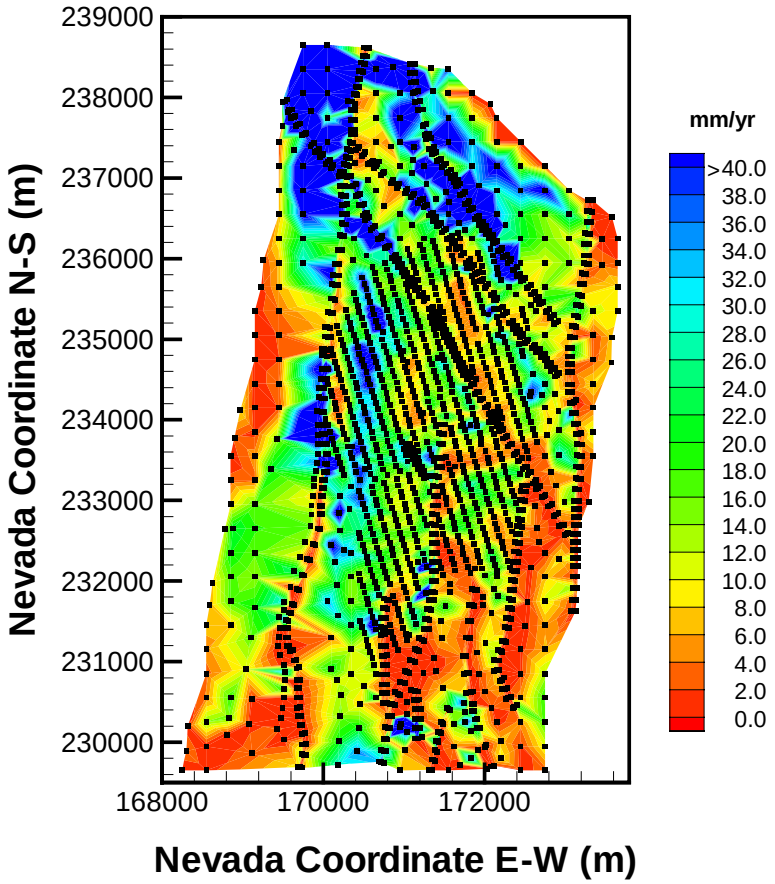

Source: LB0302PTNTSW9I.001 [162277]

NOTE: Black symbols denote center nodes of UZ model grid.

Figure 6.6-9. Contour Map of Vertical Fluxes at the PTn/TSw Interface for the Glacial Transition Climate (Mean Climate Scenario)

For use in TSPA, only those fluxes are needed that are representative of the repository area, because only these fluxes are relevant for seepage. Extracting the repository fluxes gives the distribution of percolation fluxes to be used in TSPA. Figure 6.6-10 shows the distribution of extracted PTn/TSw-fluxes for the repository columns of the UZ model grid. (Note that the so-called contingency area at the southern tip of the repository is not included.) Table 6.6-11 provides statistical measures—average percolation and maximum percolation—calculated for the flux distributions of the (a) entire UZ domain, and (b) the repository domain. Note that the statistical calculation is conducted without accounting for differences in the cross-sectional area of each vertical column. The impact of this simplification is small, however, and not relevant for the estimation of seepage. This is because the horizontal area of vertical columns is fairly uniform over the repository area.

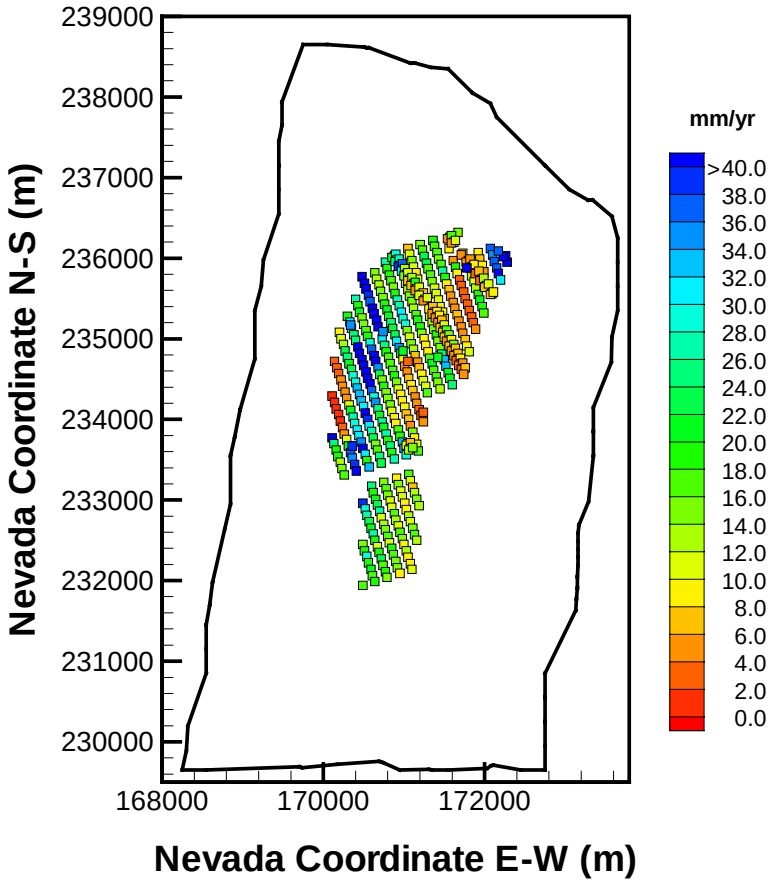

Source: LB0302PTNTSW9I.001 [162277]

NOTE: Symbols denote center nodes of UZ model grid over the repository area.

Figure 6.6-10. Extracted Vertical Fluxes at the PTn/TSw Interface for the Glacial Transition Climate (Mean Climate Scenario)

For both the mean and the upper-bound scenario in Table 6.6-11, the percolation fluxes increase significantly as a result of the imposed climate changes at 600 and at 2,000 years. This is different for the lower-bound scenario. Here, at overall small percolation rates, the glacial transition climate has less percolation than the monsoon climate. The observed trends in percolation flux over the UZ model domain are consistent with the trends in net infiltration as reported in USGS (2001 [160355], Tables 6.9, 6.13, and 6.18). In general, the fluxes extracted for the repository area are smaller than the fluxes over the entire UZ model domain, as indicated by the slightly smaller average values and the considerable differences in the maximum values. For comparison, Table 6.6-11 also gives statistics for repository fluxes without considering fault zones. While the average fluxes are hardly affected, the maximum percolation fluxes are significantly smaller without consideration of fault zones. In seepage abstraction, however, the large percolation fluxes in fault zone fluxes are included. This is because it is not clear at this point if the emplacement of waste canisters in fault zones can be entirely avoided.

Figure 6.6-11 shows histograms of the distribution of percolation flux over the repository area, for the present-day, monsoon, and glacial transition climate stages of the mean climate scenario.

The histograms demonstrate that the maximum values observed in Table 6.6-11 are in fact extreme cases that are very sparsely distributed and not representative of the majority of locations in the repository area. Most of these extreme cases are associated with fault zones.

As already mentioned, the diversion capacity of the PTn unit is very important for the spatial distribution of percolation fluxes in the TSw. However, the characterization of groundwater flow within the PTn is critically dependent on detailed knowledge of the rock properties and the heterogeneity within the PTn unit. Related uncertainties have been studied in BSC (2003 [163045], Section 6.6) by adjusting the PTn properties, allowing for considerably less lateral diversion. Based on this alternative property set, nine alternative flow fields have been simulated, and the related PTn/TSw fluxes have been provided in DTN: LB0305PTNTSW9I.001 [163690]. Table 6.6-11 gives the average and the maximum percolation value for the alternative flow model, using the mean climate scenario as an example. While the average fluxes over the repository area are not affected by the different PTn flow conceptualization, the maximum flux values are considerably smaller compared to the normal scenario. Apparently, less water is diverted towards fault zones in the alternative conceptual model. (Note that the mean fluxes over the entire UZ are slightly different between the two PTn flow concepts. Because of mass conservation, they should be identical for the respective climate stages. The differences occur as a result of neglecting the respective cross-sectional area of each vertical column in the statistical evaluation, as explained above.) Figure 6.6-12 shows histograms of the percolation flux distribution over the repository area for the alternative flow model, using the same interval size as in Figure 6.6-11. In addition to the different maximum flux values, the histograms in Figures 6.6-11 and 6.6-12 reveal some qualitative differences in the distribution of the values. The impact of these differences is examined in Section 6.8.2, where seepage rates are calculated in a Monte Carlo analysis. It will be demonstrated that the resulting seepage rates are hardly affected, so that the alternative flow scenario does not need to be analyzed within the TSPA simulations.

Table 6.6-11. Statistics of Percolation Flux Distributions at the PTn/TSw Interface

Mean Climate Scenario: Flux in mm/year			
Climate Period	**Entire UZ**	**Repository Area (used in TSPA)**	**Repository Area without Fault Zones**
Present Day Average	4.8	3.8	3.8
Present Day Maximum	111.1	39.9	20.6
Monsoon Average	13.2	11.7	11.5
Monsoon Maximum	211.6	127.9	61.3
Glacial Transition Average	18.8	17.9	17.8
Glacial Transition Maximum	276.5	192.4	90.9
Lower-Bound Climate Scenario: Flux in mm/year			
Climate Period	**Entire UZ**	**Repository Area (used in TSPA)**	**Repository Area without Fault Zones**
Present Day Average	1.1	0.4	0.4
Present Day Maximum	83.5	3.2	3.2
Monsoon Average	4.8	4.3	4.4
Monsoon Maximum	103.3	22.8	16.3
Glacial Transition Average	2.5	1.9	2.0
Glacial Transition Maximum	77.5	11.6	10.5
Upper-Bound Climate Scenario: Flux in mm/year			
Climate Period	**Entire UZ**	**Repository Area (used in TSPA)**	**Repository Area without Fault Zones**
Present Day Average	12.0	11.1	11.2
Present Day Maximum	197.5	80.3	44.0
Monsoon Average	21.7	20.3	20.1
Monsoon Maximum	358.7	161.1	97.9
Glacial Transition Average	35.6	35.1	35.3
Glacial Transition Maximum	530.2	282.2	164.1
Alternative Flow Model for PTn Unit			
Mean Climate Scenario: Flux in mm/year			
Climate Period	**Entire UZ**	**Repository Area (used in TSPA)**	**Repository Area without Fault Zones**
Present Day Average	4.4	3.8	3.9
Present Day Maximum	105.0	26.0	21.0
Monsoon Average	12.6	11.8	11.7
Monsoon Maximum	183.6	80.8	61.8
Glacial Transition Average	18.2	17.9	18.0
Glacial Transition Maximum	221.3	129.5	98.9

Sources: DTNs: LB0305PTNTSW9I.001 [163690]; LB03033DSSFF9I.001 [163047]
Output-DTN: LB0308AMRU0120.001

NOTE: Computations documented in Attachment IV

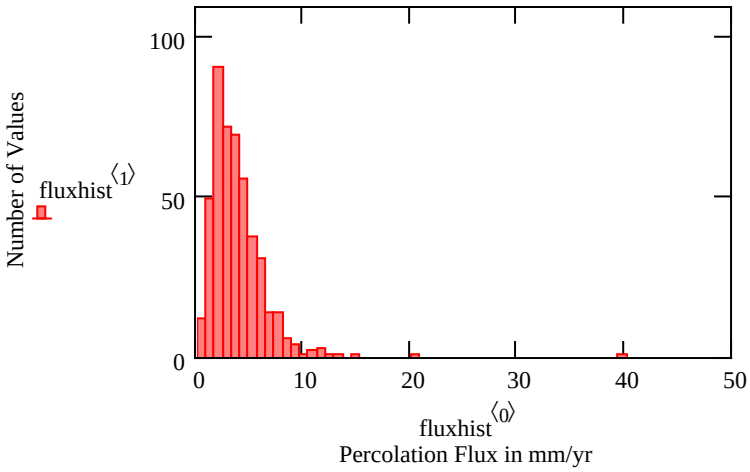

(Present-day)

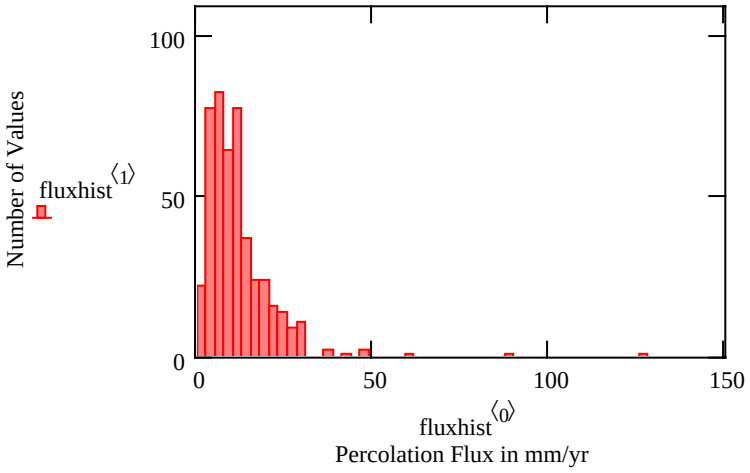

(Monsoon)

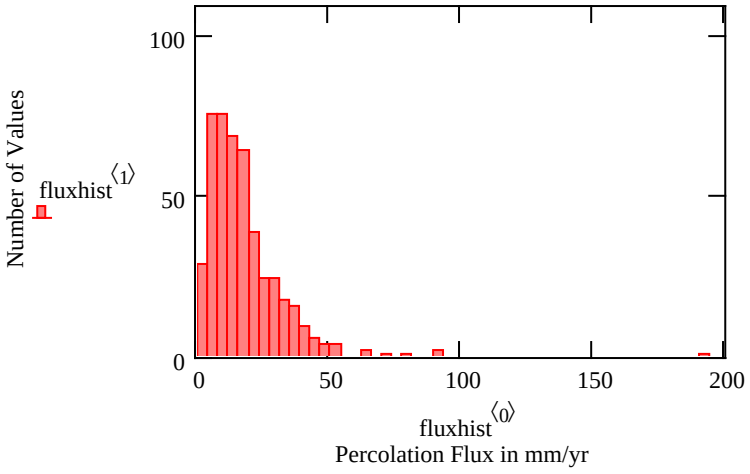

(Glacial Transition)

Sources: DTN: LB0302PTNTSW9I.001 [162277] and DTN: LB03033DSSFF9I.001[163047]

NOTE: The symbols in the histograms (i.e., fluxhist$^{<0>}$ and fluxhist$^{<1>}$) denote the variable names given in the *Mathcad 11* spreadsheet used for the calculation, see Attachment IV. Fluxes are extracted for the repository area.

Figure 6.6-11. Histograms of Vertical Fluxes at the PTn/TSw Interface for the Mean Climate Scenario

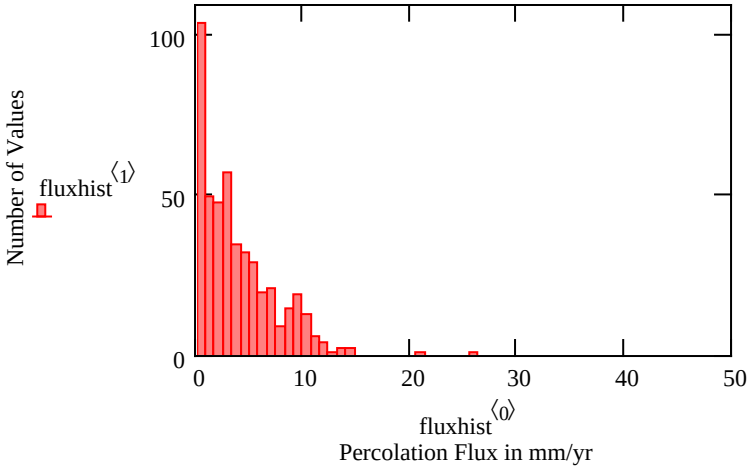

(Present-day)

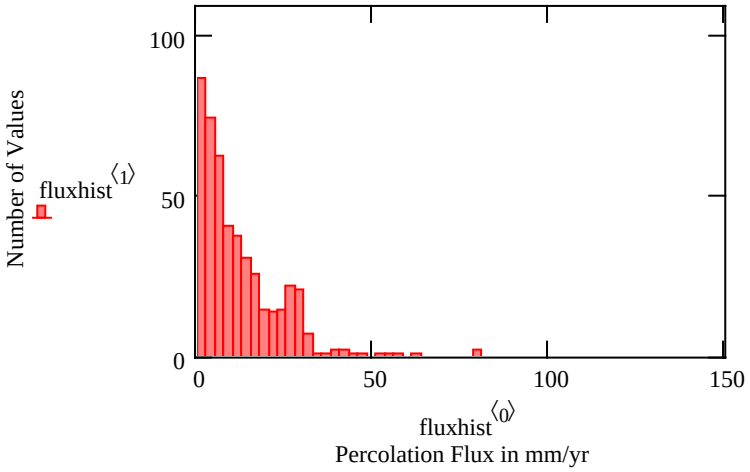

(Monsoon)

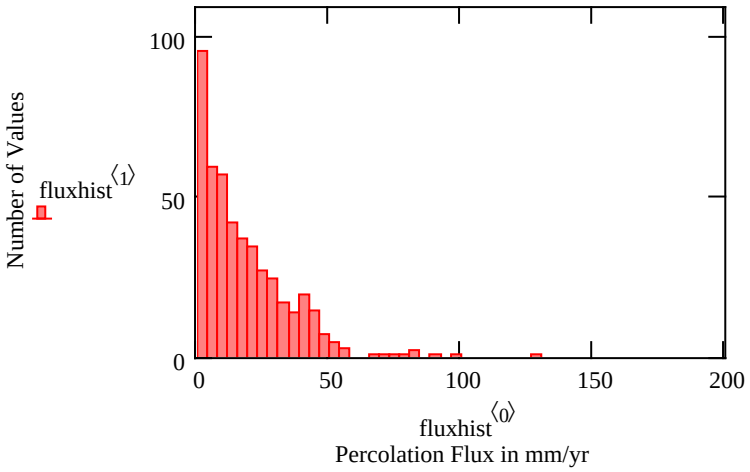

(Glacial Transition)

Sources: LB0305PTNTSW9I.001 [163690] and LB03033DSSFF9I.001 [163047]

NOTE: The symbols in the histograms (i.e., fluxhist$^{<0>}$ and fluxhist$^{<1>}$) denote the variable names given in the *Mathcad 11* spreadsheet used for the calculation, see Attachment IV. Fluxes are extracted for the repository area.

Figure 6.6-12. Histograms of Vertical fluxes at the PTn/TSw Interface for the Mean Climate Scenario Using the Alternative Flow Concept in the PTn

6.6.4.2 Flow Focusing

In the framework of seepage abstraction, flow focusing denotes the potential concentration of downward flow in the UZ onto a particular drift segment. This flow concentration could increase the local percolation flux in some locations, which would then increase the amount of seepage in those locations. The potential for flow focusing stems from the scale difference between the UZ Flow and Transport Model, which provides the 3-D distribution of percolation fluxes in the UZ, and the drift-scale seepage models, which use these percolation fluxes as inflow at the top model boundary. While the site-scale model accounts for variability in net infiltration and explicitly models the different stratigraphic units and faults, it cannot represent the intermediate-scale heterogeneity within geological units. This is because of the layer-averaged rock properties and the relatively coarse gridding (on the order of about 100 m). Drift-scale seepage models, on the other hand, have a lateral model extent on the order of a few drift diameters; the model domain typically includes the vicinity of one particular drift segment. Consequently, the distribution of percolation fluxes in seepage abstraction needs to describe the variability of this parameter on the spatial resolution of a few drift diameters. Since the site-scale model does not explicitly describe this spatial detail, the percolation flux distributions derived from this model need to be adjusted by multiplication with appropriately distributed flow focusing factors.

Note that flow focusing factors should not incorporate heterogeneity below the spatial resolution of a few drift diameters, since small-scale variability (on a scale of less than a meter) is explicitly accounted for in the drift-scale seepage models (the SMPA and the TH Seepage Model). It is shown in these models that small-scale heterogeneity is a key factor for seepage to occur; it gives rise to preferential-flow processes and increases the probability of local breaching of the capillary barrier at the rock-drift interface. (These small-scale flow processes are referred to as “flow channeling” hereafter.) In the framework of seepage abstraction, it is important to clearly distinguish between flow focusing and flow channeling. Flow focusing occurs on an intermediate scale and needs to be accounted for by appropriate factors. Flow channeling, on the other hand, occurs on a much smaller scale and is automatically included by using the seepage look-up tables of the SMPA.

Flow focusing cannot be directly measured in the field. Therefore, flow focusing phenomena are addressed through models that are able to describe the intermediate-scale heterogeneity. Indirect field evidence can be used to support the models. As described in BSC (2001 [155950], Section 4.3.2.), BSC (2001 [156609], Section 6.4.2) and further discussed in Bodvarsson et al. (2003 [163443]), an intermediate-scale flow model was developed to specifically address the issue of spatial flow focusing, bridging the gap between the site scale and the drift scale. Most of the studies with this model were conducted in a two-dimensional vertical cross section of the unsaturated zone 100 m in horizontal extent and 150 m in vertical extent. The top boundary was chosen at the bottom of the PTn unit, and the bottom boundary at the repository horizon. The 150 m vertical extent of the model corresponds to an average distance between the PTn/TSw-interface and the repository. For comparison purposes, a few additional model simulations were conducted with a 3-D model, using the same upper and lower boundaries (Bodvarsson et al. 2003 [163443]).

In contrast to the site-scale model, in which the rock properties within geological units are considered uniform, the intermediate-scale model represents the heterogeneity of the fractured

rock within the five stratigraphic layers residing in the model domain[1]. Similar to the SCM (BSC 2003 [162267]) and the SMPA (BSC 2003 [163226]), the fracture network is treated as a stochastic heterogeneous continuum with variable permeability, while flow through the matrix is neglected. Modeling simulations were conducted for the 2-D and the 3-D model where uniform and non-uniform percolation fluxes were introduced at the top boundary of the heterogeneous domain. Flow focusing phenomena were then studied by comparison of the flux distribution measured at the repository horizon (bottom boundary) with the original flux distribution introduced at the top boundary. The additional variability stemming from the downward flow in the heterogeneous model domain is the variability that cannot be described by the site-scale results, and that needs to be accounted for by appropriate distributions of flow focusing factors.

The spatial distribution of fracture permeability was based on air-permeability data stemming from surface-based boreholes and, where available, from heater test locations (BSC 2001 [156609], Section 6.4.2.2). Most of these measurements were conducted with injection intervals of a few meters length; thus, the resulting geostatistical parameters appropriately represent intermediate-scale heterogeneity (BSC 2003 [161773], Section 6.1.1.1). These geostatistical parameters (mean and standard deviation of fracture permeability), and other properties of the fracture continuum (layer-averaged porosity, capillary pressure, and relative permeability functions), were based on those reported in a previous version (Revision 00) of the *Calibrated Properties Model* (CRWMS M&O 2000 [144426], Section 6). While there are differences between these properties and the most recent model calibrations in BSC (2003 [160240], Section 6), these differences are rather small and not relevant for the scope of the flow focusing study. In particular, the variability of fracture permeability in the flow focusing study (Bodvarsson et al. 2003 [163443], Table 1), as expressed by the standard deviation, is on the order of 0.5 to 0.7 in log space, similar to the range of standard deviations for the TSw given in BSC (2003 [160240], Table 4). Two correlation lengths of 1 m and 3 m were studied, representing fairly weak spatial correlation of fracture continuum permeability. This is consistent with findings reported in BSC (2003 [162267], Section 6.6.2.1). Based on the geostatistical data, multiple realizations of 2-D and 3-D spatially distributed fracture permeability values were generated and mapped to each gridblock. Note that the grid resolution in both 2-D and 3-D cases was on the order of less than a meter. Thus grid resolution of flow focusing model was considerably finer than the typical model extent of drift-scale seepage models (which is on the order of a few drift diameters). Since flow variability is more pronounced in a fine-resolution grid, the maximum flow focusing factors derived in this study are arguably on the high end of possible values, providing cautiously realistic flux estimates. This means that application of these flow focusing factors may overestimate seepage rates (see abstraction sensitivity studies in Section 6.8.2).

Simulation runs were conducted for several flow scenarios with varying infiltration rates imposed at the top boundary (1, 5, 25, 100, and 500 mm/yr), different infiltration patterns (uniform versus localized), different correlation lengths, and 2-D versus 3-D representation (Bodvarsson et al. 2003 [163443]). As an example, Figure 6.6-13 shows the vertical liquid flux across the bottom of the model area for a 2-D simulation case with 5 mm/yr uniform percolation

[1] These stratigraphic layers are the tsw31, tsw31, tsw33, tsw34, and tsw35, using the nomenclature of the UZ model reports. Note that the tsw34 corresponds to the Tptpmn unit when using the nomenclature of the Geological Framework Model (BSC 2002 [159124]). Similarly, the tsw35 corresponds to the Tptpll unit. The relationship between these different unit names are given in several model reports, e.g., in BSC (2003 [160109], Table 11).

imposed at the top and a spatial correlation of 1 m. The flux profile demonstrates a significant variability, with flux values ranging from about 0 to almost 30 mm/yr. Additional cross sections not presented here show statistically similar behavior, suggesting that the basic flow focusing characteristics develop within tens of meters from the top of the model (or a unit contact), but remain similar within a unit over extended vertical distances.

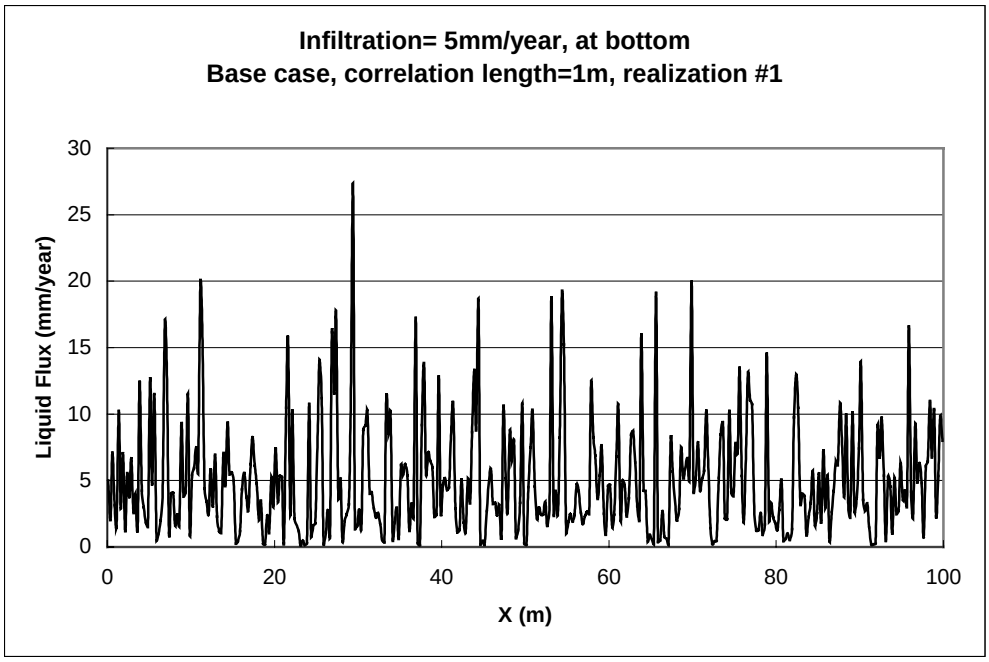

Source: BSC (2001 [156609], Figure 6.4-22b)

Figure 6.6-13. Distribution of Vertical Fluxes at the Bottom of the Model Domain, for the Simulation Case with a 5 mm/yr Uniform Infiltration and a 1 m Correlation Length

A distribution of flow focusing factors can be easily calculated from the cross-sectional flux data by normalizing the flux values to the average infiltration rate imposed at the top boundary. Factors larger than one correspond to increased percolation fluxes, and factors smaller than one correspond to decreased percolation fluxes compared to the average percolation. Figure 6.6-14 shows the frequency distributions of normalized vertical flux (flow focusing factors) across the bottom boundary for the five infiltration cases, as presented in BSC (2001 [156609], Figure 6.4-24). All infiltration cases, covering a range from 1 mm/yr to 500 mm/yr, are statistically similar. This means that flow focusing is independent of the percolation flux; i.e., the distribution of flow focusing factors is not correlated to the distribution of percolation fluxes. The majority of all normalized fluxes (focusing factors) ranges from 0 to about 2. The maximum flux that occurs in the model domain is generally about five to six times higher than the infiltration flux prescribed at the upper boundary. The minimum flux is almost zero.

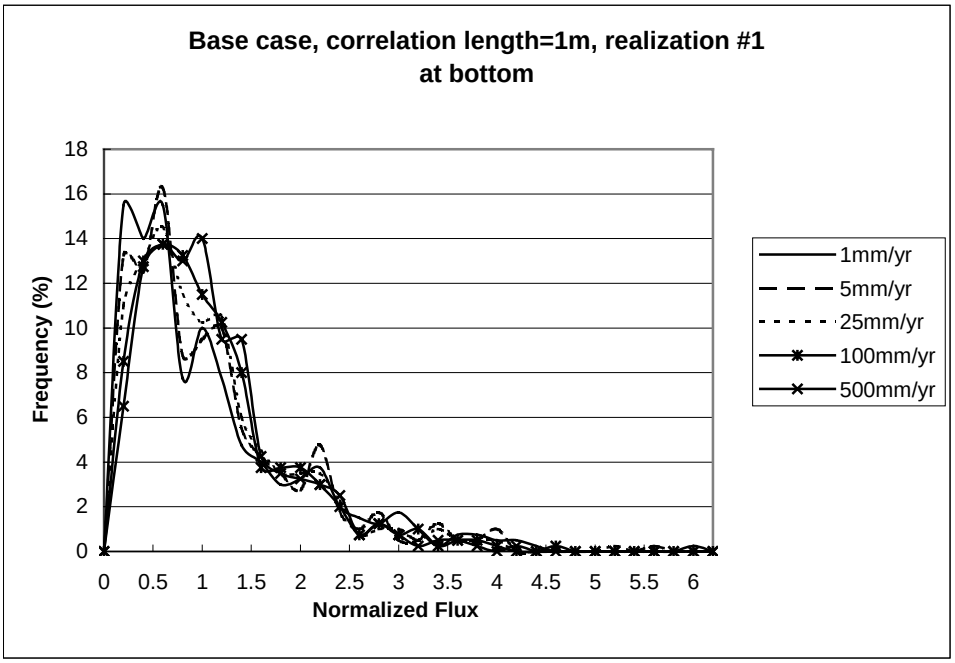

Source: BSC (2001 [156609], Figure 6.4-24)

Figure 6.6-14. Frequency Distribution of Vertical Fluxes at the Bottom of the Model Domain, for Different Uniform Infiltration Rates and a 1 m Correlation Length

As pointed out in BSC (2001 [155950], Section 4.3.2.6), BSC (2001 [156609], p. 118), and Bodvarsson et al. (2003 [163443]), all other simulation cases mentioned above also featured statistical similarity in the normalized flux-frequency distributions. It was concluded that a single frequency distribution of flow focusing factors could be developed for use in seepage abstraction. A regression analysis was conducted to derive a probability distribution function of normalized fluxes at the bottom boundary from all 2-D simulation runs. This function, provided in DTN: LB0104AMRU0185.012 [163906], is depicted in Figure 6.6-15, along with the 99% confidence band for all simulation results. The function defines the cumulative probability distribution of flow focusing factors to be used in seepage abstraction and TSPA. Note that this distribution is mass conservative, as required, so that the total amount of downward water flow remains unchanged when using flow focusing factors as multipliers to the site-scale percolation fluxes (i.e., the arithmetic mean of all flow focusing factors of a large enough ensemble of random values is 100%). Also note that the regression curve is zero at a flow focusing factor of 0.116 and approaches 100% at a flow focusing factor of 5.016. Thus, sampling from the cumulative probability distribution will give a distribution of flow focusing factors ranging from 0.116 to 5.016. The regression curve is not defined outside of this range.

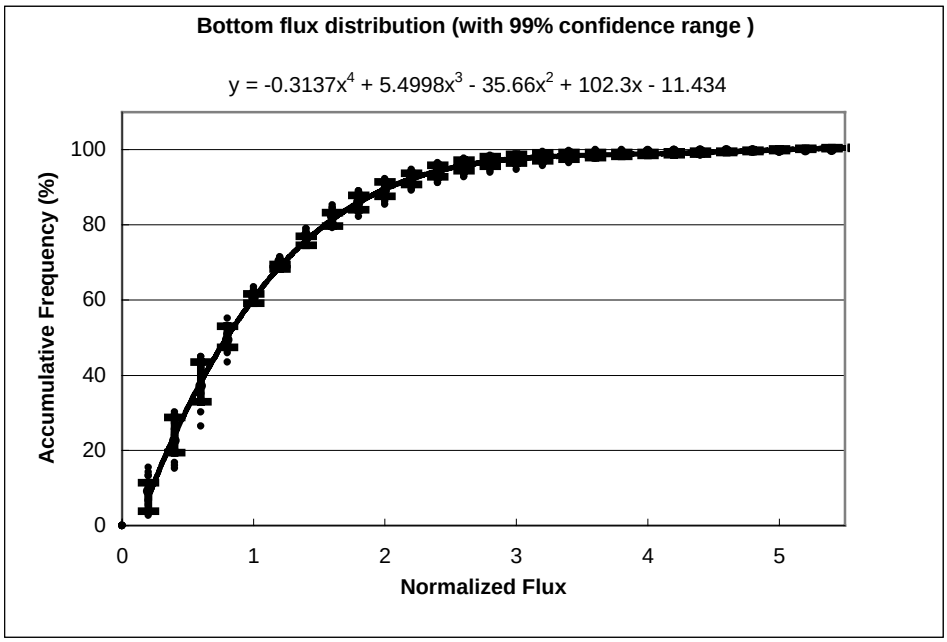

Source: DTN: LB0104AMRU0185.012 [163906])

Figure 6.6-15. Regression Curve (and 99% Confidence Band) for Cumulative Distribution of Percolation Flux at the Bottom of the Model Domain, Averaged Over All Simulations

Qualitative evidence of preferential flowpaths occurring at Yucca Mountain can be inferred from observations of secondary minerals in the UZ. These secondary minerals form coatings on fracture foot walls and cavity floors as calcite or silica deposits precipitate by percolating water. Whelan et al. (2002 [160442], p. 738) report heterogeneous distribution of these minerals within the UZ, with fewer than 6% of fractures (longer than 1 m) mineralized. This suggests that the majority of all fractures do not contribute to downward flow, and that the downward flux in the small fraction of "actively" flowing fractures should be about 15 to 20 times higher than the average percolation. However, these factors cannot be directly compared to the flow focusing factors derived above. The abundance of mineral precipitation in fractures reveals flow heterogeneity on a small scale. Thus, the spatial variability as suggested from the interpretation of fracture coatings includes components of both flow focusing (intermediate-scale heterogeneity) and flow channeling (small-scale heterogeneity). As mentioned above, flow channeling is explicitly accounted for in seepage models by a stochastic representation of the small-scale variation in the drift vicinity, giving rise to considerable flux variability on a scale less than one meter. Thus, the resulting flux variability included in seepage abstraction, stemming from large-scale variability as modeled by the UZ Flow and Transport Model, intermediate-scale variability as described by flow focusing factors, and small-scale variability, as simulated by the seepage process models, is significant. Qualitatively, it appears that this flux variability is consistent with, if not cautiously overestimating, the observed heterogeneity in mineral deposits on fracture walls as reported in Whelan et al. (2002 [160442]). Note that there is additional evidence from measurements that the effect of flow focusing should not be larger than estimated above. For example, distributions of water potential in the TSw are nearly uniform, indicating that there are many small flow paths instead of a just few large ones.

Note that the flow focusing factors derived in previous seepage abstractions (CRWMS M&O 2001 [154291], Section 6.4.3.2) were in general more widely distributed than the ones estimated above. These factors were derived using a method developed to estimate the spacing of actively flowing fractures on a scale below the resolution of the UZ site-scale model. Based on this, maximum flow focusing factors ranged between 9.7 and 47, depending on which climate scenario was applied. However, these values are believed to be overly conservative and unrealistic. This is mainly because the evaluation of active fracture spacing addresses small-scale heterogeneity. In light of the above discussion on the different scales of variability, this small-scale heterogeneity should not be included in the flow focusing factors provided for the TSPA seepage analysis. The probability distributions function defined in Figure 6.6-15 provides a cautiously realistic representation of the intermediate-scale variability of percolation flux in the TSw.

6.6.4.3 Resulting Distribution of Percolation Fluxes

The resulting spatial distributions of percolation flux $q_{perc,ff}$—to be used in TSPA as input for seepage calculation—are generated as follows:

(1) The local PTn/TSw flux q_{perc} is sampled for a large number of locations within the repository, using one of the nine site-scale flow fields, depending on the considered climate scenario and time period.

(2) Flow focusing factors f_{ff} are randomly sampled for each location, using the cumulative flux distribution given in Figure 6.6-15. The flow focusing factors are *not* correlated to the local percolation flux.

(3) The local flux values are multiplied with the local flow focusing factor to give the resulting local percolation flux $q_{perc,ff}$ for input into the seepage look-up table.

This procedure yields spatial flux distributions much wider and more heterogeneous than the ones displayed in Figures 6.6-11 and 6.6-12. In theory, the maximum fluxes of each climate scenario/period can be derived by multiplication of the values given in Table 6.6-11 with the maximum flow focusing factor of about five. (The mean values remain unchanged for a large enough sample, because of mass conservation.) This yields maximum values of about 200 mm/yr for the present-day climate, about 640 mm/yr for the monsoon climate, and about 960 mm/yr for the glacial transition climate (using the mean climate scenario). For the upper-bound scenario, the theoretical maximum flux during the glacial transition climate is over 1,400 mm/yr, which is beyond the flux range studied with the SMPA. One must note, however, that these maximum fluxes are extremely unlikely, caused by the extremely small probability that two independent events have extreme parameter values at the same time.

There are several sources of uncertainty related to the percolation flux estimates. Uncertainty related to the future climate and net infiltration at Yucca Mountain is covered using three alternative climate scenarios. These scenarios, used as input to the UZ Flow and Transport Model, lead to alternative rock property calibrations and alternative percolation flux distributions that are accounted for in TSPA with their respective occurrence probability. Uncertainty related to simulation of flow processes in the UZ has been addressed by careful calibration and validation of the model to a wide variety and large amount of data from different sources (BSC 2003 [163045], Sections 6 and 7). For the scope of evaluating seepage, the most important

sources of uncertainty are the flow diversion capacity of the PTn and the impact of spatial variability within stratigraphic units. The impact of the PTn flow diversion is addressed in Section 6.8.2, where seepage rates are estimated using results of an alternative flow model for the PTn, one that does not allow for significant lateral flow. It is shown that the alternative flow model does not significantly impact the seepage estimates. The effect of intermediate-scale spatial variability, not accounted for in the UZ model results, is explicitly incorporated in seepage abstraction using the flow focusing concept. It is recognized that the flow focusing factors developed in BSC (2001 [156609], Section 6.4.2) may be overestimating the variability of percolation flux, because a fine grid resolution was used for the numerical study. Therefore, the resulting flux distributions used for seepage evaluation are expected to cautiously cover the spatial variability of this parameter and all related uncertainties.

6.7 SUMMARY OF SEEPAGE ABSTRACTION

6.7.1 TSPA Seepage Calculation Methodology and Relevant Abstraction Results

This section provides a roadmap of the proposed methodology for the TSPA seepage calculations (Output-DTN: LB0308AMRU0120.001). The relevant calculation steps are briefly summarized together with the relevant parameter distributions and simplifications. The reader is referred to Sections 6.4, 6.5, and 6.6 of this Model Report for the rationale behind the abstraction methodology.

Seepage is treated as a probabilistic process in the TSPA-LA simulations (Figure 6.5-1). Within each time step, the TSPA seepage component conducts a stochastic evaluation of seepage over a large number of realizations R, covering seepage uncertainty, and locations r, covering seepage variability. The seepage evaluation has two main steps: (1) deriving ambient seepage rates from seepage look-up tables provided by the SMPA (for both non-degraded and collapsed drifts), and (2) adjusting the ambient seepage rates for other important factors. Both steps are explained in detail in the previous sections. According to the definitions in Section 6.1.2, the seepage rates are given for a reference drift section of 5.1 m length; as a result, they correspond to the amount of water that potentially drips on one waste package.

6.7.1.1 Step 1: Ambient Seepage

Ambient seepage is a function of three key parameters: capillary strength $1/\alpha$, permeability k, and percolation flux $q_{perc,ff}$. Probability distributions have been developed within the abstraction process to represent the spatial variability and uncertainty inherent in these parameters. These distributions distinguish explicitly between spatial variability and uncertainty.

Four different methods have been identified in Section 6.6.1 to derive statistical parameters for describing the spatial variability and uncertainty in $1/\alpha$. The four statistical methods provide four different probability distributions for spatial variability and uncertainty defined below. Methods A and B arrive at similar distributions for all the geological units, Methods C and D have separate distributions for the nonlithophysal and lithophysal units. These four methods are to be used as four equally probable alternative representations of spatial variability and uncertainty in the capillary-strength parameter.

- *Parameter Space for Capillary-Strength Parameter $1/\alpha$ using Methods A and B:*
  (Method B values in parentheses)

  Spatial Variability Distribution:
  Uniform Distribution with Mean 591 Pa (631 Pa). Lower Bound is 402 Pa (442 Pa). Upper Bound is 780 Pa (820 Pa).

  Uncertainty Distribution:
  Triangular Distribution with Mean 0. Lower Bound is –105 Pa (–162 Pa). Upper Bound is +105 Pa (+162 Pa).

  These distributions are identical for all units (Tptpll, Tptpul, Tptpmn, Tptpln).

- *Parameter Space for Capillary-Strength Parameter $1/\alpha$ using Methods C and D:*
  (Method D values in parentheses)

  Tptpmn Unit:

  Spatial Variability Distribution:
  Uniform Distribution with Mean 604 Pa (650 Pa). Lower Bound is 377 Pa (427 Pa). Upper Bound is 831 Pa (873 Pa).

  Uncertainty Distribution:
  Triangular Distribution with Mean 0. Lower Bound is –198 Pa (–273 Pa). Upper Bound is +198 Pa (+273 Pa).

  These distributions for the Tptpmn are also used for the Tptpln unit.

  Tptpll Unit:

  Spatial Variability Distribution:
  Uniform Distribution with Mean 582 Pa (613 Pa). Lower Bound is 400 Pa (384 Pa). Upper Bound is 764 Pa (841 Pa).

  Uncertainty Distribution:
  Triangular Distribution with Mean 0. Lower Bound is –129 Pa (–279 Pa). Upper Bound is +129 Pa (+279 Pa).

  These distributions for the Tptpll are also used for the Tptpul unit.

The spatial variability and uncertainty distributions for permeability are defined as follows:

- *Parameter Space for Permeability k (in log10)*

  Tptpmn Unit:

  Spatial Variability Distribution:
  Lognormal Distribution with Mean –12.2 and Standard Deviation 0.34.

  Uncertainty Distribution:
  Triangular Distribution with Mean 0. Lower Bound is –0.68. Upper Bound is +0.68.

  The permeability distributions for the Tptpmn are also used for the Tptpln unit.

  Tptpll Unit:

  Spatial Variability Distribution:
  Lognormal Distribution with Mean –11.5 and Standard Deviation 0.47.

  Uncertainty Distribution:
  Triangular Distribution with Mean 0. Lower Bound is –0.92. Upper Bound is +0.92.

  The permeability distributions for the Tptpll are also used for the Tptpul unit.

Values for $1/\alpha$ and k sampled from the spatial variability distributions are adjusted using values for $\Delta 1/\alpha$ and Δk sampled from the uncertainty distributions, to arrive at the final parameter distribution covering both spatial variability and uncertainty.

The procedure for sampling percolation fluxes is slightly different. The percolation flux distributions are provided by model results from the UZ Flow and Transport Model (DTN: LB0302PTNTSW9I.001 [162277]). These spatial distributions are time-dependent; they are given separately for three climate stages (present-day, monsoon, and glacial transition), during which the UZ flow fields are considered steady state. Uncertainty is expressed by three different

scenarios of spatial flux distributions (mean, upper-bound, and lower-bound scenario), each of them associated with a certain occurrence probability (provided to TSPA in a separate Model Report). (Note that the nine flux distributions simulated using an alternative conceptual model for flow diversion in the PTn do not need to be considered in the TSPA.) The TSPA-LA seepage component samples from the spatial flux distribution at given locations r within the repository area, using the present-day, monsoon, or glacial transition flow field, depending on the considered time step. Over the R uncertainty realizations, the three flux scenarios are weighted according to their respective occurrence probability.

These sampled percolation fluxes q_{perc} need to be adjusted for intermediate-scale heterogeneity, which is not represented in the flux distributions from the UZ Flow and Transport Model. This is done using a spatial distribution of flow focusing factors f_{ff}. Multiplication of the sampled fluxes q_{perc} from the site-scale model with the flow focusing factors f_{ff} gives the local percolation flux $q_{perc,ff}$ to be used in the TSPA calculation. The spatial variability distribution for the flow focusing factor is defined as follows (DTN: LB0104AMRU0185.012 [163906]):

- *Flow Focusing Factor f_{ff}*

  Spatial Variability Distribution:
  Cumulative Probability Distribution given as
  $Y = -0.3137\ x^4 + 5.4998\ x^3 - 35.66\ x^2 + 102.3\ x - 11.434$ (in %)

  Uncertainty Distribution:
  No Uncertainty.

Note that the respective probability distributions for capillary strength, permeability, percolation flux, and flow focusing factor are not correlated. This means that the random variables used to sample from the respective distributions should be generated independently in the TSPA.

For each set of seepage-relevant parameters $1/\alpha$, k, and $q_{perc,ff}$ derived in the random sampling procedure over R realizations and r locations, seepage rates are calculated using the seepage look-up tables provided by the SMPA simulation results. These look-up tables are available for non-degraded drifts (DTN: LB0304SMDCREV2.002 [163687]) as well as for collapsed drifts (DTN: LB0307SEEPDRCL.002 [164337]). For both look-up tables, the SMPA simulation cases cover the parameter values given below. All possible combinations of these values were simulated in the systematic SMPA analysis, and a complete suite of results is provided in the seepage look-up tables.

- *SMPA Simulation Cases*

  Capillary-Strength Parameter $1/\alpha$: 100 to 1000 Pa (intervals of 100 Pa)
  Permeability k: -14.0 to –10.0 (intervals of 0.25)
  Local Percolation Flux $q_{perc,ff}$: 1, 5, 10, 20, 50, 100, 200, 300, 400, 500, 600, 700, 800, 900, 1000 mm/year

TSPA will select the appropriate look-up table, depending on the considered geologic unit, the selected nominal or disruptive scenario, and the assumed rock strength reduction case. This selection is based on categories of drift degradation that have been introduced in Section 6.5.1.5, based on results from BSC (2003 [162711]). Category 1 comprises degraded drifts that may show local rock breakout but stay essentially intact. In this category, seepage is interpolated from

the look-up table for non-degraded drifts. Category 1 includes all drifts located in nonlithophysal rock, and, for drifts located in lithophysal rock, the thermal stress case, the 5×10^{-4} seismic hazard case, and the 0% through 40% strength reduction cases. Category 2 comprises the cases with complete drift collapse. These are the 1×10^{-6} and the 1×10^{-7} seismic hazard levels and the 60% through 100% strength reduction cases for lithophysal rock units. In this category, seepage is interpolated from the look-up table for collapsed drifts.

Information on the time-dependence of rock strength reduction is not available at this time. Therefore, the collapsed drift look-up table should be used for the entire postclosure period when one of the strength-induced collapsed drift scenarios is considered in TSPA. On the other hand, if the time of a seismic event leading to drift collapse is considered in TSPA, the collapsed drift scenario should be used starting with the assumed time of the seismic event.

The seepage results for each sampled set of seepage-relevant parameters $1/\alpha$, k, and $q_{perc,ff}$ derived in the random sampling procedure are calculated from a linear interpolation between the three independent seepage input parameters in the look-up tables. It is possible (but unlikely) that the parameter range covered in the SMPA is exceeded for parameter values sampled from the unbounded distributions of permeability and percolation flux. The following recommendations are made in this case:

- *Truncation of Parameter Distributions*

  a.) If local percolation flux is less than 1 mm/yr, set to 1 mm/yr.
  b.) If local percolation flux is more than 1,000 mm/yr, set to 1,000 mm/yr.
  c.) If permeability is less than –14, set to –14 (in log10).
  d.) If permeability is larger than –10, set to –10 (in log10).

The interpolated results from the seepage look-up tables are the mean seepage values $\overline{Q}_{seep}$ and the standard deviations σ_{seep}. The standard deviations represent the estimation uncertainty in the seepage results, which is different for each sampled set of parameters. Since this uncertainty must be included in the TSPA simulation, the interpolated mean seepage values $\overline{Q}_{seep}$ are adjusted using values for $\Delta\overline{Q}_{seep}$ sampled from appropriate uncertainty distributions. These distributions are defined as follows:

- *Uncertainty Distribution for Seepage Results*

  Uniform distribution with Mean 0.
  Lower bound is $-1.7321 \times \sigma_{seep}$. Upper bound is $+1.7321 \times \sigma_{seep}$.

After adjusting the seepage values to account for uncertainty, the results must be checked for consistency. If the resulting seepage rates are smaller than 0, they are set to 0. If the resulting seepage rates correspond to a seepage percentage larger than 100%, they are set to a rate corresponding to a seepage percentage of 100%. The final result of Step 1 of the TSPA seepage calculation is a probability distribution of ambient seepage rates (or seepage percentages) over R realizations and r locations, given for each time step studied in the TSPA simulation.

Three alternative abstraction methods are proposed for igneous events (see Section 6.5.1.7). The first method is to apply the seepage results obtained for nondegraded drifts, using the look-up

table in DTN: LB0304SMDCREV2.002 [163687]; the second method is to apply the seepage results for collapsed drifts, using the look-up table in DTN: LB0307SEEPDRCL.002 [164337]; and the third method is to set the seepage percentage in intersected drifts to 100% (i.e., the seepage flux potentially contacting the waste is equal to the local percolation flux arriving at the drifts). In view of the significant uncertainty about the in-drift conditions after an igneous event, it is recommended that TSPA conduct sensitivity analyses with the three abstraction methods. The more conservative seepage estimates should be chosen and propagated to the downstream TSPA modules. If the time of an igneous intrusion event is considered in TSPA, the selected abstraction method for igneous intrusion should be used starting with the assumed time of the event.

6.7.1.2 Step 2: Adjustments for Other Relevant Factors

The ambient seepage distributions do not account for (1) alterations of seepage-relevant parameters as a result of heat-induced THM and THC effects, (2) uncertainty related to drift degradation, and (3) thermal perturbations during the first several hundred years after emplacement when boiling occurs in the rock. The following adjustments are necessary to incorporate these additional factors into the seepage evaluation:

- *THM and THC Alteration of $1/\alpha$ and k*

  The time-dependent alterations of these seepage-relevant parameters can (and should) be neglected in the seepage abstraction.

- *Effect of Drift Degradation*

  For all collapsed drift cases, uncertainty is already accounted for in the interpolated seepage rates. For non-collapsed cases, the ambient seepage rates are increased by 20% to account for additional uncertainty. In this case, for large ambient seepage, the increased seepage rates may correspond to a seepage percentage larger than 100%. These are set to a rate corresponding to a seepage percentage of 100%. The reference area used to relate seepage rates and seepage percentages is 5.1 m $\times$ 5.5 m in this case, i.e., the footprint of a 5.1-m long section of a non-degraded drift.

- *Thermal Seepage*

  Two alternative abstraction approaches are proposed for the treatment of thermal seepage in the TSPA seepage calculation. The decision which one of the two abstraction approaches should be used will be made during the TSPA process, weighting the benefit of less seepage in Abstraction Model 2 against the complexity of implementing it into the TSPA. The two abstraction approaches are defined as follows:

  Abstraction Model 1 sets thermal seepage equal to the adjusted ambient seepage. In other words, these seepage rates are *not* adjusted for thermal perturbation effects. The abstraction is based on the model finding that ambient seepage provides an asymptotic upper limit for thermal seepage (i.e., there is no enhanced seepage as a result of thermal perturbation).

  Abstraction Model 2 sets thermal seepage to zero for the period of above-boiling temperatures in the drift vicinity. This approach takes credit for the vaporization barrier that prevents seepage during the period of above-boiling temperatures. The threshold temperature that defines the duration of the boiling period is set to 100°C. For the remaining time period, thermal seepage is set equal to the adjusted ambient seepage rates. The abstraction is based on the model findings that thermal seepage never occurs at above-boiling temperatures and that the ambient seepage values provide an asymptotic upper limit for thermal seepage. For implementation of this model in the TSPA, detailed information is required about the duration of the boiling period for a large number of parameter cases.

Seepage in ventilated drifts is highly unlikely. Therefore, in both abstraction models, seepage during the 50-year preclosure period can be neglected.

6.7.1.3 Step 3: Seepage Probability Distributions and Seepage Fraction

The final results of the TSPA seepage calculation are probability distributions of seepage rates appropriately incorporating all relevant factors, given for each time step. Statistical analyses can be conducted for a detailed evaluation of the seepage results in each time step. Such analyses can be conducted over all realizations and locations (uncertainty and spatial variability), or alternatively for one location over all realizations (uncertainty at one location) and one realization over all locations (spatial variability). Histograms reveal the shape of the respective distributions. Relating the mean seepage rate to the overall percolation flux demonstrates the barrier capability of the UZ, limiting the seepage of water into emplacement drifts. The total number of samples with a nonzero seepage rate defines the seepage fraction f_{seep}. This parameter is important because it reveals the fraction of waste packages potentially in contact with water. Other data processing of the seepage results (sorting, averaging, binning) may be needed for further use in downstream TSPA model components.

6.7.2 Propagation of Uncertainty through the Abstraction

All sources of uncertainty related to seepage-relevant parameters and seepage simulation results have been characterized in and propagated through the seepage abstraction for TSPA-LA. Uncertainty in the key parameters for ambient seepage has been explicitly represented through appropriate probability distributions (Section 6.6). The probabilities assigned to these key parameters distinguish between spatial variability (aleatory uncertainty) and uncertainty (epistemic uncertainty), using separate distributions. Spatial variability distributions for the capillary strength parameter and the local permeability have been derived in this Model Report by detailed statistical analysis of the sparsely distributed data (Sections 6.6.1 and 6.6.2). Spatial variability distributions for the local percolation flux are provided from site-scale simulations with the UZ Flow and Transport Model (Section 6.6.3). These fluxes are then adjusted to account for intermediate-scale heterogeneity, using a spatial distribution of flow focusing factors. Uncertainty has been characterized by evaluation of all potential sources for uncertainty—i.e., uncertainty in the measurements, the conceptual model, the estimation process, and the spatial variability. Information on uncertainty provided in upstream analyses or modeling has been included in this evaluation. Uncertainty inherent in the capillary strength parameter and the local permeability is described by triangular probability distributions (Sections 6.6.1 and 6.6.2). Alternative methods have been employed to derive statistical parameters describing the probability distributions for the capillary-strength parameter. It is recommended that TSPA conduct a sensitivity analysis and choose the most conservative method with respect to the overall seepage. Uncertainty in the percolation flux distributions is incorporated using three different flow scenarios (Section 6.6.4). In addition, an alternative UZ flow scenario is evaluated in Section 6.8.2, but can be neglected in TSPA because of its limited impact.

Another contribution to uncertainty in the TSPA seepage calculations stems from the simulation results of drift-scale models that describe seepage-relevant processes. Drift-scale models are introduced in Section 6.4, including a detailed assessment of the respective model validation and

corroboration with alternative conceptual models. As discussed in Section 6.5, the treatment of uncertainty in simulation results is based on this assessment and considers the respective use of the model in the abstraction. The estimation uncertainty of SMPA simulation results, used directly in TSPA-LA as a quantitative measure of seepage, is explicitly incorporated in the seepage abstraction by uniform uncertainty distributions (Section 6.5.1.4). Other drift-scale models provide quantitative and qualitative information used to adjust the SMPA seepage results for additional factors (THM and THC parameter alterations, drift degradation, rock bolts, and thermal seepage). These adjustments are generally based on simplifications of the more complex process model results. To incorporate uncertainty, these simplifications are chosen to be conservative. This means that the simplified abstractions tend to overestimate the seepage compared to the predicted process model results. THC parameter alterations, for example, were found to decrease the potential of seepage because of a precipitation umbrella forming a few meters above drifts. This process, however, is neglected in the abstraction because of considerable uncertainties in modeling the coupled THC processes (Section 6.5.1.4).

Two different approaches are chosen for seepage estimates in degraded drifts. For moderately degraded drifts, the seepage rates are increased by 20% to account for uncertainty in the prediction (Section 6.5.1.5). For collapsed drifts, this increase is not necessary because this extreme degree of damage is related to a worst-case scenario that includes sufficient conservatism. Two alternative abstractions have been proposed for thermal seepage. The first approach is simple and conservative; no incorporation of the vaporization barrier in superheated fractured rock takes place so that the thermal seepage is not different from ambient seepage. The second approach is more realistic; it considers that there is no seepage during the period of above-boiling temperatures. To account for uncertainty, the threshold temperature used to define “above-boiling conditions” is chosen to be higher than the nominal boiling temperature of water (Section 6.5.2.2).

6.8 SEEPAGE CALCULATION AND SENSITIVITIES

In this section, a probabilistic calculation of seepage is conducted following the seepage abstraction method described in Sections 6.5 through 6.7. This calculation serves two purposes: (1) to demonstrate the barrier capabilities of the UZ and (2) to evaluate sensitivities in the abstraction process. As mentioned before, results from this calculation are not utilized in the performance assessment; they merely provide information on the expected seepage behavior for different test cases. However, they may be useful as corroborating information for validation of the seepage calculation procedure in the TSPA-LA. The TSPA-LA seepage component will perform a more comprehensive probabilistic seepage calculation within its Monte Carlo simulation procedure to provide the final seepage results used in the performance assessment.

The probabilistic analysis in this Model Report is conducted in a random procedure with sample size 10,000. For simplification, spatial variability and uncertainty distributions are simultaneously sampled in one calculational loop. In each random seepage case, noncorrelated random numbers are generated to sample from spatial variability distributions (for capillary strength, permeability, percolation flux, and flow focusing factor) *and* from uncertainty distributions (for capillary strength, permeability, and seepage uncertainty). In contrast, in the TSPA-LA calculation, uncertainty is sampled in an outer calculation loop over R realizations, while spatial variability is sampled in an inner calculation loop over r spatial locations. These spatial locations will be selected in the TSPA-LA so that they are consistent with other abstractions (e.g., for the in-drift environment). In this way, the PTn/TSw flux q_{perc} will be derived from exact spatial interpolation of the respective flux distribution in the TSPA-LA. Since the selection of these locations has not been finalized at the time of writing this Model Report, a simplified sampling procedure is utilized in the calculations below. The percolation flux values are randomly sampled using the probability distribution functions from the respective percolation flux fields (see histograms in Figures 6.6-11 and 6.6-12), without explicit consideration of the location in the repository area. Note that these differences may lead to minor differences in the predicted seepage results between the TSPA-LA calculation and the calculation conducted in this report. However, the main trends are not affected by these differences.

The probabilistic seepage calculations are carried out using Mathcad 11, a standard technical calculation tool for solving mathematical problems of various kinds. The different *Mathcad 11* spreadsheets developed for the several seepage calculation cases are provided in Attachment V. The mathematical calculation follows the seepage abstraction steps summarized in Section 6.7. Note that only the non-collapsed drift cases are analyzed. In Step 1 of the calculation, random numbers are generated to sample probabilistic parameter values from spatial variability distributions and to adjust them using respective uncertainty distributions. This is done for the three key parameters of ambient seepage, capillary strength, permeability, and percolation flux (the latter using site-scale fluxes and flow focusing factors). For each random parameter set, mean seepage rates and related standard deviations are interpolated from the appropriate look-up table, and the mean seepage rates are adjusted for seepage uncertainty. (The interpolation is conducted for the k-variable first, then for $1/\alpha$, and finally for $q_{perc,ff}$.) Note that all seepage calculation cases use the same seed value for the random procedure. This ensures that the comparison of different sensitivity cases is not biased by artifacts of the random number procedure. Using a fixed random seed also ensures reproducibility of the results. In Step 2, the ambient seepage rates are corrected for the effect of drift degradation, increasing them by 20%.

Finally, the impact of thermal perturbation is accounted for. In this Model Report, we mainly apply Abstraction Model 1 for thermal seepage, using the above ambient results as an approximation of the thermal period. Since detailed results on the duration of the boiling period for all repository drifts including spatial variability and uncertainty cases are not available at the time of writing this report, Abstraction Model 2 is applied only as a sensitivity study, assuming that the duration of the boiling period in all emplacement drifts corresponds to the duration of the present-day climate period.

The following two subsections give seepage calculation results for the base-case seepage evaluation (Section 6.8.1) and for selected sensitivity cases (Section 6.8.2). Histograms of the calculated seepage rates (in kg/year per waste package) and seepage percentages (relative to the percolation flux) are given for selected cases to demonstrate the variability of seepage over the 10,000 random cases. Summary results comprise the mean seepage rate and the mean seepage percentage, both of which are calculated over all 10,000 locations with and without seepage, and the seepage fraction (fraction of locations with seepage). The mean seepage percentage is derived as the mean seepage rate (over all 10,000 samples) related to the mean percolation flux (over the repository area). (This is different from simply averaging the 10,000 seepage percentage values). The seepage fraction is calculated using a threshold seepage rate of 0.1 kg/year per waste package. Locations with less than this threshold rate are considered "no seepage," because such small values are mainly a result of the interpolation procedure (simulation cases with a seepage rate of less than 0.1 kg/year per waste package are extremely rare in the SMPA look-up table).

6.8.1 Base-Case Seepage Evaluation

First, the probabilistic seepage analysis is presented for the Tptpll unit, the main repository unit according to the current repository design. Results of the seepage calculation are given separately for the three different climate scenarios (the mean, upper-bound, and lower-bound scenarios). In the TSPA-LA calculations, these separate results will be converted into one final distribution according to the respective occurrence probability of each scenario. These probabilities are developed in the Analyses Report *Analysis of Infiltration Uncertainty* (BSC 2003 [163740]), which has not been finalized yet. Therefore, this final step is not conducted here. Thermal seepage is first accounted for using Abstraction Model 1. The seepage calculations in this section are conducted using the parameter distribution for capillary strength as derived from the statistical Method A (see Table 6.6-2 and Section 6.1.1.1). The impact of applying the other distributions (from Methods B, C, and D) is evaluated in the sensitivity analysis in Section 6.8.2.

For illustration, Figures 6.8-1 and 6.8-2 present histograms of the calculated seepage rates and percentages for the mean climate scenario, showing only the random samples with nonzero seepage. (The great majority of the samples have zero seepage.) The seepage rates vary strongly, from small values below 0.1 kg/year per waste package up to almost 10,000 kg/year per waste package. (For comparison: A percolation flux of 500 mm/year that completely seeps into a 5.1 m long drift section would give a seepage rate of more than 14,000 kg/year per waste package.) The seepage percentages also show considerable variability covering the entire range from 0% up to 100%. Most probable, however, are the small seepage percentages; only a few samples reach 80% seepage and more. In both figures, there is a clear trend of increasing seepage probability as

a result of the climate changes from present-day to monsoon climate and from monsoon to glacial transition climate.

Table 6.8-1 gives summary results of the probabilistic analysis for the Tptpll, providing the mean seepage rate, the mean seepage percentage, and the seepage fraction, during the present-day, the monsoon, and the glacial transition climate. For the mean climate scenario, seepage is expected to occur at about 8% of all waste packages during the first 600 years after emplacement. This percentage rises to about 18% during the monsoon climate, and about 24% during the glacial transition climate. On average over all waste packages, the amount of seeping water is 1.7, 17.5, and 37.9 kg/year for the three climate stages, respectively. This translates to mean seepage percentages of 1.5%, 5.3%, and 7.5%. In other words, during the present-day climate, more than 98% of the percolation flux is diverted around drifts in the Tptpll unit. For the wetter climate stages of the monsoon and the glacial transition period, the percentage of diverted flux is smaller, but still at about 95% and 92%, respectively. This illustrates the barrier capability of the unsaturated flow processes in the fractured rock at and above the repository horizon.

As expected, the lower-bound climate scenario results in considerably less seepage. Here, the seepage fraction varies from about 1% for the present-day climate to over 9% during the monsoon period to 4% during the glacial transition climate. The respective mean seepage percentages are as low as 0.3%, 1.5%, and 0.9%. The opposite trend is seen for the upper-bound climate scenario, with the seepage fraction as high as 36% during the glacial transition climate. The mean seepage percentage during this climate stage is 11.8%. Thus, even for the upper-bound climate scenario with comparably strong downward percolation, the diversion capacity of the unsaturated rock is at least 88%.

The tabular values for mean seepage rate, mean seepage percentage and seepage fraction are visualized in Figures 6.8-3 through 6.8-5, showing the evolution of seepage over time. Note that the time axis starts at 50 years after emplacement, i.e., of the beginning of the postclosure period. As a result of the forced ventilation with relatively dry air, seepage is not expected to occur during the 50-year preclosure period. For the mean and the upper-bound scenarios, the trend of seepage increase with changes in climate is clearly evident. The stepwise increases at 600 years and at 2,000 years are particularly strong for the mean seepage rates, which give the absolute amount of water seeping into drifts (Figure 6.8-3). Compared to the other two climate scenarios, the lower-bound climate scenario has much less seepage during all climate stages.

The seepage results displayed in Figures 6.8-3 through 6.8-5 can be used as a basis to discuss the benefit of using Abstraction Model 2 instead of Abstraction Model 1 for thermal seepage. Abstraction Model 2 takes credit for a fully effective vaporization barrier during the time period that local rock temperatures in the drift vicinity are above boiling. For average percolation fluxes, this time period is expected to last for about 1,000 years (Tptpmn) to about 1,400 years (Tptpll) after waste emplacement (see Figure 6.2.3.1-1 in BSC (2003 [161530])), but can be significantly shorter for larger percolation fluxes (Section 6.4.3.3). Other relevant factors affecting the duration of the boiling period in individual drift sections are the thermal load, the location in the repository, and the TH properties of the fractured rock. Since spatial variability in these factors will give rise to considerable spatial variability of the boiling period within different drift sections, the implementation of Abstraction Model 2 in TSPA-LA requires systematic TH simulations for a large number of parameter cases. In view of these systematic results, an

average boiling period of 600 years is assumed in all emplacement drifts to illustrate the differences between the thermal seepage abstraction results. (While most drift sections are expected to remain at boiling conditions for more than 600 years, there will be parameter cases with shorter boiling periods, for example the extreme percolation flux cases shown in Section 6.4.3.3.) Then, the benefit of Abstraction Model 2 can be easily derived by setting the seepage flux, percentage, and fraction to zero during the present-day climate period, in Figures 6.8-1 through 6.8-5 and in Table 6.8-1. It is obvious that the time period for a fully effective vaporization barrier coincides with the time period of relatively small ambient seepage compared to later climate stages. More benefit can be expected from Abstraction Model 2, when an average boiling period of 1,000 to 1,400 years is assumed. In this case, the no-seepage period according to Abstraction Model 2 would extend several hundred years into the monsoon climate stage, when the predicted ambient seepage is higher.

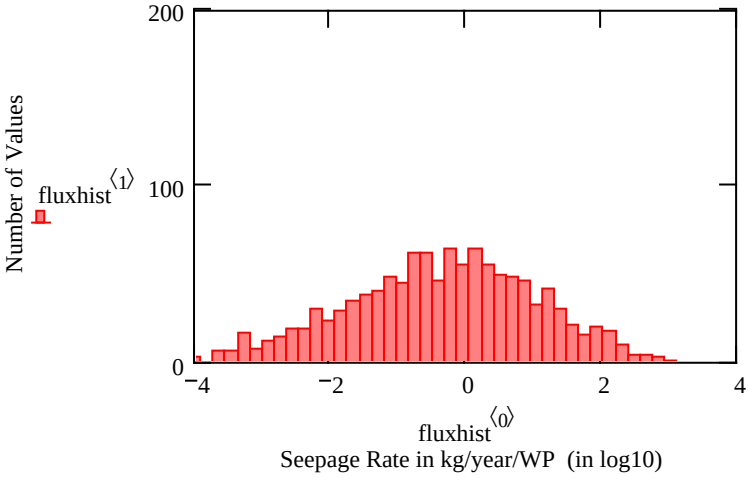

(Present-day)

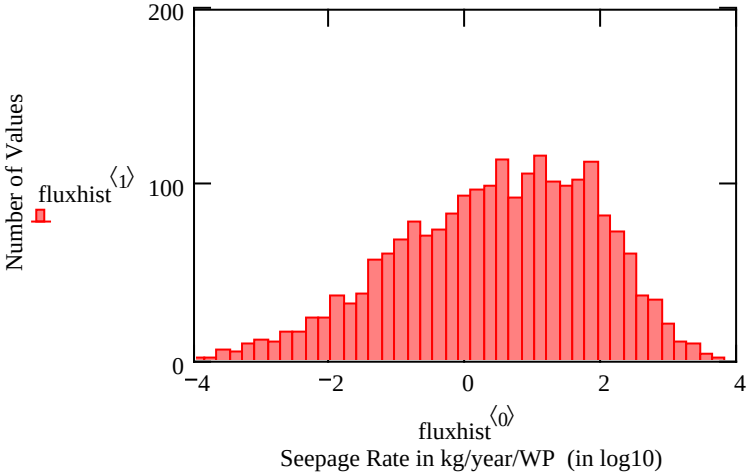

(Monsoon)

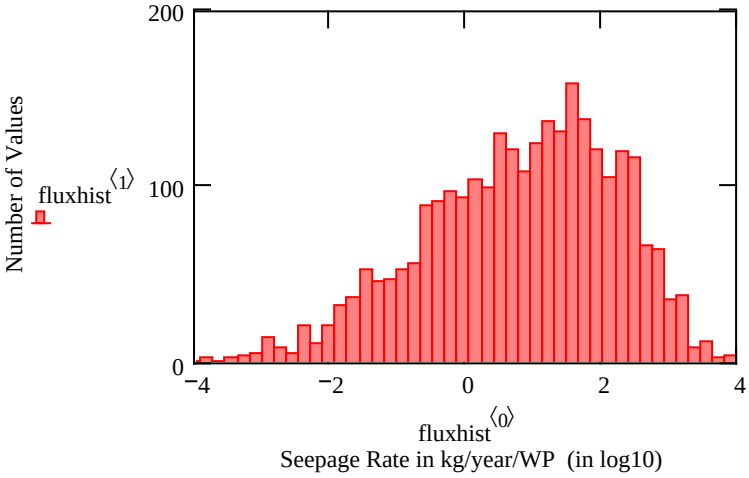

(Glacial Transition)

Output-DTN: LB0308AMRU0120.002

NOTE: The symbols in the histograms (i.e., fluxhist$^{<0>}$ and fluxhist$^{<1>}$) denote the variable names given in the *Mathcad 11* spreadsheet used for the calculation, see Attachment V. Only the samples with non-zero seepage are depicted.

Figure 6.8-1. Histograms of Seepage Rates for Tptpll Unit

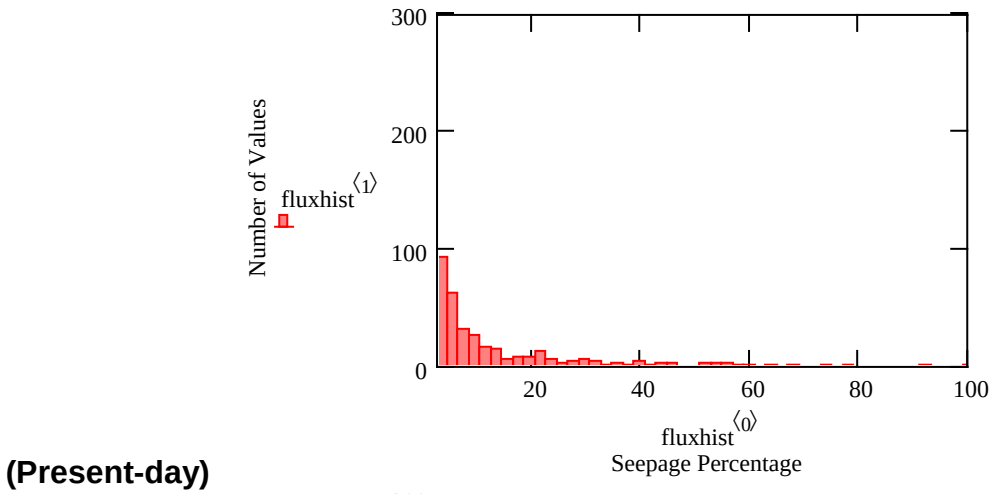

(Present-day)

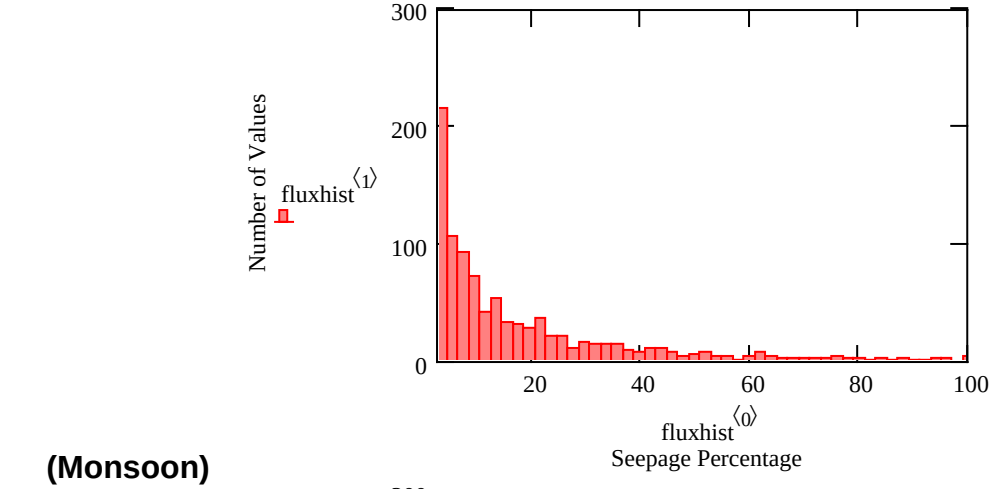

(Monsoon)

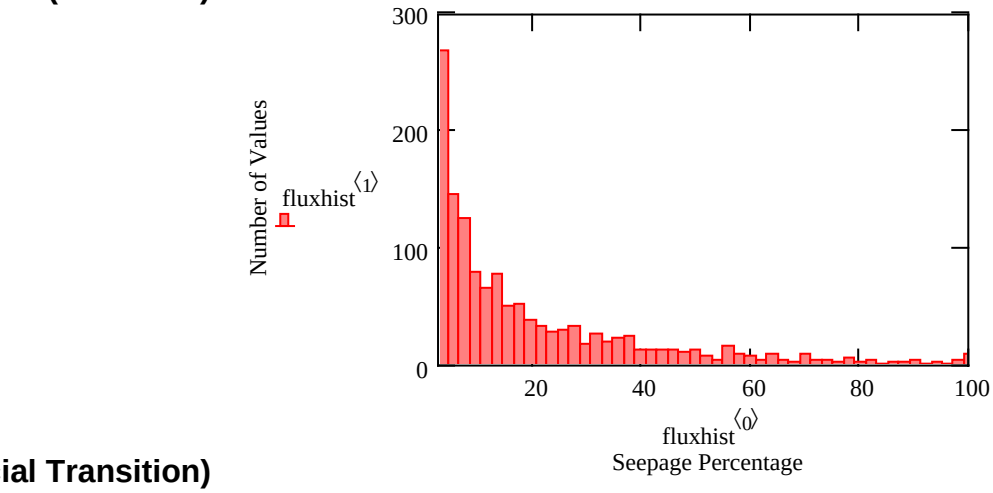

(Glacial Transition)

Output-DTN: LB0308AMRU0120.002

NOTE: The symbols in the histograms (i.e., fluxhist$^{<0>}$ and fluxhist$^{<1>}$) denote the variable names given in the *Mathcad 11* spreadsheet used for the calculation, see Attachment V. Only the samples with non-zero seepage are depicted.

Figure 6.8-2. Histograms of Seepage Percentages for Tptpll Unit

Table 6.8-1. Summary Statistics for Probabilistic Seepage Evaluation (Tptpll Unit)

Mean Climate Scenario			
Climate Period	**Mean Seepage Rate (kg/year/WP)**	**Mean Seepage Percentage (%)**	**Seepage Fraction (%)**
Present Day	1.7	1.5	7.9
Monsoon	17.5	5.3	18.3
Glacial Transition	37.9	7.5	24.2
Lower-Bound Climate Scenario			
Climate Period	**Mean Seepage Rate (kg/year/WP)**	**Mean Seepage Percentage (%)**	**Seepage Fraction (%)**
Present Day	0.0	0.3	0.8
Monsoon	1.8	1.5	8.6
Glacial Transition	0.5	0.9	3.9
Upper-Bound Climate Scenario			
Climate Period	**Mean Seepage Rate (kg/year/WP)**	**Mean Seepage Percentage (%)**	**Seepage Fraction (%)**
Present Day	13.1	4.2	18.3
Monsoon	44.7	7.8	26.6
Glacial Transition	117.5	11.8	36.0

Output-DTN: LB0308AMRU0120.002

NOTE: Computation documented in Attachment V.

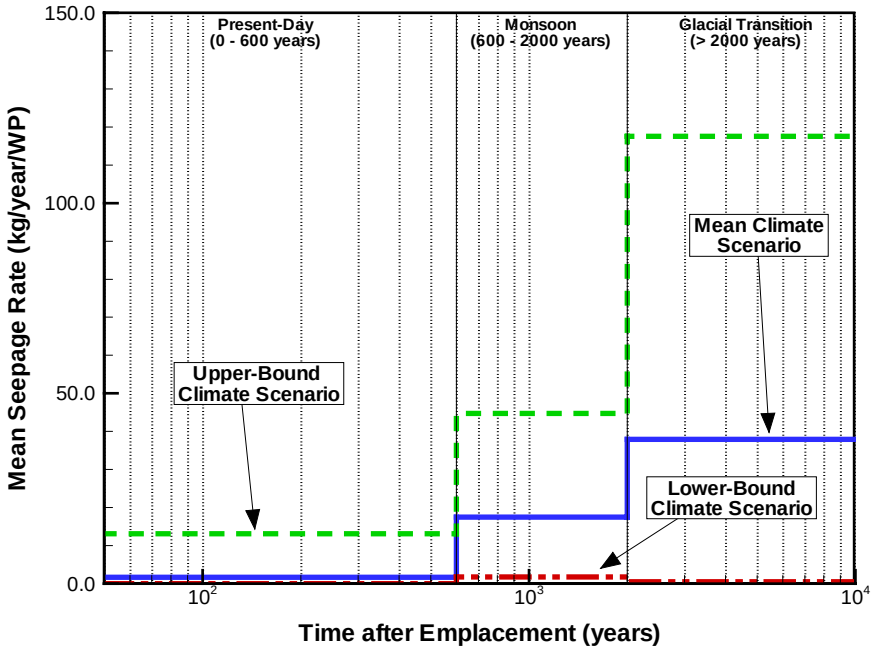

Source: Table 6.8-1; Output-DTN: LB0308AMRU0120.002

Figure 6.8-3. Mean Seepage Rate as a Function of Time after Emplacement for Tptpll Unit and Different Climate Scenarios

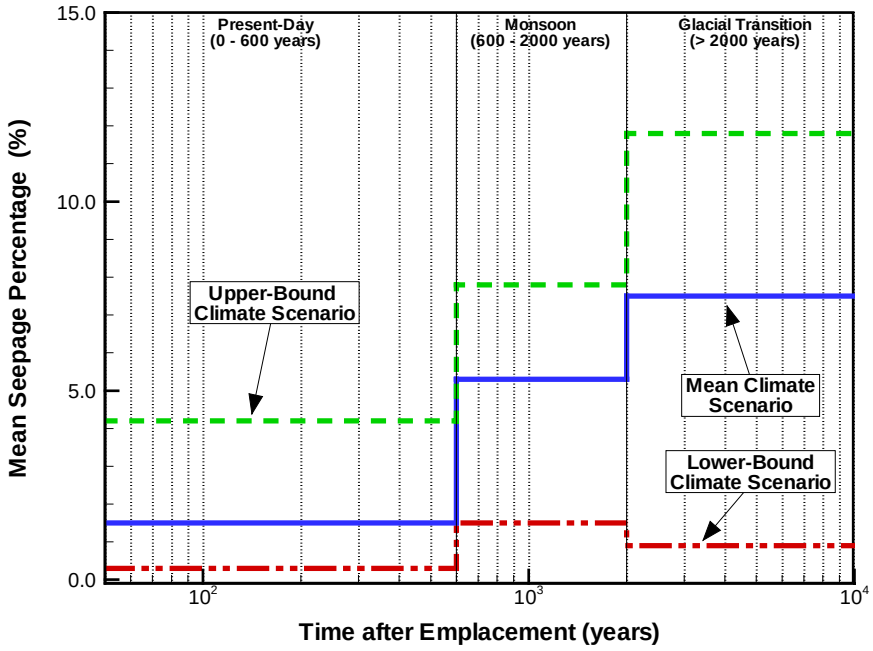

Source: Table 6.8-1; Output-DTN: LB0308AMRU0120.002

Figure 6.8-4. Mean Seepage Percentage as a Function of Time after Emplacement for Tptpll Unit and Different Climate Scenarios

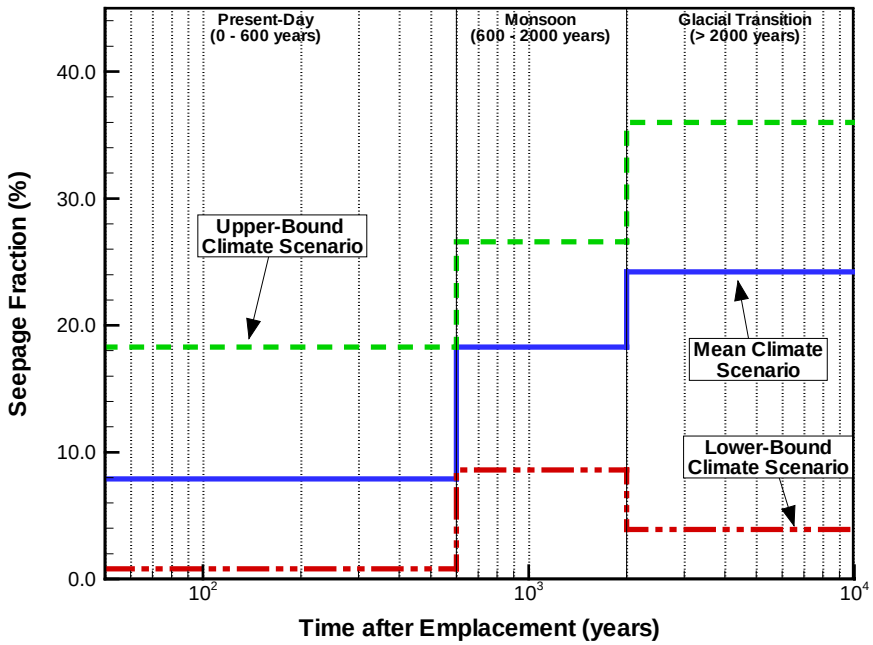

Source: Table 6.8-1; Output-DTN: LB0308AMRU0120.002

Figure 6.8-5. Seepage Fraction as a Function of Time after Emplacement for Tptpll Unit and Different Climate Scenarios

Summary statistics for seepage in the Tptpmn unit are listed in Table 6.8-2, for the three climate stages and climate scenarios. Comparison with Table 6.8-1 indicates that considerably more seepage occurs at a larger number of locations in the Tptpmn compared to the Tptpll (i.e., higher mean seepage rate and percentage, higher seepage fraction). This is mainly a result of the smaller mean permeability assigned to the spatial variability distribution of the Tptpmn unit. Thus, with respect to seepage, the Tptpll unit is the better host rock unit compared to the Tptpmn. The trends in the seepage results—between the different climate stages and scenarios—are similar to the Tptpll.

Table 6.8-2. Summary Statistics for Probabilistic Seepage Evaluation (Tptpmn Unit)

Mean Climate Scenario			
Climate Period	**Mean Seepage Rate (kg/year/WP)**	**Mean Seepage Percentage (%)**	**Seepage Fraction (%)**
Present Day	5.9	5.5	22.6
Monsoon	50.6	15.3	41.6
Glacial Transition	103.1	18.8	50.1
Lower-Bound Climate Scenario			
Climate Period	**Mean Seepage Rate (kg/year/WP)**	**Mean Seepage Percentage (%)**	**Seepage Fraction (%)**
Present Day	0.1	1.2	3.0
Monsoon	6.6	5.5	24.6
Glacial Transition	1.8	3.3	13.3
Upper-Bound Climate Scenario			
Climate Period	**Mean Seepage Rate (kg/year/WP)**	**Mean Seepage Percentage (%)**	**Seepage Fraction (%)**
Present Day	41.0	13.0	42.3
Monsoon	122.3	21.3	54.0
Glacial Transition	294.6	29.6	65.4

Output-DTN: LB0308AMRU0120.002

NOTE: Computation documented in Attachment V.

As discussed in Section 6.5.1.2, sampled parameter values for permeability and percolation flux are truncated if they fall outside of the parameter space covered by the SMPA look-up table. It is important for the validity of the seepage evaluation that the SMPA ranges are not exceeded in too many instances. Therefore, during the *Mathcad* calculation, the number of sampled values falling outside of the SMPA parameter space is counted and checked. The results are as follows: In the Tptpll unit, none of the 10,000 permeability values is smaller than –14 (in log10); about 72 values are higher than –10. (Truncating at the upper permeability value, however, is conservative, because reducing permeability tends to increase the probability of seepage. Also, at this upper bound, seepage is only expected in extreme parameter cases.) In the Tptpmn unit, with a narrower distribution for spatial variability and uncertainty, none of the sample values exceeds the parameter space. Considering the sampled percolation flux distributions, the number of flux values larger than 1,000 mm/yr is zero for all climate stages and scenarios. (Depending on the climate scenario, several sample values are smaller than 1 mm/yr, the smallest percolation flux simulated with the SMPA. Truncating at this lower bound, however, is not significant because

seepage hardly occurs at such small fluxes.) A percolation flux of 500 mm/yr, the upper flux value of the glacial transition climate analyzed with the Thermal Seepage Model, is exceeded in only one instance using the mean climate scenario (seven instances in the upper-bound scenario, none in the lower-bound scenario). These small numbers indicate that the supporting seepage process models cover parameter spaces that safely include the vast majority of the sample cases in the random seepage evaluation. This ensures that the seepage evaluation results are not biased by sample truncation.

6.8.2 Sensitivity Analysis

Several sensitivity cases have been selected to identify how the overall amount of seepage and the seepage fraction in the repository may be affected by some choices made in the abstraction process. The sensitivity analysis is conducted only for the Tptpll unit using the mean climate scenario; the trends observed should be similar for the Tptpmn unit and should also be representative of other climate scenarios. Abstraction Model 1 is used for thermal seepage. Table 6.8-3 provides summary statistics for the respective sensitivity cases, giving the mean seepage rate, the mean seepage percentage, and the seepage fraction during the present-day, the monsoon, and the glacial transition climate. For comparison, the table not only provides the absolute seepage results for the considered case, but also the differences of these results from the base case (Table 6.8-1). A negative value indicates that the sensitivity case result is smaller than that of the base case (number in blue). A positive value indicates that the sensitivity case result is larger than that of the base case (number in red). Below, the sensitivity cases are discussed item by item.

1. Normal Distribution for Spatial Variability of Capillary Strength Parameter

As discussed in Section 6.6.1.2, the shape of the spatial variability distribution for the calibrated capillary strength parameter is not clearly indicated by the histogram of the data sample (Figure 6.6-2). Therefore, the distribution of choice for the TSPA-LA is a uniform distribution. For comparison, Sensitivity Case 1 utilizes a normal distribution instead of a uniform distribution. The seepage results using a normal distribution are almost identical to the base case, indicating a very small sensitivity to the shape of the distribution.

2. Normal Distribution for Uncertainty of Seepage Rate Predictions

Analysis of the SMPA results in Section 6.4.2.3 does not reveal a consistent trend for the uncertainty distribution describing the variability in seepage predictions from different realizations. Thus, a simple uniform distribution is selected in the abstraction for the TSPA-LA. In Sensitivity Case 2, a normal distribution is assumed as an alternative case. Again, the impact of choosing a different shape of the distribution is rather marginal, indicating a small sensitivity.

3. No Spatial Variability in Permeability and Capillary Strength

Significant effort was devoted in Section 6.6 to define appropriate distributions describing the intermediate-scale variability of permeability and capillary strength over the repository area. Sensitivity Case 3 ignores the spatial variability of these seepage-relevant parameters. The seepage results in Table 6.8-3 indicates the considerable impact

of using spatially uniform (but still uncertain) parameters. The overall amount of seepage (expressed in the mean seepage rate and the mean seepage percentage), as well as the seepage fraction, is considerably smaller than in the base case.

4. No Uncertainty in Permeability and Capillary Strength

Sensitivity Case 4 assumes that the uncertainty in the parameter distribution for the seepage-relevant parameters—permeability and capillary strength—can be neglected. (Spatial variability, however, is still considered, expressed by appropriate probability distributions.) Without uncertainty, the overall amount of seepage and the seepage fraction are smaller than in the base case. Comparison with Sensitivity Case 3 indicates that the impact of neglecting uncertainty is less significant than the impact of neglecting spatial variability.

5. Adjusted Mean Value of Spatial Variability Distribution for Permeability

In Sensitivity Case 5, the spatial variability distribution for fracture permeability is shifted to a larger mean value, from initially –11.5 to –11.0 (in log10). As discussed in Section 6.6.2.2, the small-scale permeability measurements conducted in Niche 1620 and in the ECRB suggest a mean permeability of about –11.0 in the excavation-disturbed zone around drifts. However, additional analysis of surface-based boreholes indicated that these permeability measurements might be on the high side, potentially representing a rather permeable region in the Tptpll. Therefore, the mean permeability value proposed for TSPA-LA seepage calculations was set half an order of magnitude smaller, to a value of –11.5. Sensitivity Case 5 uses the initial value of –11.0 to demonstrate the impact of this shift in the mean permeability. Having a higher permeability brings down the expected seepage in the Tptpll by a significant amount. During the glacial transition climate, for example, the mean seepage percentage decreases from 7.5% (base case) to 2.6%. Similarly, the seepage fraction changes from 24.2% (base case) to 11.3% during this climate stage. Thus, an increase in permeability reduces the overall amount of seepage as well as the number of waste packages contacted by water. The calculated numbers indicate that the proposed mean permeability of –11.5 is clearly a conservative parameter choice.

6. Adjusted Flow Focusing Factors

Flow focusing is described in the seepage abstraction by a cumulative probability distribution giving maximum factors between 5 and 6. Sensitivity Cases 6a and 6b demonstrate the impact of flow focusing. Case 6a assumes that there is no flow focusing; i.e., the percolation flux distributions derived from the UZ Flow and Transport Model are directly applied for TSPA sampling (Section 6.6.4.1). In contrast, Case 6b uses more widely distributed flow focusing factors, with a maximum factor of about 33. Note that the considered distributions for flow focusing are all mass conservative; i.e., the mean of the distributions is always one. Thus, focusing of flow in one location (which tends to increase seepage) will reduce flow in other places (which tends to decrease seepage). The effect of this shift can be seen in the seepage calculation results. Having no flow focusing leads to a small increase in the seepage fraction, while the overall amount of seepage decreases slightly. Hence, more waste packages will have contact with water, but the average amount of water at these locations will be small. In contrast, a wider distribution

of flow focusing factors leads to a strong increase in overall seepage, combined with a significant decrease in the seepage fraction. As a result, many fewer waste packages will have contact with water, but the amount of seepage at these locations will be large.

7. Percolation Flux Distribution From Alternative PTn Flow Conceptualization

Alternative percolation flux distributions were introduced in Section 6.6.4.1, based on adjusted hydrological properties in the PTn unit. The impact of using these alternative distributions is analyzed in Sensitivity Case 7. The resulting differences in both the overall amount of seepage and the seepage fraction are small. Using the alternative flow fields leads to a minor increase in the mean seepage percentage combined with a small decrease in the seepage fraction. Because they have limited impact, alternative flow fields can be neglected in the TSPA-LA seepage evaluation.

8. Alternative Methods for Definition of Capillary Strength Parameter Distribution

As discussed in Section 6.6.1.2, four different methods have been employed to derive the mean and the standard deviation of sampled values of the capillary strength parameter $1/\alpha$. The methods consider alternative statistical relationships between sample values measured in different geological units and at different locations, and they arrive at four alternative probability distributions for spatial variability and uncertainty of this parameter (see Section 6.7.1.1 for the definition of the four parameter distributions). Statistical tests have not provided a clear indication about the most appropriate method. It was recommended in Sections 6.6.1.2 and Section 6.7.1 that all four methods be included in TSPA as equally probable alternative representations of spatial variability and uncertainty in the $1/\alpha$-parameter. The base-case seepage results in Section 6.8.1 have been calculated using Method A. For comparison, Sensitivity Cases 8a, 8b, and 8c use parameter distributions for $1/\alpha$ based on the statistical values derived using Methods B, C, and D, respectively. The resulting values of seepage percentage and fraction are slightly lower for Method B compared to Method A, whereas Methods C and D lead to slightly higher seepage estimates compared to Method A. Overall, the sensitivity of the seepage results to the evaluation method is rather small, providing confidence that the seepage calculation is not greatly affected by uncertainty about the statistical independence of the sample values.

Table 6.8-3. Summary Statistics for Seepage Sensitivity Cases (Tptpll Unit)

1. Normal Distribution for 1/α Instead of Uniform Distribution						
Climate Period	Mean Seepage Rate (kg/year/WP)		Mean Seepage Percentage (%)		Seepage Fraction (%)	
Present Day	1.6	-0.1	1.5	0.0	7.8	-0.1
Monsoon	17.2	-0.3	5.2	-0.1	18.2	-0.1
Glacial Transition	37.5	-0.4	7.4	-0.1	24.0	-0.2
2. Normal Distribution for Seepage Uncertainty Instead of Uniform Distribution						
Climate Period	Mean Seepage Rate (kg/year/WP)		Mean Seepage Percentage (%)		Seepage Fraction (%)	
Present Day	1.4	-0.3	1.3	-0.2	7.6	-0.3
Monsoon	16.6	-0.9	5.0	-0.3	18.7	+0.4
Glacial Transition	36.6	-1.3	7.3	-0.2	24.8	+0.6
3. No Spatial Variability in Permeability and Capillary-Strength Parameter						
Climate Period	Mean Seepage Rate (kg/year/WP)		Mean Seepage Percentage (%)		Seepage Fraction (%)	
Present Day	0.1	-1.6	0.1	-1.4	1.7	-6.2
Monsoon	5.6	-11.9	1.7	-3.6	10.3	-8.0
Glacial Transition	14.9	-23.0	3.0	-4.5	16.4	-7.8
4. No Uncertainty in Permeability and Capillary-Strength Parameter						
Climate Period	Mean Seepage Rate (kg/year/WP)		Mean Seepage Percentage (%)		Seepage Fraction (%)	
Present Day	0.9	-0.8	0.8	-0.7	4.8	-3.1
Monsoon	12.5	-5.0	3.8	-1.5	15.4	-2.9
Glacial Transition	28.6	-9.3	5.7	-1.8	21.0	-3.2
5. Adjusted Mean Permeability for Tptpll: k = -11.0 instead of k = -11.5 (in log10)						
Climate Period	Mean Seepage Rate (kg/year/WP)		Mean Seepage Percentage (%)		Seepage Fraction (%)	
Present Day	0.4	-1.3	0.4	-1.1	2.4	-5.5
Monsoon	5.7	-11.8	1.7	-3.6	8.0	-10.3
Glacial Transition	13.3	-24.6	2.6	-4.9	11.3	-12.9
6a. No Flow Focusing						
Climate Period	Mean Seepage Rate (kg/year/WP)		Mean Seepage Percentage (%)		Seepage Fraction (%)	
Present Day	0.9	-0.8	0.9	-0.6	8.1	+0.2
Monsoon	10.4	-7.1	3.2	-2.1	19.8	+1.5
Glacial Transition	23.6	-14.3	4.7	-2.8	26.6	+2.4
6b. Increased Flow Focusing (Maximum Flow Focusing Factor f_{ff} = 33)						
Climate Period	Mean Seepage Rate (kg/year/WP)		Mean Seepage Percentage (%)		Seepage Fraction (%)	
Present Day	10.6	+8.9	9.5	+8.0	5.3	-2.6
Monsoon	68.2	+50.7	19.8	+14.5	11.2	-7.1
Glacial Transition	127.2	+89.3	24.1	+16.6	14.1	-10.1
7. Percolation Flux Distribution From Alternative PTn Flow Conceptualization						
Climate Period	Mean Seepage Rate (kg/year/WP)		Mean Seepage Percentage (%)		Seepage Fraction (%)	
Present Day	2.1	+0.4	2.0	+0.5	7.7	-0.2
Monsoon	20.1	+2.6	6.0	+0.7	17.2	-1.1
Glacial Transition	42.9	+5.0	8.4	+0.9	22.6	-1.6

Table 6.8-3. Summary Statistics for Seepage Sensitivity Cases (Tptpll Unit) (continued)

8a. Spatial Variability and Uncertainty Distributions for 1/α Defined From Method B						
Climate Period	Mean Seepage Rate (kg/year/WP)		Mean Seepage Percentage (%)		Seepage Fraction (%)	
Present Day	1.2	-0.5	1.1	-0.4	6.0	-1.9
Monsoon	14.0	-3.5	4.2	-1.1	15.0	-3.3
Glacial Transition	30.7	-7.2	6.1	-1.4	20.5	-3.7
8b. Spatial Variability and Uncertainty Distributions for 1/α Defined From Method C						
Climate Period	Mean Seepage Rate (kg/year/WP)		Mean Seepage Percentage (%)		Seepage Fraction (%)	
Present Day	1.8	+0.1	1.7	+0.2	8.6	+0.7
Monsoon	18.8	+1.3	5.7	+0.4	19.4	+1.1
Glacial Transition	40.1	+2.2	8.0	+0.5	25.4	+1.2
8c. Spatial Variability and Uncertainty Distributions for 1/α Defined From Method D						
Climate Period	Mean Seepage Rate (kg/year/WP)		Mean Seepage Percentage (%)		Seepage Fraction (%)	
Present Day	3.2	+1.5	3.0	+1.5	10.9	+3.0
Monsoon	24.1	+6.6	7.3	+2.0	20.4	+2.1
Glacial Transition	48.3	+10.4	9.6	+2.1	25.8	+1.6

Output-DTN: LB0308AMRU0120.002

NOTE: Left values in each column given seepage results for sensitivity case, right values give changes to base case. Computation documented in Attachment V.

The main results from the sensitivity analysis can be briefly summarized. The first two sensitivity cases prove that the chosen shape of the probability distributions for spatial variability of capillary strength and the uncertainty in seepage rates does not affect the seepage evaluation. As a consequence, the abstraction choice to use uniform distributions is supported. Sensitivity Cases 3 and 4 demonstrate that the consideration of spatial variability and uncertainty in seepage-relevant parameters $1/\alpha$ and k is important for seepage evaluation in TSPA-LA. Sensitivity Case 5 indicates the strong impact of the conservative parameter choice for permeability in the Tptpll unit. Additional air injection testing could be beneficial for this unit, to provide evidence that the mean permeability in the Tptpll should be higher than the one chosen in the abstraction. As shown in Sensitivity Case 6, the distribution of flow focusing factors is also important for the seepage evaluation. In contrast to Sensitivity Cases 3, 4, and 5, where a consistent trend is seen in both the seepage percentage and the seepage fraction, a change in flow focusing factors results in opposite trends for these seepage parameters. An increase in the overall amount of seepage is associated with a decrease in the number of waste packages affected by seepage, and vice versa. Since both the amount of seepage and the seepage fraction are important for TSPA-LA, the overall impact of using different distributions for flow focusing factors should be evaluated in further sensitivity testing using the full TSPA model. Sensitivity Case 7 shows that the alternative flow conceptualization in the PTn unit is not important for the overall seepage evaluation. The final sensitivity cases demonstrate that the seepage estimates are not strongly influenced by the evaluation method employed to define the spatial variability and uncertainty distribution for the capillary strength parameter.

INTENTIONALLY LEFT BLANK

7. VALIDATION

The seepage abstraction developed in this Model Report is based on seepage predictions from detailed process models that have been validated in previous analyses, to ensure appropriate representation of the physical processes and relevant parameters (Section 6.4). As explained in Section 6.5, these results are either propagated to the TSPA-LA without changes (i.e., seepage look-up table) or have been simplified within the abstraction process (i.e., thermal seepage, THC and THM alterations, drift degradation, rock bolts). From the seepage look-up tables and the respective simplifications for additional factors, probabilistic seepage rates and uncertainties can be calculated as a function of seepage-relevant parameters. In the abstraction, appropriate spatial variability and uncertainty distributions have been developed for these parameters, based on either process model results (i.e., capillary strength, percolation flux) or *in situ* measurements (permeability).

Application of the developed abstraction model gives probabilistic seepage estimates for the future conditions in the entire repository, e.g., the expected probability distribution of seepage rates and the number of locations in the repository where seepage may occur. The validity of these final results depends on (1) the validity of the parameter distributions that feed into the seepage look-up table, and (2) the validity of the seepage predictions that provide the look-up tables or serve as bases for certain simplifications. Thus, validation of the seepage abstraction must demonstrate that (1) the input parameters for the seepage abstraction are justified, (2) the seepage abstraction captures the results provided by the process models in a qualitative and quantitative manner, and (3) uncertainties in the input parameters and the model results are appropriately incorporated.

The validation activities conducted for the seepage abstraction are consistent with the TWP for this Model Report (BSC 2002 [160819], Attachment I, Section I-4-3-1). These include activities that are conducted during the model development process (discussion and justification of input parameters, discussion and evaluation of uncertainties) and activities for testing the model after development (corroboration of abstraction with process models). Note that no initial conditions are established in the seepage abstraction model, i.e., a discussion and justification of the approach for the establishment of initial conditions do not apply to this Model Report. Results obtained from validation are presented and discussed in the remainder of this section.

Confidence Building during Model Development: Justification of Input Parameters

The parameters used in the abstraction process have been carefully selected from appropriate seepage process models and from *in situ* testing; they are reasonable and consistent with the data. Process models that provide parameter input to the abstraction have been discussed and evaluated in Section 6.4. These process models have all been validated, typically in comparison with experimental data and through corroboration with alternative conceptual models. The seepage process models all have a consistent conceptual modeling framework similar to the SCM, an important requirement for predictive modeling of ambient and thermal seepage. The boundary conditions and parameter ranges applied to these process models are appropriate; they sufficiently cover the expected conditions and ranges at Yucca Mountain, including temporal changes and

spatial variability. This ensures that the seepage abstraction does not extrapolate process model results to conditions beyond the model simulation ranges.

Confidence Building during Model Development: Evaluation of Uncertainties

A significant effort was spent in the abstraction process to define appropriate probability distributions for the spatial variability and uncertainty of seepage-relevant parameters (Section 6.6). The spatial variability distributions for the capillary-strength parameter and the permeability were developed from statistical calculations in Excel spreadsheets, using input from the SCM and from *in situ* air-injection tests (spreadsheets are given in Attachments II and III). Both parameters have been derived on the appropriate scale representing the location of interest, i.e., the near-drift excavation-disturbed zone. Uncertainty in these spatial variability distributions, stemming from the limited number of intermediate-scale measurement locations, was identified and incorporated in the abstraction by use of triangular probability distributions. The spatial variability of percolation fluxes was provided by simulation results from the UZ Flow and Transport Model. To account for heterogeneity occurring below the resolution of this site-scale model, additional flux variability was incorporated using a spatial distribution of flow focusing factors. Furthermore, measurement and model uncertainty identified in the upstream sources feeding into this abstraction was accounted for. For example, seepage prediction uncertainty is explicitly included in the seepage abstraction by random sampling from a uniform uncertainty distribution, while uncertainty in the future climates and percolation fluxes is accounted for by three different climate scenarios. Other uncertainties are incorporated in the abstraction by means of conservative upper-bound seepage estimates. A sensitivity study was conducted in Section 6.8.2 to evaluate the sensitivity of the overall seepage in the repository to certain abstraction choices with regard to the treatment of spatial variability and uncertainty.

Post-Development Validation Activities: Corroboration with Process Models

The main validation method for an abstraction model is to show that the abstraction results are sufficiently close to the predictions of the supporting models. Since the supporting models in turn are validated, the abstraction results can be considered validated ensuring an appropriate representation of the relevant processes in the TSPA-LA. The validation criterion suggested in the TWP (BSC 2002 [160819], Attachment I, Section I-4-3-1) calls for an agreement within 20% between the abstracted results and the process model results. It should be added that this 20% threshold may be exceeded if the abstracted results lead to more seepage; i.e., if the abstraction method uses conservative bounds for seepage. This ensures that the simplifications required in the seepage abstraction do not lead to an underestimation of seepage.

In seepage abstraction, the supporting models providing simulated seepage rates are the SMPA for ambient seepage and the Thermal Seepage Model for thermal seepage. In addition, the impact of THM and THC alterations is evaluated with the Drift-Scale THM Model and the THC Seepage Model, respectively. The agreement between these models and the abstracted results can be summarized as follows:

1. *SMPA* Results

The seepage look-up tables for ambient seepage provided by the SMPA are propagated through the seepage abstraction without further simplification (Section 6.5.1). For given random parameter cases, the seepage results are directly interpolated from the predicted values in the look-up table. Thus, there is very good agreement between the process model results and the abstracted results. Specific simulation cases were devoted to analyze the impact of degraded drift shapes on ambient seepage (Sections 6.4.2.4 and 6.4.2.5). In order to incorporate uncertainties in the results for moderately degraded drifts, the ambient seepage rates were increased by 20% in the abstraction (Section 6.5.1.5). While there is a difference of about 20% between the process model and the abstraction, the abstraction method is on the conservative side.

2. *TH Seepage Model* Results
   The temporal evolution of seepage at thermally perturbed conditions is abstracted using simplified time-dependent seepage estimates that provide an asymptotic upper limit to the process model results (Figures 6.5-3 and 6.5-4). During early heating stages, these asymptotic estimates are more than 20% off from the process model results. However, the abstracted results are always conservative.

3. *Drift-Scale THM Model* Results
   The impact of THM parameter alterations is neglected in the seepage abstraction, based on model results that predict slightly smaller seepage for simulation runs including THM effects (Section 6.4.4.1). The differences between the abstracted results and the THM process model results are small, as demonstrated in Figure 6.4-17, with the abstraction results on the conservative side.

4. *THC Seepage Model* Results
   The impact of THC parameter alterations on seepage has been qualitatively evaluated with the THC Seepage Model (Section 6.4.4.2). The precipitation cap that may potentially form 7-8 m above waste emplacement drifts after several hundred years of heating is expected to decrease seepage into drifts, since the percolating water is diverted sideways by the low-permeability cap before reaching the drift crown (Figure 6.4-18). This effect, however, is not accounted for in the seepage abstraction because of significant uncertainties related to these estimates. While the resulting disagreement between the process model results and the seepage abstraction cannot be exactly quantified because of the qualitative nature of the THC predictions with respect to seepage, the abstraction method is conservative.

Items 1 through 4 above demonstrate that the seepage abstraction is reasonably consistent with the respective process model results and conservative where they differ.

The validation activities conducted during and after development of the seepage abstraction provide confidence into the suggested abstraction methodology. The validation criteria defined in the TWP (BSC 2002 [160819], Attachment I, Section I-4-3-1) have been met. No further activities are needed to complete the validation of the seepage abstraction model for its intended use.

INTENTIONALLY LEFT BLANK

8. CONCLUSIONS

Seepage into waste emplacement drifts affects the performance of the high-level nuclear waste repository at Yucca Mountain, Nevada. Theoretical analyses, numerical modeling studies, and field experiments have shown that seepage into underground openings excavated in unsaturated formations is smaller than the percolation flux at the given location. This is mainly a result of capillary pressures holding the water in the formation, diverting it around the cavity, and preventing it from entering the drifts. During the first several hundred to thousands of years after waste emplacement at Yucca Mountain, when above-boiling temperatures will develop in the formation as a result of heat generated by the decaying waste, seepage can also be prevented by the vaporization of percolating water.

In this Model Report, an abstraction model was developed for evaluating the future amount and distribution of seepage into the waste emplacement drifts at Yucca Mountain. The purpose of this abstraction is to provide the necessary methodology, parameters, and simplifications to the TSPA-LA, so that probabilistic seepage calculations can be conducted within the TSPA simulation loops. These probabilistic calculations provide estimates of seepage rates and the seepage fraction averaged over drifts segments for given TSPA simulation time steps; they are not expected to predict individual seepage events or the precise spatial seepage distribution along the drifts and within the repository.

The seepage abstraction is based on several input sources such as drift-scale and site-scale process models as well as *in situ* testing in the unsaturated zone at Yucca Mountain. This Model Report evaluates the respective input sources, analyzes relevant results, and discusses the related uncertainties (Section 6.4). On this basis, the abstraction input is then synthesized, integrated, and simplified into a form that can be used in the TSPA-LA. All relevant uncertainties are characterized and propagated through the abstraction. A short summary of the treatment of natural variability and uncertainty in the abstraction is given in Section 6.7.2. All the NRC acceptance criteria listed in Section 4.2 are adequately addressed in Section 6.

The proposed abstraction methodology is explained in detail in Section 6.5 of this Model Report. It is recognized that the amount of seepage is sensitive to key hydrological properties that are both spatially variable and uncertain. For ambient seepage, these key hydrological properties are the capillary-strength parameter, the permeability, and the local percolation flux. One of the main tasks of this seepage abstraction model is to define appropriate probability distributions that represent the spatial variability and uncertainty inherent in these parameters in a cautiously realistic manner. Section 6.6 explains the data evaluation methodology and provides the resulting parameter distributions separately for spatial variability and uncertainty. All relevant sources of data uncertainty have been identified, described, and accounted for in this process, potentially stemming from measurement uncertainty, conceptual model uncertainty, estimation uncertainty, and spatial variability uncertainty.

Based on these parameter distributions, ambient seepage can be derived in a random process using predictive seepage simulations from the SMPA (Section 6.5.1). The SMPA results are given in the form of seepage look-up tables (DTN: LB0304SMDCREV2.002 [163687]) that provide seepage results as a function of the seepage-relevant parameters. For a particular set of

these parameters, randomly sampled from the respective distributions, the mean seepage rate and its inherent estimation uncertainty, expressed by the standard deviation over the 20 realizations conducted, are linearly interpolated between the table values. The standard deviation is used to define a uniform uncertainty distribution. A seepage uncertainty value is then randomly sampled from this distribution and used to adjust the mean seepage values, giving the final ambient seepage rate for the considered parameter set. Conducting this procedure over a large number of random parameter sets results in the final distribution of ambient seepage.

It is possible that the initially circular-shaped drifts degrade with time as a result of rock fatigue or seismic events. Based on the SMPA modeling results, the impact of drift degradation is accounted for by using separate look-up tables for non-degraded and collapsed drifts. TSPA will select the appropriate look-up table depending on the considered geologic unit, the selected nominal or disruptive scenario, and the assumed rock strength reduction case. This selection is based on categories of drift degradation that have been introduced in Section 6.5.1.5, based on results from BSC (2003 [162711]). Category 1 comprises degraded drifts that may show local rock breakout but stay essentially intact. In this category, seepage is interpolated from the look-up table for non-degraded drifts. Category 1 includes all drifts located in nonlithophysal rock, and, for drifts located in lithophysal rock, the nominal scenario, the 5×10^{-4} seismic hazard case, and the 0% through 40% strength reduction cases. Category 2 comprises the cases with complete drift collapse. These are the 1×10^{-6} and the 1×10^{-7} seismic hazard levels and the 60% through 100% strength reduction cases for lithophysal rock units. In this category, seepage is interpolated from the look-up table for collapsed drifts. Note that three alternative abstraction methods are proposed for igneous events (see Section 6.5.1.7). In view of the significant uncertainty about the in-drift conditions after an igneous event, it is recommended that TSPA conduct sensitivity analyses with the three abstraction methods. The more conservative seepage estimates should be chosen and propagated to the downstream TSPA modules.

Since the SMPA look-up tables account for seepage at ambient and somewhat idealized conditions, the impact of additional factors affecting seepage needs to be evaluated in a second step (Section 6.5.2). These factors include the ground support with rock bolts, the expected transient changes in hydrological properties as a result of THM and THC effects, and the thermal perturbation of the flow field as a result of boiling in the rock. The method proposed in this abstraction is to account for these factors in a simplified form, using the ambient seepage results as a basis and adjusting them as suggested by the relative importance of each factor. To incorporate uncertainty, the simplifications made in this process are usually conservative, yet strive to be as realistic as possible. Conservatism means that the simplified abstractions tend to overestimate seepage compared to the predicted process model results.

The impact of rock bolts as well as THM and THC parameter alterations can be neglected in the abstraction, as demonstrated by the drift-scale process models simulating these processes. Two alternative abstraction models are proposed for seepage during the period of strong thermal perturbation at Yucca Mountain. The first model is very simple; it does not take credit for the vaporization barrier that prevents seepage at above-boiling rock temperatures. The second abstraction model is more realistic (less conservative), but requires more complex implementation into the TSPA-LA. In this model, thermal seepage is set to zero for the period of above-boiling rock temperatures in the drift vicinity. The decision on which one of the two models should be used will be made during the TSPA process.

For illustration of the expected seepage behavior in the repository, a probabilistic seepage calculation was conducted within this Model Report following the proposed abstraction method (Section 6.8). Summary results indicate the importance of the natural barrier formed by the unsaturated rock at and above the repository horizon. For drifts located in the main geological unit in the repository (Tptpll) and assuming the most probable climate scenario, the mean seepage percentage is about 8% during the "wet" glacial transition climate, when most seepage is expected. This means that on average, more than about 92% of the percolating water is diverted around the emplacement drifts. The calculation procedure was also applied to understand the impact of certain abstraction choices by analysis of various sensitivity cases. Note that the calculation results are not directly utilized in the performance assessment, because the seepage component in the TSPA simulations will conduct a similar seepage calculation embedded in the Monte Carlo simulation procedure.

The use of the results presented in this Model Report is restricted to a probabilistic TSPA simulation that follows the methodology outlined in Section 6.6, summarized in Section 6.7, and demonstrated in Section 6.8. Specifically, the distributions of seepage-relevant parameters developed in this Model Report can only be used for seepage evaluations if combined with look-up tables that were generated based on a consistent conceptual model (such as the SMPA). Furthermore, the use of the seepage abstraction model is limited to the conditions considered and described in the upstream process models (see Figure 1-1).

A short roadmap of the proposed abstraction methodology is given in Section 6.7.1. This roadmap can be directly followed by the TSPA-LA seepage calculations. The relevant content of Section 6.7.1 was submitted to the TDMS under DTN: LB0308AMRU0120.001. This DTN also comprises several statistical calculations needed for evaluating parameter distributions. Another DTN: LB0308AMRU0120.002 includes the probabilistic seepage calculations conducted in Section 6.8. For the purposes of traceability and reproducibility, all files submitted to the TDMS are described in detail in Attachments I to V. All file dates and file sizes can be obtained from the TDMS.

INTENTIONALLY LEFT BLANK

9. INPUTS AND REFERENCES

The following is a list of the references cited in this document. Column 1 represents the unique six digit numerical identifier (the Document Input Reference System [DIRS] number), which is placed in the text following the reference callout (e.g., BSC 2002 [160819]). The purpose of these numbers is to assist the reader in locating a specific reference. Within the reference list, multiple sources by the same author (e.g., BSC 2002) are sorted alphabetically by title.

9.1 DOCUMENTS CITED

163686 Birkholzer, J. 2003. "Penetration of Liquid Fingers into Superheated Fractured Rock." *Water Resources Research, 39*, (4), SBH 9-1 to SBH 9-21. [Washington, D.C.]: American Geophysical Union. TIC: 254362.

105170 Birkholzer, J.; Li, G.; Tsang, C-F.; and Tsang, Y. 1999. "Modeling Studies and Analysis of Seepage into Drifts at Yucca Mountain." *Journal of Contaminant Hydrology, 38*, (1-3), 349-384. New York, New York: Elsevier. TIC: 244160.

164526 Birkholzer, J.T. 2003. YMP-LBNL-JTB-2 Unsaturated Zone Synthesis & Modeling - Abstraction of Drift Seepage. Scientific Notebook SN-LBNL-SCI-231-V1. ACC: MOL.20030728.0385.

164525 Birkholzer, J.T. 2003. YMP-LBNL-JTB-3 Unsaturated Zone Synthesis & Modeling - Abstraction of Drift Seepage. Scientific Notebook SN-LBNL-SCI-231-V2. ACC: MOL.20030728.0383.

154608 Birkholzer, J.T. and Tsang, Y.W. 2000. "Modeling the Thermal-Hydrologic Processes in a Large-Scale Underground Heater Test in Partially Saturated Fractured Tuff." *Water Resources Research, 36*, (6), 1431-1447. Washington, D.C.: American Geophysical Union. TIC: 248278.

120055 Bodvarsson, G.S.; Boyle, W.; Patterson, R.; and Williams, D. 1999. "Overview of Scientific Investigations at Yucca Mountain—The Potential Repository for High-Level Nuclear Waste." *Journal of Contaminant Hydrology, 38*, (1-3), 3-24. New York, New York: Elsevier. TIC: 244160.

163443 Bodvarsson, G.S.; Wu, Y-S.; and Zhang, K. 2003. "Development of Discrete Flow Paths in Unsaturated Fractures at Yucca Mountain." *Journal of Contaminant Hydrology, 62-63*, 23-42. New York, New York: Elsevier. TIC: 254205.

156304 BSC (Bechtel SAIC Company) 2001. *Drift Degradation Analysis*. ANL-EBS-MD-000027 REV 01 ICN 01. Las Vegas, Nevada: Bechtel SAIC Company. ACC: MOL.20011029.0311.

155950 BSC (Bechtel SAIC Company) 2001. *FY 01 Supplemental Science and Performance Analyses, Volume 1: Scientific Bases and Analyses*. TDR-MGR-MD-000007 REV

00 ICN 01. Las Vegas, Nevada: Bechtel SAIC Company. ACC: MOL.20010801.0404; MOL.20010712.0062; MOL.20010815.0001.

154659 BSC (Bechtel SAIC Company) 2001. *FY01 Supplemental Science and Performance Analyses, Volume 2: Performance Analyses*. TDR-MGR-PA-000001 REV 00. Las Vegas, Nevada: Bechtel SAIC Company. ACC: MOL.20010724.0110.

155187 BSC (Bechtel SAIC Company) 2001. *Ground Control for Emplacement Drifts for SR*. ANL-EBS-GE-000002 REV 00 ICN 01. Las Vegas, Nevada: Bechtel SAIC Company. ACC: MOL.20010627.0028.

158463 BSC (Bechtel SAIC Company) 2001. *In Situ Field Testing of Processes*. ANL-NBS-HS-000005 REV 01. Las Vegas, Nevada: Bechtel SAIC Company. ACC: MOL.20020108.0351.

158204 BSC (Bechtel SAIC Company) 2001. *Multiscale Thermohydrologic Model*. ANL-EBS-MD-000049 REV 00 ICN 02. Las Vegas, Nevada: Bechtel SAIC Company. ACC: MOL.20020123.0279.

156609 BSC (Bechtel SAIC Company) 2001. *Unsaturated Zone Flow Patterns and Analysis*. MDL-NBS-HS-000012 REV 00. Las Vegas, Nevada: Bechtel SAIC Company. ACC: MOL.20011029.0315.

159124 BSC (Bechtel SAIC Company) 2002. *Geologic Framework Model (GFM2000)*. MDL-NBS-GS-000002 REV 01. Las Vegas, Nevada: Bechtel SAIC Company. ACC: MOL.20020530.0078.

158794 BSC (Bechtel SAIC Company) 2002. *Guidelines for Developing and Documenting Alternative Conceptual Models, Model Abstractions, and Parameter Uncertainty in the Total System Performance Assessment for the License Application*. TDR-WIS-PA-000008 REV 00, ICN 01. Las Vegas, Nevada: Bechtel SAIC Company. ACC: MOL.20020904.0002.

160405 BSC (Bechtel SAIC Company) 2002. *Natural Analogue Synthesis Report*. TDR-NBS-GS-000027 REV 00 ICN 02. Las Vegas, Nevada: Bechtel SAIC Company. ACC: MOL.20020520.0288.

160780 BSC (Bechtel SAIC Company) 2002. *Risk Information to Support Prioritization of Performance Assessment Model*s. TDR-WIS-PA-000009 REV 01 ICN 01. Las Vegas, Nevada: Bechtel SAIC Company. ACC: MOL.20021017.0045.

160819 BSC (Bechtel SAIC Company) 2002. *Technical Work Plan for: Performance Assessment Unsaturated Zone*. TWP-NBS-HS-000003 REV 02. Las Vegas, Nevada: Bechtel SAIC Company. ACC: MOL.20030102.0108.

160319 BSC (Bechtel SAIC Company) 2002. *Thermal Conductivity of the Potential Repository Horizon Model Report.* MDL-NBS-GS-000005 REV 00. Las Vegas, Nevada: Bechtel SAIC Company. ACC: MOL.20020923.0167.

160771 BSC (Bechtel SAIC Company) 2002. *Thermal Testing Measurements Report*. ANL-NBS-HS-000041 REV 00. Las Vegas, Nevada: Bechtel SAIC Company. ACC: MOL.20021004.0314.

160146 BSC (Bechtel SAIC Company) 2002. *Total System Performance Assessment-License Application Methods and Approach*. TDR-WIS-PA-000006 REV 00. Las Vegas, Nevada: Bechtel SAIC Company. ACC: MOL.20020923.0175.

161773 BSC (Bechtel SAIC Company) 2003. *Analysis of Hydrologic Properties Data*. MDL-NBS-HS-000014 REV 00. Las Vegas, Nevada: Bechtel SAIC Company. ACC: DOC.20030404.0004.

163740 BSC (Bechtel SAIC Company) 2003. *Analysis of Infiltration Uncertainty*. ANL-NBS-HS-000027 REV 01D. Las Vegas, Nevada: Bechtel SAIC Company. ACC: MOL.20030807.0339.

160240 BSC (Bechtel SAIC Company) 2003. *Calibrated Properties Model*. MDL-NBS-HS-000003 REV 01. Las Vegas, Nevada: Bechtel SAIC Company. ACC: DOC.20030219.0001.

160109 BSC (Bechtel SAIC Company) 2003. *Development of Numerical Grids for UZ Flow and Transport Modeling*. ANL-NBS-HS-000015 REV 01. Las Vegas, Nevada: Bechtel SAIC Company. ACC: DOC.20030404.0005.

161839 BSC (Bechtel SAIC Company) 2003. *Dike/Drift Interactions*. MDL-MGR-GS-000005 REV 00A. Las Vegas, Nevada: Bechtel SAIC Company. ACC: MOL.20030711.0105.

162711 BSC (Bechtel SAIC Company) 2003. *Drift Degradation Analysis*. ANL-EBS-MD-000027 REV 02. Las Vegas, Nevada: Bechtel SAIC Company. ACC: DOC.20030709.0003.

162318 BSC (Bechtel SAIC Company) 2003. *Drift Scale THM Model*. MDL-NBS-HS-000017 REV 00. Las Vegas, Nevada: Bechtel SAIC Company. ACC: DOC.20030818.0003.

161530 BSC (Bechtel SAIC Company) 2003. *Drift-Scale Coupled Processes (DST and TH Seepage) Models*. MDL-NBS-HS-000015 REV 00. Las Vegas, Nevada: Bechtel SAIC Company. URN-1087

162050 BSC (Bechtel SAIC Company) 2003. *Drift-Scale Coupled Processes (DST and THC Seepage) Models*. MDL-NBS-HS-000001 REV 02. Las Vegas, Nevada: Bechtel SAIC Company. ACC: DOC.20030804.0004.

163938 BSC (Bechtel SAIC Company) 2003. *Drift-Scale Radionuclide Transport*. MDL-NBS-HS-000016 REV 00C. Las Vegas, Nevada: Bechtel SAIC Company. ACC: MOL.20030804.0205.

164603 BSC (Bechtel SAIC Company) 2003. *Repository Design Project, RDP/PA IED Typical Waste Package Components Assembly 1 of 9*. 800-IED-WIS0-00201-000-00B. Las Vegas, Nevada: Bechtel SAIC Company. ACC: ENG.20030808.0004.

164101 BSC (Bechtel SAIC Company) 2003. *Repository Design Project, Repository/PA IED Emplacement Drift Committed Materials (2)*. 800-IED-WIS0-00302-000-00A. Las Vegas, Nevada: Bechtel SAIC Company. ACC: ENG.20030627.0004.

164069 BSC (Bechtel SAIC Company) 2003. *Repository Design Project, Repository/PA IED Emplacement Drift Configuration 1 of 2*. 800-IED-EBS0-00201-000-00A. Las Vegas, Nevada: Bechtel SAIC Company. ACC: ENG.20030630.0002.

162289 BSC (Bechtel SAIC Company) 2003. *Repository Design, Repository/PA IED Subsurface Facilities*. 800-IED-EBS0-00401-000-00C. Las Vegas, Nevada: Bechtel SAIC Company. ACC: ENG.20030303.0002.

162267 BSC (Bechtel SAIC Company) 2003. *Seepage Calibration Model and Seepage Testing Data*. MDL-NBS-HS-000004 REV 02. Las Vegas, Nevada: Bechtel SAIC Company. ACC: DOC.20030408.0004.

163226 BSC (Bechtel SAIC Company) 2003. *Seepage Model for PA Including Drift Collapse*. MDL-NBS-HS-000002 REV 02. Las Vegas, Nevada: Bechtel SAIC Company. ACC: DOC.20030709.0001.

164325 BSC (Bechtel SAIC Company) 2003. *Underground Layout Configuration*. 800-P0C-MGR0-00100-000-00D. Las Vegas, Nevada: Bechtel SAIC Company. ACC: ENG.20030716.0002.

163045 BSC (Bechtel SAIC Company) 2003. *UZ Flow Models and Submodels*. MDL-NBS-HS-000006 REV 01. Las Vegas, Nevada: Bechtel SAIC Company. ACC: DOC.20030818.0002.

161770 Canori, G.F. and Leitner, M.M. 2003. *Project Requirements Document*. TER-MGR-MD-000001 REV 01. Las Vegas, Nevada: Bechtel SAIC Company. ACC: DOC.20030404.0003.

124052 CRWMS M&O (Civilian Radioactive Waste Management System Management and Operating Contractor) 1997. *The Site-Scale Unsaturated Zone Transport Model of*

Yucca Mountain. Milestone SP25BM3, Rev. 1. Las Vegas, Nevada: CRWMS M&O. ACC: MOL.19980224.0314.

143244 CRWMS M&O 2000. *Analysis of Infiltration Uncertainty*. ANL-NBS-HS-000027 REV 00. Las Vegas, Nevada: CRWMS M&O. ACC: MOL.20000525.0377.

100356 CRWMS M&O 1998. "Unsaturated Zone Hydrology Model." Chapter 2 of *Total System Performance Assessment-Viability Assessment (TSPA-VA) Analyses Technical Basis Document*. B00000000-01717-4301-00002 REV 01. Las Vegas, Nevada: CRWMS M&O. ACC: MOL.19981008.0002.

144426 CRWMS M&O 2000. *Calibrated Properties Model*. MDL-NBS-HS-000003 REV 00. Las Vegas, Nevada: CRWMS M&O. ACC: MOL.19990721.0520.

141187 CRWMS M&O 2000. *Conceptual and Numerical Models for UZ Flow and Transport*. MDL-NBS-HS-000005 REV 00. Las Vegas, Nevada: CRWMS M&O. ACC: MOL.19990721.0526.

152286 CRWMS M&O 2000. *Fracture Geometry Analysis for the Stratigraphic Units of the Repository Host Horizon*. ANL-EBS-GE-000006 REV 00. Las Vegas, Nevada: CRWMS M&O. ACC: MOL.20000918.0286.

148384 CRWMS M&O 2000. *Total System Performance Assessment (TSPA) Model for Site Recommendation*. MDL-WIS-PA-000002 REV 00. Las Vegas, Nevada: CRWMS M&O. ACC: MOL.20001226.0003.

153246 CRWMS M&O 2000. *Total System Performance Assessment for the Site Recommendation*. TDR-WIS-PA-000001 REV 00 ICN 01. Las Vegas, Nevada: CRWMS M&O. ACC: MOL.20001220.0045.

151940 CRWMS M&O 2000. *Unsaturated Zone Flow and Transport Model Process Model Report*. TDR-NBS-HS-000002 REV 00 ICN 02. Las Vegas, Nevada: CRWMS M&O. ACC: MOL.20000831.0280.

151945 CRWMS M&O 2000. *Yucca Mountain Site Description*. TDR-CRW-GS-000001 REV 01 ICN 01. Las Vegas, Nevada: CRWMS M&O. ACC: MOL.20001003.0111.

154291 CRWMS M&O 2001. *Abstraction of Drift Seepage*. ANL-NBS-MD-000005 REV 01. Las Vegas, Nevada: CRWMS M&O. ACC: MOL.20010309.0019.

135997 Doughty, C. 1999. "Investigation of Conceptual and Numerical Approaches for Evaluating Moisture, Gas, Chemical, and Heat Transport in Fractured Unsaturated Rock." *Journal of Contaminant Hydrology*, *38*, (1-3), 69-106. New York, New York: Elsevier. TIC: 244160.

100145 Fabryka-Martin, J.T.; Wolfsberg, A.V.; Dixon, P.R.; Levy, S.S.; Musgrave, J.A.; and Turin, H.J. 1997. *Summary Report of Chlorine-36 Studies: Sampling, Analysis, and Simulation of Chlorine-36 in the Exploratory Studies Facility*. LA-13352-MS. Los Alamos, New Mexico: Los Alamos National Laboratory. ACC: MOL.19980812.0254.

151875 Finsterle, S. 2000. "Using the Continuum Approach to Model Unsaturated Flow in Fractured Rock." *Water Resources Research, 36*, (8), 2055-2066. [Washington, D.C.]: American Geophysical Union. TIC: 248769.

154365 Freeze, G.A.; Brodsky, N.S.; and Swift, P.N. 2001. *The Development of Information Catalogued in REV00 of the YMP FEP Database*. TDR-WIS-MD-000003 REV 00 ICN 01. Las Vegas, Nevada: Bechtel SAIC Company. ACC: MOL.20010301.0237.

101700 LeCain, G.D. 1995. *Pneumatic Testing in 45-Degree-Inclined Boreholes in Ash-Flow Tuff Near Superior, Arizona*. Water-Resources Investigations Report 95-4073. Denver, Colorado: U.S. Geological Survey. ACC: MOL.19960715.0083.

105729 Liu, H.H.; Doughty, C.; and Bodvarsson, G.S. 1998. "An Active Fracture Model for Unsaturated Flow and Transport in Fractured Rocks." *Water Resources Research, 34*, (10), 2633-2646. Washington, D.C.: American Geophysical Union. TIC: 243012.

163603 Mishra, S. 2002. *Assigning Probability Distributions to Input Parameters of Performance Assessment Models*. SKB TR-02-11. Stockholm, Sweden: Svensk Kärnbränsleförsörjning A.B. TIC: 252794.

149850 Mongano, G.S.; Singleton, W.L.; Moyer, T.C.; Beason, S.C.; Eatman, G.L.W.; Albin, A.L.; and Lung, R.C. 1999. *Geology of the ECRB Cross Drift - Exploratory Studies Facility, Yucca Mountain Project, Yucca Mountain, Nevada*. [Deliverable SPG42GM3]. Denver, Colorado: U.S. Geological Survey. ACC: MOL.20000324.0614.

105731 Neuman, S.P. 1994. "Generalized Scaling of Permeabilities: Validation and Effect of Support Scale." *Geophysical Research Letters, 21*, (5), 349-352. Washington, D.C.: American Geophysical Union. TIC: 240142.

163274 NRC (U.S. Nuclear Regulatory Commission) 2003. *Yucca Mountain Review Plan, Final Report*. NUREG-1804, Rev. 2. Washington, D.C.: U.S. Nuclear Regulatory Commission, Office of Nuclear Material Safety and Safeguards. TIC: 254568.

144773 Or, D. and Ghezzehei, T.A. 2000. "Dripping into Subterranean Cavities from Unsaturated Fractures under Evaporative Conditions." *Water Resources Research, 36*, (2), 381-393. Washington, D.C.: American Geophysical Union. TIC: 246982.

105736 Paleologos, E.K.; Neuman, S.P.; and Tartakovsky, D. 1996. "Effective Hydraulic Conductivity of Bounded, Strongly Heterogeneous Porous Media." *Water Resources Research, 32*, (5), 1333-1341. Washington, D.C.: American Geophysical Union. TIC: 245760.

105743 Philip, J.R.; Knight, J.H.; and Waechter, R.T. 1989. "Unsaturated Seepage and Subterranean Holes: Conspectus, and Exclusion Problem for Circular Cylindrical Cavities." *Water Resources Research, 25*, (1), 16-28. Washington, D.C.: American Geophysical Union. TIC: 239117.

100819 Pruess, K.; Wang, J.S.Y.; and Tsang, Y.W. 1990. "On Thermohydrologic Conditions Near High-Level Nuclear Wastes Emplaced in Partially Saturated Fractured Tuff, 2. Effective Continuum Approximation." *Water Resources Research, 26*, (6), 1249-1261. [Washington, D.C.]: American Geophysical Union. TIC: 224854.

158378 USGS (U.S. Geological Survey) 2001. *Future Climate Analysis*. ANL-NBS-GS-000008 REV 00 ICN 01. Denver, Colorado: U.S. Geological Survey. ACC: MOL.20011107.0004.

160355 USGS (U.S. Geological Survey) 2001. *Simulation of Net Infiltration for Modern and Potential Future Climates*. ANL-NBS-HS-000032 REV 00 ICN 02. Denver, Colorado: U.S. Geological Survey. ACC: MOL.20011119.0334.

163702 Wang, J.S. 2003. "Scientific Notebooks Referenced in Model Report U0120, Abstraction of Drift Seepage, MDL-NBS-HS-000019 REV 00." Correspondence from J.S. Wang (BSC) to File, August 18, 2003, with attachments. ACC: MOL.20030818.0371.

104366 Wang, J.S.Y. and Elsworth, D. 1999. "Permeability Changes Induced by Excavation in Fractured Tuff." *Rock Mechanics for Industry, Proceedings of the 37th U.S. Rock Mechanics Symposium, Vail, Colorado, USA, 6-9 June 1999*. Amadei, B.; Kranz, R.L.; Scott, G.A.; and Smeallie, P.H., eds. *2*, 751-757. Brookfield, Vermont: A.A. Balkema. TIC: 245246.

101309 Wang, J.S.Y.; Flint, A.L.; Nitao, J.J.; Chesnut, D.A.; Cook, P.; Cook, N.G.W.; Birkholzer, J.; Freifeld, B.; Flint, L.E.; Ellet, K.; Mitchell, A.J.; Homuth, E.F.; Griego, G.J.; Cerny, J.A.; and Johnson, C.L. 1996. *Evaluation of Moisture Evolution in the Exploratory Studies Facility*. Milestone TR31K6M. Berkeley, California: Lawrence Berkeley National Laboratory. ACC: MOL.19961231.0089.

160442 Whelan, J.F.; Paces, J.B.; and Peterman, Z.E. 2002. "Physical and Stable-Isotope Evidence for Formation of Secondary Calcite and Silica in the Unsaturated Zone, Yucca Mountain, Nevada." *Applied Geochemistry, 17*, ([6]), 735-750. [New York, New York]: Elsevier. TIC: 253462.

164334 Williams, H. and McBirney, A.R. 1979. *Volcanology*. San Francisco, California: Freeman, Cooper, and Company. TIC: 254575.

161058 Wu, Y-S.; Zhang, W.; Pan, L.; Hinds, J.; and Bodvarsson, G.S. 2002. "Modeling Capillary Barriers in Unsaturated Fractured Rock." *Water Resources Research, 38*, (11), 35-1 through 35-12. [Washington, D.C.]: American Geophysical Union. TIC: 253854.

Software Cited

154783 LBNL (Lawrence Berkeley National Laboratory) 2001. *Software Code: FLAC3D*. V2.0. PC. STN: 10502-2.0-00.

161491 LBNL (Lawrence Berkeley National Laboratory) 2003. *Software Code: TOUGH2*. V1.6. PC/MS-DOS under Windows 98, Sun UltraSparc OS 5.5.1, DEC-Alpha OSF1 V4.0. 10007-1.6-01.

9.2 CODES, STANDARDS, REGULATIONS, AND PROCEDURES

156605 10 CFR 63. Energy: Disposal of High-Level Radioactive Wastes in a Geologic Repository at Yucca Mountain, Nevada. Readily available.

AP-2.22Q, Rev. 1. *Analyses and Maintenance of the Q-List.* Washington, D.C.: U.S. Department of Energy, Office of Civilian Radioactive Waste Management. ACC: DOC.20030807.0002.

AP-SI.1Q, Rev. 05, ICN 01. *Software Management*. Washington, D.C.: U.S. Department of Energy, Office of Civilian Radioactive Waste Management. ACC: DOC.20030708.0001.

AP-SIII.10Q, Rev. 1, ICN 2. *Models*. Washington, D.C.: U.S. Department of Energy, Office of Civilian Radioactive Waste Management. ACC: DOC.20030627.0003.

AP-SV.1Q, Rev. 0, ICN 3. *Control of the Electronic Management of Information*. Washington, D.C.: U.S. Department of Energy, Office of Civilian Radioactive Waste Management. ACC: MOL.20020917.0133.

YMP-LBNL-QIP-SV.0, Rev. 2, Mod. 1. *Management of YMP-LBNL Electronic Data*. Berkeley, California: Lawrence Berkeley National Laboratory. ACC: MOL.20020717.0319.

9.3 SOURCE DATA, LISTED BY DATA TRACKING NUMBER

105574 GS960908312232.013. Air-Injection Testing in Vertical Boreholes in Welded and Non-Welded Tuff, Yucca Mountain, Nevada. Submittal date: 09/26/1996.

153155 LB0011AIRKTEST.001. Air Permeability Testing in Niches 3566 and 3650. Submittal date: 11/08/2000.

154586 LB0012AIRKTEST.001. Niche 5 Air K Testing 3/23/00-4/3/00. Submittal date: 12/21/2000.

163906 LB0104AMRU0185.012. Section 6.4.2 Focusing and Discrete Flow Paths in the TSW - Data Summary. Submittal date: 05/15/2001.

163689 LB0301DSCPTHSM.002. Drift-Scale Coupled Process Model for Thermohydrologic Seepage: Data Summary. Submittal date: 01/29/2003.

162277 LB0302PTNTSW9I.001. PTN/TSW Interface Percolation Flux Maps for 9 Infiltration Scenarios. Submittal date: 02/28/2003.

162273 LB0302SCMREV02.002. Seepage-Related Model Parameters K and 1/A: Data Summary. Submittal date: 02/28/2003.

163047 LB03033DSSFF9I.001. 3-D Site Scale UZ FLow Fields for 9 Infiltration Scenarios: Simulations Using Alternative Hydraulic Properties. Submittal date: 03/28/2003.

163688 LB0303DSCPTHSM.001. Drift-Scale Coupled Process Model for Thermohydrologic Seepage: Simulation Files. Submittal date: 03/20/2003.

163687 LB0304SMDCREV2.002. Seepage Modeling for Performance Assessment, Including Drift Collapse: Summary Plot Files and Tables. Submittal date: 04/11/2003.

163691 LB0304SMDCREV2.004. Impact of Thermal-Hydrologic-Mechanical Effects on Seepage: Summary Plot Files and Tables. Submittal date: 04/23/2003.

163690 LB0305PTNTSW9I.001. PTN/TSW Interface Percolation Flux Maps for 9 Alternative Infiltration Scenarios. Submittal date: 05/12/2003.

164337 LB0307SEEPDRCL.002. Seepage Into Collapsed Drift: Data Summary. Submittal date: 07/21/2003.

136593 LB980901233124.101. Pneumatic Pressure and Air Permeability Data from Niche 3107 and Niche 4788 in the ESF from Chapter 2 of Report SP33PBM4: Fracture Flow and Seepage Testing in the ESF, FY98. Submittal date: 11/23/1999.

123273 LB990901233124.004. Air Permeability Cross-Hole Connectivity in Alcove 6, Alcove 4, and Niche 4 of the ESF for AMR U0015, “In Situ Testing of Field Processes”. Submittal date: 11/01/1999.

161496 MO0301SEPFEPS1.000. LA FEP List. Submittal date: 01/21/2003.

164736 MO0306MWDDPPDR.000. Drift Profile Prediction and Degraded Rock Mass Characteristics. Submittal date: 06/18/2003.

9.4 OUTPUT DATA, LISTED BY DATA TRACKING NUMBER

LB0308AMRU0120.001. Supporting Calculations and Analysis for Seepage Abstraction and Summary of Abstraction Results. Submittal date: 07/17/2003.

LB0308AMRU0120.002. Mathcad 11 Spreadsheets for Probabilistic Seepage Evaluation. Submittal date: 07/17/2003.

ATTACHMENT I—HISTOGRAMS OF SMPA REALIZATION RESULTS

Histograms of SMPA realization results were analyzed in Section 6.4.2.3 (Figure 6.4-7). A *Mathcad 11* spreadsheet was used to read the SMPA look-up table results for the non-degraded drift and calculate the seepage histograms for selected cases. The following procedure was followed to conduct the analysis (see also Scientific Notebook, Birkholzer 2003 [164525], pp. 20–25):

1. Copy file Fig6-3toFig6-8.xls from DTN: LB0304SMDCREV2.002 [163687] into appropriate working directory

2. Open a new Excel file named ResponseSurfaceSMPA_all_realizations_selected.xls, with three different Worksheets "-12 and 500","-12 and 100","-12 and 1000"

3. Choose three parameter cases in k and $1/\alpha$, representing SMPA results with average, large and small seepage (Case 1: k = -12, $1/\alpha$ = 500 Pa, Case 2: k = -12, $1/\alpha$ = 1,00 Pa, Case 3: k = -12, $1/\alpha$ = 1,000 Pa)

4. Copy SMPA results for each selected case from Fig6-3toFig6-8.xls into ResponseSurfaceSMPA_all_realizations_selected.xls. For each case, copy the full line of all percolation rates included in the look-up table. Copy all lines for Case1 into Worksheet "-12 and 500", all lines for Case 2 into Worksheet "-12 and 100", and all lines for Case 3 into Worksheet "-12 and 1000".

5. Delete the first seven columns in each Worksheet, so that only the 20 columns for each realization are left in the Excel file.

6. Use *Mathcad 11* spreadsheet histogram_seepage_uncertainty.mcd to calculate and display the seepage histograms over the 20 realizations. The calculation reads the Excel file ResponseSurfaceSMPA_all_realizations_selected.xls. It then calculates and displays histograms for each case, choosing four percolation fluxes (50 mm/yr, 200 mm/yr, 500 mm/yr, and 1000 mm/yr). The resulting histograms can be evaluated.

ResponseSurfaceSMPA_all_realizations_selected.xls and histogram_seepage_uncertainty.mcd are in Output-DTN: LB0308AMRU0120.001 (Directory: seepage_uncertainty_evaluation).

INTENTIONALLY LEFT BLANK

ATTACHMENT II—STATISTICAL ANALYSIS OF CAPILLARY-STRENGTH PARAMETER VALUES

The calibrated capillary-strength parameters from the SCM were statistically analyzed in Section 6.6.1.2 (see also Scientific Notebook, Birkholzer 2003 [164526], pp. 59–65, 118–127). The analysis was conducted with a *Microsoft Excel 97 SR-2* calculation. The capillary-strength parameters are provided in DTN: LB0302SCMREV02.002 [162273]. The DTN gives six calibrated capillary-strength parameter values in the Tptpll unit, available at two locations (Niche 1620 and systematic testing borehole in the ECRB), and four parameter values in the Tptpmn unit, available at two locations (Niche 3107 and Niche 4788). The statistical parameters calculated are the mean μ, the standard deviation σ and the mean error SE—an estimate for the uncertainty in the mean value caused by a limited number of measurements. Four different methods of deriving these statistical parameters are chosen to support the above approach. These methods are as follows:

A. Derive mean and standard deviation from all ten samples in both units

B. Calculate average values from multiple tests in one location, then derive mean and standard deviation from the resulting four samples in both units

C. Derive mean and standard deviation separately for geological units, from six samples in the Tptpll and four samples in the Tptpmn

D. Calculate average values from multiple tests in one location, then derive mean and standard deviation separately for each geological unit

Excel spreadsheet capillary_strength_variability_analysis.xls conducts the calculation. Methods A and B are included in Worksheet “both units”. Methods C and D are included in Worksheets “tptpm” and “tptpl”, separately for the two units. The Excel spreadsheet is provided in Output-DTN: LB0308AMRU0120.001 (Directory: capillary_strength_analysis). The results support Table 6.6-2 of this Model Report.

INTENTIONALLY LEFT BLANK

ATTACHMENT III—STATISTICAL ANALYSIS OF PERMEABILITY VALUES

Permeability values measured in air-injection testing were statistically analyzed in Section 6.6.2.2 (see also Scientific Notebooks, Birkholzer 2003 [164526], pp. 42–58, 128–132; Birkholzer 2003 [164525], pp. 69–70). The analyses were conducted with *Microsoft Excel 97 SR-2* calculations. The Excel spreadsheets used for the different calculations are provided in Output-DTN: LB0308AMRU0120.001 (Directory: permeability_analysis).

In a first step, permeability values from small-scale injection testing in close vicinity to niches or the ECRB tunnel were analyzed. Except for the systematic testing in the ECRB tunnel, permeability values are available for the conditions prior to and after niche construction (undisturbed versus disturbed). In most cases, summary statistics (mean and standard deviation) of these small-scale measurements had been conducted prior to this seepage abstraction and were available in the TDMS, in DTN: LB0302SCMREV02.002 [162273] (disturbed measurements statistics) and DTN: LB990901233124.004 [123273] (undisturbed measurements statistics). In the case of Niche 1620, summary statistics of the undisturbed small-scale measurements were not available. These were therefore calculated directly from DTN: LB0012AIRKTEST.001 [154586], containing permeability values for all small-scale test intervals. The statistical calculation was conducted in Excel spreadsheet niche_1620_preexcavation.xls. The procedure is as follows:

1. Tables 01048_001 from DTN: LB0012AIRKTEST.001 [154586] was extracted from the TDMS. File zz_sep_278799.zip was copied to an appropriate working directory and unzipped. A text file named zz_sep_278799.txt opens.

2. A new Excel file named niche_1620_preexcavation.xls was generated. The text file zz_sep_278799.txt was opened into Excel, using space and tab delimited options. The last data column contains the permeability values in log10 space. This column was analyzed. From the 208 measurements in this column, stemming from different boreholes, the mean and standard deviation was calculated, also minimum and maximum values were derived.

3. Finally, editorial changes were conducted in Excel file niche_1620_preexcavation.xls. These include adding/changing headers and deleting columns that are not needed.

The statistics derived from niche_1620_preexcavation.xls support Table 6.6-3 of this Model Report. The mean permeability value derived in niche_1620_preexcavation.xls, as well as the other mean values from small-scale permeability measurements as provided in DTN: LB0302SCMREV02.002 [162273] and DTN: LB990901233124.004 [123273], are used then to calculate the intermediate-scale variability over the Yucca Mountain. This calculation is done in Excel spreadsheet permeability_variability_analysis_small_scale.xls. Worksheet “undisturbed” comprises analysis of pre-excavation measurements, for four niches in the Tptpmn and one niche in the Tptpll. Worksheet “disturbed” comprises analyses of post-excavation measurements, from three niches in the Tptpmn and one niche plus and one systematic testing borehole. The statistical parameters calculated are the mean μ, the standard deviation σ and the mean error SE. Worksheet “comparison” analyzes undisturbed versus disturbed permeability values, looking at the changes in the mean values and changes in the standard deviation. The Excel spreadsheet is

provided in Output-DTN: LB0308AMRU0120.001 (Directory: Permeability_Analysis). The results of this support Tables 6.6-4 and 6.6-7 of this Model Report.

In a second step, permeability values from injection testing conducted in surface-based boreholes were analyzed. Measurements from surface-based boreholes, performed at four borehole locations in various units at the Yucca Mountain, are available in DTN: GS960908312232.013 [105574]. The boreholes included in this DTN: are NRG-6, NRG-7a, SD-12, and UZ#16. The relevant units for this Model report are the Tptpll, the Tptpmn, the Tptpul, and the Tptpln. A varying number of injection tests had been conducted in each unit and at each location, depending on the local thickness of the unit and the chosen injection interval length. For further analysis, the mean permeability value of all measurements at each location and each relevant unit was calculated in Excel spreadsheet vertical_boreholes.xls. The procedure was as follows:

1. Table s01163_001 from DTN: GS960908312232.013 [105574] was extracted from the TDMS. File zz_sep_208683.zip was copied to an appropriate working directory and unzipped. A text file named zz_sep_208683.txt opens.

2. A new Excel file named vertical_boreholes.xls was generated. The text file zz_sep_208683.txt was opened into Excel, using space and tab delimited options. The last data column contains the permeability values in log10 space. This column was analyzed. Information on locations and units for each measurement is given in the second column (borehole) and the tenth column (unit). All data lines that do not represent the Tptpll, Tptpmn, Tptpul, and Tptpln units were deleted. This left two units for borehole NRG-6 (Tptpul and Tptpmn), three units at NRG-7a (Tptpul, Tptpmn, and Tptpll), three units at SD-12 (Tptpul, Tptpmn, and Tptpln), and four units at UZ#16 (Tptpul, Tptpmn, Tptpll, and Tptpln). Some measurement intervals intersect two units. In such cases, the measured permeability value was applied to the statistical calculation of both units (i.e. the respective data line was copied and assigned to both units). Then, for each borehole and each unit, the mean and standard deviation was calculated, also minimum and maximum values were derived.

3. Finally, several editorial changes were conducted in Excel file vertical_boreholes.xls.

The mean permeability values derived from vertical_boreholes.xls support Tables 6.6-5, 6.6-8, and 6.6-10 of this Model report. These values are then used to calculate the intermediate-scale variability over the Yucca Mountain. This calculation is done in Excel spreadsheet permeability_variability_analysis_vertical_boreholes.xls. The statistical parameters calculated are the mean μ, the standard deviation σ and the mean error SE, separately for the different units. The results of this calculation support Tables 6.6-5, 6.6-8, and 6.6-10 of this Model Report.

A final calculation analysis was performed in Section 6.6.2.2 in order to evaluate the effect of measurement interval differences between the niche air injection tests (1-foot-intervals) and those conducted in surface-based boreholes (interval lengths between 3.5 and 4.6 m). The mean effective permeability increases with the interval length, so that upscaling laws have to be applied in order to make the permeability values comparable. One of the methods used in Section 6.6.2.2 was to use the 1-foot measurements in the niches and presume that these represent the exact spatial variability along the borehole. The individual permeability values were then divided

into several groups of twelve consecutive 1-foot measurements; i.e., one group represents the length of a 3.6-m interval. The arithmetic mean of the twelve 1-foot values in each group gives the permeability value that would have been measured in a 3.6-m-injection interval. The arithmetic mean values of all groups in one niche location can then be statistically analyzed to evaluate the scaling effects directly from the data.

The upscaling analysis was conducted using the pre-excavation measurements in Niches 1620, 3107, 3566, 3650, and 3566. These data are given in DTN: LB0012AIRKTEST.001 [154586] (Niche 1620), DTN: LB980901233124.101 [136593] (Niches 3107 and 4788), and DTN: LB0011AIRKTEST.001 [153155] (Niches 3650 and 3566), containing permeability values for all small-scale test intervals. The statistical calculation was conducted with different Excel spreadsheets. The procedure was as follows:

Niche 1620:

1. Table s01048_001 from DTN: LB0012AIRKTEST.001 [154586] was extracted from the TDMS. File zz_sep_278799.zip was copied to an appropriate working directory and unzipped. A text file named zz_sep_278799.txt opens.

2. A new Excel file named niche_1620_preexcavation_upscaling.xls was generated. The text file zz_sep_278799.txt was opened into Excel, using space and tab delimited options. The second last data column contains the permeability values in non-logarithmic space. Starting with the first measurement interval, the arithmetic mean of groups of twelve consecutive values was calculated. Four measurement intervals at the end of the data set were disregarded in this analysis since they do not comprise a full group of twelve. The arithmetic mean values were transformed into log10 values. Finally, the arithmetic mean over all log10 values was calculated, giving the upscaled mean permeability value for the Niche 1620 measurements.

3. Finally, editorial changes were conducted in niche_1620_preexcavation_upscaling.xls. These include adding/changing headers and deleting columns that are not needed.

Niche 3107:

1. Table s99469_001 from DTN: LB980901233124.101 [136593] was extracted from the TDMS. File zz_sep_208706.zip was copied to an appropriate working directory and unzipped. A text file named zz_sep_208706.txt opens.

2. A new Excel file named niche_3107_preexcavation_upscaling.xls was generated. The text file zz_sep_208706.txt was opened into Excel, using space and tab delimited options. The last data column contains the permeability values in non-logarithmic space. Starting with the first measurement interval, the arithmetic mean of groups of twelve consecutive values was calculated. Three measurement intervals at the end of the data set were disregarded in this analysis since they do not comprise a full group of twelve. The arithmetic mean values were transformed into log10 values. Finally, the arithmetic mean over all log10 values was calculated, giving the upscaled mean permeability value for the Niche 3107 measurements.

3. Finally, editorial changes were conducted in niche_3107_preexcavation_upscaling.xls. These include adding/changing headers and deleting columns that are not needed.

Niche 4788:

1. Table s99469_002 from DTN: LB980901233124.101 [136593] was extracted from the TDMS. File zz_sep_208707.zip was copied to an appropriate working directory and unzipped. A text file named zz_sep_208707.txt opens.

2. A new Excel file named niche_4788_preexcavation_upscaling.xls was generated. The text file zz_sep_208707.txt was opened into Excel, using space and tab delimited options. The last data column contains the permeability values in non-logarithmic space. Starting with the first measurement interval, the arithmetic mean of groups of twelve consecutive values was calculated. The last group contains only eleven permeability values. The arithmetic mean values were transformed into log10 values. Finally, the arithmetic mean over all log10 values was calculated, giving the upscaled mean permeability value for the Niche 4788 measurements.

3. Finally, editorial changes were conducted in niche_4788_preexcavation_upscaling.xls. These include adding/changing headers and deleting columns that are not needed.

Niche 3650:

1. Tables s00434_006 through s00434_009, S00434_011, S00434_013, and S00434_015 from DTN: LB980901233124.101 [136593] were extracted from the TDMS. Each table relates to a separate zip file for the boreholes tested in prior to construction of Niche 3107. The zip files were copied to an appropriate working directory and unzipped. Several text files containing the measurements of the different boreholes open.

2. A new Excel file named niche_3650_preexcavation_upscaling.xls was generated. All text files for the different boreholes were opened into Excel, using space and tab delimited options, and were then copied, one boreholes after the other, into one spreadsheet. The second last data column contains the permeability values in non-logarithmic space. Starting with the first measurement interval, the arithmetic mean of groups of twelve consecutive values was calculated. Nine measurement intervals at the end of the data set were disregarded in this analysis since they do not comprise a full group of twelve. The arithmetic mean values were transformed into log10 values. Finally, the arithmetic mean over all log10 values was calculated, giving the upscaled mean permeability value for the Niche 3650 measurements.

3. Finally, editorial changes were conducted in niche_3650_preexcavation_upscaling.xls. These include adding/changing headers and deleting columns that are not needed.

Niche 3566:

1. Tables s00434_001, S00434_002, and S00434_003 from DTN: LB980901233124.101 [136593] were extracted from the TDMS. Each table relates to a separate zip file for the boreholes tested in prior to construction of Niche 3566. The zip files were copied to an

appropriate working directory and unzipped. Several text files containing the measurements of the different boreholes open.

2. A new Excel file named niche_3566_preexcavation_upscaling.xls was generated. All text files for the different boreholes were opened into Excel, using space and tab delimited options, and were then copied, one borehole after the other, into one spreadsheet. The second last data column contains the permeability values in non-logarithmic space. Starting with the first measurement interval, the arithmetic mean of groups of twelve consecutive values was calculated. Eight measurement intervals at the end of the data set were disregarded in this analysis since they do not comprise a full group of twelve. The arithmetic mean values were transformed into log10 values. Finally, the arithmetic mean over all log10 values was calculated, giving the upscaled mean permeability value for the Niche 3566 measurements.

3. Finally, editorial changes were conducted in niche_3566_preexcavation_upscaling.xls. These include adding/changing headers and deleting columns that are not needed.

The statistics derived from the upscaling analysis for the five niches support Tables 6.6-6 and 6.6-9 of this Model report.

INTENTIONALLY LEFT BLANK

ATTACHMENT IV—ANALYSIS OF PERCOLATION FLUX FIELDS

The percolation flux distributions predicted by the UZ Flow and Transport Model (BSC 2003 [163045]) were statistically analyzed in Section 6.6.4.1 of this Model Report (see also Scientific Notebook, Birkholzer 2003 [164526], pp. 97–117, 140–146). These fluxes were provided in DTN: LB0302PTNTSW9I.001 [162277] (base case) and DTN: LB0305PTNTSW9I.001 [163690] (alternative conceptual model for flow in the PTn). Several *Mathcad 11* spreadsheets were used to calculate the mean, minimum, and maximum fluxes in these flow fields, and to analyze the distribution of fluxes using histograms. As pointed out in Section 6.6.4.1, the model domain of the UZ Flow and Transport Model is much larger than the repository area. Since only fluxes over the repository area are relevant for the seepage evaluation, the *Mathcad* calculation must extract the repository fluxes from the overall flux distribution for the entire UZ model domain. In addition, it is interesting to evaluate the potential impact of major fault zones that intersect the model domain. Therefore, fluxes that represent fault zones need to be identified in the *Mathcad* spreadsheets, and statistical parameters need to be calculated for flux distributions with and without fault zones.

The *Mathcad* calculation uses file REPO_ZONE.cell from DTN: LB03033DSSFF9I.001 [163047] to identify the repository fluxes. This file lists the 469 repository elements in the UZ model grid by their 7-digit names. The last three digits denote the columns of the numerical grid; the first one of these three digits is a letter followed by a two-digit number. An upper-case letter indicates that the column represents a fault element, lower case letters stand for non-fault (fractured rock) elements. Based on the given list of repository element names, an Excel file REPO_ZONE_for_mathcad.xls was generated containing two worksheets. The first worksheet "Repository Columns" includes a list of the 469 repository elements with only the last three digits; the first four digits have been eliminated because they are not needed for identification of repository elements. The second worksheet "No Fault Repo Columns" includes a list of all non-fault 433 repository elements, again only giving the last three digits. This list was generated by eliminating all repository elements from Worksheet "Repository Columns" that have an upper case letter.

The nine flow fields from DTN: LB0302PTNTSW9I.001 [162277] are given in separate data files; these are named as follows in the DTN:

preq_ma_ptn.q	mean climate scenario, present-day climate
monq_ma_ptn.q	mean climate scenario, monsoon climate
glaq_ma_ptn.q	mean climate scenario, glacial transition climate
preq_la_ptn.q	lower-bound climate scenario, present-day climate
monq_la_ptn.q	lower-bound climate scenario, monsoon climate
glaq_la_ptn.q	lower-bound climate scenario, glacial transition climate
preq_ma_ptn.q	upper-bound climate scenario, present-day climate
monq_ma_ptn.q	upper-bound climate scenario, monsoon climate
glaq_ma_ptn.q	upper-bound climate scenario, glacial transition climate

The nine flow fields from DTN: LB0305PTNTSW9I.001 [163690], for the alternative flow model in the PTn, are given in separate data files; these are named as follows in the DTN:

preq_mb_ptn.q	mean climate scenario, present-day climate

monq_mb_ptn.q	mean climate scenario, monsoon climate
glaq_mb_ptn.q	mean climate scenario, glacial transition climate
preq_lb_ptn.q	lower-bound climate scenario, present-day climate
monq_lb_ptn.q	lower-bound climate scenario, monsoon climate
glaq_lb_ptn.q	lower-bound climate scenario, glacial transition climate
preq_mb_ptn.q	upper-bound climate scenario, present-day climate
monq_mb_ptn.q	upper-bound climate scenario, monsoon climate
glaq_mb_ptn.q	upper-bound climate scenario, glacial transition climate

Each of these files contains the PTn/TSw-fluxes for all element columns of the UZ model grid. The first two variables in each line give the element coordinates, the third variable gives the vertical percolation flux at the PTn/TSw-interface in mm/yr, and the fourth variable gives the element name (7-digits). For the *Mathcad* calculation, the list of element names was copied into an Excel file ptntsw_elements_for_mathcad.xls. The first four digits of each name were deleted, so that only the 3-digit column name remains in the Excel file.

The statistical analysis of these percolation flux fields is conducted with various *Mathcad* spreadsheets. Basically, the calculation procedure in these spreadsheets is identical; only the input and output file names are different. The *Mathcad* spreadsheets (1) read Excel files REPO_ZONE_for_mathcad.xls and ptntsw_elements_for_mathcad.xls, (2) read one of the 18 files for the percolation flux fields, (3) calculate over all fluxes (entire UZ domain), (4) identify and extract the repository fluxes, (4) write the extracted fluxes into an Excel file for further use in seepage evaluation, (5) calculate statistics for the extracted fluxes, and (6) plot a histogram of the distribution of extracted fluxes. The statistical analysis is conducted for *all* repository elements and for *all non-fault* repository elements, in separate spreadsheets. For the base case flow concept in the PTN, all nine flow fields are analyzed. For the alternative flow concept in the PTn, only the three climate stages of the mean climate scenario are analyzed.

Table IV-1 provides a list of the *Mathcad* spreadsheets for the percolation flux analysis using the base case flow fields, conducted for all repository elements. Table IV-2 provides a list of the *Mathcad* spreadsheets for the same flow fields, but conducted for no-fault repository elements. Table IV-3 gives a list of the *Mathcad* spreadsheets for the alternative flow fields analysis, conducted for the mean climate scenario for all repository elements. Table IV-4 provides a list of the *Mathcad* spreadsheets for the same flow fields, but conducted for no-fault repository elements.

Table IV-1. Mathcad Spreadsheets for Percolation Flux Analysis Using the Base Case Flow Fields from DTN: LB0302PTNTSW9I.001 [162277]. Calculation is Conducted for All Repository Elements

Spreadsheet: Repo_Flux_preq_ma.mcd Input File: preq_ma_ptn.q Output-File: Extracted_preq_ma_from_Mathcad.xls
Spreadsheet: Repo_Flux_monq_ma.mcd Input File: monq_ma_ptn.q Output-File: Extracted_monq_ma_from_Mathcad.xls
Spreadsheet: Repo_Flux_glaq_ma.mcd Input File: glaq_ma_ptn.q Output-File: Extracted_glaq_ma_from_Mathcad.xls
Spreadsheet: Repo_Flux_preq_la.mcd Input File: preq_la_ptn.q Output-File: Extracted_preq_la_from_Mathcad.xls

Spreadsheet: Repo_Flux_monq_la.mcd Input File: monq_la_ptn.q Output-File: Extracted_monq_la_from_Mathcad.xls
Spreadsheet: Repo_Flux_glaq_la.mcd Input File: glaq_la_ptn.q Output-File: Extracted_glaq_la_from_Mathcad.xls
Spreadsheet: Repo_Flux_preq_ua.mcd Input File: preq_ua_ptn.q Output-File: Extracted_preq_ua_from_Mathcad.xls
Spreadsheet: Repo_Flux_monq_ua.mcd Input File: monq_ua_ptn.q Output-File: Extracted_monq_ua_from_Mathcad.xls
Spreadsheet: Repo_Flux_glaq_ua.mcd Input File: glaq_ua_ptn.q Output-File: Extracted_glaq_ua_from_Mathcad.xls

Table IV-2. Mathcad Spreadsheets for Percolation Flux Analysis Using the Base Case Flow Fields from DTN: LB0302PTNTSW9I.001 [162277]. Calculation is Conducted for No-Fault Repository Elements

Spreadsheet: Repo_Flux_preq_ma_no_fault.mcd Input File: preq_ma_ptn.q Output-File: NA
Spreadsheet: Repo_Flux_monq_ma_no_fault.mcd Input File: monq_ma_ptn.q Output-File: NA
Spreadsheet: Repo_Flux_glaq_ma_no_fault.mcd Input File: glaq_ma_ptn.q Output-File: NA
Spreadsheet: Repo_Flux_preq_la_no_fault.mcd Input File: preq_la_ptn.q Output-File: NA
Spreadsheet: Repo_Flux_monq_la_no_fault.mcd Input File: monq_la_ptn.q Output-File: NA
Spreadsheet: Repo_Flux_glaq_la_no_fault.mcd Input File: glaq_la_ptn.q Output-File: NA
Spreadsheet: Repo_Flux_preq_ua_no_fault.mcd Input File: preq_ua_ptn.q Output-File: NA
Spreadsheet: Repo_Flux_monq_ua_no_fault.mcd Input File: monq_ua_ptn.q Output-File: NA
Spreadsheet: Repo_Flux_glaq_ua_no_fault.mcd Input File: glaq_ua_ptn.q Output-File: NA

Table IV-3. Mathcad Spreadsheets for Percolation Flux Analysis Using the Alternative Flow Fields from DTN: LB0305PTNTSW9I.001 [163690]. Calculation is Conducted for All Repository Elements

Spreadsheet: Repo_Flux_preq_mb.mcd Input File: preq_mb_ptn.q Output-File: Extracted_preq_mb_from_Mathcad.xls
Spreadsheet: Repo_Flux_monq_mb.mcd Input File: monq_mb_ptn.q Output-File: Extracted_monq_mb_from_Mathcad.xls
Spreadsheet: Repo_Flux_glaq_mb.mcd Input File: glaq_mb_ptn.q Output-File: Extracted_glaq_mb_from_Mathcad.xls

Table IV-4. Mathcad Spreadsheets for Percolation Flux Analysis Using the Alternative Flow Fields from DTN: LB0305PTNTSW9I.001 [163690]. Calculation is Conducted for No-Fault Repository Elements

Spreadsheet: Repo_Flux_preq_mb_no_fault.mcd Input File: preq_mb_ptn.q Output-File: NA
Spreadsheet: Repo_Flux_monq_mb_no_fault.mcd Input File: monq_mb_ptn.q Output-File: NA
Spreadsheet: Repo_Flux_glaq_mb_no_fault.mcd Input File: glaq_mb_ptn.q Output-File: NA

The *Mathcad* spreadsheets and all input/output files are provided in Output-DTN: LB0308AMRU0120.001. The files listed in Tables IV-1 and IV-2 are provided in directory: Norm_Flow_Field_Analysis. Results from these files support Table 6.6-11 and Figure 6.6-11 of this Model Report. The files listed in Tables IV-3 and IV-4 are provided in directory: Alternative_Concept_Flow_Field_Analysis. Results from these files support Table 6.6-11 and Figure 6.6-12 of this Model Report.

ATTACHMENT V—PROBABILISTIC SEEPAGE CALCULATION

The results from probabilistic seepage calculations were described and discussed in Section 6.8.3. Several *Mathcad 11* spreadsheets were used to conduct these calculations for various evaluation cases. The *Mathcad* spreadsheets read the SMPA look-up table and the extracted repository percolation fluxes (see Attachment IV), perform a random seepage calculation over 10,000 random samples, and derive seepage histograms as well as seepage summary statistics. The following procedure was followed to conduct the analysis (see also Scientific Notebook, Birkholzer 2003 [164525], pp. 96–142):

1. Copy file Fig6-3toFig6-8.dat from DTN: LB0304SMDCREV2.002 [163687] into appropriate working directory for *Mathcad* calculation, subdirectory SMPA Input.

2. Rename file Fig6-3toFig6-8.dat to ResponseSurfaceSMPA_for_Mathcad.dat. Delete first two lines.

3. Copy the Excel files containing the extracted repository fluxes (see Attachment IV, Table IV-1 and IV-3) into subdirectories UZ Flow Fields Norm (for base case flow fields) and UZ Flow Fields Alternative (for alternative flow fields)

4. Conduct *Mathcad* calculations using the various *Mathcad* spreadsheets listed in Tables V-1, V-2 and V-3. Tables V-1 and V-2 give the base case calculations described in Section 6.8.1, for the Tptpll and the Tptpmn units, respectively. Table V-2 lists the sensitivity case calculations described in Section 6.8.2.

Table V-1. Mathcad Spreadsheets for Probabilistic Seepage Calculation for the Tptpll Unit (Base Case Seepage Evaluation)

tptpll_preq_ma.mcd	seepage calculation for present-day climate, mean climate scenario
tptpll_monq_ma.mcd	seepage calculation for monsoon climate, mean climate scenario
tptpll_glaq_ma.mcd	seepage calculation for glacial transition climate, mean climate scenario
tptpll_preq_la.mcd	seepage calculation for present-day climate, lower-bound climate scenario
tptpll_monq_la.mcd	seepage calculation for monsoon climate, lower-bound climate scenario
tptpll_glaq_la.mcd	seepage calculation for glacial transition climate, lower-bound climate scenario
tptpll_preq_ua.mcd	seepage calculation for present-day climate, upper-bound climate scenario
tptpll_monq_ua.mcd	seepage calculation for monsoon climate, upper-bound climate scenario
tptpll_glaq_ua.mcd	seepage calculation for glacial transition climate, upper-bound climate scenario

Table V-2. Mathcad Spreadsheets for Probabilistic Seepage Calculation for the Tptpmn Unit (Base Case Seepage Evaluation)

tptpmn_preq_ma.mcd	seepage calculation for present-day climate, mean climate scenario
tptpmn_monq_ma.mcd	seepage calculation for monsoon climate, mean climate scenario
tptpmn_glaq_ma.mcd	seepage calculation for glacial transition climate, mean climate scenario
tptpmn_preq_la.mcd	seepage calculation for present-day climate, lower-bound climate scenario
tptpmn_monq_la.mcd	seepage calculation for monsoon climate, lower-bound climate scenario
tptpmn_glaq_la.mcd	seepage calculation for glacial transition climate, lower-bound climate scenario
tptpmn_preq_ua.mcd	seepage calculation for present-day climate, upper-bound climate scenario
tptpmn_monq_ua.mcd	seepage calculation for monsoon climate, upper-bound climate scenario
tptpmn_glaq_ua.mcd	seepage calculation for glacial transition climate, upper-bound climate scenario

Table V-3. Mathcad Spreadsheets for Probabilistic Seepage Calculation for the Tptpll Unit (Sensitivity Cases)

tptpll_preq_ma_normal_dist_alpha.mcd tptpll_monq_ma_normal_dist_alpha.mcd tptpll_glaq_ma_normal_dist_alpha.mcd	sensitivity case 1: normal distribution for spatial variability of capillary strength, three climate stages, mean climate scenario
tptpll_preq_ma_normal_dist_uncertainty_seep.mcd tptpll_monq_ma_normal_dist__uncertainty_seep.mcd tptpll_glaq_ma_normal_dist_uncertainty_seep.mcd	sensitivity case 2: normal distribution for uncertainty of seepage rate predictions, three climate stages, mean climate scenario
tptpll_preq_ma_mean_k_alpha.mcd tptpll_monq_ma_mean_k_alpha.mcd tptpll_glaq_ma_mean_k_alpha.mcd	sensitivity case 3: no spatial variability in permeability and capillary strength, three climate stages, mean climate scenario
tptpll_preq_ma_no_uncertainty_k_alpha.mcd tptpll_monq_ma_no_uncertainty_k_alpha.mcd tptpll_glaq_ma_no_uncertainty_k_alpha.mcd	sensitivity case 4: no uncertainty in permeability and capillary strength, three climate stages, mean climate scenario
tptpll_preq_ma_niche_1620.mcd tptpll_monq_ma_niche_1620.mcd tptpll_glaq_ma_niche_1620.mcd	sensitivity case 5: adjusted mean value for permeability distribution, three climate stages, mean climate scenario
tptpll_preq_ma_no_focus.mcd tptpll_monq_ma_no_focus.mcd tptpll_glaq_ma_no_focus.mcd tptpll_preq_ma_large_focus.mcd tptpll_monq_ma_large_focus.mcd tptpll_glaq_ma_large_focus.mcd	sensitivity cases 6a and 6b: adjusted flow focusing factors (no flow focusing and increased flow focusing), three climate stages, mean climate scenario
tptpll_preq_mb_alternative_Ptn.mcd tptpll_monq_mb_alternative_Ptn.mcd tptpll_glaq_ mb_alternative_Ptn.mcd	sensitivity case 7: percolation flux distribution from alternative Ptn flow concept, three climate stages, mean climate scenario
tptpll_preq_mb_alphamethodB.mcd tptpll_monq_mb_alphamethodB.mcd tptpll_glaq_ mb_alphamethodB.mcd tptpll_preq_mb_alphamethodC.mcd tptpll_monq_mb_alphamethodC.mcd tptpll_glaq_ mb_alphamethodC.mcd	sensitivity cases 8a, 8b, 8c: percolation flux distribution for alternative methods B, C, and D for deriving statistical parameters for capillary strength, three climate stages, mean climate scenario

tptpll_preq_mb_alphamethodC.mcd tptpll_monq_mb_alphamethodC.mcd tptpll_glaq_ mb_alphamethodC.mcd	

All *Mathcad* spreadsheets listed above are provided in Output-DTN: LB0308AMRU0120.002. Results from these files support Figures 6.8-1 through 6.8-3 and Tables 6.8-1 through 6.8-3.

INTENTIONALLY LEFT BLANK